

# **HYDROGEN-FREE CONVERSION OF LIPIDS INTO FUEL RANGE HYDROCARBONS OVER THREE REACTION STAGES**

Morenike Ajike Peters

Doctor of Philosophy

ASTON UNIVERSITY

JUNE 2023

© Morenike Ajike Peters, 2023

Morenike Ajike Peters asserts their moral right to be identified as the author of this thesis

This copy of the thesis has been supplied on condition that anyone who consults it is understood to recognise that its copyright belongs to its author and that no quotation from the thesis and no information derived from it may be published without appropriate permission or acknowledgement

**Hydrogen-free Conversion of Lipids into Fuel-range Hydrocarbons over Three Reaction Stages**

Morenike Ajike Peters

Doctor of Philosophy

2023

**Thesis summary**

The chemical composition of lipids is much closer to hydrocarbons than any other type of biomass-derived feedstocks and could contribute to the source of feedstocks for large-scale production of fuels and chemicals. In this present work, a three-step process involving hydrothermal hydrolysis, catalytic decarboxylation and catalytic cracking has been investigated for hydrogen-free conversion of lipid feedstocks into liquid hydrocarbon fuels with high yields of aliphatics and aromatics using batch reactors.

The hydrothermal hydrolysis stage investigated in the absence of catalysts was optimised and results show that the best conditions for the hydrolysis of rapeseed oil were 1 h at 300 °C, and oil-to-water mass ratio of 1:2. This led to a high conversion of rapeseed oil to give 88 wt.% yield of semi-solid product, dominated by C18 fatty acids, with oleic acid accounting for over 62 wt.% yield.

Over 97% deoxygenation was achieved at 400 °C for 2 h, with heptadecane as the dominant compound. Further experiments at temperatures of 420 °C and 450 °C led to simultaneous decarboxylation and cracking of the hydrolysed oil to obtain organic liquid products with high proportions of gasoline and biojet fuel range hydrocarbons at the optimal conditions of 450 °C for 1 h.

Finally, catalytic cracking of the decarboxylated oil was carried out and the optimal oil product found with 10:1 oil-to-ZSM-5 mass ratio, 400 °C for 1 h contained C7- C16 hydrocarbons with a dominance of single ring compounds. Significant shifts of aromatic contents towards undesirable soot-forming polycyclic aromatic hydrocarbons (PAHs) occurred with increased reaction severity.

Overall, the three-stage process produced around 50 wt. % - 65 wt.% yield of liquid hydrocarbons, without the use of expensive hydrogen gas. The innovative combination of reaction steps, catalysts and reaction conditions presented a potentially low-cost for obtaining fuel range liquid hydrocarbons.



## Acknowledgements

I dedicate this Thesis to the Omnipotent God Almighty who has continuously endowed me with the grace and numerous blessings to take advantage of this amazing opportunity. Next, I would like to give huge thanks to my Supervisor, Dr Jude Onwudili without whose unflinching support I would not have even dared to start this PhD programme. His expertise, exceptional resilience, constant motivation, finesse in supervision style have made it possible for me to complete this PhD programme. I would like to express great gratitude to my Associate Supervisor, Dr Jiawei Wang, who was always present and ready to lend a helping hand when I needed it. My gratitude also goes to all the members of Dr Onwudili's Sustainable Fuels and Chemicals Group whose friendships and shared experiences were both inspirational and motivational to me as I navigated the challenges of my PhD research. Special thanks to Dr Iram Razaq, Dr Cristiane Scaldaferri, Dr Carine Alves, Dr Onajite Diejomaoh who shared their research skills and experiences with me within the group and to other PhD students in EBRI including Omar Mohammad. When it really got down to it, we went through the challenges together, and their support helped in so many ways. I would like to also appreciate my friends for constantly motivating me and cheering me on. With a grateful heart and unparalleled appreciation, I would like to thank my parents Mr Gboyega and Mrs Funmilayo Peters for their support and belief in me all my life and for funding my PhD. To my lovely sister Bimbo Adebiyi, brothers Lekan Peters and Yemi Adebiyi, and nephew Adriel Adebiyi, I love you loads for all the support and encouragement.

## Table of contents

1	Introduction .....	21
1.1	Policy drivers for biofuel production and utilisations.....	22
1.2	Why should we explore other sources of aviation fuels?.....	22
1.3	Properties of aviation fuels.....	24
1.4	Research aims and objectives .....	25
1.4.1	Aim .....	25
1.4.2	Organisation of this Thesis .....	26
1.4.3	Justification for process selection for experimental work.....	27
1.5	References.....	29
2	Literature review .....	32
2.1	Current state of biojet fuels production.....	32
2.2	ASTM-approved biojet fuel pathways .....	34
2.2.1	Biojet fuel technology based on lipid feedstocks .....	34
2.2.2	Biojet production routes based on alcohol feedstocks Alcohol to Jet (ATJ) .....	39
2.2.3	Biojet fuel production routes based on sugar feedstocks (Direct Sugar to Hydrocarbon (DSHC)) .....	42
2.3	Fischer Tropsch (syngas to Jet).....	45
2.4	Comparison of biojet properties and yields from different routes .....	46
2.5	Pyrolysis and hydrothermal liquefaction (HTL) to jet fuel .....	50
2.6	Research Objectives .....	52
2.7	References.....	54
3	Methodology .....	63
3.1	Materials .....	63
3.1.1	Feedstock.....	63
3.1.2	Reagents .....	64
3.1.3	Catalysts.....	64
3.2	Methods .....	65
3.2.1	Detailed description of experimental equipment.....	65

3.2.2	Detailed description of experimental procedures.....	73
3.2.3	Analytical equipment and procedures.....	76
3.3	Computation of mass balances.....	106
3.4	References .....	109
4	Hydrothermal Hydrolysis of Rapeseed oil and WCOs .....	113
4.1	Selection of optimum conditions for hydrolysis experiments .....	113
4.2	Results and Discussions .....	114
4.2.1	Results from TGA characterisation of samples.....	116
4.2.2	Characterisation of RSO, WCO-A and WCO-B by GC/MS after esterification .....	120
4.3	Results from hydrothermal hydrolysis of RSO .....	122
4.3.1.	Effect of temperature on hydrolysis of RSO .....	123
4.3.2.	Effect of reaction time.....	125
4.3.3.	Effect of RSO – water mass ratio on hydrolysis of rapeseed oil .....	126
4.3.4	Effect of stirring speed and reactor wall.....	127
4.4	Results from hydrolysis of WCO samples .....	128
4.4.1	Fatty acid yields and mass balances from hydrolysis of WCO samples .	128
4.4.2	Quantification of fatty acids in hydrolysed lipids as FAMES by GC/MS ...	129
4.4.3	TGA quantification of fatty acids and FAMES obtained from hydrolysis of lipids .....	131
4.4.4	Comparing quantification of fatty acids by titration, GC/MS and TGA .....	134
4.5	References.....	136
5	Catalytic decarboxylation of hydrolysis product up to 400 °C .....	140
5.1	Catalyst characterisation.....	141
5.2	Influence of different reaction parameters on the decarboxylation of hydrolysis products .....	143
5.2.1	Screening of different catalysts for the decarboxylation of fatty acids from hydrolysis of RSO .....	143
5.2.2	Effect of decarboxylation temperature .....	151

5.2.3 Effect of 5 wt% Pt/C catalyst loading of the decarboxylation of fatty acids from hydrolysis stage.....	164
5.2.4 Effect of reaction time on the decarboxylation of fatty acids from hydrolysis of RSO with 5 wt% Pt/C catalyst.....	173
5.3 References .....	186
6 Catalytic decarboxylation and cracking of hydrolysis product up to 450 °C .....	190
6.1 Effect of reaction temperature .....	190
6.1.1 Product yields and mass balance .....	191
6.1.2 Gas composition .....	192
6.1.3 Characterisation of liquid products obtained from combined decarboxylation and cracking at higher temperatures .....	194
6.2 Effect of different catalysts on combined decarboxylation and cracking of hydrolysed RSO at 450 °C.....	201
6.2.1 Product yields and mass balance .....	201
6.2.2 Gas composition .....	203
6.2.3 Characterisation of liquid products from combined decarboxylation and cracking of hydrolysed RSO at 450° C with different catalysts .....	204
6.3 Effect of reaction time on the simultaneous decarboxylation and cracking of hydrolysed RSO.....	211
6.3.1 Product yields and mass balance .....	211
6.3.2 Gas composition in relation to reaction times at 450 °C .....	213
6.3.3 Characterisation of liquid products obtained in relation to reaction time at 450 °C in the presence of 5 wt% Pt/C catalyst .....	214
6.4 Reusability of 5 wt% Pt/C for combined decarboxylation and cracking at 450 °C .....	218
6.4.1 Product yields and mass balance .....	218
6.4.2 Gas composition .....	219
6.4.3 Characterisation of liquid products obtained from reusing Pt/C catalyst over three reaction cycles.....	221
6.4.4 Characterisation of the used Pt/C catalysts by x-ray diffraction (XRD) spectroscopy .....	227

6.5	Simultaneous decarboxylation and cracking of hydrolysed waste cooking oils (WCOs).....	228
6.5.1	Product yields and mass balance .....	228
6.5.2	Gas composition .....	229
6.5.3	Characterisation of liquid products.....	231
6.6	References.....	241
7	Cracking .....	243
7.1	Selection of optimum condition for preparation of feedstock for cracking ..	244
7.2	Characteristics of the fresh catalysts used for cracking of decarboxylated oil from RSO.....	246
7.3	Effect of reaction temperature with and without catalyst .....	247
7.3.1	Product yields and mass balance .....	247
7.3.2	Composition of gas products .....	248
7.3.3	Characteristics of liquid products in relation to cracking temperature and catalyst .....	249
7.4	Comparison of different catalyst for cracking of decarboxylated oil .....	258
7.4.1	Product yields and mass balance in relation of different catalysts.....	259
7.4.2	Gas composition in relation to different catalysts.....	260
7.4.3	Characterisation of liquid products obtained from cracking with different catalysts.....	260
7.5	Effect of reaction time on the cracking of decarboxylated oil from RSO.....	273
7.5.1	Product yields and mass balance in relation to reaction time for cracking .....	273
7.5.2	Gas composition in relation to reaction time .....	274
7.5.3	Characterisation of liquid products in relation to reaction time during cracking .....	274
7.6	Simple distillation of oil products from cracking of decarboxylated oil .....	280
7.7	Mechanism for formation of aromatics during cracking .....	283
7.8	Cracking of decarboxylated oils from real-world waste cooking oils (WCOs)	284

7.8.1 Product yields and mass balance .....	284
7.8.2 Gas composition from the cracking of decarboxylated oils from three feedstocks .....	285
7.8.3 Characterisation of liquid products obtained from the cracking of WCOs	286
7.9 Improving yield of single ring aromatic compounds .....	292
7.9.1 Chemical composition of oil products from cracking at extended residence times .....	293
7.10 References .....	302
8 Conclusion and future work .....	307
8.1 Conclusion to results chapters .....	307
8.2 Overall recommendation and future work .....	311
8.3 References.....	313

## List of Abbreviations

Al <sub>2</sub> O <sub>3</sub>	Alumina
APR	Aqueous Phase Reforming
ASTM	American Society for Testing and Materials
ATAG	Air Transport Action Group
ATJ	Alcohol-To-Jet
BECCS	Bioenergy With Carbon Capture and Storage
BET	Brunauer-Emmett-Teller
BJH	Barrett, Joyner and Halenda
BTEX	Benzene, Toluene, Ethylbenzene and Xylene
CAF	conventional aviation fuels
CH	Catalytic Hydrothermolysis
CHNS	Carbon, Hydrogen, Nitrogen, and Sulphur
CHNSO	Carbon, Hydrogen, Nitrogen, Sulphur, and Oxygen
CI	Chemical Ionisation
CO	Carbon monoxide
CO <sub>2</sub>	Carbon dioxide
CoMo	Cobalt Molybdenum
CoMo-Al <sub>2</sub> O <sub>3</sub>	Cobalt Molybdenum Alumina
CoMoS <sub>2</sub>	Cobalt Molybdenum Sulphide
COSHH	Control of Substances Hazardous to Health
COVID-19	Coronavirus disease 2019
CrCl <sub>2</sub>	Chromium Chloride
DC	Direct current
DCM	Dichloromethane
DSHC	Direct sugar to hydrocarbon
DTG	Derivative Thermogravimetric
EBRI	Energy and Bioproduct Research Institute
EI	Electron Impact
EU	European Union
FA	Fatty Acids
FAMEs	Fatty Acid Methyl Esters

FFA	Free Fatty Acids
FID	Flame Ionisation Detector
FT	Fischer Tropsch
GC	Gas Chromatography
GHSV	Gas Hourly Space Velocities
GTJ	Gas To Jet
h	hour
H <sub>2</sub> S	Hydrogen Sulphide
H <sub>2</sub> SO <sub>4</sub>	Sulphuric acid
H <sub>3</sub> PO <sub>4</sub>	Phosphoric acid
HCl	Hydrochloric acid
HDO	Hydrodeoxygenation
HDRD	Hydrogenated Derived Renewable Diesel
<i>H<sub>eff</sub></i>	Heating Efficiency
HEFA	Hydroprocessed Esters and Fatty Acids
HHV	Higher Heating Value
HRJ	Hydroprocessed Renewable Jet
HTL	Hydrothermal Liquefaction
IATA	International Air Transport Association
ICEs	Internal Combustion Engines
Jet-A	Jet Fuel
KWh	Kilowatt Hour
LCA	Life Cycle Analysis
LDPE	Low Density Polyethylene
LED	Light-Emitting Diode
LHSV	Liquid Hourly Velocity
N <sub>2</sub>	Nitrogen
NaOH	Sodium hydroxide
Nb <sub>2</sub> O <sub>5</sub>	Niobium oxide
NH <sub>3</sub>	Ammonia
NH <sub>4</sub> Cl	Ammonium chloride
Ni-Cu	Nickel Copper
Ni-Mo	Nickel Molybdenum
Ni-MoS <sub>2</sub>	Nickel Molybdenum Sulphide



Ni-W	Nickel Tungsten
NiAg	Nickel silver
NIST	National Institute of Standards and Technology
PAHs	Polycyclic Aromatic Hydrocarbons
Pd	Palladium
PID	Proportional–Integral–Derivative Controller
PMMA	Polymethyl Methacrylate
PPM	Parts Per Million
PTCM	Primary Temperature Control Module
PTFE	Polytetrafluoroethylene
RF	Response Factors
RRF	Relative Response Factor
RSO	Rapeseed Oil
RTFO	Renewable Transport Fuel Obligation
RuO <sub>2</sub>	Ruthenium oxide
SAF	sustainable aviation fuels
SAXS	Small angle X-ray scattering
SiO <sub>2</sub>	Silica
SIP	Synthesized Iso-Paraffinic fuel
TANs	Total acid numbers
TCD	Thermal Conductivity Detector
TGA	Thermogravimetric Analysis
TRL	Technology Readiness level
WAXD	Wide-angle X-ray diffraction
WCO	Waste Cooking Oils
WHSV	Weight hourly space velocity
Wt	Weight
XRD	X-ray diffraction

## List of Tables

Table 1.1: Specification standard of aviation fuel ICAO SAF, 2020; Elhaj and Lang, 2014) ..25	25
Table 2.1: Biojet fuel technologies and production companies (Beginner's Guide to Sustainable Aviation Fuel, 2017; Geleynse et al., 2018; Van Dyk et al., 2019; Wang et al., 2020; Bosch et al., 2020).....33	33
Table 2.2: Technology readiness level of biojet fuel technologies (Van Dyk et al., 2019; Bosch et al., 2020) .....35	35
Table 2.3: Conversion of sugars and cellulose to HMF .....44	44
Table 2.4: Comparison of properties of biojet fuel technologies (Elhaj and Lang, 2014; Brooks et al., 2016; Wright, 2012; ICAO, 2017).....46	46
Table 2.5: Some current results from literature on conversion of different feedstock to hydrocarbons .....48	48
Table 2.6: Types of pyrolysis (Bridgwater and Bridge, 1991).....50	50
Table 2.7: Comparison of properties; biooil and crude oil (Mortensen et al., 2011; Beims et al., 2017).....51	51
Table 2.8: Some current literature on catalytic upgrading of bio-oil (Mortensen et al., 2011) 51	51
Table 3.1: Preliminary experiments to test reactor temperature and pressure profiles .....71	71
Table 3.2: Peak areas for the standard hydrocarbon gases.....83	83
Table 3.3: Peak areas for the standard permanent gases .....84	84
Table 3.4: Preliminary GC/MS analysis results of FAME standards.....90	90
Table 3.5: Preliminary GC/MS analysis results of hydrocarbon standards.....93	93
Table 3.6: Results from repeatability tests on the acid-base titration of hydrolysis products .96	96
Table 3.7: Reproducibility of acid-base titration using products from hydrolysis stage .....96	96
Table 3.8: Reproducibility of acid-base titration using products from decarboxylation stage.97	97
Table 3.9: Results of testing standard on CHNS equipment.....99	99
Table 3.10: Solvent-free mixtures of hydrocarbons for elemental analysis by CHNS analyser and GC/MS method (0.1 g of each compound used in each mixture).....100	100
Table 3.11: Comparison between elemental analysis by CHNS and GC-MS.....101	101
Table 4.1: Some physicochemical properties of the samples used in this present study ....115	115
Table 4.2: Temperature profiles and mass losses during the degradation of components of lipids samples in a TGA.....119	119
Table 4.3: Types and compositions of fatty acids in 'as-received' RSO, WCO-A and WCO-B .....122	122
Table 4.4: Mass balance closures and fatty acids yields after hydrothermal hydrolysis of WCO .....129	129
Table 4.5: Types and compositions of fatty acids in hydrolysed RSO.....131	131
Table 4.6: Temperature profiles and mass losses during the degradation of components of lipids samples in a TGA.....133	133
Table 5.1: Physical and morphological properties of the catalysts used in this study* .....141	141
Table 5.2: Mass balance for reaction products from decarboxylation of hydrolysed rapeseed oil at 400 °C, 2 h with various catalysts .....144	144
Table 5.3: Physicochemical properties, density, acid content, elemental composition and calorific value obtained from varying catalyst types .....146	146
Table 5.4: List of compounds from decarboxylation of hydrolysed rapeseed oil at 400 °C, 2 h with various catalysts .....149	149
Table 5.5: Mass balance for reaction products from decarboxylation of hydrolysed rapeseed oil for 1 h at different temperatures (feed = 10 g).....152	152
Table 5.6: Density, acid content, elemental composition and calorific value obtained from varying reaction temperature.....156	156
Table 5.7: List of compounds from decarboxylation of hydrolysed rapeseed oil for 1 h at different temperatures (feed = 10 g) .....159	159

Table 5.8: Mass balance for reaction products from decarboxylation of hydrolysed rapeseed oil at 400 °C, 1 h with different 5 wt% Pt/C catalyst/feed mass ratios .....	164
Table 5.9: Density, acid content, elemental composition and calorific value obtained from varying 5 wt% Pt/C catalyst/feed mass ratios .....	167
Table 5.10: List of compounds from decarboxylation of hydrolysed rapeseed oil at 400 °C, 1 h with different 5 wt% Pt/C catalyst/feed mass ratios.....	170
Table 5.11: Mass balance for reaction products from decarboxylation of hydrolysed rapeseed oil at 400 °C with different reaction times with 5 wt% Pt/C catalyst.....	174
Table 5.12: Density, acid content, elemental composition and calorific value obtained of oil/wax products obtained from RSO in relation to reaction time in the presence of 5 wt% Pt/C catalyst.....	176
Table 5.13: List of compounds from decarboxylation of hydrolysed rapeseed oil at 400 °C with different reaction times with 5 wt% Pt/C catalyst .....	180
Table 5.14: Summary table showing compiled results of decarboxylation experiments .....	183
Table 6.1: Mass balance for reaction products from decarboxylation of hydrolysed rapeseed oil for 1 h at different temperatures.....	191
Table 6.2: Density, acid content, elemental composition and calorific value obtained combined decarboxylation and cracking at higher temperatures .....	194
Table 6.3: List of compounds in the oil products obtained from combined decarboxylation and cracking of hydrolysed RSO for 1 h at different temperatures (*reaction with 5 wt% Pt/C catalyst).....	199
Table 6.4: Mass balance for reaction products from decarboxylation of hydrolysed RSO at 450 °C, 1 h with different catalysts .....	202
Table 6.5: Density, acid content, elemental composition and calorific value obtained from varying select catalyst types .....	204
Table 6.6: List of compounds in the oil products obtained from combined decarboxylation and cracking of hydrolysed RSO for 1 h varying catalyst types .....	207
Table 6.7: Mass balance for reaction products from simultaneous decarboxylation and cracking of hydrolysed RSO at 450 °C with different reaction times .....	212
Table 6.8: Density, acid content, elemental composition and calorific value of liquid products in relation to reaction time at 450 °C with 5 wt% Pt/C catalyst.....	214
Table 6.9: Mass balance for reaction products from decarboxylation of hydrolysed rapeseed oil at 450 °C for 1 h assessing repeatability of results.....	218
Table 6.10: Density, acid content, elemental composition and calorific value obtained from reusing catalyst .....	221
Table 6.11: List of compounds in the oil products obtained from combined decarboxylation and cracking of hydrolysed RSO for 1 h repeating catalyst.....	224
Table 6.12: Mass balance for reaction products from decarboxylation of hydrolysed WCOs at 450 °C for 1 h.....	229
Table 6.13: Physicochemical properties, density, acid content, elemental composition and calorific value obtained from using different feedstock sources .....	231
Table 6.14: List of compounds in the oil products obtained from combined decarboxylation and cracking of hydrolysed RSO for 1 h repeating catalyst.....	234
Table 6.15: Summary table showing compiled results of decarboxylation and cracking experiments.....	236
Table 7.1: Energy efficiency optimisation for cracking feedstock .....	245
Table 7.2: Some properties of the catalysts used in the cracking reactions .....	246
Table 7.3: Mass balance for reaction products from cracking of hydrocarbons for 1 h at different temperatures .....	248
Table 7.4: Colour, elemental composition and calorific value of oil products in relation to cracking temperature.....	249
Table 7.5: List of compounds obtained from cracking of decarboxylated oil for 1 h at different temperatures (** indicates reactions carried out with catalyst, ZSM-5) .....	254

Table 7.6: Mass balance for reaction products from cracking at 400 °C, 1 h with various catalysts .....	259
Table 7.7: Colour, elemental composition and calorific value obtained from varying catalysts .....	261
Table 7.8: List of hydrocarbon compounds in the oil products obtained with the different catalysts at 400 °C for 1 h .....	263
Table 7.9: Distribution of carbon in cracking products .....	268
Table 7.10: Surface areas, pore volumes and pore diameters of used and recalcined catalysts used for the cracking reactions .....	272
Table 7.11: Mass balance for reaction products from the cracking of decarboxylated oils at 400 °C with different reaction times .....	273
Table 7.12: Colour, elemental composition and calorific value obtained from varying reaction time .....	275
Table 7.13: List of compounds in the oils obtained from the cracking reactions in relation to reaction time.....	276
Table 7.14: Mass balance for reaction products from cracking of decarboxylated oils from RSO and WCOs with ZSM-5 at 400 °C for 1 h .....	284
Table 7.15: Elemental composition and calorific values of the oil products from the cracking of decarboxylated WCOs.....	286
Table 7.16: List of compounds in the oil products obtained from the cracking of decarboxylated WCOs .....	288
Table 7.17: Product distribution, mass balances and densities of oil product from the extended reaction times at 400 °C, 1 h with various catalysts .....	292
Table 7.18: List of compounds in the oil products obtained from cracking decarboxylated RSO for extended reaction times.....	293
Table 7.19: Summary table showing compiled results of cracking experiments .....	300

## List of Figures

Figure 1.1: Energy consumption in transport: growth by mode (BP Global, 2020) .....	23
Figure 1.2: Current and projected commercial aircraft in service (CAPA, 2020) .....	24
Figure 2.1: Biojet fuel technology pathways .....	34
Figure 2.2: HRJ flow chart (Scaldaferri and Pasa, 2019) .....	36
Figure 2.3: Catalytic Hydrothermolysis (CH) process .....	38
Figure 2.4: Alcohol to jet flow chart.....	40
Figure 2.5: Approved pathway for ATJ .....	40
Figure 2.6: DSHC pathways to biojet fuel .....	42
Figure 2.7: Pyrolysis to jet fuel pathway .....	50
Figure 3.1: Photos of; a) the fresh supermarket rape seed oil; b) WCO-A from Aston University Pub, and c) WCO-B from Aston University cafeteria .....	64
Figure 3.2: Photos of main batch reactor system for hydrothermal hydrolysis; (a) 450ml fixed head bench top Parr reactor; (b) controller for 4848 Parr Reactor .....	65
Figure 3.3: Photo of 75ml bench top Parr batch reactor used for decarboxylation and cracking experiments .....	66
Figure 3.4: Arrangement for loading and unloading the 450 ml reactor using a laboratory vice .....	67
Figure 3.5: Photo of the main weighing balance used in this study .....	68
Figure 3.6: Photo of a typical Tedlar gas sampling bag used in this study .....	70
Figure 3.7: Reactor temperature profile in relation to quantity of water/oil loaded .....	71
Figure 3.8: Reactor pressure profile in relation to quantity of water/oil loaded .....	72
Figure 3.9: Reactor temperature profile in relation to volume of water added .....	73
Figure 3.10: Reactor temperature profile in relation to volume of water added .....	73
Figure 3.11: Process route for conversion of vegetable oil to biojet fuel range hydrocarbons .....	74
Figure 3.12: Procedure in hydrothermal hydrolysis, catalytic deoxygenation, and cracking ..	74
Figure 3.13: Photos of (a) Vacuum filtration setup; (b) liquid-liquid extraction apparatus .....	77
Figure 3.14: Stuart solvent evaporation system.....	78
Figure 3.15: Photos relating to solid product drying; (a) solids collected on filter paper (b) drying oven .....	79
Figure 3.16: Schematic of a typical gas chromatograph (Torres, 2016) .....	80
Figure 3.17: A typical GC chromatogram (Spangler, 2015) .....	80
Figure 3.18: Schematic of an FID .....	81
Figure 3.19: Wheatstone bridge basis of TCD .....	82
Figure 3.20: GC used for gas analysis.....	82
Figure 3.21: GC/FID chromatogram of standard hydrocarbon gases.....	83
Figure 3.22: GC/FID chromatogram of standard permanent gases .....	84
Figure 3.23: Schematic of electron Ionisation used in GC/MS (Rockwood, Kushnir and Clarke, 2018).....	86
Figure 3.24: Pathway to detecting ions in a mass spectrometer (Domingues, García and Skrzydlewska, 2018) .....	86
Figure 3.25: Photo of Shimadzu GC-2010 GC/MS used for qualitative and quantitative analyses of liquid products .....	87
Figure 3.26: Photo of reflux set up used for esterification .....	89
Figure 3.27: GC/MS chromatogram of FAMEs standards.....	90
Figure 3.28: Photo of distillation set up.....	92
Figure 3.29: GC/MS chromatogram of hydrocarbon standards containing 3000 ug of each compound .....	93
Figure 3.30: Photo of titration setup used .....	94
Figure 3.31: Results from fatty acid determination with acid-base titration method .....	96
Figure 3.32: Photo of CHNS equipment used.....	98

Figure 3.33: Photos of materials used for CHNS analysis of oil products; (a) adsorbent pads b) tin crucibles c) vanadium pentoxide d) sulphanilamide .....	98
Figure 3.34: Photo of TGA used in this study .....	102
Figure 3.35: Photo of nitrogen adsorption used .....	104
Figure 3.36: Photo of XRD used .....	105
Figure 3.37: Repeatability results on yield of products from each process stage .....	108
Figure 4.1: Schematic of hydrolysis experimental procedure .....	113
Figure 4.2: TGA thermograms and degradation temperature profiles of pure glycerol, oleic acid and methyl oleate .....	116
Figure 4.3: TGA thermograms of RSO, WCO-A and WCO-B, indicating the degradation profiles with Stage I (free fatty acids), Stage II (mono- & diglycerides and Stage III (triglycerides).....	119
Figure 4.4: Compositions of fatty acids in the 'as-received' samples; (a) rapeseed oil, (b) WCO-A and (c) WCO-B .....	121
Figure 4.5: Influence of reaction temperature on yields of fatty acids from hydrolysis of RSO (vegetable oil – water mass ratio = 1:2; reaction time of 60 min and stirring speed of 50 rpm) .....	123
Figure 4.6: Influence of reaction time on conversion of RSO at 300 °C and vegetable oil – water mass ratio of 1:2 (stirring speed of 50 rpm); (a) yields of fatty acids; (b(i) – (iii)) TGA thermograms of hydrolysis products obtained at 0 min, 30 min and 60 min, res.....	124
Figure 4.7: Influence of vegetable oil-water mass ratios on fatty acid yields from RSO at 300 °C and reaction time of 60 min (stirring speed of 50 rpm) .....	126
Figure 4.8: Images of rapeseed oil, reactor vessel/liner and hydrolysis product .....	127
Figure 4.9: Influence of stirring speed on the yields of total fatty acids from the hydrolysis of RSO at 300 °C, reaction time of 60 min and vegetable oil – water mass ratio of 1:2 .....	128
Figure 4.10: Annotated GC/MS chromatograms of the esterified hydrolysis products for (a) RSO, (b) WCO-A and (c) WCO-B.....	130
Figure 4.11: TGA thermograms of hydrolysis products of RSO, WCO-A and WCO-B before and after esterification with methanol, indicating their degradation profiles with Stage I (fatty acids/FAMES), Stage II (unreacted triglycerides and others).....	132
Figure 4.12: Results from comparative analysis studies; (a) quantification of fatty acid yields using the three different analytical methods .....	135
Figure 5.1: Schematic of decarboxylation experimental procedure .....	140
Figure 5.2: XRD patterns of fresh catalysts used (# Al <sub>2</sub> O <sub>3</sub> , # SiO <sub>2</sub> , < Pt, * MgSilicate, < C, ~ NiCu, ~ Pd) .....	142
Figure 5.3: Appearance of products obtained from using different catalysts .....	144
Figure 5.4: Mass yields of gas products obtained from decarboxylation of hydrolysed rapeseed oil at 400 °C, 2 h with various catalysts.....	145
Figure 5.5: Mass yields of hydrocarbon products obtained from decarboxylation of hydrolysed RSO at 400 °C, 2 h with various catalysts based.....	147
Figure 5.6: Mass yields of heptadecane and other hydrocarbon products obtained from decarboxylation of hydrolysed rapeseed oil at 400 °C, 2 h with various catalysts .....	148
Figure 5.7: Liquid fuels characterisation from varying catalyst type by H/C and O/C molar ratios in Van Krevelen diagram .....	151
Figure 5.8: Appearance of liquid/wax products .....	152
Figure 5.9: Mass yield, wt% of gases obtained from decarboxylation of hydrolysed RSO for 1 h at different temperatures (*reactions with 5 wt% Pt/C catalyst).....	154
Figure 5.10: Mass yields of compounds groups obtained from decarboxylation of hydrolysed RSO for 1 h at different temperatures (*with 5 wt% Pt/C catalyst) .....	157
Figure 5.11: Mass yields of heptadecane and other hydrocarbon products obtained from decarboxylation of hydrolysed RSO for 1 h at different temperatures (*with 5 wt% Pt/C catalyst).....	158
Figure 5.12: Liquid fuels characterisation from varying reaction temperature by H/C and O/C molar ratios in Van Krevelen diagram.....	162

Figure 5.13: Appearance of products in relation to 5 wt% Pt/C catalyst/feed mass ratios from decarboxylation of hydrolysed RSO .....	165
Figure 5.14: Mass yields and calorific values of gas products obtained from decarboxylation of hydrolysed RSO at 400 °C, 1 h with different 5 wt% Pt/C catalyst/feed mass ratios .....	166
Figure 5.15: Conversion of fatty acids in hydrolysed RSO and mass yields of hydrocarbon products at 400 °C, 1 h with different 5 wt% Pt/C catalyst/feed mass ratios .....	168
Figure 5.16: Mass yields of heptadecane and other hydrocarbon products from decarboxylation of hydrolysed RSO at 400 °C, 1 h with 5 wt% Pt/C catalyst/feed ratios .....	169
Figure 5.17: Van Krevelen diagram of liquid fuels characterisation from varying catalyst to feed mass ratios .....	173
Figure 5.18: Appearance of products in relation to reaction time at 400 °C .....	175
Figure 5.19: Mass yields and calorific values of gas products obtained from decarboxylation of hydrolysed RSO at 400 °C at different reaction times with 5 wt% Pt/C catalyst .....	175
Figure 5.20: Mass yields of groups of hydrocarbon products obtained from decarboxylation of hydrolysed RSO at 400 °C with different reaction times with 5 wt% Pt/C catalyst .....	178
Figure 5.21: Mass yields of heptadecane and other hydrocarbons from decarboxylation of hydrolysed RSO at 400 °C with different reaction times with 5 wt% Pt/C catalyst .....	178
Figure 6.1: Appearance of liquid products obtained from high temperature decarboxylation and cracking tests .....	192
Figure 6.2: Mass yields of gas products and their calorific values obtained from decarboxylation and cracking of hydrolysed RSO for 1 h at different temperatures without and with 5 wt% Pt/C catalyst .....	193
Figure 6.3: Mass yields of groups of compounds in liquid products and conversion of hydrolysed RSO during simultaneous decarboxylation and cracking at 450 °C (* reaction with 5 wt% Pt/C) .....	196
Figure 6.4: Mass yields of heptadecane and other hydrocarbon products from combined decarboxylation and cracking of hydrolysed RSO for 1 h at different temperatures (*reaction with 5 wt% Pt/C catalyst) .....	197
Figure 6.5: GC/MS chromatograms of combined decarboxylation and cracking of hydrolysed RSO for 1 h: (a) reaction at 420 °C without catalyst (b) reaction at 450 °C without catalyst (b) reaction at 450 °C in the presence of 5 wt% Pt/C .....	198
Figure 6.6: Liquid fuels characterisation from varying reaction temperature by H/C and O/C molar ratios in Van Krevelen diagram .....	201
Figure 6.7: Appearance of the liquid products obtained from different catalysts during combined decarboxylation and cracking of hydrolysed RSO at 450 °C for 1 h .....	202
Figure 6.8: Mass yield of gas products are their calorific values during combined decarboxylation and cracking of hydrolysed RSO at 450 °C, 1 h with different catalysts ....	203
Figure 6.9: Mass yields of groups of compounds in the oil products and the conversion of hydrolysed RSO at 450 °C after 1 h with different catalysts .....	206
Figure 6.10: Mass yields of heptadecane and other hydrocarbon products obtained from combined decarboxylation and cracking of hydrolysed RSO at 450 °C, 1 h with different catalysts .....	206
Figure 6.11: Liquid fuels characterisation from varying catalyst type by H/C and O/C molar ratios in Van Krevelen diagram .....	210
Figure 6.12: Appearance of products from simultaneous decarboxylation and cracking of hydrolysed RSO in relation to reaction time at 450 °C .....	212
Figure 6.13: Mass yields of gas products and their calorific values from simultaneous cracking and decarboxylation of hydrolysed RSO at 450 °C at different reaction times .....	213
Figure 6.14: Mass yields of groups of hydrocarbon products and conversion of hydrolysed RSO during simultaneous decarboxylation and cracking at 450 °C and different reaction times .....	215
Figure 6.15: Mass yields of heptadecane and other hydrocarbon products from the simultaneous decarboxylation and cracking of hydrolysed RSO at 450 °C and different reaction times .....	216

Figure 6.16: Liquid fuels characterisation from varying reaction time by H/C and O/C molar ratios in Van Krevelen diagram .....	217
Figure 6.17: Appearance of oil products obtained from reusing the Pt/C catalysts over 3 reaction cycles .....	219
Figure 6.18: Mass yields of gas products obtained from reusing catalyst at decarboxylation stage .....	220
Figure 6.19: Mass yields of groups of products obtained from reusing Pt/C catalyst for simultaneous decarboxylation and cracking .....	222
Figure 6.20: Mass yields of heptadecane and hydrocarbon products obtained from reusing Pt/C catalyst for simultaneous decarboxylation and cracking at 450 °C for 1 h.....	223
Figure 6.21: Liquid fuels characterisation from reusing Pt/C catalyst by H/C and O/C molar ratios in Van Krevelen diagram .....	226
Figure 6.22: XRD diffractograms of fresh and spent Pt/C catalyst from the simultaneous decarboxylation and cracking of hydrolysed RSO .....	227
Figure 6.23: Appearance of liquid products from the simultaneous decarboxylation and cracking of hydrolysed vegetable oils .....	229
Figure 6.24: Mass yield, wt % of gases obtained from decarboxylation of hydrolysed WCOs at 450 °C for 1 h .....	230
Figure 6.25: Mass yield, wt % of groups of hydrocarbon products obtained from decarboxylation of hydrolysed WCOs at 450 °C for 1 h .....	232
Figure 6.26: Mass yields of heptadecane and other hydrocarbon products obtained from simultaneous decarboxylation and cracking of hydrolysed WCOs at 450 °C for 1 h .....	233
Figure 6.27: Liquid fuels characterisation from varying feedstock sources by H/C and O/C molar ratios in Van Krevelen diagram.....	235
Figure 7.1: Schematic of procedure used for catalytic cracking experiments .....	244
Figure 7.2: Appearance of oil products from catalytic and non-catalytic cracking of decarboxylated oil at different temperatures .....	248
Figure 7.3: Mass yield % of gases obtained from cracking of decarboxylated oil for 1 h at different temperatures (** indicates reactions carried out with catalyst, ZSM-5).....	249
Figure 7.4: Mass yields of groups of compounds obtained from catalytic and non-catalytic cracking of decarboxylated oil for 1 h at different temperatures (** indicates reactions carried out with catalyst, ZSM-5).....	251
Figure 7.5: Mass yields of heptadecane and other hydrocarbons in the oil products obtained from cracking of decarboxylated oil for 1 h at different temperatures (** indicates reactions carried out with catalyst, ZSM-5) .....	253
Figure 7.6: Van Krevelen plot of the liquid/wax products from RSO to the post-cracking oil product in comparison with conventional hydrocarbon fuels .....	257
Figure 7.7: Simulated distillation curves from varying reaction temperature (ASTM D2887) .....	258
Figure 7.8: Appearance of liquid products obtained with the different cracking catalysts ....	259
Figure 7.9: Mass yields of gas products obtained from cracking of decarboxylated oil at 400 °C with various catalysts for 1 h.....	260
Figure 7.10: Mass yields of compound groups in oil products obtained from the cracking of decarboxylated oil at 400 °C with various catalysts for 1 h .....	261
Figure 7.11: Yield wt% of heptadecane and other hydrocarbon products obtained from cracking of hydrocarbons at 400 °C, 1 h with various catalysts .....	262
Figure 7.12: Van Krevelen plots of the oil products obtained with different catalysts at 400 °C for 1 h in comparison with conventional fuels .....	266
Figure 7.13: Simulated distillation curves for oil products obtained with different catalysts at 400 °C for 1 h .....	267
Figure 7.14: Appearance of the fresh, used and recalcined catalysts used for the cracking reactions .....	270
Figure 7.15: XRD patterns of (a) ZSM-5 (b) Zeolite Y (c) MCM-41 (d) Ru HSAalumina ( =Al <sub>2</sub> O <sub>3</sub> , =SiO <sub>2</sub> , =Ru, =RuO <sub>2</sub> , =Zeolite Y, =ZSM-5).....	271



Figure 7.16: Appearance of liquid products obtained from the catalytic cracking of the decarboxylated oils from RSO at different reaction times .....	273
Figure 7.17: Mass yield, wt % of gases obtained from cracking hydrocarbons at 400 °C with different reaction times .....	274
Figure 7.18: Mass yields of groups of hydrocarbon products obtained from cracking of decarboxylated oil at 400 °C in relation to reaction time .....	275
Figure 7.19: Mass yields of heptadecane and other hydrocarbon in the oil products obtained from cracking decarboxylated oil at 400 °C in relation to reaction time .....	276
Figure 7.20: Liquid fuels characterisation from varying reaction time by H/C and O/C molar ratios in Van Krevelen diagram .....	279
Figure 7.21: Simulated distillation curves from varying reaction time .....	280
Figure 7.22: Distribution and appearance of liquid products after distillation.....	281
Figure 7.23: (a) GC-MS chromatogram of pre-distilled cracked oil (b) GC-MS chromatogram of distilled cracked oil .....	282
Figure 7.24: Comparison of peak area between cracked and distilled oils .....	283
Figure 7.25: Reaction pathways for the catalytic cracking of hydrocarbons (Singh et al., 2021).....	284
Figure 7.26: Appearance of liquid products from the cracking of decarboxylated oils with ZSM-5 at 400 °C, for 1 h.....	285
Figure 7.27: Mass yields of gas products obtained from cracking of decarboxylated oils from WCOs at 400 °C for 1 h in comparison with RSO .....	285
Figure 7.28: Mass yields of groups of hydrocarbons obtained from cracking of decarboxylated WCOs .....	287
Figure 7.29: Mass yields of hydrocarbon products obtained from cracking WCOs according to carbon number .....	288
Figure 7.30: Van Krevelen plots of the oil products from cracking of decarboxylated WCOs in comparison with conventional fuels .....	291
Figure 7.31: Simulated distillation curves from varying feed sources .....	292
Figure 7.32: Appearance of liquid products from the cracking of decarboxylated oils with ZSM-5 at 400 °C, for longer reaction times.....	293
Figure 7.33: GC-MS chromatogram of (a) 1 h reaction (b) 6 h reaction (c) 12 h reaction....	297
Figure 8.1: Overall yields of liquid hydrocarbons from the 3-stage conversion of rapeseed oil .....	310

## **Publications arising from thesis**

Disclaimer: The results from Chapter 4 have been published in a journal paper:

**Peters, Morenike A.**, Alves, Carine Tondo, Wang, Jiawei and Onwudili, Jude A. (2022). Subcritical Water Hydrolysis of Fresh and Waste Cooking Oils to Fatty Acids Followed by Esterification to Fatty Acid Methyl Esters: Detailed Characterization of Feedstocks and Products. *Omega (ACS)*, 7 (50), 46870-46883.

## 1 Introduction

The current global energy consumption increased by 18% over the last decade and now stands at 14.3 billion tonnes of oil equivalent (BTOE) (BP Global, 2020). All four of the world's primary energy sectors (industry, transport, commercial and residential) have recorded increased demands during this period, which have been mainly satisfied from conventional fossil-based energy sources including crude oil, gas and coal. However, the depletion of the fossil fuels along with the global concern on the greenhouse effect (i.e., Global Warming and Climate Change), is facilitating the paradigm shift to replace the non-renewables by more sustainable and renewable alternatives. Thus, the quest for and development of renewable energy sources have become a necessity in the fields of science and technology. Apart from energy sources like solar, wind and geothermal, biomass has been recognised as one of the renewable energy resources. Indeed, biomass has the most potential in the transition from petroleum to low-carbon fuels because it can easily be converted to energy carriers (gas, liquid and solid fuels) similar to those obtained from fossil fuels on which modern lifestyles depend.

The concept of Net Zero carbon emissions to the atmosphere has been globally accepted and stakeholders are working towards achieving this by 2050. The transition to Net Zero requires two further concepts that can be worked side-by-side: defossilisation and decarbonisation. There are overlaps between these two concepts and the Net Zero target inspires a continuum of approaches between these two. In the purest sense, defossilisation refers to the gradual replacement of carbon-based energy from non-renewable fossil fuels with those from renewable carbon such as biomass resources. The purest form of decarbonisation refers to the rejection of carbon-based energy in all its forms, so that only non-carbon-based energy resources would provide all our energy needs. A recent perspective published by Lange (2021), indicates that during the transition to net Zero, between 400 – 500 billion tonnes of carbon will need to be injected into the chemical sector every year to achieve a smooth shift. It is therefore clear that a green transition will rely on biomass, which is the only source of renewable carbon on Earth. In particular, using biomass-derived liquid fuels (biofuels) is seen as the drop-in replacement to defossilise the transport sector (Gomez, Steele-King and McQueen-Mason, 2008). With the growing research into bioenergy with carbon capture and storage (BECCS), biomass can become a source of negative carbon emissions, with significant contributions to the decarbonisation efforts to achieve Net Zero (Yang et al., 2022).

## 1.1 Policy drivers for biofuel production and utilisations

This transition to low-carbon energy sources has been supported by a range of national and international policies to provide incentives or palliatives to enable large scale changes. In particular, for the transportation sector, this has been very effective. For example, the successful implementation of the Renewable Transport Fuel Obligation (RTFO) in 2008 provided incentivised use of sustainable fuel for road transport in the UK. This legislation and other similar international obligations made a significant impact on the biofuel industry globally with production of over 90 Mtoe (Alalwan et al., 2019).

Examples of other national and international policies that have contributed to the promotion of the use of biofuels include (Pandey, 2020):

- US Mandate to produce 164 billion litres of biofuel by 2022
- Brazil's Directive to use biodiesel to replace at least 10% of its fuel consumption by 2020
- EU's Directive of substituting a minimum of 10% of its transport fuel with sustainable fuel by 2020
- China replacing 15% of total fuel consumption with biofuel by 2020

## 1.2 Why should we explore other sources of aviation fuels?

The total demand of the transportation industry in 2020 was estimated at 3.1 BTOE with less than 1% contribution from the renewable sector. This demand is forecast to increase by 20% over the next two decades (BP Global, 2020). As seen in Figure 1.1, the aviation sector currently leads the increased demand and is projected to do so in the future. Global jet fuel demand prior to the COVID-19 pandemic stood at about 4.5 trillion litres/yr (Kaya, 2020). Even though it is a challenge to directly determine the quantity of emissions solely based on the aircraft, especially due to this occurring at high altitudes and the time spent there, an estimate can be derived based on the distance travelled and the fuel efficiency (ICAO, 2020). CO<sub>2</sub> has the greatest share (70%) of emissions in the exhaust of an aircraft (Overton, 2019).

With over 36 billion tonnes of CO<sub>2</sub> emissions annually, about 2.5% of this total was related to the commercial aviation sector as at 2018 (Friedlingstein et al., 2019). This low percentage still contributes to the growing problem of global warming. The global COVID-19 pandemic played a huge role in cutting down emissions with an estimated quantity of 2 billion tonnes by the end of 2020. However, the definite rise in post-COVID air travel demands even more sustainable ways of curbing emissions (Evans, 2020).

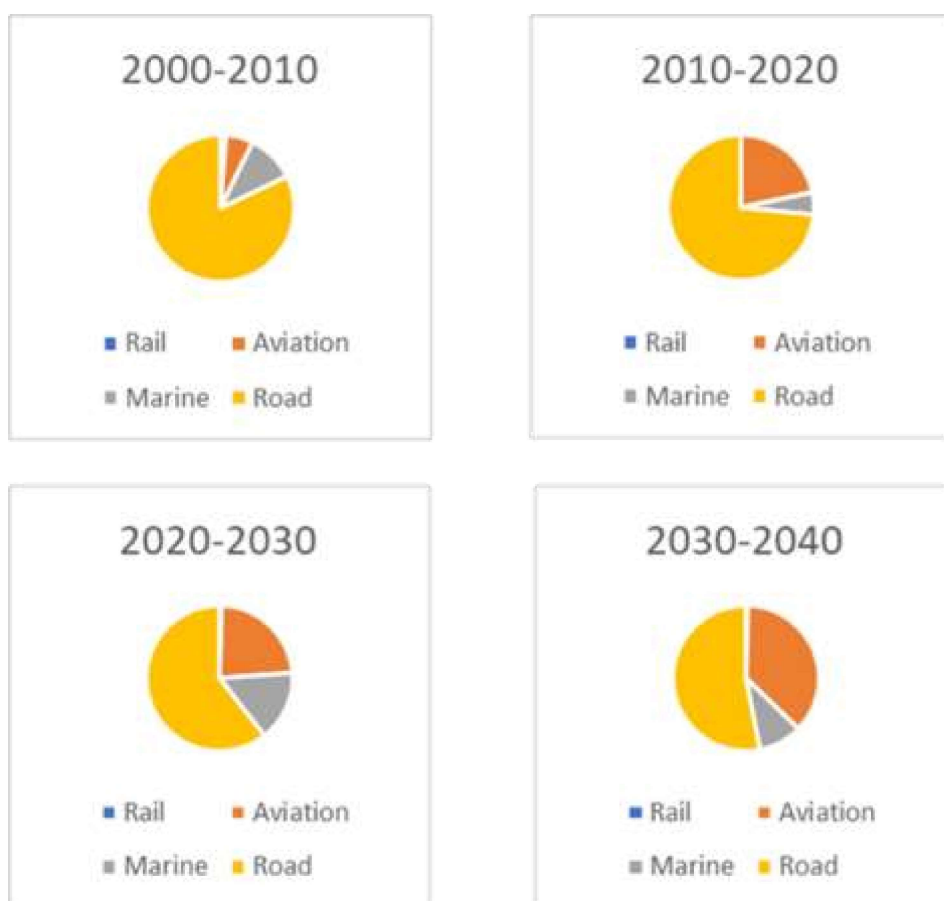


Figure 0.1: Energy consumption in transport: growth by mode (BP Global, 2020)

Among the efforts to achieve Net Zero, the aviation industry appears to be lagging in terms of the use of alternative fuels or energy. Specifically, for the aviation industry, IATA (International Air Transport Association) set three goals in 2009 to combat the problems of environmental pollution by aircrafts. These include (IATA, 2020):

- improve fuel efficiency by 1.5% by 2020
- cap carbon emissions from 2020 to maintain carbon neutral growth
- halve the emissions of 2005 by 2050

The Air Transport Action Group (ATAG) has taken various measures to reduce emission of CO<sub>2</sub> based on two major approaches. The first strategy is the modification of the technology associated with aircrafts and the second strategy is the application of fuels which emit lower amount of CO<sub>2</sub>. The option of modification is viable but for the long term as many aircrafts operate for 25 – 30 years before coming to their end-of-life and replacing them with highly efficient ones would be plausible. Furthermore, currently, there are about 25,830 commercial aircrafts available globally (Mazareanu,2020), added to the forecasted increase as seen in

Figure 1.2, this long lifespan, coupled with the backlog of manufacturing airplanes, would delay the suggested engine modification and contribute to the difficulty of controlling and reducing greenhouse gas emissions in the aviation industry. For instance, there is a 10-year backlog of about 50% of contracted aircrafts yet to be produced; therefore, the change in technology will take some time before implementation (CAPA, 2020). A different situation has been observed in the car industry, where conventional cars with internal combustion engines (ICEs) are being replaced by electric vehicles (Hausfather, 2020). However, electrification of aircrafts is still a while away as batteries that will power commercial planes will weigh a lot and in turn affect the energy efficiency of the aircraft.

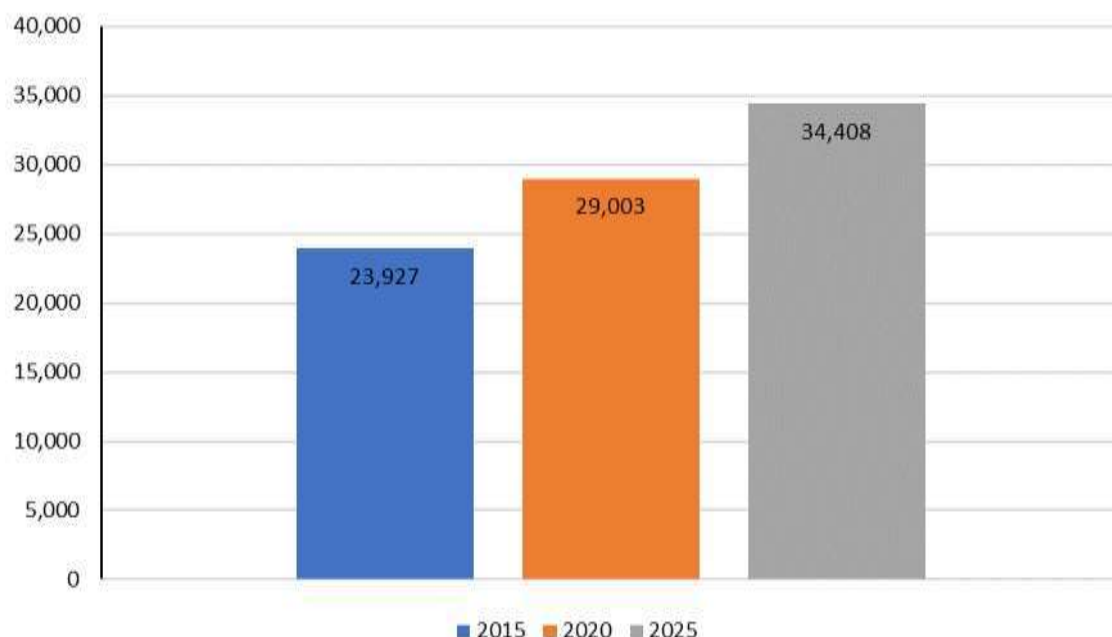


Figure 0.2: Current and projected commercial aircraft in service (CAPA, 2020)

### 1.3 Properties of aviation fuels

The benefit of liquid fuels for transportation lies mainly in their physical state and high energy densities, making them convenient for handling and storage. The most commonly used fuel type for commercial aircraft is ASTM D1655 standard specification for aviation turbine fuels. Its properties are summarised in the Table 1.1. Therefore, any fuel, including biofuels, which come under the name of sustainable aviation fuels (SAF) destined for aircraft engines must satisfy these properties required of conventional aviation fuels (CAF) in order to prevent negative impact on conventional engines (ICAO SAF, 2020). Jet fuel consists of paraffins which contribute high energy density properties, naphthenes (cycloparaffins) which help reduce the freezing point (a property essential due to high altitude operations), and aromatics

for seal swell properties but with a limit to minimise smoke formation (Brooks et al., 2016) (Khan et al., 2019).

Clearly any biomass-derived liquid jet fuel (biojet) fuel that is to be used as a substitute of commercial jet fuel will have to meet the standard of this specification. This remains the goal of current biojet fuel production technologies. Another important property of liquid fuels is the cetane number. This characteristic determines the engine compatibility as low cetane number fuels could lead to a faulty engine due to incomplete combustion (Malinowski et al., 2015).

Table 0.1: Specification standard of aviation fuel ICAO SAF, 2020; Elhaj and Lang, 2014)

Property	Meaning	Value
Density	Measure of mass per volume	775.0 -840.0 Kg/m <sup>3</sup> @ 15 °C
Flash point	Minimum temperature ignition occurs in the presence of air near liquid's surface	38 °C min.
Freezing point	Temperature at which it freezes	47 °C max.
Aromatics content	Molecules with a carbon ring of unsaturated bonds	25%, volume max.
Sulphur content	Amount of sulphur in fuel	0.30ppm max.
Specific energy	Energy per unit mass produced when burned	42.8 MJ/Kg

## 1.4 Research aims and objectives

### 1.4.1 Aim

The aim of this research project is to develop a 3-stage novel route to convert triglycerides into high yields of liquid hydrocarbon fuels from which aviation fuel may be obtained as a high fraction without the use of hydrogen. This route will include hydrothermal hydrolysis, decarboxylation, and cracking reactions. One of the major challenges of producing biojet fuels is the large consumption of hydrogen gas to deoxygenate the biomass-derived feedstocks that are available for conversion. The goal is to find an alternative hydrogen-free method that can produce high yields of liquid hydrocarbons. It is hoped that such a method will help reduce the cost of processing biomass-derived feedstocks to make alternative sustainable hydrocarbon fuels, from which SAF can be obtained. This work will focus on the technical development of the processing route. It will not cover the techno-economics and other environmental assessments that are important for optimisation and commercialisation, which can be carried out once available data generated from this work are validated.

### 1.4.2 Organisation of this Thesis

Here the organisation of this thesis is given to provide the reading audience a smooth pathway to navigate its contents.

Chapter 2: This chapter contains a comprehensive literature review on the background theory and important previous work done on the development of sustainable aviation fuels from biomass-derived feedstocks. Firstly, this chapter looks at the state-of-the-art of different technologies for biojet fuel production, their successes, and limitations as well as gaps in their implementation. Therefore, the influence of different experimental parameters on the yields of products and conversions of feedstocks are reviewed to provide a basis for the development of the experimental programme for this present work.

Chapter 3: This chapter covers the systematic methods used carry out experiment and to collect and interpret data. This chapter first discusses the reactor used to carry out all experimental tests, its specification, and the description from how it was used to successfully run experimental tests to how the reactor was reused. Next, the materials used, and the procedures followed in carrying out these tests and in collecting samples for data analysis. Some tests were done on each process stage to confirm the reliability of the method designed to achieve results by running three repeats and collating and comparing their results. Finally, all analytical equipment and the procedures followed for the analysis of the samples are discussed.

Chapter 4: This fourth section focuses on the first stage of the process, hydrolysis. Specifically, the non-catalytic hydrothermal conversion of vegetable oil as well as waste cooking oils (WCO) to fatty acids. Tests are carried out to examine the effect of temperature, time, oil to water mass ratio, and stirring speed, and determine the optimum reaction conditions to produce the highest yield. Analytical methods such as CHNS, TGA, GC/MS, and titration were used to quantify the product samples, and the results obtained were discussed.

Chapter 5: The subject matter of this fifth chapter is the second stage of the process, catalytic decarboxylation. The product of the first stage, fatty acids from vegetable oil and WCOs, were used as the feedstock for this stage and converted to hydrocarbons. Mostly saturated hydrocarbons to be more specific. This chapter investigates the effect of varying temperature, catalyst loading, time, and catalyst type to determine the combination of reaction conditions that will give the optimum yield and composition. After carrying out experiments varying the earlier listed reaction conditions, the product oils are analysed using GC/MS, CHNS, and titration methods to estimate their conversions, yields, and compositions. The gas product was also analysed on the GC/FID. Following the analysis, there was a discussion of the collated results.



Chapter 6: This chapter consists of experiments carried out to achieve both decarboxylation and cracking. There are some similarities with the previous chapter, in terms of the types of parameters examined like catalyst type, temperature, and time. However, this section examines more severe reaction conditions, meaning, the tests reported here were done at higher reaction temperatures to explore the effect of, as mentioned earlier, both decarboxylation and cracking. Afterwards, there was a discussion of the results obtained from analysing the product samples through GC/FID, GC/MS, titration, and CHNS.

Chapter 7: This seventh chapter covers the cracking and aromatisation of saturated hydrocarbons produced in chapter 6, which is also the final stage of the process. Reaction parameters such as temperature, catalyst type, and time were explored to determine the optimum conditions to obtain the highest yield of aromatics. The gas products were analysed on the GC/FID, while the product oils were analysed on the GC/MS. In addition to the direct interpretation of the results obtained from these analytical equipment, further interpretation of the results using tools such as the Van Krevelen diagram, and simulated distillation were also utilised. All results were discussed in detail.

Chapter 8: This final chapter provides a review of the methodology used and the key findings in summary. It would highlight the discoveries, outcomes, and prospects of these in relation to the gap that had been set out to be filled. Furthermore, this section will discuss the limitations of the research and recommendations of directions to take to answer questions that were not addressed but could contribute to the research scope.

### 1.4.3 Justification for process selection for experimental work

The initial stage of this 3-stage process route, hydrolysis, was employed because the part of the feedstock, the triglyceride, that will produce the target products, hydrocarbons, is the carboxylic acids. Therefore, hydrolysis was considered an important process as it releases these fatty acids from the triglyceride, leaving behind glycerol. As a separate stream that allows for valorisation of this by-product, glycerol. In comparison with existing technologies such as the HEFA process, this glycerol is converted to propane, which puts a limitation on the exploitation of the glycerol for other applications as mentioned in Section 2.2.3.1 and Section 8.2. This separation to extract the carboxylic acids will minimise, and therefore, simplify and aid the understanding of the process chemistries required in the conversion to the target product.

Similarly, this is the idea in employing the decarboxylation step. After obtaining a feedstock that is mainly fatty acids, the reactions become more controllable with the understanding of the deoxygenation reaction. The use of a specific functional group, for example, carboxylic

acids, helps the focus on what deoxygenation pathway is followed. Otherwise, without obtaining these defined feedstocks after each stage, the specific chemistries of these reactions might not be so emphasised and as easily comprehensible.

Likewise, the cracking, if deoxygenation is achieved and giving the carbon chain length will yield diesel range hydrocarbons. However, by carrying out cracking, other fuels with different and shorter carbon chain lengths can be produced, which adds to the robustness of the process.

## 1.5 References

- Alalwan, H., Alminshid, A. and Aljaafari, H., (2019). Promising evolution of biofuel generations. Subject review. *Renewable Energy Focus*, 28, pp.127-139.
- BP global. (2020). Energy Demand by Sector | Energy Economics | Home. [online] Available at: <<https://www.bp.com/en/global/corporate/energy-economics/energy-outlook/demand-by-sector.html>> [Accessed 23 March 2020].
- Brooks, K., Snowden-Swan, L., Jones, S., Butcher, M., Lee, G., Anderson, D., Frye, J., Holladay, J., Owen, J., Harmon, L., Burton, F., Palou-Rivera, I., Plaza, J., Handler, R. and Shonnard, D. (2016). Low-Carbon Aviation Fuel Through the Alcohol to Jet Pathway. *Biofuels for Aviation*, pp.109-150.
- CAPA - Centre for Aviation (2020). Record Global Aircraft Deliveries In 2017: Boeing Ahead of Airbus Again, But Behind on Order Backlog. [online] Available at: <<https://centreforaviation.com/analysis/reports/record-global-aircraft-deliveries-in-2017-boeing-ahead-of-airbus-again-but-behind-on-order-backlog-393914>> [Accessed 23 March 2020].
- Elhaj, H.F.A. and Lang, A. (2014) (PDF) The worldwide production of bio-jet fuels - The current developments regarding technologies and feedstocks, and innovative new developments., ResearchGate. Available at: [https://www.researchgate.net/publication/273765924\\_The\\_worldwide\\_production\\_of\\_bio-jet\\_fuels\\_-\\_The\\_current\\_developments\\_regarding\\_technologies\\_and\\_feedstocks\\_and\\_innovative\\_new\\_RD\\_developments](https://www.researchgate.net/publication/273765924_The_worldwide_production_of_bio-jet_fuels_-_The_current_developments_regarding_technologies_and_feedstocks_and_innovative_new_RD_developments) (Accessed: 2020).
- Evans, S. (2020). Analysis: Coronavirus Set to Cause Largest Ever Annual Fall In CO2 Emissions | Carbon Brief. [online] Carbon Brief. Available at: <<https://www.carbonbrief.org/analysis-coronavirus-set-to-cause-largest-ever-annual-fall-in-co2-emissions>> [Accessed 13 March 2020].
- Friedlingstein, P., Jones, M. W., O'Sullivan, M., Andrew, R. M., Hauck, J., Peters, G. P., Peters, W., Pongratz, J., Sitch, S., Le Quéré, C., Bakker, D. C. E., Canadell, J. G., Ciais, P., Jackson, R. B., Anthoni, P., Barbero, L., Bastos, A., Bastrikov, V., Becker, M., . . . Zaehle, S. (2019). Global Carbon Budget 2019. *Earth System Science Data*, 11(4), 1783–1838. <https://doi.org/10.5194/essd-11-1783-2019>.
- Gomez, L., Steele-King, C. and McQueen-Mason, S. (2008). Sustainable liquid biofuels from biomass: the writing's on the walls. *New Phytologist*, 178(3), pp.473-485.

Hausfather, Z. (2020). Factcheck: How Electric Vehicles Help to Tackle Climate Change. [online] Carbon Brief. Available at: <<https://www.carbonbrief.org/factcheck-how-electric-vehicles-help-to-tackle-climate-change>> [Accessed 13 March 2020].

Iata.org. (2020). Annual Review 2019. [online] Available at: <<https://www.iata.org/contentassets/c81222d96c9a4e0bb4ff6ced0126f0bb/iata-annual-review-2019.pdf>>.

ICAO (2020). ICAO SAF. [online] Available at: <[https://www.icao.int/environmental-protection/knowledge-sharing/Docs/Sustainable%20Aviation%20Fuels%20Guide\\_vf.pdf](https://www.icao.int/environmental-protection/knowledge-sharing/Docs/Sustainable%20Aviation%20Fuels%20Guide_vf.pdf)> [Accessed 13 March 2020].

ICAO.int. (2020). [online] Available at: [https://www.icao.int/environmental-protection/knowledge-sharing/Docs/Sustainable%20Aviation%20Fuels%20Guide\\_vf.pdf](https://www.icao.int/environmental-protection/knowledge-sharing/Docs/Sustainable%20Aviation%20Fuels%20Guide_vf.pdf) [Accessed 10 Jan. 2020].

Kaya, N. (2020). World Jet Fuel Demand Could Drop By 70% Due To COVID-19. [online] Aa.com.tr. Available at: <<https://www.aa.com.tr/en/economy/world-jet-fuel-demand-could-drop-by-70-due-to-covid-19/1778544>> [Accessed 3 April 2020].

Khan, S., Kay Lup, A. N., Qureshi, K. M., Abnisa, F., Wan Daud, W. M. A., and Patah, M. F. A. (2019). A review on deoxygenation of triglycerides for jet fuel range hydrocarbons. *Journal of Analytical and Applied Pyrolysis*, 140, 1–24.  
<https://doi.org/10.1016/j.jaap.2019.03.005>

Lange, J.-P. (2021) “Towards circular carbo-chemicals – the metamorphosis of Petrochemicals,” *Energy and Environmental Science*, 14(8), pp. 4358–4376. Available at: <https://doi.org/10.1039/d1ee00532d>.

Malinowski, A., Wrzosek, P., Turlej, A. and Wardzińska, D. (2015). A Review of Selected Methods of Measurement Used for the On-Line Analysis of Liquid Fuels. *Storage Stability of Fuels*.

Mazareanu, E., 2020. Size Of Aircraft Fleets Worldwide (2018) | Statista. [online] Statista. Available at: <<https://www.statista.com/statistics/262971/aircraft-fleets-by-region-worldwide/>>.

Overton, J. (2019) “The United States 2021 Aviation Climate Action Plan.” Available at: [https://www.eesi.org/files/IssueBrief\\_Climate\\_Impacts\\_Aviation\\_2019rev2022.pdf](https://www.eesi.org/files/IssueBrief_Climate_Impacts_Aviation_2019rev2022.pdf) (Accessed: February 20, 2020).

Pandey, A. Biomass, Biofuels, Biochemicals. Piccirilli Dorsey, I., (2020). Fact Sheet: The Growth in Greenhouse Gas Emissions from Commercial Aviation | White Papers | EESI. [online] Eesi.org. Available at: <<https://www.eesi.org/papers/view/fact-sheet-the-growth->

in-greenhouse-gas-emissions-from-commercial-aviation> [Accessed 23 March 2020].

Yang, C., Kwon, H., Bang, B., Jeong, S., and Lee, U. (2022). Role of biomass as low-carbon energy source in the era of net zero emissions. *Fuel*, 328, 125206.

<https://doi.org/10.1016/j.fuel.2022.125206>

## 2 Literature review

This chapter examines the development of sustainable aviation fuels using feedstocks derived from biomass. This includes an extensive review of the literature on the several state-of-the-art technologies used for the production of biojet fuel. The merits, demerits and knowledge gaps are highlighted. At the end, this chapter provides the basis for formulating the main objectives of this study, defining its novelty and contribution to knowledge. The objectives then form the basis of the design of the experimental programme to contribute towards filling the observed knowledge gaps.

### 2.1 Current state of biojet fuels production

There is an increased drive to develop and deploy aviation biofuels (biojet). Since the take-off of the first aircraft using sustainable fuel in 2008, ten years later by 2018, over 450,000 flights have been powered by biojet (Net zero 2050: IATA, 2022). This drive is promoted by the potential of sustainable aviation fuels to reduce emissions by 80% over the life cycle of aircrafts when compared with conventional jet fuel (Annual Review 2019, 2020). In particular, there is a growing trend to adopt the use of cheap low-quality feedstocks and wastes. Although, there are several processes for the production of aviation biofuels, the choice of an efficient process that uses low-quality feedstocks while simultaneously having the capability to avoid reduced yield is a challenging task.

The standard specification for biojet fuel containing hydrocarbons derived from coal, gas, biomass and hydroprocessed plant oils and animal fats known as ASTM D7566 was approved in 2009. Although this standard is yet to be met, sustainable aviation fuel used today contains a maximum of 50% blend from biofuel mixed with fossil jet fuel for use in conventional engines (Brooks et al., 2016).

There are a lot of collaborations going on between airline companies that are keen on the deployment of biojet fuels in their fleets and fuel production companies as seen in Table 2.1.

Table 2.1: Biojet fuel technologies and production companies (Beginner's Guide to Sustainable Aviation Fuel, 2017; Geleynse et al., 2018; Van Dyk et al., 2019; Wang et al., 2020; Bosch et al., 2020)

Biojet Fuel Technology	Technology Readiness Level (TRL)	Feedstock type	Production company	Airline company	Blends (%)
Alcohol-To-Jet (ATJ)	Development	Sugars, starches, alcohol	Terrabon/MixAlco, LanzaTech/Swedish Biofuels, Coskata, Gevo, Byogy, Albemarle/Cobalt Solazyme	Boeing, Virgin Atlantic, Continental Airlines, United Airlines	50
Gasification and Fischer Tropsch (FT)	Near commercial	Woody and lignocellulosic biomass	Syntroleum, SynFuels, Rentech, Shell, Solena, Coskata, INEOS, Bio/Lanza Tech, Swedish Biofuels, Fulcrum, Red Rock	Qatar Airways, United Airlines, Airbus, British Airways, Virgin Atlantic	50
Hydroprocessed Renewable Jet (HRJ)	Commercial	Plant oils, food industry waste oils, algal oil, animal fats	UOP, SG Biofuels, AltAir Fuels, Agrisoma Biosciences, Neste Oil, Petrochina, Sapphire Energy, Syntroleum/Tyson Food, PEMEX, ASA, Renewable Energy Group, ENI, UPM Diamond Green Diesel	Boeing, Lufthansa, Virgin Atlantic, Virgin Blue, GE Aviation, Air New Zealand, Rolls-Royce, Continental, CFM, JAL, Airbus, KLM, Pratt & Whitney, Air China, TAM Airlines, Jet BLUE Airways, IAE, United Airlines, Air France, Finnair, Air Mexico, Thomson Airways, Porter Airlines, Alaska Airlines, Horizon Air, Ethiad Airways, Romanian Air, Bombardier	50
Catalytic Hydrothermolysis (CH)	Development	Plant oils, food industry waste oils, algal oil, animal fats	Applied Research Association, Aemetis/Chevron Lummus Global	Rolls-Royce, Pratt & Whitney	50
Direct Sugar to Hydrocarbons (DSHC/SIP)	Development	Sugars, cellulosic materials	Amyris/Total, Solazyme, LS9	Boeing, Embraer, Azul Airlines, GE, Trip Airlines	50

## 2.2 ASTM-approved biojet fuel pathways

Figure 2.1 presents the five ASTM approved production pathways for biojet fuel. These pathways differ based on the types of feedstocks used in the production of the biojet fuel and these differences are discussed in this section.

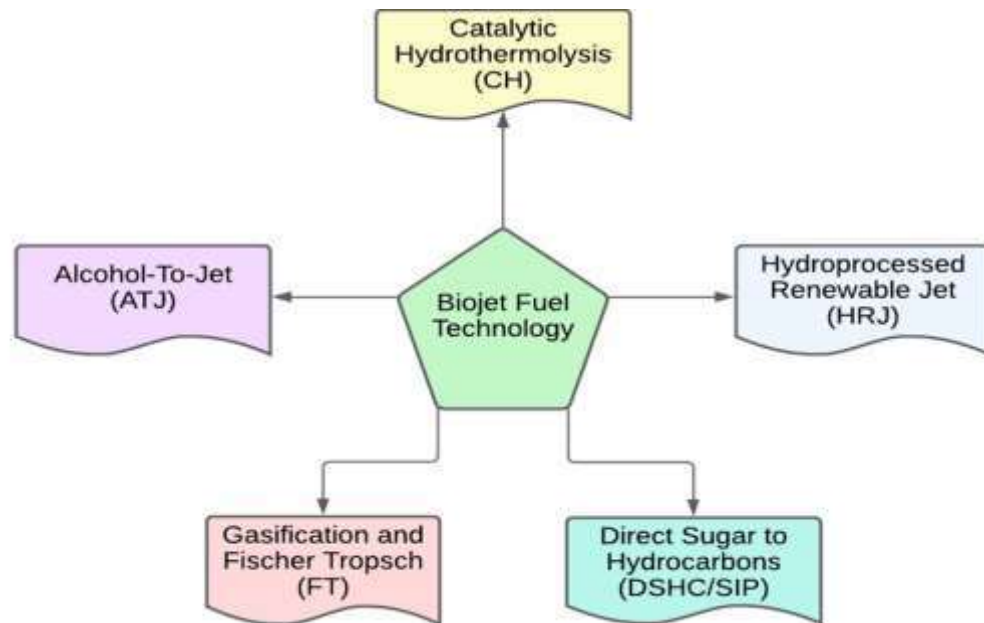


Figure 2.1: Biojet fuel technology pathways (Beginner's Guide to Sustainable Aviation Fuel, 2017; Geleynse et al., 2018; Van Dyk et al., 2019; Wang et al., 2020; Bosch et al., 2020)

### 2.2.1 Biojet fuel technology based on lipid feedstocks

Both HRJ and CH utilise lipid-based feedstocks, triglycerides to be precise, for biojet fuel production. The main differences stem from the steps employed to reach biojet fuel. CH produces free fatty acids (FFA) and glycerol through thermal hydrolysis, followed by the hydrogenation of the FFA, while HRJ employs propane cleavage in the conversion of triglycerides into hydrocarbons.

#### 2.2.1.1 Hydroprocessed renewable jet (HRJ)

HRJ also known as HEFA (Hydroprocessed Esters and Fatty Acids) is so far the only technology that produces and distributes jet fuel at a commercial scale. The production of HRJ follows a similar process utilised in the petrochemical industry to produce jet fuel (Brooks et al., 2016). The commercial scale facilities which produce HEFA currently have a total global capacity of 5.5 billion litres/yr (Table 2.2). Presently, these facilities do not produce only HEFA biojet, but also HEFA biodiesel.



Table 2.2: Technology readiness level of biojet fuel technologies (Van Dyk et al., 2019; Bosch et al., 2020)

Biofuel	Company	Technology	Feedstock	Capacity L/yr	Status
HEFA/HRJ	Neste	NEXBTL	Veg. oil, WCO, animal fat	3.3 B	Operational
	ENI	Ecofining™	Veg. oil	462 M	Operational
	Diamond Green Diesel	Ecofining™	Veg. oil, WCO, animal fat	1.04 B	Operational
	World energy (Alt Air)	LA MEDE	Non-edible oil, waste oil	150 M	Operational
	Total	UPM Bioverno	WCO, veg. oil	64 M	Start up
	UPM	Developed by Dynamic Fuels LLC	Crude tall oil	120 M	Operational
	Renewable Energy Group	-	High and low free fatty acid feedstocks	284 M	Operational
	Fulcrum Bioenergy	-	MSW	37 M	Planned
	RedRock	-	Wood	45 M	Planned
	Swedish Biofuel Technology	-	Ethanol	10 M	Operational
ATJ	Biochemtex	-	Lignocellulosic biomass	<10 M	Operational
	LanzaTech	-	Ethanol	180 M	Operational

The biodiesel market is larger than the biojet market. Therefore, a greater proportion of this capacity is not directed at the production of biojet fuel. However, even if the total capacity (5.5 BL/yr) was invested in biojet fuel, this will only represent 1% of the global jet fuel demand (6.3 trL/yr) (Erkul Kaya, 2020; Van Dyk et al., 2019).

The main limitations associated with the HRJ process are related to the high cost of the use of excess hydrogen to minimise carbon loss, and hence increasing biojet yield. The cost of obtaining feedstock accounts for 70% of the production cost, a major issue for airline companies as fuel represents 30% of their total expense (IRENA, 2017). Nonetheless, other challenges include pre-treatment of feedstock to obtain high yields, and thorough process control required due to high heat (exotherms) generated from reaction (ICAO, 2017).

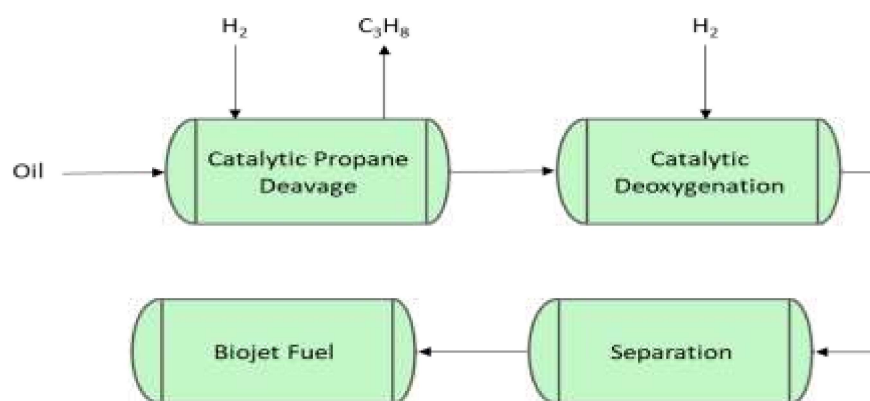
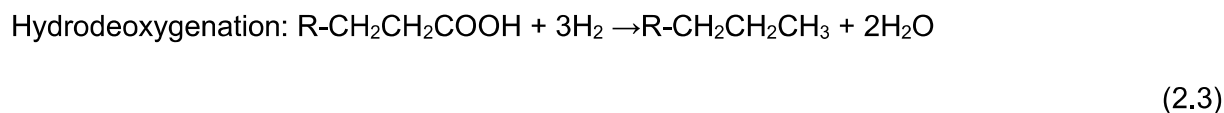
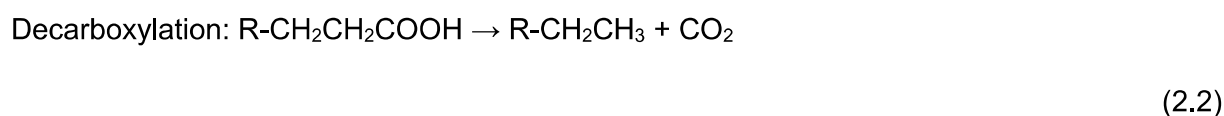
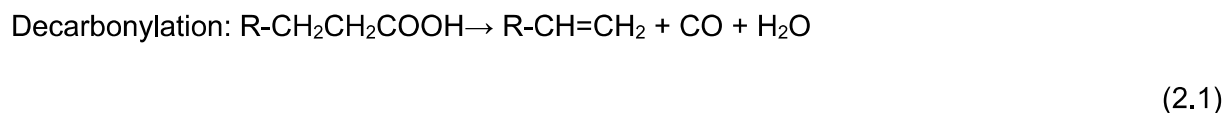


Figure 2.2: HRJ flow chart (Scaldaferri and Pasa, 2019)

The HRJ process involves deoxygenation and other wide range of catalytic processes like hydrogenation, hydro-isomerization, and hydrocracking (Figure 2.2). In most cases, the deoxygenation of biomass-derived liquids is generally carried out in the presence of hydrogen and suitable catalysts (Chu et al., 2017). It results into hydroprocessed renewable jet (HRJ) fuel, which in comparison to fatty acid methyl esters (FAMES) in biodiesel, has higher heating value, higher energy density, as well as superior cold point qualities (Zanon et al. 2020).

Common feedstocks for HRJ include soybean oil, sunflower oil and palm oil (Mousavi-Avval and Shah, 2021). The triglycerides are initially taken through hydrogenation of C=C to produce saturated carbon chains. Thereafter, hydrogenolysis of carbon to oxygen bond is carried out to facilitate release of fatty acids and a molecule of propane. It is at this stage that the deoxygenation technique takes place to ensure oxygen are removed as water to produce alkanes (Wang and Hsieh, 2020).

Several techniques for deoxygenation that are popularly applied in biojet fuel hydro-processing comprises of decarbonylation (Equation 2.1), decarboxylation (Equation 2.2), and hydrodeoxygenation (HDO) (Equation 2.3) (Vasquez et al., 2017; Martinez-Hernandez et al., 2019). Under the process of decarboxylation, a carboxyl group is eliminated by releasing of carbon dioxide and paraffinic hydrocarbon. Also, decarbonylation deals with the elimination of carbonyl group and produces olefins, carbon monoxide and water. Finally, hydrodeoxygenation deals with the cleavage of carbon to oxygen bond especially in fatty acids and is achieved by using excess hydrogen gas pressures resulting in the formation of hydrocarbons and water.



The final conversion of lipids to hydrocarbons depends on the fatty acids and significant amount of literature is dedicated to this. Fatty acids have carbon chains that range throughout the length from roughly C8 to C24, but C12, C16, and C18 fatty acids are often the most prevalent (Doll et al. 2021). Deoxygenation of fatty acids produces paraffinic hydrocarbons, with the capability to replace or even be transformed into paraffinic petrochemical feedstocks and traditional petroleum-derived liquid transportation fuels.

Extensive research has been done on the liquid-phase deoxygenation of free fatty acids and fatty acid esters in the presence of hydrogen (Hu et al. 2019) . When aliphatic and aromatic carboxylic acids were deoxygenated at 330 °C over Pd/SiO<sub>2</sub> and Ni/Al<sub>2</sub>O<sub>3</sub> catalysts in various gas phase conditions (H<sub>2</sub> or N<sub>2</sub>), hydrogen was preferable to ensure a stable catalytic activity during its decarboxylation reaction (Jeništová et al., 2017). Pd/C catalyst was also used to conduct liquid-phase deoxygenation of oleic acid in a continuous-flow reactor with N<sub>2</sub> as well as H<sub>2</sub> as the environment and no solvents at 330 °C for 3 h (Cheah et al. 2019). However, less than 10 mol% of hydrocarbons, primarily olefins including aromatics, were produced.

There are also several investigations on the “decarboxylation of the unsaturated oleic acid” described in literature (Krobkrong et al., 2018; Popov and Kumar, 2015; Çakman et al., 2022). Due to the high proportion of oleic acid in many lipids, it has been used as model compound for the catalytic conversion of triglycerides to hydrocarbons. In the majority of these experiments, the catalyst support is either a comparatively non-acidic substance, including silica or non-acidic alumina, or a catalytically inert substance (like carbon) (Smoljan

et al. 2020). However, substantial research has been done mostly on hydrocracking as well as isomerization of hydrocarbons using Pt maintained on highly acidic supports (such as Pt-zeolites). Cheah et al. (2020) also pointed out that the distribution of hydrocarbons produced was influenced by the strength, surface density, and pore size of such acidic sites.

According to Hossain et al. (2018), hydrogenated derived renewable diesel (HDRD), a liquefied fuel manufactured from vegetable oils and animal fat was produced via catalytic HDO using  $\text{Mo}/\text{Al}_2\text{O}_3$  as catalyst, 1:5 oleic acid to water volume ratio for 4 h at 375 °C under  $\text{N}_2$  pressure. The product, which had a 71% yield, was found to contain linear paraffinic hydrocarbons, which are hydrocarbons that are physically as well as chemically related to those present in petroleum distillate.

#### 2.2.1.2 Catalytic hydrothermolysis (CH)

Catalytic hydrothermolysis (CH) is a novel process (Figure 2.3) developed by Applied Research Associates for producing renewable drop in and aromatic fuels from the algal oil or plant with the promised potential to give 100% conventional biofuel substitute. CH jet fuel can be used without blending (Gorlova, 2020). Jet fuel from this process attains military and ASTM specification with quality and better cold flow stability and properties.

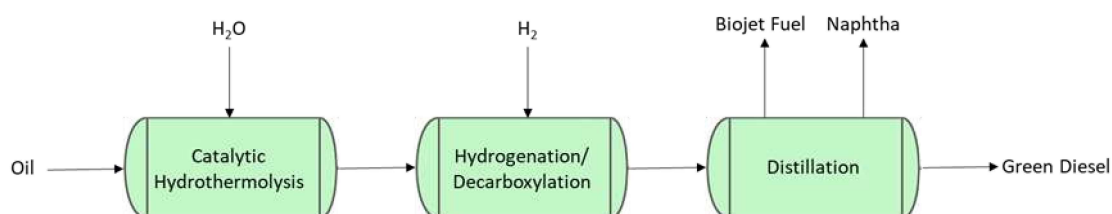


Figure 2.3: Catalytic Hydrothermolysis (CH) process

The process of catalytic hydrothermolysis applies the use of triglyceride feedstock to produce fatty acid, which are then hydrotreated to hydrocarbons (McGarvey, 2018). Catalytic hydrothermolysis involves a chain of reactions which includes thermal hydrolysis, decarboxylation, cracking, cyclization and isomerization (Elkelawy et al., 2022). The hydrolysis reaction is carried out with catalyst and water. The initial liquid products are composed of oxygenated species, unsaturated molecules and FFAs as shown in Equations 2.4 – 2.6. These oxygenates are taken through a hydrotreating and decarboxylation process for saturation and removal of oxygen. The products obtained after hydrotreatment range from 6 - 28 carbon number with iso-alkanes, n-alkanes, aromatics, and cyclo-alkanes, which are separated into fractions by distillation. These are then fractionated into naphtha, diesel fuel and jet fuel separation (Hashmi, 2017). The overall hydrolysis of triglycerides with three moles water produces one mole of glycerol and three moles of FFA (Equations 2.4 -

2.6). Catalytic hydrothermolysis conversion process depends on five main parameters, including pressure, temperature, oil to water ratio, catalyst, hydrogen gas pressure, and residence time. High pressure and temperature are required for water to dissolve in oil phase and for both reactants to stay in liquid phase (Wang et al., 2012).



Utilising operating conditions of 450 °C - 475 °C and pressures of 210 bar in the presence of water, CH could proceed in the presence or absence of a catalyst (Hashmi et al., 2017). Li et al. (2010) reported catalytic conversion of soybean oil, tung oil and jatropha oil under conditions 450 °C to 475 °C, using nickel catalyst, and a pressure of 210 bar. Although tung oil gave the highest naval distillate yield (24.3%), soybean showed potential having the highest JP-8 fraction yield (11.7%).

Therefore, CH produces a fuel that meets the ASTM specification as the resulting jet fuel consists of not only high flash point but also excellent cold flows characteristics. Research have indicated that isomers of straight-chain alkanes exist as the process starts and sequential reaction cracks them to branched structure (Grau and Parera, 1993).

Hydrocracking results in production of gases and shorter chain hydrocarbons, and the saturation of olefins. After cracking, light hydrocarbon species containing carbon numbers from C5 to C8 (within the naphtha) are produced, which are out of range for jet fuel.

Currently, the CH process is promising alternative jet fuel and diesel production method. Variety of feedstocks such as palm oil, corn oil soybean and canola have been extensively explored. For example, in USA jet fuel and diesel are produced via this method using soybean oil. Hence, for jet fuel, the hydrocracking step is omitted.

### 2.2.2 Biojet production routes based on alcohol feedstocks Alcohol to Jet (ATJ)

Alcohol-to-jet fuel refers to aviation fuel-range hydrocarbons produced from the various alcohols including methanol, butanol, and ethanol alongside long-chain fatty alcohols. The alcohol required for this process is obtained from sugars or lignocellulosic biomass. The production of alcohol can be done either by conventional sugar fermentation or by catalytic syngas conversion as seen in Figure 2.4. Ethanol and isobutanol are the most commonly used intermediates (Geleynse et al., 2018). The process of conversion of alcohols to jet fuel

includes three main stages: dehydration, oligomerization, which converts alcohol into linear olefins, and hydrogenation, to saturate the olefinic bonds (Beckham et al., 2019).

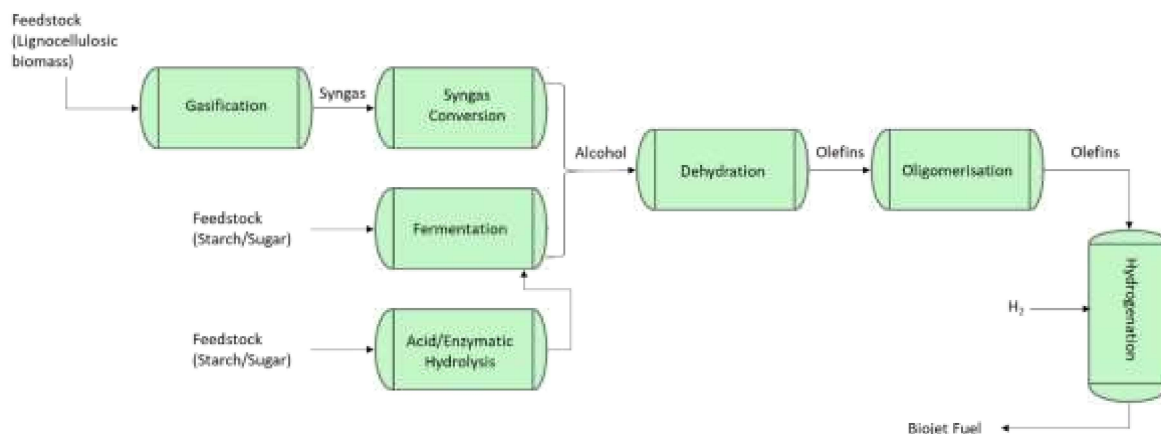


Figure 2.4: Alcohol to jet flow chart

The only route ASTM-D7566 certified for ATJ conversion is seen in Figure 2.5a (Geleynse et al., 2018). Dagle et al., (2016) reported the conversion of biomass-derived syngas into hydrocarbons. In their work, ethanol obtained from the syngas was converted into isobutene using a mixed oxide catalyst  $Zn_xZr_yO_2$ . Isobutene was then oligomerised over solid acid catalyst, Amberlyst-36 to produce olefins that were further hydrogenated to produce approximately 75% jet fuel range hydrocarbons.

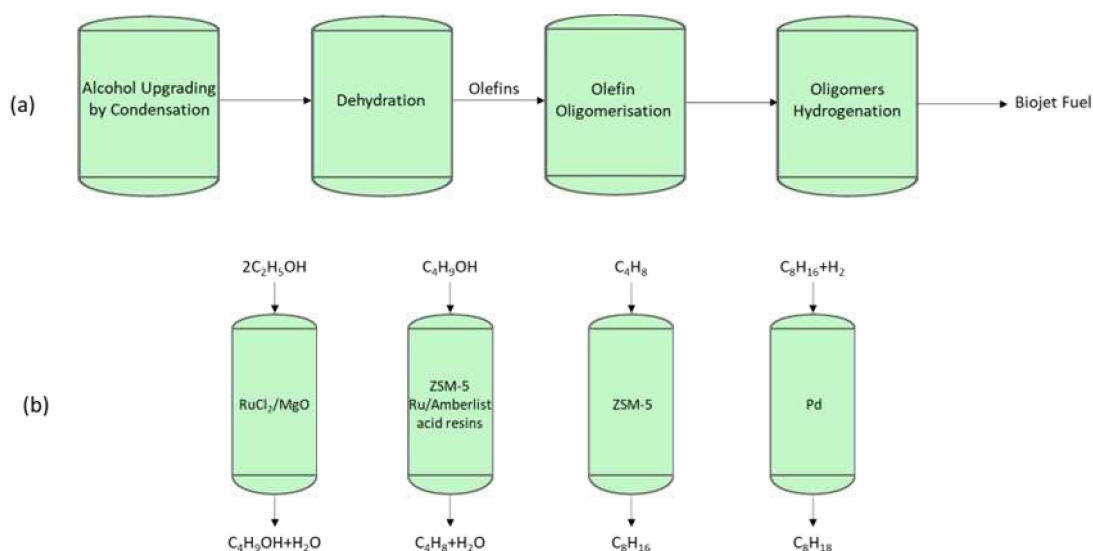


Figure 2.5: Approved pathway for ATJ

Even though alcohols with lower carbon numbers produce hydrocarbons with more even distribution, alcohols with higher carbon numbers require a lower degree of oligomerisation (Geleynse et al., 2018). The use of upgraded alcohols (higher carbon alcohols) as seen in Figure 2.5b as reported by Atsonios et al. (2015), can possibly result in lower costs due the avoidance of oligomerisation and dehydration chemistries.

Dehydration catalysts are needed in the upgrading of alcohols to hydrocarbon and research on catalysis has explored alumina and transition metal, silicoaluminophosphates, H-ZSM-5 zeolite catalyst, heteropolyacid. H-ZSM-5 zeolite catalyst proves to be the most reliable returning nearly 100% conversion and 99% ethylene yield from ethanol at 350 °C (Tao et al., 2017). A catalytic oligomerization process was used in the conversion of the dehydrated ethanol to  $\alpha$ -olefins. Tao et al. (2017) obtained 95%  $\alpha$ -olefins over Ziegler catalyst at 90-120 °C and (Aldrett and H. Worstell, 2015) produced a higher yield (97%) over ZieglerNatta type catalyst at 100 °C and 89 bar pressure. The resultant  $\alpha$ -olefins were then distilled to produce both diesel range fuels as well as jet range fuels alongside light olefins. The light olefins were subjected to further oligomerization step. Such jet fuel-range alkenes can be hydrogenated into alkanes over Pd/C or Pt/C catalyst at 370°C and 3h<sup>-1</sup> WHSV (Gevo Inc, 2008).

At a temperature of 380 °C and pressure of 2.1 bar, it is possible to attain dehydration of n-butanol to form 1-butene using  $\gamma$ -alumina as the catalyst. The yield of biobutenes is about 98% on the highest side with a selectivity of 95% for 1-butene. The remaining products was 2-butene, which was isomerised from 1-butene. The formed 1-butene was taken through the process of oligomerization to generate olefins in the range of C8 to C32 at 97% conversion rate. The distributions of the product for mixed olefins in the jet fuel range included 26.46% C8, 25.4 %C12, and 17.64% C16 with ZnAl<sub>2</sub>O<sub>4</sub> as catalyst (US Secretary of Navy, 2012; Wright, 2012).

Lanzatech operates the first global ATJ facility operating at a commercial scale, converting ethanol from waste into biojet fuel (Fivga et al., 2019). Oak Ridge National (ORN) in the US, has developed a catalytic upgrading process which converts ethanol and other alcohols to hydrocarbons in a single step. The reported process operates in the absence of hydrogen and at temperatures from 275 °C - 350 °C. Despite the high yields obtained, this pathway is still not approved by the ASTM-D7566 and will still require qualification (Wyman, 1993).

### 2.2.3 Biojet fuel production routes based on sugar feedstocks (Direct Sugar to Hydrocarbon (DSHC))

Sugars can also serve as a feedstock to produce biojet fuel. Sugars and their chemical derivatives have a maximum number of six carbon atoms and also have various oxygen-based functional groups. To convert these molecules into jet fuel which has carbon atoms C8 – C16, deoxygenation reactions and C-C coupling reactions such as aldol condensation and oligomerisation need to be carried out (Díaz-Pérez and Serrano-Ruiz, 2020; Serrano-Ruiz and Dumesic, 2011).

These reactions are favourable in the aqueous phase, with the added advantage that the hydrocarbon products are insoluble in water, hence, easier separation leading to better energy savings (Wang et al., 2014). Figure 2.6 highlights the pathways sugars can be converted into biojet fuel.

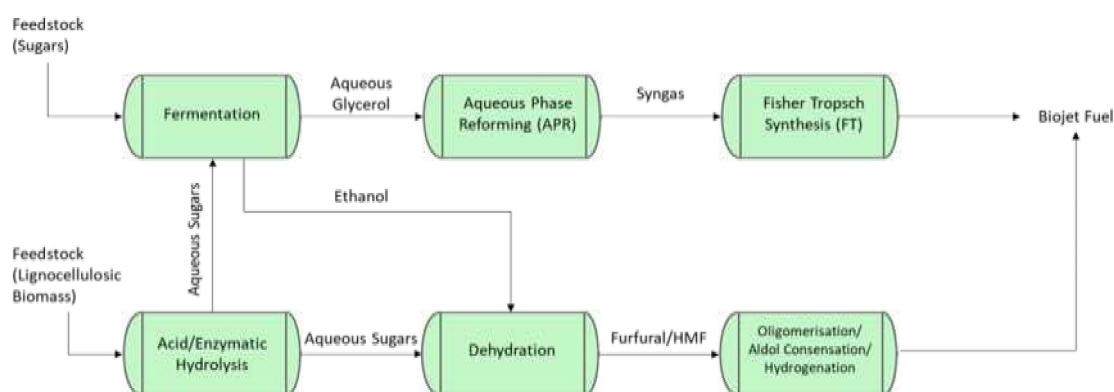


Figure 2.6: DSHC pathways to biojet fuel

#### 2.2.3.1 Aqueous Phase Reforming (APR)

In Figure 2.6, one route highlights the conversion through APR of glycerol to produce syngas. Syngas is upgraded into liquid hydrocarbon fuels through Fischer-Tropsch (FT) synthesis. This APR route which requires relatively mild temperatures (225 °C – 300 °C) has been adopted by Virent Energy Systems, renamed as the Bioforming Process but yet to be commercialised (Pagliaro et al., 2008; Biddy et al., 2016).

This is an attractive route because glycerol which is a by-product of the fermentation of sugar to produce ethanol, usually at levels of around 3 wt%. However, large amount of glycerol is produced as by-product of biodiesel industry (Pagliaro et al., 2008). A Pt-Re/C is known to catalyse deoxygenation and hydrogenation, which can be used in upgrading C-C coupling reactions to increase yield of alkane products. For instance, Kunkes et al., 2008 used a



combined process of glycerol conversion into syngas over Pt-Re/C catalyst to obtain C5+ liquid alkanes.

Wang et al. (2014) produced 32.8% aviation fuel yield from sorbitol conversion using HZSM-5/MCM-41 catalyst. The reaction conditions were temperature of 280 °C, weight hourly space velocity (WHSV) of 1.25 h<sup>-1</sup>, gas hourly space velocities (GHSV) of 2500 h<sup>-1</sup> and 40 bar pressure.

### 2.2.3.2 Furanics

Figure 2.7 also shows a second route that explores the use of precursors such as furfurals or HMF, also known as furanics for conversion into biofuels and other sustainable chemicals. First, lignocellulosic biomass is fractionated to remove lignin and obtain the cellulose and hemi-cellulose fractions for conversion to hydrocarbons. The lignin generated in this process is often dewatered and combusted to generate process heat. The fractionated hemicellulose and cellulose are hydrolysed into sugars that have five (pentoses) or even six (hexoses) carbons with the use of acid or enzyme catalysts. The carbohydrates are converted through hydrogenation or hydrogenolysis into polyhydric alcohols or short-chain length oxygenates, respectively (Cortright, 2015).

Furfural and HMF are viable intermediates for biojet fuel production because of the carbonyl group in these compounds which allow a cascade process of dehydration, hydrogenations, and aldol condensations reactions (Huber, 2005). Unlike the production of HMF from C<sub>6</sub> sugars like glucose, which is complicated and still a challenge, obtaining furfurals from C<sub>5</sub> sugars such as xylose is a mature industrial process. The complications related to the use of HMF include:

- i. the limited control over side reactions
- ii. the limited control associated with glucose the feedstock
- iii. the extra steps required to isomerise glucose into fructose as fructose gives higher yields of HMF with better selectivity and rates as seen in Table 2.6.

Furanics serve as aromatics contributors to the jet fuel hydrocarbon pool as reported by Williams (2014). The reaction of dimethylfuran with ethylene via Diels-Alder Cycloaddition reaction, followed by hydrogenation to give 90% p-xylene yield. Besides being a source for aromatics, HMF and furfural can produce liquid hydrocarbon fuels. Sutton et al. (2013) examined the production of alkanes from mono-HMF and di-HMF. In their work, Pd/C catalyst was used for hydrogenation while La(OTf)<sub>3</sub> catalyst was applied for HDO, with 20.7 bar H<sub>2</sub>. After 16 hours of reaction, mono-HMF gave 87% C<sub>9</sub> alkane yield (1:1 HMF and acetone) and di-HMF gave 76% C<sub>12</sub> alkane yield (2:1 HMF and acetone).

Table 2.3: Conversion of sugars and cellulose to HMF

Feedstock	Solvent	Catalyst	Temp (°C)	Time (min)	Yield (%)	Reference
Fructose	CHClO	Malonic acid	80	60	41	(Hu et al., 2019)
	CHClO	Oxalic acid	80	60	62	(Hu et al., 2019)
	Water	HCl (aq)	95	90	68	(Nicholas, 2016)
	Water-acetone	Dowex-50wx8-100	150	15	73	(Nicholas, 2016)
	CHClO	Citric acid	80	60	76.3	(Hu et al., 2019)
	1:1 water-DMSO/ 7:3 MIBK/ 2-BuOH	HCl	170	4	85	(Nicholas, 2016)
	DMSO	CNT-PSSA	120	30	89	(Hu et al., 2019)
Glucose	[HexylMIM]Cl	SO <sub>4</sub> <sup>2-</sup> /ZrO <sub>2</sub>	100	30	89	(Nicholas, 2016)
	[BMIM]Cl	LS	100	10	94.3	(Xie, Zhao and Wang, 2012)
	[BMIM]Cl	NHC/CrCl <sub>2</sub>	100	360	96	(Nicholas, 2016)
	1:7 DMSO/MIBK	Acidic ion exchange resin	76	-	97	(Nicholas, 2016)
	DMSO	NH <sub>4</sub> Cl	100	45	100	(Nicholas, 2016)
	DMSO	Amberlyst-15 powder	120	120	100	(Nicholas, 2016)
	Water	TiO <sub>2</sub> /ZrO <sub>2</sub>	250	5	29	(Nicholas, 2016)
	[EMIM]Cl	Boric acid	120	180	41	(Stahlberg et al., 2011)
	Water	H <sub>3</sub> PO <sub>4</sub> /Nb <sub>2</sub> O <sub>5</sub>	120	180	52	(Nicholas, 2016)
	DMSO	CNT-PSSA	140	60	57	(Nicholas, 2016)
Cellulose	1:2.25 Water-MIBK	AgPW <sub>12</sub> O <sub>40</sub>	130	240	76	(Nicholas, 2016)
	Water	HCL	300	30	21	(Nicholas, 2016)
	1:5 Water/MIBK	TiO <sub>2</sub>	270	2	30	(Nicholas, 2016)
	[EMIM]Cl	Boric acid	120	480	32	(Stahlberg et al., 2011)
	Water	Cr[(DS)H <sub>2</sub> PW <sub>12</sub> O <sub>40</sub> ]3	150	120	53	(Nicholas, 2016)
	[EMIM]Cl	CrCl <sub>2</sub>	120	360	89	(Nicholas, 2016)

Key: DMSO (dimethyl sulfoxide), MIBK (methylisobutylketone), (1-butyl-3-methylimidazolium chloride), (1-hexyl-3-methylimidazolium chloride), (1-ethyl-3-methylimidazolium chloride), CHClO (choline chloride) (Sutton et al., 2013)

To prevent coking during HDO, HMF and acetone are made water-soluble by hydrogenation. Huber (2005) obtained  $\approx 70\%$  C<sub>16</sub> using Pt/SiO<sub>2</sub>-Al<sub>2</sub>O<sub>3</sub>, at temperatures from 250 °C - 265 °C, pressures of 50 - 52 bar and GSHV from 1000 - 3000 h<sup>-1</sup> H<sub>2</sub> gas hourly space velocities. HMF production is known to promote catalyst deactivation (Malinowski and Wardzińska, 2012).

## 2.3 Fischer Tropsch (syngas to Jet)

This syngas to jet (GTJ) pathway is able to generate liquid hydrocarbon fuel from syngas ((a mixture of carbon monoxide and hydrogen) produced via biomass gasification. Unlike gasoline and diesel, Fisher Tropsch hydrocarbons are sulphur free and composed of very few aromatics. Initial process involves drying of biomass feedstocks in order to minimize the sizes of the particle in the course of pretreatment.

Particularly, slagging gasification is applied in converting biomass to syngas in which the dried biomass is pressurized then converted to raw synthesis gas at about 1300°C in presence of limited oxygen and steam. A combustor is integrated into the system to supply heat for drying biomass while direct quench syngas cooling arrangement eliminates ash and tars. The process also takes place in the reformer. Generated syngas is refined using zinc oxide and stimulated carbon sorbent and pressurised to 25 bar. Purification of hydrogen used in hydro-processing stage is done by pressure swing adsorption. Eventually, syngas is processed via Fisher-Tropsch synthesis to yield liquid fuel (Shahabuddin et al., 2020).

Fisher-Tropsch synthesis can be operated at high temperature and low temperature. High temperature process operates at 300 °C - 350°C with iron as a catalyst, yielding gasoline and linear low-molecular weight olefins. In contrast, low temperature process runs at 200 °C – 240 °C using iron or cobalt as catalysts generating linear waxes of high molecular weight. In general FT process yields alkanes, alkenes as well as oxygen-based compounds like alcohols, aldehydes, and carboxylic acids. In addition, ketones and aromatics are generated in high temperature process. The use of cobalt-based catalysts yields more output compared to iron catalysts at high level of conversion (Shahabuddin et al., 2020). In existing plants, a portion of the unconverted syngas is taken back to the FT reactor after acid gas removal system while the remaining is used to power for air separation unit.

Hydrogenolysis, isomerization, hydrogenation and fractionation are used in upgrading FT synthesis products to high-quality, low-aromatic and sulphur free fuels. Hydrogenolysis converts wax into low weight products with shorter chain length and lower boiling points. These are then heated and distilled to generate jet fuel, diesel fuel and lubricants.

Hydrogenation is used to generate naphtha from liquid Fisher- Tropsch. Hydrogen, water, methane, carbon monoxide, carbon dioxide, nitrogen, argon and dense hydrocarbons which are components of Fisher Tropsch tail gas are reused in generation of syngas. Hydrogen is cleaned via pressure swing absorber and eventually utilized in hydrogenolysis or process of isomerization (Weber, 2018).

In addition to high and low temperature FT processes, micro and monolithic FT reactors are under investigation to improve rates of reaction, with enhanced heat as well as mass transfer features (Guettel and Turek, 2009). Microlithic structures proposed and developed to include minute parallel channels, one using FT reaction while other is for circulating cooling water therefore increasing the efficiency of transferring heat between channels leading to isothermal operation. Monolithic catalysts are basically ceramic structures composed of supports like Alumina or Silica (Boger et al., 2004).

## 2.4 Comparison of biojet properties and yields from different routes

Due to the different process routes available for producing biojet fuel, it is important to compare the physical and fuel properties of the final liquid products against the commercial jet fuel. This is presented in Table 2.4.

Table 2.4: Comparison of properties of biojet fuel technologies (Elhaj and Lang, 2014; Brooks et al., 2016; Wright, 2012; ICAO, 2017)

Properties	JET-A	HRJ	ATJ	FT	DSHC
Acid no. (mgKOH/g)	0.10 max.	0.02 max.	0.02 max.	0.02 max.	0.02 max.
Flash point (°C)	38 min.	38 min.	48 min.	38 min.	100 min
Freezing point (°C)	-47 max.	-40 max.	-80 max.	-40 max.	-60 max.
Density @ 15 °C (kg/m <sup>3</sup> )	775-840	730-770	763	730-770	765-780
Net heat of combustion (MJ/Kg)	42.8 min.	42.8 min.	43.2 min.	42.8 min.	43.5 in.
Additive antioxidants (mg/L)	24.0 max.	17 min. 24 max.	17.2 min 24 max.	17 min. 24 max.	17 min. 24 max.
Aromatics (%)	25 max.	0.5 max.	-	0.5 max.	0.5 max.
Sulphur content (ppm)	0.30 max.	15 max.	10 max.	15 max.	2 max.

Table 2.4 shows that there are mostly subtle variations in the properties of the biojet fuels from the different process routes considered except for properties like the aromatics content. Table 2.4 shows that the maximum aromatics contents of these potential biojet products are still 98% less than the amount required to be a potential Jet-A substitute. Therefore, one method to accommodate this difference would be to blend with aromatics. As stated previously in Section 1.3, jet fuel consists of a paraffins, naphthenes, and aromatics. Table

2.5 shows a summary of the many studies done in attempt to convert different bio-feedstock sources into hydrocarbons that have the potential to substitute commercial jet fuel. Majority of the research done (Table 2.8) only made mention of the hydrocarbons produced falling in the jet fuel range of C9-16. However, some authors went further to specify the yield and group of compounds. For instance, Chen et al. (2016) obtained 26.9% C9-C16 alkane yield from the deoxygenation of FAME with Ni/HZM-5 at 300 °C and 8 bar H<sub>2</sub> pressure. Both Cheng et al. (2014) and Li et al. (2015) carried out decarbonylation reactions for 8 h to produce hydrocarbons. The former used soybean oil with Ni-Mo/HY as catalyst at 390 °C and 1 MPa H<sub>2</sub> and obtained 30% alkanes and 30% aromatics. While the latter used waste cooking oil and Ni/Meso-Y catalyst at 400 °C under 30 bar H<sub>2</sub> pressure to obtain 37.5% alkanes and 10% aromatics. Wang et al. (2017) reported that very high yields of products consisting of 80% alkanes, 3% alkenes and 6% aromatics were obtained from the hydrodeoxygenation of soybean oil for 7.5 h at 300 °C under 40 bar H<sub>2</sub> with Ni-Mo/ $\gamma$ -Al<sub>2</sub>O<sub>3</sub> as catalyst.

Table 2.5: Some current results from literature on conversion of different feedstock to hydrocarbons

Feedstock	Process route	Operating conditions	Catalysts	Yields	Reference
Algal oil	Decarboxylation	Solvent = water Residence time = 45 min T=360 °C	Pt/C	53.63% heptadecane	(Fu et al., 2015) [104]
Castor oil	Hydrodeoxygenation	T = 300 °C – 360 °C P = 3 MPa (H <sub>2</sub> ) WHSV=2h <sup>-1</sup> T=300 °C	NiAg/SAPO-11	87.12% C <sub>8</sub> -C <sub>15</sub> hydrocarbons	(Li et al., 2015) [102]
FAME	Deoxygenation	P = 0.8 MPa (H <sub>2</sub> ) LHSV = 4 h <sup>-1</sup> H <sub>2</sub> /oil molar ratio = 15 T=200 °C	Ni/HZSM-5	26.90% C <sub>8</sub> -C <sub>16</sub> alkane yield	(Chen et al., 2016) [101]
Jatropha oil	Deoxygenation without H <sub>2</sub>	P=4 MPa (N <sub>2</sub> ) LHSV = 1.33 h <sup>-1</sup>	WO <sub>3</sub> /Pt/TiO <sub>2</sub>	75% C <sub>8</sub> -C <sub>16</sub> hydrocarbons	(Choi et al., 2018) [105]
Macauba oil	Decarboxylation	T=300 °C P=1 MPa (H <sub>2</sub> ) Residence time = 5 h	Pd/C	33% C <sub>9</sub> -C <sub>16</sub> hydrocarbons	(Silva et al., 2016) [106]
Microalgae biodiesel	Deoxygenation	T=275 °C Injection rate= 0.02 ml/min	Ni/meso-Y zeolite	48.6% alkanes 2.7% aromatics 0.18 % alkenes	(Cheng et al., 2019) [107]
Oleic acid	Deoxygenation without H <sub>2</sub>	T=300 °C P = 1 atm. (N <sub>2</sub> ) Residence time = 3 h	CoMo	20.1% C <sub>9</sub> -C <sub>16</sub> hydrocarbons	(Shim et al., 2018) [108]
Palm oil	Hydrodeoxygenation	T=300 °C P=1 MPa (H <sub>2</sub> ) Residence time = 5 h	Pd/C	90% C <sub>9</sub> -C <sub>15</sub> hydrocarbons	(de Sousa, Cardoso and Pasa, 2016) [109]
	Hydrodeoxygenation	P=5 MPa (H <sub>2</sub> ) LHSV=1h <sup>-1</sup> H <sub>2</sub> /oil = 1000 Ncm <sup>3</sup> /cm <sup>3</sup> T=330 °C	Ni-MoS <sub>2</sub> /γ-Al <sub>2</sub> O <sub>3</sub>	60% C <sub>10</sub> -C <sub>12</sub> hydrocarbons	(Itthibenchapong et al., 2017) [110]
	Decarbonylation	T=390 °C P=1 MPa (H <sub>2</sub> ) Residence time = 8 h	Ni-Mo/HY	30% aromatics 30% alkanes	(Cheng et al., 2014) [111]
Soybean oil	Hydrodeoxygenation	T = 370–385 °C P=3 MPa (H <sub>2</sub> ) LHSV=1h <sup>-1</sup> H <sub>2</sub> /oil = 800 NL/L	Pt/Al <sub>2</sub> O <sub>3</sub> /SAPO-11	15% aromatics	(Rabaev et al., 2015) [112]
	Decarboxylation	T=350 °C	NbOPO <sub>4</sub>	62% C <sub>9</sub> -C <sub>16</sub> hydrocarbons	

	P=1 MPa (H <sub>2</sub> ) Residence time = 5 h			(Scalaferrì and Pasa, 2019) [21]
Deoxygenation	T=350 °C	Ni-Al	80% C <sub>8</sub> -C <sub>17</sub> hydrocarbons	(Morgan et al., 2012) [113]
Deoxygenation	P=0.7 MPa (N <sub>2</sub> ) Residence time = 4 h T=400 °C	CoMo-Al <sub>2</sub> O <sub>3</sub>	13.5% biojet fuel range hydrocarbons	(Veriansyah et al., 2012) [114]
Decarbonylation	P=9.2 MPa (H <sub>2</sub> ) Residence time = 1 h T=400 °C	Ni/Meso-Y	37.5% alkanes 10% aromatics	(Li et al., 2015) [115]
Waste cooking oil	P=3 MPa (H <sub>2</sub> ) Residence time = 8 h T=300 °C	Ni-Mo/γ-Al <sub>2</sub> O <sub>3</sub>	80% alkanes 3% alkenes 6% aromatics	(Wang et al., 2017) [116]
Hydrodeoxygenation	P=4 MPa (H <sub>2</sub> ) Residence time = 7.5 h	Ni-Mo/Al <sub>2</sub> O <sub>3</sub>	65% kerosene range hydrocarbons	(El-Sawy, Hanafi, Ashour and Aboul-Fotouh, 2020) [117]
Waste cooking oil + waste lubricating oil + vacuum gas oil	T=380 °C P=7 MPa (H <sub>2</sub> ) LHSV=1.5 h <sup>-1</sup> H <sub>2</sub> /oil = 400/400 Nm <sup>3</sup> /m <sup>3</sup>	Ni-W/SiO <sub>2</sub> /Al <sub>2</sub> O <sub>3</sub>		
Deoxygenation				

## 2.5 Pyrolysis and hydrothermal liquefaction (HTL) to jet fuel

In addition to the above standardised methods, biojet fuel could be produced from biomass via bio-oil(pyrolysis) and biocrude (HTL) routes. Pyrolysis and HTL are yet to be approved by ASTM as a jet fuel conversion route. However, pyrolysis produces biooils which can undergo deoxygenation, a step common to CH and HRJ. Pyrolysis is the thermal decomposition of biomass. This usually occurs in the absence of oxygen or air, and temperatures 400 - 600 °C(Jenkins et al., 2016).

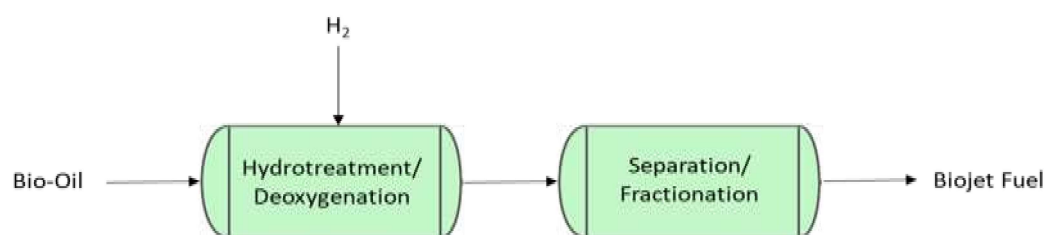


Figure 2.7: Pyrolysis to jet fuel pathway

Table 2.6: Types of pyrolysis (Bridgwater and Bridge, 1991)

Pyrolysis type	Residence time	Heating rate	Temperature (°C)	Major product
Carbonisation	hrs - days	very low	400	char
Conventional	10 s -10 min	low - moderate	<600	gas, char, liquid
Flash (liquid)	<1s	high	<600	liquid
Flash (gas)	<1s	high	>700	gas, char, liquid
Ultra	<0.5 s	very high	1000	gas, chemicals
Vacuum	2 - 30 s	moderate	400	liquid

Depending on the process variables such as: feedstock composition, heat transfer rate, residence times, and the intended aim of experiment, there are various types of pyrolysis as seen in Table 2.3. HTL is similar to pyrolysis but involved the use of pressurised-hot water medium to degrade biomass into bio-crude, biochar and gases. The bio-crude has similar properties as pyrolysis bio-oil but with reduced acid contents (Park et al., 2017; Banks and Bridgwater, 2016; Ramirez et al., 2015).

One of the products of biomass pyrolysis is bio-oil and is the main product when fast pyrolysis is carried out between 500 °C and 600 °C. Bio-oil is mainly composed of alcohols, aldehydes, carboxylic acids, alkenes, aromatics, sugars, ketones, furans, phenols, and heavy molecular weight oligomers. These oxygenated compounds can be converted to hydrocarbons via HDO in the presence of hydrogen and appropriate catalysts. Kumar et al. (2019), Westerhof et al. (2012), Yildiz et al. (2014), have all explored the pyrolysis of pinewood to produce bio-oil. Westerhof et al. (2012) found that although a two-step reaction



produced less moisture and char, a one step process produced more bio-oil (59%) at 530 °C. Kumar et al. (2019) obtained the highest bio-oil yield at 500 °C (62.7%) when compared with other temperatures; 600 °C (47.1%) and 700 °C (17.9%).

Although in principle, bio-oil can be used as fuel for boilers, turbines, gasifiers, and engines, upgrading to remove oxygen and crack the oligomers present to a certain degree would be required for use as a liquid transportation fuel (Yildiz et al., 2014). The catalytic upgrading of bio-oil is aimed at increasing the heating value, improving compatibility with petroleum hydrocarbons due to reduced oxygen content, improving chemical stability and decreasing its viscosity. Table 2.7 shows the comparison between bio-oil and crude oil, hence highlighting the incompatibility of the latter.

Table 2.7: Comparison of properties; biooil and crude oil (Mortensen et al., 2011; Beims et al., 2017)

Properties	Bio-oil	Crude oil
Density (kg/m <sup>3</sup> @ 15 °C)	818.4-923.6	772.1 - 936.0
Total acid number (mgKOH/g)	116.2-207.5	0.0 - 2.0
Aromatics (%)	20.4-60.5	32.6 - 53.0
C (%)	55-65	83 - 86
H (%)	5-7	9-14
O (%)	28-40	<1
Water (%)	15-30	0.1
Heating value (MJ/Kg)	16-19	44

Table 2.8: Some current literature on catalytic upgrading of bio-oil (Mortensen et al., 2011)

Catalyst	Reactor type	Time (h)	P (bar)	T (°C)	Degree of deoxygenation (%)	Upgraded oil yield (%)
Hydrodeoxygenation (HDO)						
CoMoS <sub>2</sub> /Al <sub>2</sub> O <sub>3</sub>	Batch	4	200	350	81	26
CoMoS <sub>2</sub> /Al <sub>2</sub> O <sub>3</sub>	Continuous	4	300	370	100	33
NiMoS <sub>2</sub> /Al <sub>2</sub> O <sub>3</sub>	Batch	4	200	350	74	28
NiMoS <sub>2</sub> /Al <sub>2</sub> O <sub>3</sub>	Continuous	0.5	85	400	28	84
Pd/C	Batch	4	200	350	85	65
Pd/C	Continuous	4	140	85	64	48
Pt/Al <sub>2</sub> O <sub>3</sub> /SiO <sub>2</sub>	Continuous	0.5	85	400	45	81
Ru/Al <sub>2</sub> O <sub>3</sub>	Batch	4	200	350	78	36
Ru/C	Continuous	0.2	230	350-400	73	38
Ru/C	Batch	4	200	350	86	53
Ru/TiO <sub>2</sub>	Batch	4	200	350	77	67
Zeolite cracking						
HZSM-5	Continuous	0.32	1	380	50	24
HZSM-5	Continuous	0.91	1	500	53	12

Figure 2.4 shows the pathway route for conversion of bio-oil into biojet fuel (Czernik and Bridgwater, 2004; Mosier, 2005; Mythili et al., 2013). Mortensen et al. (2011) reviewed the catalytic upgrading of bio-oil (Table 2.5). This review summarised the process variables and the yield produced under two main categories: HDO and zeolite cracking. The main differences that stand out are the relatively less pressure required, and low yields obtained over the zeolite cracking reactions.

Besides the challenge of storage as the acidic nature of bio-oils lead to corrosion (Shah et al., 2019), another major problem with catalytic pyrolysis to obtain hydrocarbons is the efficiency of deoxygenation reactions, especially at an industrial scale. An improvement in the type of catalysts used and the process chemistries will be essential to improve the quality of the process (Yildiz et al., 2014). Research has shown that hydrothermal liquefaction of cornstalk can produce bio-oil to be converted to jet fuel range hydrocarbons. The catalyst for the process was Ni/ZrO<sub>2</sub> in supercritical cyclohexane. The conditions include a moderate temperature of 300°C and 50 bar pressure of hydrogen. The catalyst converted all the components of the bio-oil, obtaining 73.44% yield of biojet and biodiesel range hydrocarbons (Shi et al., 2014).

Following the fast pyrolysis of straw stalk at temperature 550 °C, the bio-oil produced was catalytically cracked and deoxygenated over HZSM-5 catalyst to obtain C<sub>2</sub>-C<sub>4</sub> olefins and C<sub>6</sub>-C<sub>8</sub> aromatics, which are further upgraded to jet fuel range hydrocarbons with a selectivity of 88.4% (Wang et al. 2015). Duan et al. (2020) explored the catalytic processing of combined feeding of lignocellulosic biomass and low-density polyethylene (LDPE) to mitigate catalyst deactivation by reducing coke generating and to increase aromatic yield. This process produced bio-oil yield of 50% with selectivity of jet fuel range hydrocarbons at 88%.

## 2.6 Research Objectives

This chapter shows that significant amounts of research have been carried out and are being carried out on the production of hydrocarbon fuels from biomass feedstocks. Primarily, lipids (oils and fats) have been targeted due to their high hydrogen-carbon (H/C) ratio compared to other biomass feedstocks. Essentially, it can be argued that nature has valorised lipids to be so close to hydrocarbons in properties. However, there are still challenges of feedstock availability, processing costs (most lipid conversion processes rely on hydrogen to remove oxygen), yields of hydrocarbon molecules and selectivity towards the useful fuels and chemicals. In addition, most reported SAF production routes yield products with very low aromatic contents (0.5%), whereas conventional aviation fuel contains up to 25% aromatics, which offer benefits to increase the fuel's seal swell properties as mentioned in Chapter 1. Hence, the low aromatic contents in SAF places a limitation on the blending ratio of SAF with conventional jet fuel at 50%. Apart from CH, all other routes require blending with fossil jet

fuel to maintain jet engine performance. However, CH still relies on the heavy use of hydrogen gas. Therefore, there is need to develop production routes that can cater to both high yields of hydrocarbons as well as sufficient aromatic contents in SAF. Extensive literature search has identified these challenges for which the following research objectives have been set:

1. To develop a novel hydrogen-free thermochemical process for the conversion of lipids to hydrocarbons by deconstructing the chemistries involved into steps to study each one in detail. These chemistries have been identified from literature to include hydrothermal hydrolysis, catalytic decarboxylation, and catalytic cracking.
2. To use the experimental design to produce liquid green hydrocarbons from lipids with the potential to obtain both fuel range aliphatic and aromatic hydrocarbons, which can be used directly or blended in appropriate ratios to make a SAF product with similar properties to conventional jet fuel (Jet-A).
3. To develop and/or adapt robust analytical methodologies for the measurements of the specific products from each reaction step to determine the conversion of feedstocks and the yields and selectivities of expected products. This would help to construct complete mass balances for the whole system.
4. To investigate the influence of reaction conditions of temperature, reaction time, feedstock concentration/loading, catalyst types, catalyst loading and feedstock/catalyst ratios on the conversion of feedstocks and yields of products during each stage of the process.
5. To analyse the data obtained from each stage and produce a comprehensive discussion of the results of this work as a contribution to this field of research. This would involve linking the research questions to the experimental results to discuss how the objectives have been achieved.

## 2.7 References

- Aldrett, S. and H. Worstell, J. (2015). Improved Ethylene Oligomerization Modelling using Aspentech's Polymers Plus. [online] Available at: <[https://www.researchgate.net/publication/242218224\\_Improved\\_Ethylene\\_Oligomerization\\_Modeling\\_using\\_AspenTech%27s\\_Polymers\\_Plus](https://www.researchgate.net/publication/242218224_Improved_Ethylene_Oligomerization_Modeling_using_AspenTech%27s_Polymers_Plus)> [Accessed 28 April 2020].
- Atsonios, K., Kouglioumtzis, M., D. Panopoulos, K. and Kakaras, E. ( 2015). Alternative thermochemical routes for aviation biofuels via alcohols synthesis: Process modelling, techno-economic assessment, and comparison. *Applied Energy*, 138, pp.346-366.
- Aviationbenefits.org. (2017). Beginner's Guide to Sustainable Aviation Fuel. [online] Available at: <[https://aviationbenefits.org/media/166152/beginners-guide-to-saf\\_web.pdf](https://aviationbenefits.org/media/166152/beginners-guide-to-saf_web.pdf)> [Accessed 28 April 2020].
- Banks, S.W., and Bridgwater, A.V. (2016) "Catalytic fast pyrolysis for improved liquid quality," *Handbook of Biofuels Production*, pp. 391–429. Available at: <https://doi.org/10.1016/b978-0-08-100455-5.00014-x>.
- Beckham, G., Linger, J., Vardon, D., Guarnieri, M., Karp E., Centennial M., Johnson C., Strathmann C., Pienko P. (2019). [online] [Patentimages.storage.googleapis.com](https://patentimages.storage.googleapis.com/c7/d7/80/50248b7d92aac5/US10266852.pdf). Available at: <<https://patentimages.storage.googleapis.com/c7/d7/80/50248b7d92aac5/US10266852.pdf>> .
- Beims, R., Bertoli, S., Botton, V., Ender, L., Simionatto, E., Meier, H. and Wiggers, V., (2017). Co-processing of thermal cracking bio-oil at petroleum refineries. *Brazilian Journal of Petroleum and Gas*, 11(2), pp.99-113.
- Biddy, M., Wang, W., Tao, L., Markham, J., Zhang, Y., Tan, E., Batan, L. and Warner, E., (2016). Review of Biojet Fuel Conversion Technologies. [online] Available at: <<https://www.nrel.gov/docs/fy16osti/66291.pdf>> [Accessed 28 May 2020].
- Boger, T., Heibel, A.K. and Sorensen, C.M. (2004) "Monolithic catalysts for the Chemical Industry," *Industrial and Engineering Chemistry Research*, 43(16), pp. 4602–4611. Available at: <https://doi.org/10.1021/ie030730q>.
- Bosch, J., De Jong, S., Hoefnagels, D. and Slade, D., (2020). [online] [Imperial.ac.uk](https://www.imperial.ac.uk). Available at: <<https://www.imperial.ac.uk/media/imperial-college/grantham-institute/public/publications/briefing-papers/BP-23-Aviation-Biofuels.pdf>> [Accessed 28 March 2020].

- Brooks, K., Snowden-Swan, L., Jones, S., Butcher, M., Lee, G., Anderson, D., Frye, J., Holladay, J., Owen, J., Harmon, L., Burton, F., Palou-Rivera, I., Plaza, J., Handler, R. and Shonnard, D. (2016). Low-Carbon Aviation Fuel Through the Alcohol to Jet Pathway. *Biofuels for Aviation*, pp.109-150.
- Çakman, G., Ceylan, S. and Balci, S. (2022) “Catalytic deoxygenation of oleic acid over synthesized ni@cmk-3 catalyst using analytical PY-GC/MS and TG-FTIR,” *Journal of Porous Materials* [Preprint]. Available at: <https://doi.org/10.1007/s10934-022-01392-1>.
- Cheah, K.W., Taylor, M.J., Osatiashtiani, A., Beaumont, S.K., Nowakowski, D.J., Yusup, S., Bridgwater, A.V. and Kyriakou, G. (2020). Monometallic and bimetallic catalysts based on Pd, Cu and Ni for hydrogen transfer deoxygenation of a prototypical fatty acid to diesel range hydrocarbons. *Catalysis Today*, 355, pp.882-892.
- Cheah, K.W., Yusup, S., Kyriakou, G., Ameen, M., Taylor, M.J., Nowakowski, D.J., Bridgwater, A.V. and Uemura, Y. (2019). In-situ hydrogen generation from 1, 2, 3, 4-tetrahydronaphthalene for catalytic conversion of oleic acid to diesel fuel hydrocarbons: Parametric studies using Response Surface Methodology approach. *International Journal of Hydrogen Energy*, 44(37), pp.20678-20689.
- Chen, L., Li, H., Fu, J., Miao, C., Lv, P., and Yuan, Z. (2016). Catalytic hydroprocessing of fatty acid methyl esters to renewable alkane fuels over Ni/HZSM-5 catalyst. *Catalysis Today*, 259, 266–276. <https://doi.org/10.1016/j.cattod.2015.08.023>
- Cheng, J., Li, T., Huang, R., Zhou, J., and Cen, K. (2014). Optimizing catalysis conditions to decrease aromatic hydrocarbons and increase alkanes for improving jet biofuel quality. *Bioresource Technology*, 158, 378–382. <https://doi.org/10.1016/j.biortech.2014.02.112>.
- Cheng, J., Zhang, Z., Zhang, X., Fan, Z., Liu, J., and Zhou, J. (2019). Continuous hydroprocessing of microalgae biodiesel to jet fuel range hydrocarbons promoted by Ni/hierarchical mesoporous Y zeolite catalyst. *International Journal of Hydrogen Energy*, 44(23), 11765–11773. <https://doi.org/10.1016/j.ijhydene.2019.03.073>
- Choi, I.-H., Lee, J.-S., Kim, C.-U., Kim, T.-W., Lee, K.-Y., and Hwang, K.-R. (2018). Production of bio-jet fuel range alkanes from catalytic deoxygenation of *Jatropha* fatty acids on a WO<sub>x</sub>/Pt/TiO<sub>2</sub> catalyst. *Fuel*, 215, 675–685. <https://doi.org/10.1016/j.fuel.2017.11.094>
- Chu, P. L., Vanderghem, C., MacLean, H. L., and Saville, B. A. (2017). Process modeling of hydrodeoxygenation to produce renewable jet fuel and other hydrocarbon fuels. *Fuel*, 196, 298–305. <https://doi.org/10.1016/j.fuel.2017.01.097>
- Cortright, R. (2015). Cellulosic Biomass Sugars to Advantaged Jet Fuel – Catalytic Conversion of Corn Stover to Energy Dense, Low Freeze Point Paraffins and Naphthenes.

- Czernik, S. and Bridgwater, A. (2004). Overview of Applications of Biomass Fast Pyrolysis Oil. *Energy and Fuels*, 18(2), pp.590-598.
- Dagle, V., Smith, C., Flake, M., Albrecht, K., Gray, M., Ramasamy, K. and Dagle, R. (2016). Integrated process for the catalytic conversion of biomass-derived syngas into transportation fuels. *Green Chemistry*, 18(7), pp.1880-1891.
- de Sousa, F., Cardoso, C. and Pasa, V. (2016). Producing hydrocarbons for green diesel and jet fuel formulation from palm kernel fat over Pd/C. *Fuel Processing Technology*, 143, pp.35-42.
- de Sousa, F.P., Cardoso, C.C. and Pasa, V.M.D. (2016) "Producing hydrocarbons for green diesel and jet fuel formulation from palm kernel fat over Pd/C," *Fuel Processing Technology*, 143, pp. 35–42. Available at: <https://doi.org/10.1016/j.fuproc.2015.10.024>.
- Doll, K.M., Moser, B.R. and Knothe, G. (2021). Decarboxylation of oleic acid using iridium catalysis to form products of increased aromatic content compared to ruthenium systems. *International Journal of Sustainable Engineering*, 14(6), pp.2018-2024.
- Duan, D., Zhang, Y., Lei, H., Qian, M., Villota, E., Wang, C., Wang, Y. and Ruan, R. (2020). A novel production of phase-divided jet-fuel-range hydrocarbons and phenol-enriched chemicals from catalytic co-pyrolysis of lignocellulosic biomass with low-density polyethylene over carbon catalysts. *Sustainable Energy and Fuels*.
- Elhaj, H.F.A. and Lang, A. (2014) "The worldwide production of bio-jet fuels - The current developments regarding technologies and feedstocks, and innovative new R&D developments." Available at: <https://doi.org/10.13140/RG.2.1.2898.6400>.
- Elkelawy, M., Bastawissi, H., Radwan, A., Ismail, M., El-Sheekh, M. (2022) "Biojet fuels production from algae: Conversion Technologies, characteristics, performance, and process simulation," *Handbook of Algal Biofuels*, pp. 331–361. Available at: <https://doi.org/10.1016/b978-0-12-823764-9.00003-0>.
- El-Sawy, M., Hanafi, S., Ashour, F. and Aboul-Fotouh, T. (2020). Co-hydroprocessing and hydrocracking of alternative feed mixture (vacuum gas oil/waste lubricating oil/waste cooking oil) with the aim of producing high quality fuels. *Fuel*, 269, p.117437.
- Erkul Kaya, N. (2020). World Jet Fuel Demand Could Drop By 70% Due To COVID-19. [online] *Aa.com.tr*. Available at: <https://www.aa.com.tr/en/economy/world-jet-fuel-demand-could-drop-by-70-due-to-covid-19/1778544#>> [Accessed 28 April 2020].
- Fivga, A., Galileu Speranza, L., Musse Branco, C., Ouadi, M. and Hornung, A. (2019). A review on the current state of the art for the production of advanced liquid biofuels. *AIMS Energy*, 7(1), pp.46-76.

- Fu, J., Yang, C., Wu, J., Zhuang, J., Hou, Z., and Lu, X. (2015). Direct production of aviation fuels from microalgae lipids in water. *Fuel*, 139, 678–683.  
<https://doi.org/10.1016/j.fuel.2014.09.025>.
- Geleynse, S., Brandt, K., Garcia-Perez, M., Wolcott, M. and Zhang, X. (2018). The Alcohol-to-Jet Conversion Pathway for Drop-In Biofuels: Techno-Economic Evaluation. *ChemSusChem*, 11(21), pp.3728-3741.
- Gevo Inc. (2008). Renewable Compositions. US8193402B2.
- Gorlova, A. K.. (2020). Hydrogen for Fuel Cells: Effect of Copper and Iron Oxides on the Catalytic Hydrolysis and Hydrothermolysis of Ammonia Borane. *Russian Journal of Electrochemistry*, Volume 56, pp. 170-173.
- Grau, J.M. and Parera, J.M. (1993) “Conversion of heavy n-alkanes into light isomers over H-Mordenite, platinum/h-mordenite, platinum/alumina and composite catalysts,” *Applied Catalysis A: General*, 106(1), pp. 27–49. Available at: [https://doi.org/10.1016/0926-860x\(93\)80154-i](https://doi.org/10.1016/0926-860x(93)80154-i).
- Green Chemistry Series (2008). Aqueous Phase Reforming. pp.18-31.
- Hashmi, S. (2017). Hydrothermolysis of organosolv lignin for the production of bio-oil rich in monoaromatic phenolic compounds. *Fuel Processing Technology*, Volume 168, pp. 74-83.
- Hossain, M.Z., Chowdhury, M.B., Jhawar, A.K., Xu, W.Z., Biesinger, M.C. and Charpentier, P.A. (2018). Continuous hydrothermal decarboxylation of fatty acids and their derivatives into liquid hydrocarbons using Mo/Al<sub>2</sub>O<sub>3</sub> catalyst. *ACS omega*, 3(6), pp.7046-7060.
- Hu, W., Wang, H., Lin, H., Zheng, Y., Ng, S., Shi, M., Zhao, Y. and Xu, R. (2019). Catalytic decomposition of oleic acid to fuels and chemicals: Roles of catalyst acidity and basicity on product distribution and reaction pathways. *Catalysts*, 9(12), p.1063.
- Huber, G. (2005). Production of Liquid Alkanes by Aqueous-Phase Processing of Biomass-Derived Carbohydrates. *Science*, 308(5727), pp.1446-1450.
- Iata.org. (2020). Annual Review 2019. [online] Available at: <<https://www.iata.org/contentassets/c81222d96c9a4e0bb4ff6ced0126f0bb/iata-annual-review-2019.pdf>>.
- Icao.int. (2017). ICAO. [online] Available at: <[https://www.icao.int/environmental-protection/knowledge-sharing/Docs/Sustainable%20Aviation%20Fuels%20Guide\\_vf.pdf](https://www.icao.int/environmental-protection/knowledge-sharing/Docs/Sustainable%20Aviation%20Fuels%20Guide_vf.pdf)>.
- IRENA (2017) Irena.org. Available at:[https://www.irena.org/documentdownloads/publications/irena\\_biofuels\\_for\\_aviation\\_2017.pdf](https://www.irena.org/documentdownloads/publications/irena_biofuels_for_aviation_2017.pdf).

- Irena.org. (2017). IRENA. [online] Available at:  
[https://www.irena.org/documentdownloads/publications/irena\\_biofuels\\_for\\_aviation\\_2017.pdf](https://www.irena.org/documentdownloads/publications/irena_biofuels_for_aviation_2017.pdf)
- Itthibenchapong, V., Srifa, A., Kaewmeesri, R., Kidkhunthod, P., and Faungnawakij, K. (2017). Deoxygenation of palm kernel oil to jet fuel-like hydrocarbons using Ni-MoS<sub>2</sub> /  $\gamma$ -Al<sub>2</sub>O<sub>3</sub> catalysts. *Energy Conversion and Management*, 134, 188–196.  
<https://doi.org/10.1016/j.enconman.2016.12.034>.
- Jeništová, K., Hachemi, I., Mäki-Arvela, P., Kumar, N., Peurla, M., Čapek, L., Wärnå, J., and Murzin, D. Y. (2017). Hydrodeoxygenation of stearic acid and tall oil fatty acids over Ni-alumina catalysts: Influence of reaction parameters and kinetic modelling. *Chemical Engineering Journal*, 316, 401–409. <https://doi.org/10.1016/j.cej.2017.01.117>
- Jenkins, R.W., Sutton, A.D. and Robichaud, D.J. (2016) “Pyrolysis of biomass for Aviation Fuel,” *Biofuels for Aviation*, pp. 191–215. Available at: <https://doi.org/10.1016/b978-0-12-804568-8.00008-1>.
- Krobkrong, N., Itthibenchapong, V., Khongpracha, P., and Faungnawakij, K. (2018). Deoxygenation of oleic acid under an inert atmosphere using molybdenum oxide-based catalysts. *Energy Conversion and Management*, 167, 1–8.  
<https://doi.org/10.1016/j.enconman.2018.04.079>
- Kumar, R., Strezov, V., Kan, T., Weldekidan, H., He, J. and Jahan, S. (2019). Investigating the Effect of Mono- and Bimetallic/Zelite Catalysts on Hydrocarbon Production during Bio-oil Upgrading from Ex Situ Pyrolysis of Biomass. *Energy and Fuels*, 34(1), pp.389-400.
- Kumar, V., Sharma, N., Sourirajan, A., Khosla, P. and Dev, K. (2018). Comparative evaluation of antimicrobial and antioxidant potential of ethanolic extract and its fractions of bark and leaves of *Terminalia arjuna* from north-western Himalayas, India. *Journal of Traditional and Complementary Medicine*, 8(1), pp.100-106.
- Kunkes, E., Simonetti, D., West, R., Serrano-Ruiz, J., Gartner, C. and Dumesic, J. (2008). Catalytic Conversion of Biomass to Monofunctional Hydrocarbons and Targeted Liquid-Fuel Classes. *Science*, 322(5900), pp.417-421.
- Li, L., Coppola, E., Rine, J., Miller, J. and Walker, D. (2010). Catalytic Hydrothermal Conversion of Triglycerides to Non-ester Biofuels. *Energy and Fuels*, 24(2), pp.1305-1315.
- Li, T., Cheng, J., Huang, R., Zhou, J., and Cen, K. (2015). Conversion of waste cooking oil to jet biofuel with nickel-based mesoporous zeolite Y catalyst. *Bioresource Technology*, 197, 289–294. <https://doi.org/10.1016/j.biortech.2015.08.115>.
- Liu, S., Zhu, Q., Guan, Q., He, L., and Li, W. (2015). Bio-aviation fuel production from hydroprocessing castor oil promoted by the nickel-based bifunctional catalysts. *Bioresource Technology*, 183, 93–100. <https://doi.org/10.1016/j.biortech.2015.02.056>.



- Malinowski, A. and Wardzińska, D. (2012). Catalytic conversion of furfural towards fuel biocomponents. [online] Available at: <[https://www.researchgate.net/publication/281835425\\_Catalytic\\_conversion\\_of\\_furfural\\_towards\\_fuel\\_biocomponents/stats](https://www.researchgate.net/publication/281835425_Catalytic_conversion_of_furfural_towards_fuel_biocomponents/stats)>.
- Martinez-Hernandez, E., Ramírez-Verduzco, L., Amezcua-Allieri, M. and Aburto, J. (2019). Process simulation and techno-economic analysis of bio-jet fuel and green diesel production — Minimum selling prices. *Chemical Engineering Research and Design*, 146, pp.60-70.
- McGarvey, E. (2018). . A stochastic techno-economic analysis of the catalytic hydrothermolysis aviation biofuel technology. *Biofuels, Bioproducts and Biorefining*, 3(12), pp. 474-484.
- Morgan, T., Santillan-Jimenez, E., Harman-Ware, A. E., Ji, Y., Grubb, D., and Crocker, M. (2012). Catalytic deoxygenation of triglycerides to hydrocarbons over supported nickel catalysts. *Chemical Engineering Journal*, 189-190, 346–355. <https://doi.org/10.1016/j.cej.2012.02.027>.
- Mortensen, P., Grunwaldt, J., Jensen, P., Knudsen, K. and Jensen, A. (2011). A review of catalytic upgrading of bio-oil to engine fuels. *Applied Catalysis A: General*, 407(1-2), pp.1-19.
- Mosier, N. (2005). Features of promising technologies for pretreatment of lignocellulosic biomass. *Bioresource Technology*, 96(6), pp.673-686.
- Mousavi-Avval, S.H. and Shah, A. (2021). “Techno-economic analysis of hydroprocessed renewable jet fuel production from Pennycress Oilseed,” *Renewable and Sustainable Energy Reviews*, 149, p. 111340. Available at: <https://doi.org/10.1016/j.rser.2021.111340>.
- Mythili, R., Venkatachalam, P., Subramanian, P. and Uma, D. (2013). Characterization of bioresidues for biooil production through pyrolysis. *Bioresource Technology*, 138, pp.71-78.
- Net zero 2050: IATA (2022). Net zero 2050: sustainable aviation fuels. IATA. Available at: <https://www.iata.org/en/iata-repository/pressroom/fact-sheets/fact-sheet---alternative-fuels/>.
- Pagliaro, M., Rossi, M., Clark, J. and Kraus, G. (2008). *The Future of Glycerol*. Cambridge: Royal Society of Chemistry.
- Park, L. K.-E., Liu, J., Yiacoumi, S., Borole, A. P., and Tsouris, C. (2017). Contribution of acidic components to the total acid number (TAN) of bio-oil. *Fuel*, 200, 171–181. <https://doi.org/10.1016/j.fuel.2017.03.022>.
- Popov, S. and Kumar, S. (2015) “Rapid hydrothermal deoxygenation of oleic acid over activated carbon in a continuous flow process,” *Energy & Fuels*, 29(5), pp. 3377–3384. Available at: <https://doi.org/10.1021/acs.energyfuels.5b00308>.

- Rabaeu, M., Landau, M. V., Vidruk-Nehemya, R., Koukouliev, V., Zarchin, R., and Herskowitz, M. (2015). Conversion of vegetable oils on Pt/Al<sub>2</sub>O<sub>3</sub>/SAPO-11 to diesel and jet fuels containing aromatics. *Fuel*, 161, 287–294. <https://doi.org/10.1016/j.fuel.2015.08.063>.
- Ramirez, J., Brown, R. and Rainey, T. (2015) “A review of hydrothermal liquefaction bio-crude properties and prospects for upgrading to transportation fuels,” *Energies*, 8(7), pp. 6765–6794. Available at: <https://doi.org/10.3390/en8076765>.
- Scaldeferri, C. and Pasa, V. (2019). Production of jet fuel and green diesel range biohydrocarbons by hydroprocessing of soybean oil over niobium phosphate catalyst. *Fuel*, 245, pp.458-466.
- Shahabuddin, M., Alam, M. T., Krishna, B. B., Bhaskar, T., and Perkins, G. (2020). A review on the production of renewable aviation fuels from the gasification of biomass and residual wastes. *Bioresource Technology*, 312, 123596. <https://doi.org/10.1016/j.biortech.2020.123596>.
- Shah, Z., Veses, R., Vaggetti, J., Amorim, V. and Silva, R. (2019). Preparation of jet engine range fuel from biomass pyrolysis oil through hydrogenation and its comparison with aviation kerosene. *International Journal of Green Energy*, 16(4), pp.350-360.
- Shi, W., Gao, Y., Song, S. and Zhao, Y. (2014). One-Pot Conversion of Bio-oil to Diesel- and Jet-Fuel-Range Hydrocarbons in Supercritical Cyclohexane. *Industrial and Engineering Chemistry Research*, 53(28), pp.11557-11565.
- Shim, J.-O., Jeon, K.-W., Jang, W.-J., Na, H.-S., Cho, J.-W., Kim, H.-M., Lee, Y.-L., Jeong, D.-W., Roh, H.-S., and Ko, C. H. (2018). Facile production of biofuel via solvent-free deoxygenation of oleic acid using a CoMo catalyst. *Applied Catalysis B : Environmental*, 239, 644–653. <https://doi.org/10.1016/j.apcatb.2018.08.057>.
- Silva, L. N., Fortes, I. C. P., de Sousa, F. P., and Pasa, V. M. D. (2016). Biokerosene and green diesel from macauba oils via catalytic deoxygenation over Pd/C. *Fuel*, 164, 329–338. <https://doi.org/10.1016/j.fuel.2015.09.081>.
- Smoljan, C.S., Crawford, J.M. and Carreon, M.A. (2020). Mesoporous microspherical NiO catalysts for the deoxygenation of oleic acid. *Catalysis Communications*, 143, p.106046.
- Sutton, A., Waldie, F., Wu, R., Schlaf, M., ‘Pete’ Silks, L. and Gordon, J. (2013). The hydrodeoxygenation of bioderived furans into alkanes. *Nature Chemistry*, 5(5), pp.428-432.
- Tao, L., Markham, J., Haq, Z. and Bidy, M. (2017). Techno-economic analysis for upgrading the biomass-derived ethanol-to-jet blendstocks. *Green Chemistry*, 19(4), pp.1082-1101.
- US Secretary of Navy (2012). Process For the Dehydration Of Aqueous Bio-Derived Terminal Alcohols To Terminal Alkenes.

Van Dyk, S., Ebadian. M., Su. J., Larock, F., Zhang. Y., Monnier, J., Wang. H., Santosa, D., Olarte, M., Neuenschwander, G., Rotness, L., Elliot, D., Drennan, C., O'Connor D., Meijerincx, O., Burns, A., Reid, C. and Claro, G. (2019). [online] Task39.sites.olt.ubc.ca. Available at: <<http://task39.sites.olt.ubc.ca/files/2019/11/GARDN-NEC-21-ATM-project-final-report-public-release.pdf>>.

Veriansyah, B., Han, J. Y., Kim, S. K., Hong, S.-A., Kim, Y. J., Lim, J. S., Shu, Y.-W., Oh, S.-G., and Kim, J. (2012). Production of renewable diesel by hydroprocessing of soybean oil: Effect of catalysts. *Fuel*, 94, 578–585. <https://doi.org/10.1016/j.fuel.2011.10.057>.

Wang, J., Bi, P., Zhang, Y., Xue, H., Jiang, P., Wu, X., Liu, J., Wang, T. and Li, Q. (2015). Preparation of jet fuel range hydrocarbons by catalytic transformation of bio-oil derived from fast pyrolysis of straw stalk. *Energy*, 86, pp.488-499.

Wang, M., He, M., Fang, Y., Baeyens, J., and Tan, T. (2017). The Ni-Mo/ $\gamma$ -Al<sub>2</sub>O<sub>3</sub> catalyzed hydrodeoxygenation of FAME to aviation fuel. *Catalysis Communications*, 100, 237–241. <https://doi.org/10.1016/j.catcom.2017.07.009>.

Wang, T., Tan, J., Qiu, S., Zhang, Q., Long, J., Chen, L., Ma, L., Li, K., Liu, Q. and Zhang, Q. (2014). Liquid Fuel Production by Aqueous Phase Catalytic Transformation of Biomass for Aviation. *Energy Procedia*, 61, pp.432-435.

Wang, W., Tao, L., Markham, J., Zhang, Y., Tan, E., Batan, L., Warner, E. and Biddy, M. (2020). [online] Nrel.gov. Available at: <<https://www.nrel.gov/docs/fy16osti/66291.pdf>>.

Wang, W.-C. (2016) Nrel.gov. Available at: <https://www.nrel.gov/docs/fy16osti/66291.pdf> (Accessed: 2020).

Wang, W.-C. and Hsieh, C.-H. (2020) “Hydro-processing of biomass-derived oil into straight-chain alkanes,” *Chemical Engineering Research and Design*, 153, pp. 63–74. Available at: <https://doi.org/10.1016/j.cherd.2019.10.030>.

Weber, D. (2018). [online] Scholarcommons.usf.edu. Available at: <<https://scholarcommons.usf.edu/cgi/viewcontent.cgi?article=8440&context=etd>> [Accessed 28 March 2020].

Westerhof, R., Brilman, D., Garcia-Perez, M., Wang, Z., Oudenhoven, S. and Kersten, S. (2012). Stepwise Fast Pyrolysis of Pine Wood. *Energy and Fuels*, 26(12), pp.7263-7273.

Wright, D. (2012). Biomass To Alcohol to Jet/Diesel.

Wyman, C. E., R. L. Bain, N. D. Hinman and D. J. Stevens (1993). Chapter 21. Ethanol and Methanol from Cellulosic Materials. *Renewable Energy: Sources for Fuels and Electricity*. T. B. Johansson, ed. Washington, D.C., Island Press.

Yildiz, G., Lathouwers, T., Toraman, H., van Geem, K., Marin, G., Ronsse, F., van Duren, R., Kersten, S. and Prins, W. (2014). Catalytic Fast Pyrolysis of Pine Wood: Effect of Successive Catalyst Regeneration. *Energy and Fuels*, 28(7), pp.4560-4572.

## 3 Methodology

The methodical techniques used to conduct experiments, gather, and analyse data for scientific interpretations are covered in this chapter. The two batch reactor systems used to conduct all experimental testing is covered along with their specifications and descriptions of how they were used to conduct successful tests for the three-stage conversion of lipids to liquid hydrocarbons. The tools and processes used to conduct these tests and collect samples for analyses are then discussed. The analytical and characterisation methods used for the examination of the feedstocks, reaction products and catalysts are also fully discussed in this chapter. In the experimental procedures, three repeats were conducted to compile and compare results, helping to establish the validity of the tests.

### 3.1 Materials

#### 3.1.1 Feedstock

Three lipid feedstocks were used in this study, and they included a sample of fresh rapeseed oil bought from an on-campus Tesco supermarket and two samples of waste cooking oils (WCO) were respectively obtained from a cafeteria and a pub around Aston University campus. The rapeseed oil, (a common vegetable oil in UK and Europe) was used, without any further treatment, to conduct all parametric studies, and to establish the best conditions for each of the three steps of the conversion (hydrothermal hydrolysis, deoxygenation, and cracking). The two waste cooking oil samples were filtered and tested under the best conditions established with the rapeseed oil. In the current investigation, the waste cooking oil sample from the pub is labelled as WCO-A, while the one from the cafeteria Was WCO-B. Personal communications with the managers of the pub and cafeteria indicated that WCO-A composed of a mixture of rapeseed, sunflower, and palm oil, while WCO-B was primarily from rapeseed oil. The photos of the oil samples are shown in Figure 3.1. There are differences in the visual appearance of these oils because they were used for frying, and the frying process allows for different factors to influence the colour of the oil. These factors include: temperature, an increase in temperature could cause thermal degradation which lead to browning reaction occurring, which is the formation of coloured compounds as larger molecules are broken down smaller molecules. The increase in temperature in combination with oxidation, that is, exposure to oxygen, in addition to the type of food also being fried are also factors that can cause the darkening of cooking oils.



Figure 3.1: Photos of; a) the fresh supermarket rape seed oil; b) WCO-A from Aston University Pub, and c) WCO-B from Aston University cafeteria

### 3.1.2 Reagents

A Milli-Q Advantage A10 Water Purification System was used in-house to generate deionised water for laboratory use. Solvents and chemicals including dichloromethane (+99%), anhydrous ethanol (+99%), oleic acid, glycerol, anhydrous methanol (+99%), sodium hydroxide pellets (+98%), sulphuric acid (+98%), petroleum ether (97%), and phenolphthalein indicator (97%) were also purchased from Fisher Scientific, Leicester, UK. Oleic acid was chosen as a model fatty acid molecule to determine the contents of fatty acids produced after hydrothermal hydrolysis of the lipids, which also produced glycerol. Furthermore, concentrated (37%) hydrochloric acid (HCl) obtained from Sigma-Aldrich in the UK was used to prepare 0.1 M hydrochloric acid standard solution.

### 3.1.3 Catalysts

The decarboxylation and cracking stages required the use of catalysts. A selection of different heterogeneous catalysts based on literature were purchased and used during these stages. 5 wt% platinum of carbon (5 wt% Pt/C), and zeolite-type catalysts including ZSM-5, Zeolite Y and MCM-41 catalysts were purchased from Sigma Aldrich, UK. In addition, 1 wt% platinum on silica powder (1 wt% Pt/SiO<sub>2</sub>), 5 wt% platinum on silica powder (5 wt% Pt/SiO<sub>2</sub>), 5 wt% platinum of alumina powder (5 wt% Pt/ Al<sub>2</sub>O<sub>3</sub>) 5 wt% platinum on magnesium silicate powder (5 wt% Pt/MgSiO<sub>3</sub>), 5 wt% palladium on magnesium silicate powder (5 wt% Pd/MgSiO<sub>3</sub>), 1:1 5 wt% nickel and copper on alumina powder (10 wt% Ni-Cu/Al<sub>2</sub>O<sub>3</sub> (P)), 1:1 10 wt% nickel and copper on alumina spheres (10 wt% Ni-Cu/Al<sub>2</sub>O<sub>3</sub> (S)) and 5 wt% ruthenium on alumina powder (5 wt% Ru/Al<sub>2</sub>O<sub>3</sub>) were sourced from Catal Limited, Sheffield, UK.

## 3.2 Methods

### 3.2.1 Detailed description of experimental equipment

A 450ml 4575A fixed head bench top Parr batch reactor (Figure 3.2a) with I.D 63.5 mm and depth 167.6 mm was used for the first step (hydrothermal hydrolysis) of the three-stage conversion of lipids to liquid hydrocarbons. This reactor has a magnetic stirrer to promote mass and heat transfer. There are also 6 screws used to tighten the split ring cap closure for extra fastening, with a PTFE gasket inserted between the head and the vessel for proper sealing. The temperature and stirrer motor speed are regulated by a 4848 Parr reactor controller, which also has a display to monitor system pressures (Figure 3.2b). The maximum operating pressure and temperature are 345 bar and 350 °C. Other parts of the reactor attached to the reactor head include the pressure gauge, a digital pressure sensor, gas, and liquid sample valves, and a thermowell for K-type thermocouple.

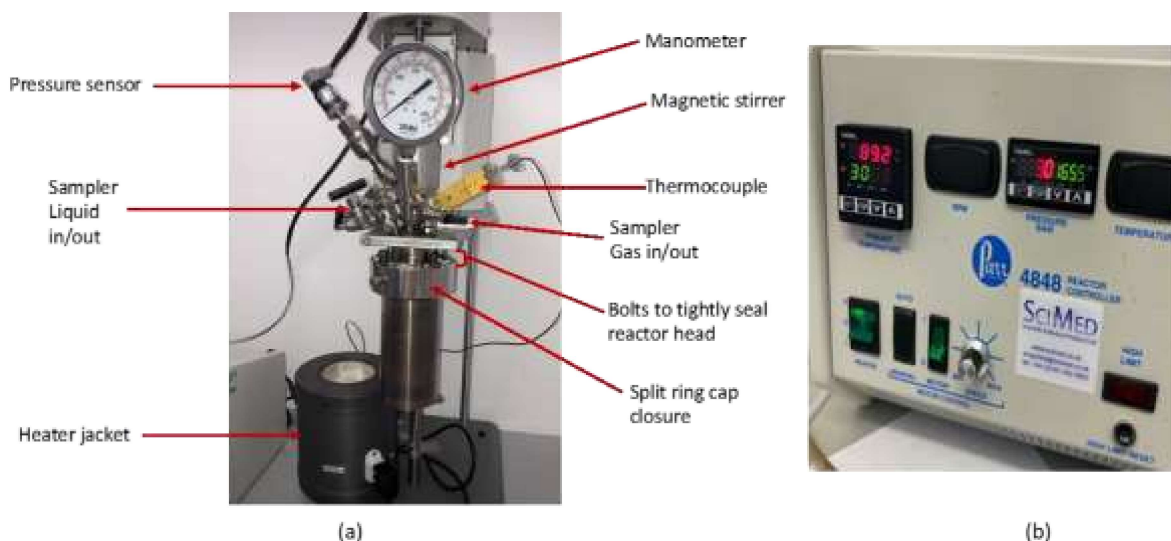


Figure 3.2: Photos of main batch reactor system for hydrothermal hydrolysis; (a) 450ml fixed head bench top Parr reactor; (b) controller for 4848 Parr Reactor

In addition, a 75ml batch reactor with I.D 25.4 mm and depth 142.2 mm was used for the decarboxylation (deoxygenation) of main hydrolysis products (fatty acids) and cracking of long-chain alkanes obtained from the decarboxylation stage. This reactor shown in Figure 3.3 has 6 screws, and a ring cap closure, housing a graphite gasket, which ensured the reactor is properly fastened and sealed. The same 4848 Parr reactor controller was used to regulate the temperature and to monitor the system pressures. The reactor also had similar parts such as the gas sampler, thermocouple, and pressure sensors. The maximum operating pressure and temperature were 450 bar and 600 °C, respectively.

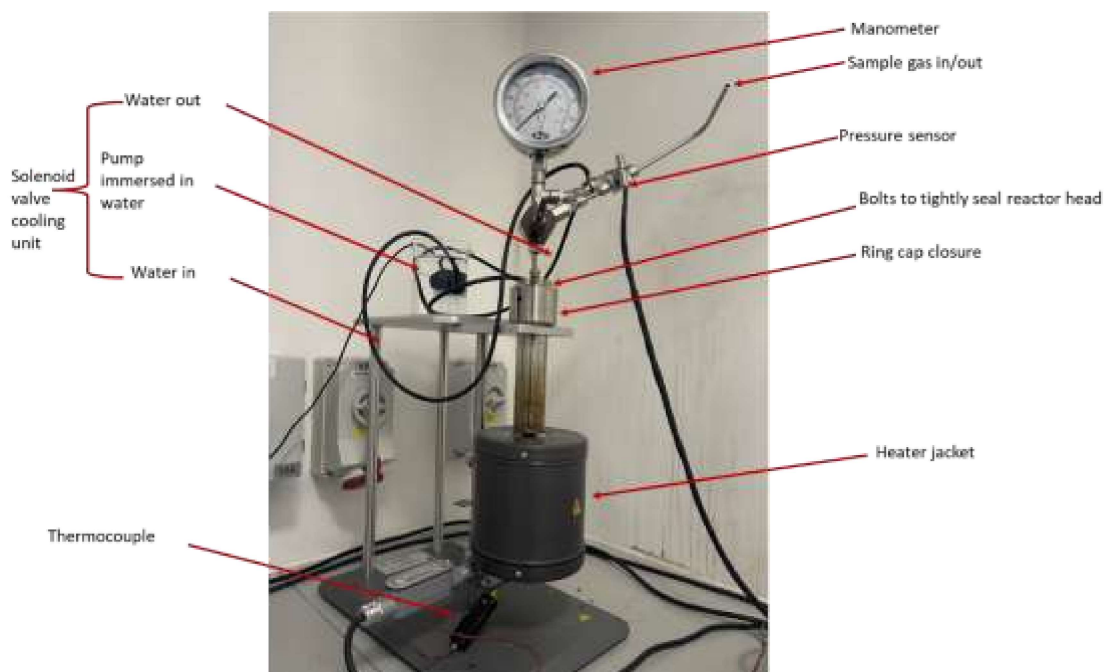


Figure 3.3: Photo of 75ml bench top Parr batch reactor used for decarboxylation and cracking experiments

The gas sample valve is used to feed in gas to purge the reactor system as well as to serve as an outlet to collect gaseous products for analysis. Each batch reactor was electrically heated to raise temperatures using the respective heating jackets provided.

#### 3.2.1.1 Operating the reactor

Apart from their different sizes and head types, the procedures for operating the reactors (opening, loading, closing, and mounting for heating) to carry out the experiments and collecting (unloading and discharging reactor contents) after experiments were similar. However, the hydrolysis experiments included the addition of water, whereas no water was added to either decarboxylation or cracking experiments. Hence, the procedure for using the reactors is described here but mostly for the 450 ml reactor.

##### 3.2.1.1.1 Preparing for safe laboratory work

Before the commencement of experimental work, thorough laboratory training was provided by the supervisor on the use of the reactor. The training was followed by a detailed Risk and COSHH Assessments on the experimental work with reactor, the use of chemicals and the disposal of waste. To do this, a list of chemicals and reagents envisaged for use in the research was made and their Material Safety Data Sheets were consulted to make notes of the associated health and safety implications of their use. In addition, other hazards of using



the reactor such as high temperatures, high pressures, and possible exposure to electrical power were considered as part of the detailed risk assessments. In addition, a Safe Operating Procedure was developed for the whole experimental procedure (from feedstock to product recovery and analysis) in conjunction with the supervisor. Copies of the safety documents were duly approved by supervisor and submitted to the designated responsible persons and online storage platform. In addition, for ease of reference, hardcopies were placed in a dedicated file in the main laboratory used for the research in Industrial Laboratory 1 in the Energy and Bioproduct Research Institute (EBRI) at Aston University.

#### 3.2.1.1.2 Opening the reactor

For health and safety reasons, it was essential practice to check the pressure and temperature of each reactor in case it might have been used by another operator. Following this confirmation, the pressure sensor and thermocouple could be detached from reactors, which would then be taken out from their respective fixed bench rigs first before loading or unloading them for the experiments.

Due to the weights of the reactors, they were disassembled and assembled by holding them firmly in a laboratory vice (Figure 3.4). For the 450 ml reactor, in addition to the six fastening bolts on the split ring cap, there was another groove fastening. For the 75 ml reactor, there were also six bolts and a screw head for fastening the head to the main vessel.



Figure 3.4: Arrangement for loading and unloading the 450 ml reactor using a laboratory vice

#### 3.2.1.1.3 Loading the reactor

As the experiments were carried out in a batch autoclave reactor, all the feedstock was added at once, before closing reactor prior to reaction. In a typical hydrolysis experiment, first, the oil was weighed using a beaker and a laboratory balance (Figure 3.5). The weighing of the reactor was carried out using a VWR weighing balance VWR1611-3472 Model LP-6292i, with a maximum load of 6200 g and the precision of 0.01 g. The balance is first set to true zero before weighing the oil in a beaker and pouring into reactor. The distilled water was measured using an appropriate measuring cylinder, depending on the amount required, then poured into the reactor. This sample weighing and loading process was maintained during subsequent reactions to improve reliability of the results and hence reduce error margins.



Figure 3.5: Photo of the main weighing balance used in this study

#### 3.2.1.1.4 Closing the loaded reactors

The feed components were loaded into reactor vessels in the fume cupboard, to prevent the exposure of operators and other lab users to harmful volatile substances or gases. The sealing PTFE gasket was checked to confirm its physical integrity for the planned experiment. The gasket would be replaced, in case of any visual signs of wear and tear or break in the gasket to avoid spillage of reactor contents under high temperatures and pressures. With the head closures placed and bolts screwed in until finger-tight, the reactor heads were then fastened using a dedicated spanner at the vice (Figure 3.4). The gas and liquid samplers were checked and closed to prevent gas or vapours from escaping during the

reaction. The next step was to mount reactors back on their fixed rigs and the respective heating jackets inserted to carry out a specified experiment.

#### 3.2.1.1.5 Cooling of the reactors

At the end of a specified reaction, the respective heater jacket was first pulled down from the reactor vessel using a pair of heat resistant gloves. A laboratory fan was used to rapidly cool the hot reactors, reducing time spent to get reactor to room temperature for sampling and collection of products. The thermocouple stayed attached to the reactors to be able to monitor temperature reading and confirm when reactor had reached room temperature to avoid handling it while unsafe (above 50 °C). The gas pressures recorded once reactors reached room temperature were an indication of the formation and quantity of gas products generated during the reactions.

#### 3.2.1.1.6 Unloading of the reactors

Following the cooling of the reactors, the gas products (if produced) were collected in Tedlar gas sampling bags made of Polytetrafluoroethylene (PTFE), through the gas outlet valves on the reactor heads as seen in Figure 3.3. In a typical procedure, the gas sampling bag (Figure 3.6) was evacuated with a vacuum pump to make sure no gas was left in the bag before adding new batch of gas product, and the empty gas bag weighed before gas product collection. The sample bag was attached to the reactor through a pipe which was fastened at one end to the reactor. Once bag is filled, the gas bag was re-weighed to record the weight of gas product. After this, reactor was taken to the vice to detach the head and the vessel weight to obtain the combined mass of the liquid and solid products on the weighing balance. As the combined weight of the 450 ml vessel and its head exceeded the maximum load of the balance, these parts were weighed separately.



Figure 3.6: Photo of a typical Tedlar gas sampling bag used in this study

Following this, the reactors were moved to the fume cupboard to extract the liquid and solid products. For the hydrolysis stage, the extraction was carried out using dichloromethane (DCM), a volatile solvent that is immiscible with water but could dissolve the hydrolysis product. The extracted product was then poured and contained in a 250 ml glass sample bottle. Thereafter, a spatula was then used to remove any solid products that stuck to reactor wall that would not easily flow out with the liquids.

#### 3.2.1.1.7 Cleaning of the reactors

The cleaning of the reactors was done immediately after unloading them to reduce chemical wear and tear, and to prepare vessels for next experiments. The cleaning was carried out in the laboratory sink using laboratory detergent and a thick bristled scrubbing brush. The inside walls of the reactors were scrubbed with detergent and water and rinsed three or four times with water to ensure proper cleaning for subsequent experiments. For the 450 ml reactor, the head was also scrubbed and cleaned gently, to avoid any damage to the fixed parts including stirring rod, dip tube and thermocouple.

#### 3.2.1.1.8 Preliminary hydrothermal hydrolysis work for reactor testing

The temperature and pressure profiles of the 450 ml reactor was initially checked with water only and with mixtures of water and rapeseed oil during the hydrolysis stage. The response of the reactor to the different reaction conditions tested are shown in Table 3.1.

Table 3.1: Preliminary experiments to test reactor temperature and pressure profiles

Run	Water (g)	RSO (g)	Set Temperature (°C)	End Temperature (°C)	End pressure (bar)	Reaction time (h)
1	20	-	300	299.0	51.6	2
2	10	-	300	301.3	31.9	2
3	20	10	300	300.3	60.1	2
4	10	10	300	299.9	30.1	1
5	20	10	300	301.6	68.8	1
6	30	10	300	300.8	78.8	1

Reaction parameters such as temperature, reaction time and oil to water ratio were varied based on similar findings in literature for laboratory training and validation (Salimon et al., 2011; Satyarthi et al., 2011; Nitbani et al., 2020). Temperature was set at 300 °C as the solubility of oil and fatty acids in water is low at temperatures below 200 °C (Alam, 2019). Different oil to water mass ratios (1:1, 1:2, 1:3) and reaction times (1-3 h) were examined.

In these tests, the reactor heat-up period lasted between 30 and 40 minutes on each occasion before reaching steady state, and the reaction time recorded afterwards. At the end of each experiment, the heating jacket was detached, and a fan was used to cool down reactor to room temperature for safe extraction of products. The mixture inside the reactor was extracted using DCM and placed in 250 ml glass vial. No gas products were obtained during these initial experiments, possibly due to the low temperature (300 °C) used, thereby insufficient to cause any significant thermal degradation of the vegetable oil and its hydrolysis products.

Figure 3.7 shows the temperature profiles of three reactions carried out for a reaction time of two hours. This preliminary study helped to understand how temperature changed with time based on the reactants in the reactor.

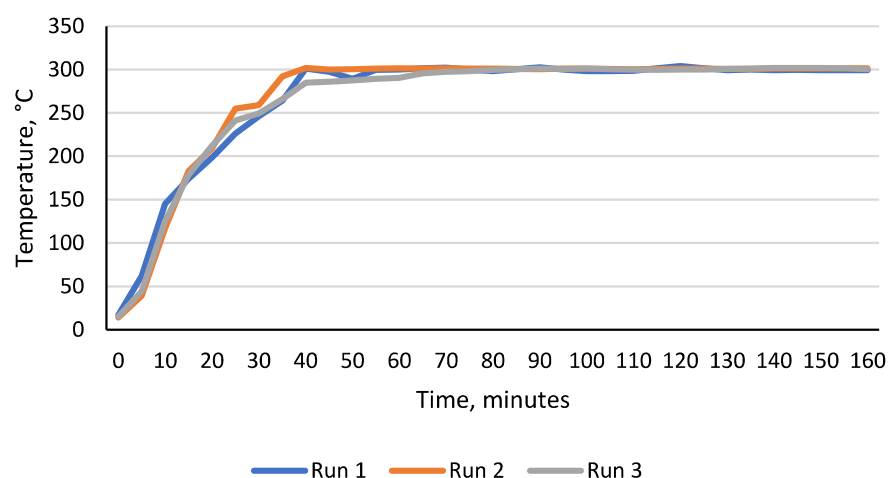


Figure 3.7: Reactor temperature profile in relation to quantity of water/oil loaded

The starting temperature depended on the room temperature. The graph shows a rapid temperature increase in all three reactions in the first 40 minutes as reaction approached set point (300°C) and steady state. However, Run 2 reached 300°C first because it contained least quantity of contents. Energetically, considering the specific heat capacity of water (4.186 J/g°C) compared to that of vegetable oils (< 2 J/g°C), more energy would be required to heat up the samples with more water from Figure 3.7. In most cases all tests remained steady at about 300 °C over the course of these experiments.

Figure 3.8 shows the pressure profiles of the same three experiments as seen in Figure 3.7. All three reactions had a sharp pressure rise in the first 40 minutes from the start, 0 bar gauge pressure. There was a distinct difference in the pressure reached at steady state, even though they all had similar curves. The experiment with the least volume of reactants (Run 2) had the least pressure of about 30 bar. Run 3, which had the highest volume ran at about 60 bar pressure while Run 1 only ran at approximately 50 bar pressure. These tests showed that the operating pressures depended on the amount of water loaded.

Figure 3.9 presents the temperature profiles of three different experiments with reaction times of one hour. The only condition that changed was the volume of water added. Even though all three experiments gave similar profiles, Run 4 which occupied the least volume reached 300 °C (set point) first. In contrast, the experiment with the highest volume of reactants (Run 6), reached the set point last as more heat was required to heat up larger quantities.

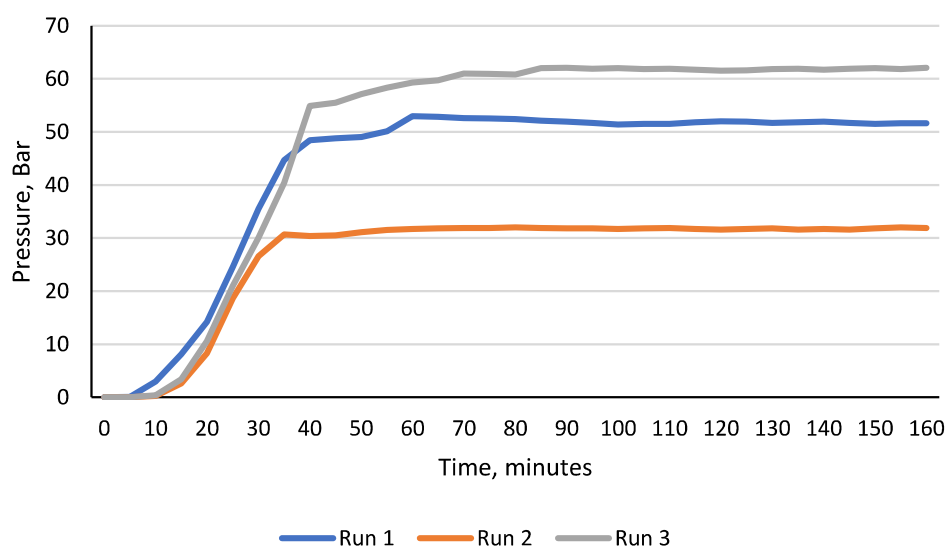


Figure 3.8: Reactor pressure profile in relation to quantity of water/oil loaded

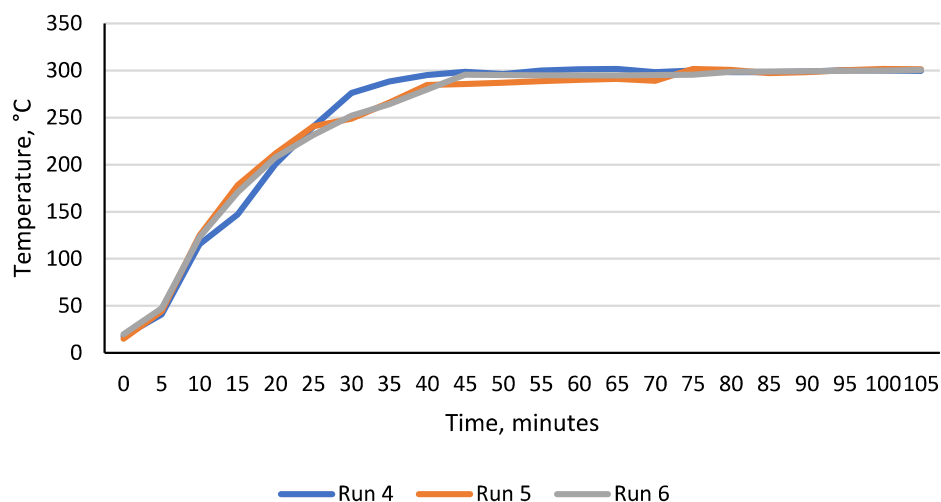


Figure 3.9: Reactor temperature profile in relation to volume of water added

Figure 3.10 represents the pressure profiles for the same experiments shown in Figure 3.9. The difference in the volume of water added resulted in reactions been run at three different pressures. Nonetheless, all reactions followed similar curves. The sample with Run 4, which occupied the least volume had a steady increase in pressure for the first 25 minutes before plateauing. The reaction which occupied the most volume (Run 6) had a significant pressure increase rate for the first 40 minutes, just like the Run 5 experiment. However, the former ran at the highest pressure, with a slight steady increase even till the end of the reaction.

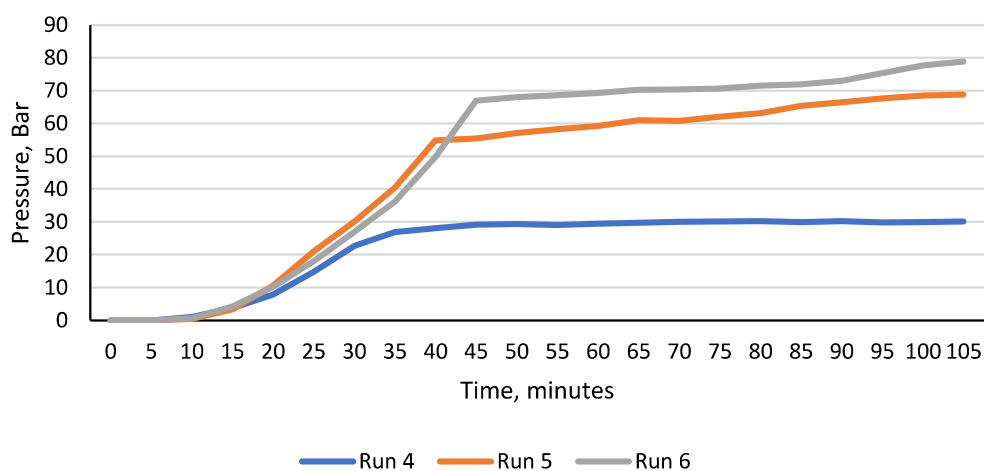


Figure 3.10: Reactor pressure profile in relation to volume of water added

### 3.2.2 Detailed description of experimental procedures

The process route proposed in this research for the production of liquid hydrocarbons from vegetable oils included the reaction steps depicted in Figure 3.11. Additionally, Figure 3.12 shows the procedure followed to carry out reactions and obtain results.



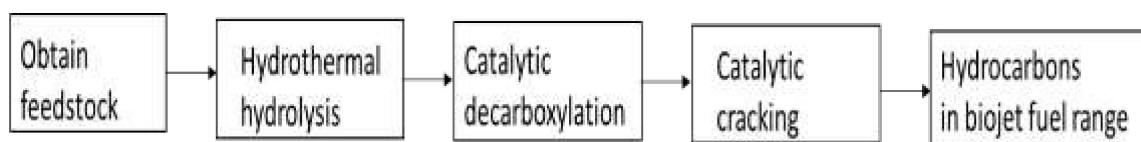


Figure 3.11: Process route for conversion of vegetable oil to biojet fuel range hydrocarbons

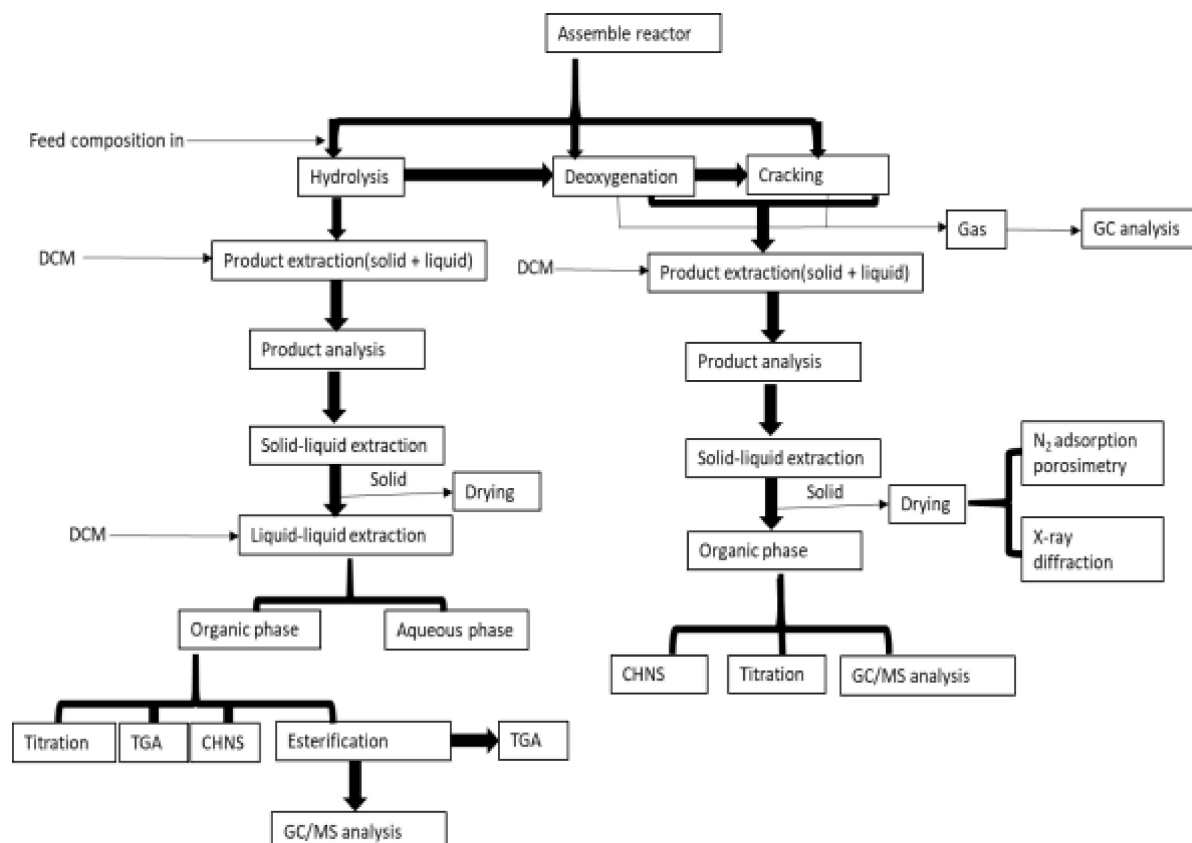


Figure 3.12: Procedure in hydrothermal hydrolysis, catalytic deoxygenation, and cracking

### 3.2.2.1 Experimental procedure for hydrothermal hydrolysis of rapeseed oil

The hydrolysis of rapeseed oil was carried out with 10 or 20 g of vegetable oil in the absence of a catalyst at 200 °C, 250 °C, and 300 °C, and corresponding autogenic pressures ranging from 9 bar to 51 bar. In addition, the effects of reaction time (1 min to 180 min) and oil/water mass ratios (1:0.1 to 1:3) on the yields of fatty acids from rapeseed oil were studied at set temperature of 300 °C. All reactions were carried out in a 450 ml stainless steel batch reactor (Parr Instruments Co. Illinois, USA), with a maximum working temperature of 350 °C and a pressure of 345 bar. After loading and sealing the reactor, it was purged for 5 min and then pressurised with nitrogen to 5 bar prior to heating at a rate of 10 °C/min to the reaction temperature. Once the set temperature was reached, the reactor was held for 1 h for the hydrolysis of the vegetable oil. At the end of the reaction, the reactor was cooled to room temperature with a laboratory fan, taking about 30 min to reach ambient temperature.



The reaction products were quantitatively transferred from the reactor vessel into a 250 ml sample bottle using aliquots of 30 mL of dichloromethane (DCM), to dissolve and recover the fatty acid product and any unreacted rapeseed oil. Thereafter, a known amount of deionised water was used to rinse the reactor, and the aqueous phase added to the product mixture in the sample bottle. The additional water was added to ensure the separation of the glycerol product (soluble in water) from the fatty acids (soluble in DCM). The aqueous and DCM phases were separated in a separating funnel. The slightly turbid aqueous phase was weighed separately. Thereafter, the organic phase was passed through anhydrous sodium sulphate to dry it and then, the DCM solvent was removed by gentle evaporation at 40 °C. The final semi-solid oily phase (wax) was transferred into a storage bottle and kept in a laboratory fridge prior to further analysis and use.

#### 3.2.2.2 Experimental procedure for catalytic decarboxylation of hydrolysis products

The oily products from the hydrolysis stage were used in the decarboxylation stage as the deoxygenation step. These deoxygenation reactions were performed in a Hastelloy batch reactor with 75 ml capacity and able to reach 600 °C and 450 bar. Each experiment was carried out using about 10 g of hydrolysed oil and 0 - 2 g of different catalysts, from 350 °C - 400 °C and reaction times 0 – 3 h. No water was added in these decarboxylation tests. The reactor was initially purged with nitrogen to exclude air and then pressurised to 5 bar with nitrogen. Nitrogen was used to help recover gas products after reaction and as internal standard during gas analysis. The operating pressures during these experiments ranged from 60-70 bar. At the end of the reaction, the reactor was rapidly cooled with laboratory fan to ambient temperatures. After cooling, the temperature and pressure of the reactor were noted, and the gas product sampled for analysis. Thereafter, the reactor was opened to sample any liquid products and solid residues. About 80% of the liquid product was first recovered without any solvent, and this oil product was used for the cracking tests as described in Section 3.2.2.3. Subsequently, DCM was used to wash the reactor to recover the remaining liquid product and solid residues. The solid residues were separated via vacuum filtration using a KNF LABOPORT vacuum filtration system, dried and weighed. Furthermore, the DCM solvent was removed by evaporation 40 °C. The oil product obtained was weighed and stored separately. The total mass of the two oil product fractions was noted for mass balance.

#### 3.2.2.3 Experimental procedure for catalytic cracking of decarboxylated products

The deoxygenated oil from the second stage was catalytically cracked into lower molecular weight hydrocarbons using with Pt/C and ZSM-5. The ZSM-5 had been calcined at 550 °C

for 6 h (Si/Al = 360:1). While zeolites are well-known for catalytic cracking, the use of Pt/C in this present work was based on the observation that increasing the severity of decarboxylation (e.g., using extended reaction times at 400 °C), led to formation of lower molecular weight compounds. To avoid any solvent contamination, only the deoxygenated oil products recovered without the use of solvent were used for cracking. Therefore, the amount of 'neat' solvent-free oil ranged from about 6 g to 8 g, but the experiment was repeated three times to gather enough oil to feed into the next stage. The reactor was loaded with 10 g of deoxygenated oil and 0 - 1 g of different catalysts in the same 75 ml Hastelloy batch reactor used for the decarboxylation step. No water was used in this test. The reactor was also purged and pressurised to 5 bar with nitrogen. Cracking experiments were carried out also at 400 °C – 450 °C for 0 - 2 h, with final running pressures between 50 and 60 bar. The post-reaction procedures for product separation and recovery used here were similar to those used for the decarboxylation step.

### 3.2.3 Analytical equipment and procedures

In general, after the reaction, the product mixture consisted of solids (see sections 3.2.3.1, 3.2.3.4, and 3.2.3.13 – 3.2.3.14), liquids (see sections 3.2.3.1 – 3.2.3.3, 3.2.3.5, and 3.2.3.9 – 3.2.3.11), and gases (see sections 3.2.3.6 – 3.2.3.8). In order to achieve accurate quantitation and computation of mass balances, the products from the reactor would need to be separated for. During hydrothermal hydrolysis of vegetable oil, it was expected that the reactor content would be a mixture of aqueous and organic phases and possibly solids. Therefore, an organic solvent would be required to quantitatively recover the organic phase from the reactor. The choice of the organic solvent was important to ensure that it could only solubilise the organic products and could be used as a solvent for the subsequent analysis of the organic products to determine compositions and yields.

In the preliminary hydrolysis experiment, it was found that the oil and fatty acids were soluble in DCM and since DCM is denser than water, the organic layer was at the bottom while the aqueous layer containing glycerol sat at the top as shown in Figure 3.13b. The three components (solid, organic layer and aqueous later) could be obtained separated using two separation methods; solid-liquid separation by filtration and liquid-liquid separation (solvent extraction).

#### 3.2.3.1 Solid-liquid separation

This was carried out using a vacuum filtration kit as seen in Figure 3.13a. This system included a filtering flask, Buchner funnel, one-hole rubber stopper, vacuum tubing, filter

forceps, filter paper and a vacuum pump. This first stage of separation removed the solid carbon produced, (or solid catalysts when used), allowing just the liquids to flow through. A filter paper was placed into the Buchner funnel and wetted with water to ensure paper was properly sitting in the funnel. The obtained product mixture was poured slowly into the Buchner funnel and the liquid products and products smaller than the pore size of the filter paper pass through. Particles larger than the pore size, stayed on the filter paper. The vacuum pump was turned off over short intervals to minimise volatilisation, hence minimising loss of product. The liquid product obtained post-filtration was poured into a clean glass sample jar for storage. The filter paper was removed from Buchner funnel with a pair of tweezers and stored.

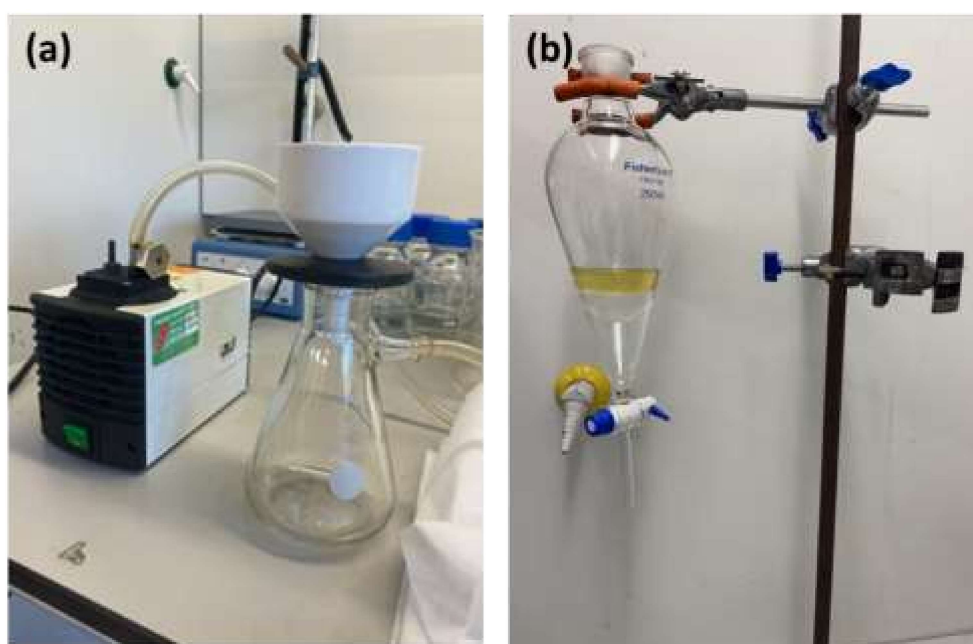


Figure 3.13: Photos of (a) Vacuum filtration setup; (b) liquid-liquid extraction apparatus

#### 3.2.3.2 Liquid-liquid separation

This separation process was used to isolate each of the two immiscible layers in the liquid mixture as seen in Figure 3.13b. The system for this included a separatory funnel, stand set, and two empty flasks to collect each layer. The funnel tap was closed to prevent leaking before separation began. The mixture was allowed to settle for about five minutes after it was poured into separatory funnel. After this, the two distinct layers appeared. The organic layer sat at the bottom because of the higher density of DCM relative to water, hence, it was drawn off first. The cork at the top of the funnel was taken off to prevent pressure build up, hence mixing of both layers due to the volatility of DCM. This bottom layer which was also identified due to its darker colour relative to the top layer was then collected into a clean glass sampling jar. After this, the aqueous layer was collected into a separate glass sampling jar.

### 3.2.3.3 Solvent evaporation

For all samples recovered by DCM (hydrolysis, decarboxylation, and cracking), the solvent was removed by heating at 40 °C with a sample concentrator. A Stuart sample concentrator was used to separate the solvent DCM (boiling point = 39.6 °C) from the oil products obtained from the decarboxylation and cracking stages (Figure 3.14). In order to minimise the loss of light chain hydrocarbons in the form of volatiles, low temperature, 40 °C is used. This drives off the DCM, and leaves behind liquid organic product. This was particularly useful during the hydrolysis stage, as the products comprised of high molecular weight fatty acids (e.g., oleic acid boiling point = 360 °C) and glycerol (boiling point = 290 °C).



Figure 3.14: Stuart solvent evaporation system

### 3.2.3.4 Drying of solid residues

After filtration with the vacuum kit, the caked filter paper (Figure 3.15a) was dried using the oven (Figure 3.15b) for 2 h, at 105 °C. Post-drying, a pair of heater tongs were used to move the weighing boat from the oven into the vacuum desiccator while wearing heat resistant gloves. The desiccant is used to remove any moisture present while the solids cool down was silica gel. A scale (Figure 3.5) was used to weigh the weighing boat and filter paper in order to calculate mass of solids. The solid product obtained after filtration of the decarboxylation and cracking reactions was dried before further analyses.



(a)



(b)

Figure 3.15: Photos relating to solid product drying; (a) solids collected on filter paper (b) drying oven

#### 3.2.3.5 Density measurement for liquid products

The densities of the product oils were measured using a 5 ml Blaubrand density bottle using the standard test method for specific gravity of oils (ASTM D5355-93) and density formula (Stauffer et al., 2008). First, the volume of the bottle was confirmed by doing a preliminary test with water, which has a known density of 997 kg/m<sup>3</sup> (Stauffer et al., 2008). Then the apparatus was used to obtain the density of the product oils using Equation 3.1.

$$D = \frac{m_{(a+b)} - m_{(a)}}{V(b)} \quad (3.1)$$

Where;  $m_{(a)}$  = mass of bottle;  $m_{(a+b)}$  = mass of bottle filled with sample;  $V_{(b)}$  = volume of sample;  $D$  = density of sample

#### 3.2.3.6 Analysis of gas product by gas chromatography

Although no gas product was obtained from hydrolysis experiments, gas was produced in the decarboxylation and cracking stages. The composition of the gaseous products collected in the gas sample bag were analysed using gas chromatography (GC). Figure 3.16 shows a schematic of how a GC operates. The Shimadzu GC-2014ATF was available for use in this research and carried out the analysis of the hydrocarbons fraction of each gas sample in 13

mins runs, and the permanent gas fraction in twenty minutes. This GC used argon at a purge flow of 1 mL/min as carrier gas. The time required for the sample to get through the column is called retention time. This factor is determined by the strength of the interaction between the sample and the stationary phase. The stronger the interaction, the longer the retention time (Saitman, 2019; Gröger et al., 2020).

The GC was switched on prior to analysis run to allow system to stabilise and reach steady state to achieve accurate analysis. Once this was achieved, the lab solution software was opened on the computer connected to the GC. The successful connection of the computer to the GC was indicated by a beep sound on the GC. Next, “start single run” was selected on the computer which prompts the gas injector to inject 1 mL of the sample gas with a septum, the start button on the GC was hit right after to commence analysis. The interpretation given by the detector is identified by Gaussian peaks printed on a chart, known as chromatograms (Figure 3.17). The amber flashing LED for temperature and flow indicated the end of the analysis. A reboot was done in 7 – 9 mins and the green lit LED signified the GC was ready for another analysis run and next sample can be injected (Turner, 2020).

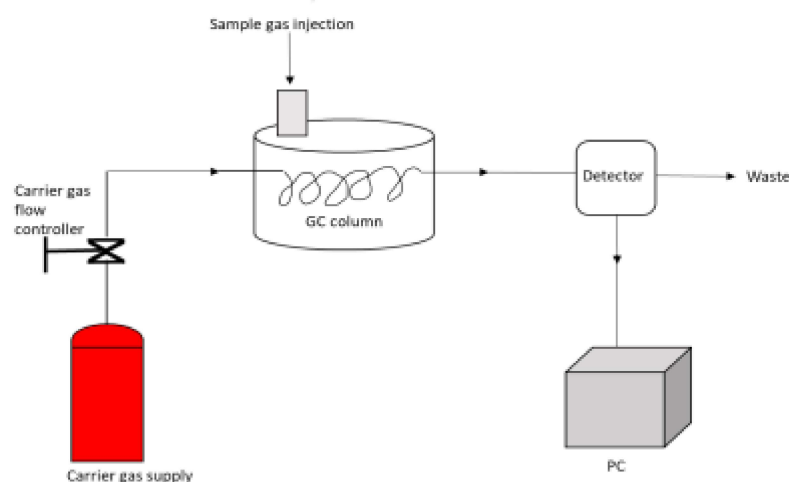


Figure 3.16: Schematic of a typical gas chromatograph (Torres, 2016)

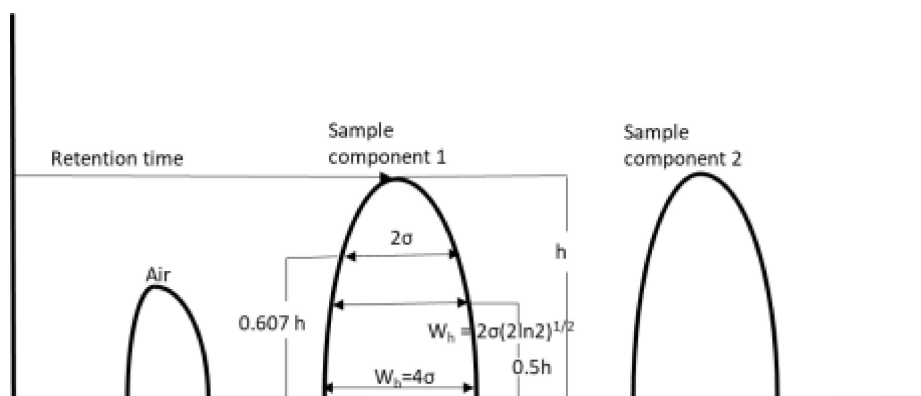


Figure 3.17: A typical GC chromatogram (Spangler, 2015)

The FID has a high selectivity for organic compounds, and uses hydrogen, oxygen, or air to ignite a flame which burns sample or organic compound to produce ions.

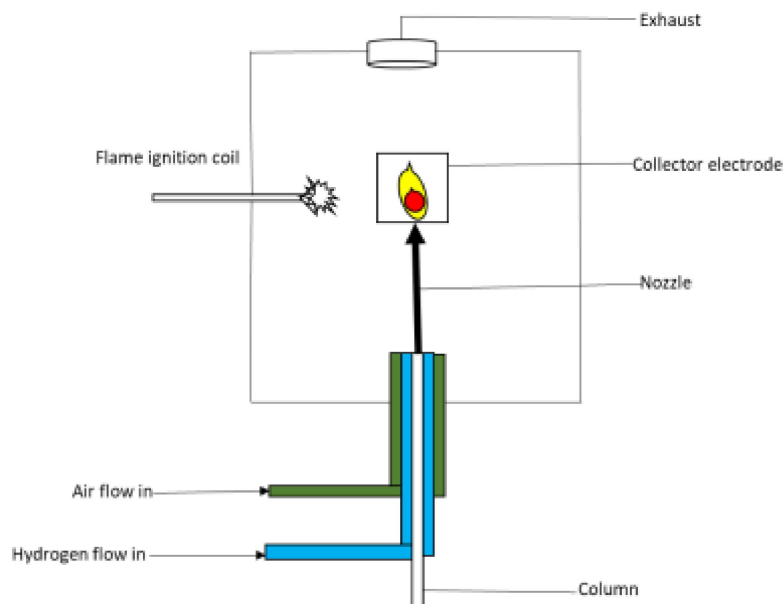


Figure 3.18: Schematic of an FID

Typically, the hydrocarbons in the sample become ionised after the ignition of the flame and sample. The positive ions are attracted to the negatively charged plate, the collector electrode. This triggers a response, a peak that is directly proportional to the carbon mass flow. The setup of an FID is shown in Figure 3.18. A major downside to the use of this type of detector is that the sample ends up combusted or burnt which hinders the detector from being combined with other analytical techniques or to be used for preparative GC (Rahman, El-Aty and Shim, 2015) (Zuo, Yang, Huang and Xia, 2013).

#### 3.2.3.6.1 Thermal Conductivity Detectors (TCD)

TCD on the other hand is suitable for preparative GC as the sample is not destroyed during analysis. The analysis is done based on the difference in thermal conductivity between two gas streams, one containing the carrier gas alone, and the other containing the carrier gas and the sample gas.



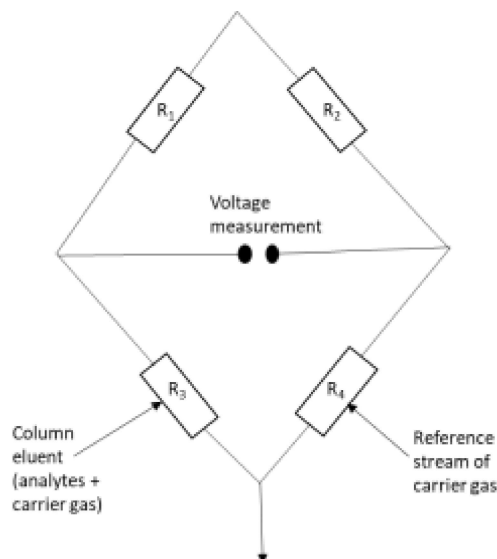


Figure 3.19: Wheatstone bridge basis of TCD

This detector consists of four resistors in an electric circuit called the Wheatstone bridge (Figure 3.19). The resistors in the circuit get heated up by passing electric current through them. Since there are two different types of gases passing through (a blank and one with the sample), the temperature of the resistors decreases at different rates, indicating different thermal conductivities.

The difference in these thermal conductivities cause the circuit to become unstable and produce an electric signal. This signal symbolises the amount of sample gas removed from the column and is seen on the chromatogram. The drawback of this detector is that it is not as sensitive as other GC detectors (Rahman, El-Aty and Shim, 2015).

### 3.2.3.7 Repeatability of standard gas injection



Figure 3.20: GC used for gas analysis



Table 3.2: Peak areas for the standard hydrocarbon gases

Run	Methane	Ethene	Ethane	Propene	Propane	Butene	Butane
1	41770235	82151545	83655961	133442078	137610532	188290396	190290396
2	45305289	89081017	90541278	133536731	138450607	180389334	183389334
3	42583314	89147311	92199838	138885993	145521204	190436480	194436480
4	41687956	87577182	90536045	136402106	143244509	190838534	191238534
5	42989782	89273715	90407667	136455472	133121459	181875937	182475937
Average	42867315.2	87446154	89468158	135744476	139589662	186366136	188366136.2
SD %	±3.43	±3.48	±3.72	±1.69	±3.50	±2.63	±2.76

SD = standard Deviation

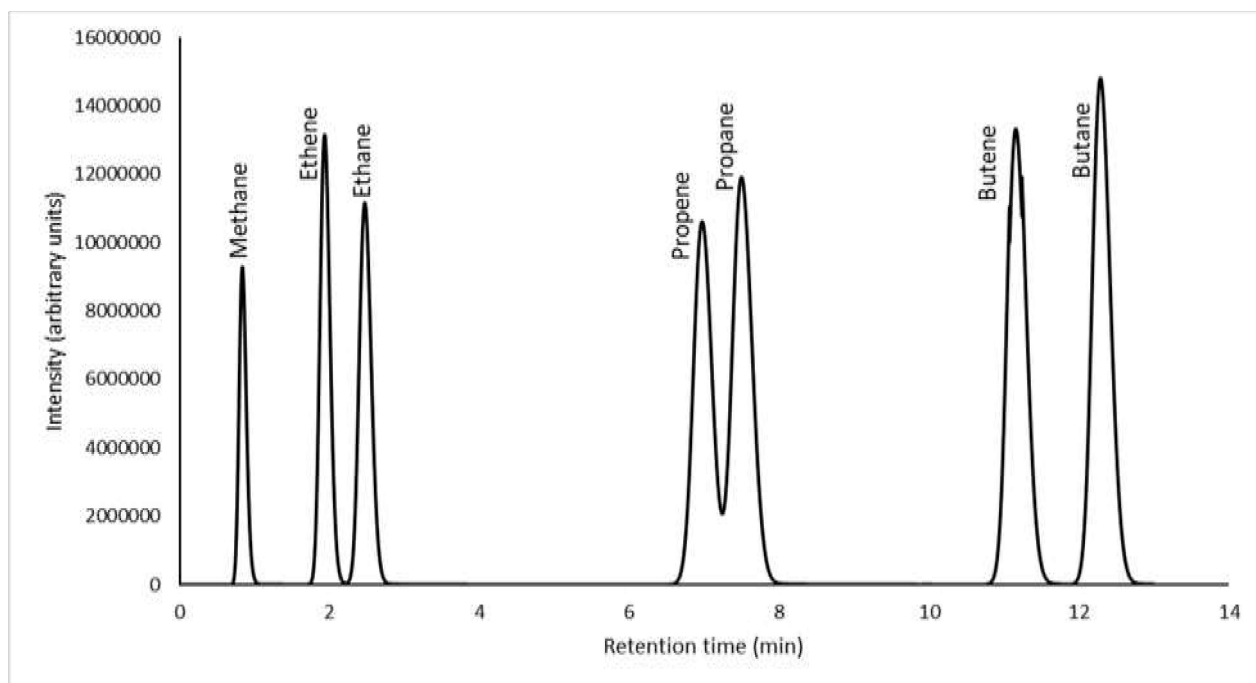


Figure 3.21: GC/FID chromatogram of standard hydrocarbon gases

Hydrocarbon and permanent gases standards were injected into the GC (Figure 3.20) in order to confirm that the equipment and the methods used are working effectively. Tables 3.2 and 3.3 show the peak areas of the hydrocarbon and permanent gases, while Figures 3.21 and 3.22 show their chromatograms respectively. The tables also show their average and relatively low standard deviation values, which imply minimal systemic errors.

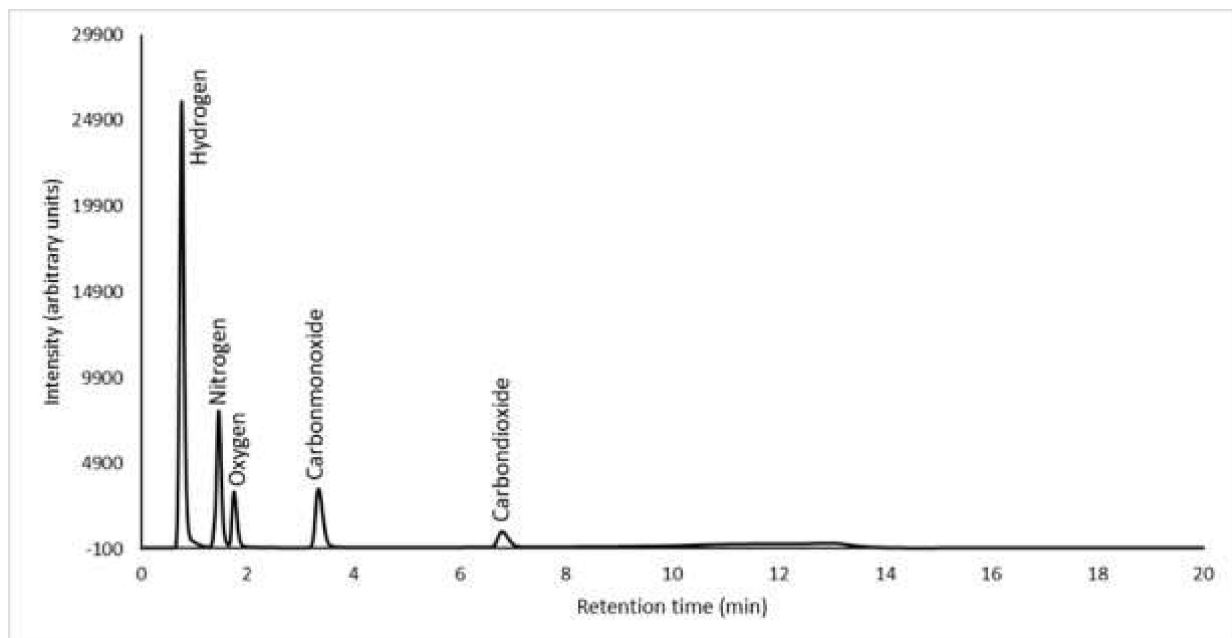


Figure 3.22: GC/FID chromatogram of standard permanent gases

Table 3.3: Peak areas for the standard permanent gases

Run	H <sub>2</sub>	O <sub>2</sub>	N <sub>2</sub>	CO	CO <sub>2</sub>
1	20626	2828	193915	5742	2026
2	19821	2909	198295	5809	2158
3	21255	2781	213594	5708	2138
4	20549	2810	208009	5601	2177
5	20094	2803	200175	5703	2078
Mean	20469	2826.20	202797.60	5712.60	2115.40
SD %	±2.69	±1.74	±3.90	±1.32	±2.94

SD = Standard Deviation

### 3.2.3.8 Quantitative analysis of gas products

Using data from the study of standard gases, the volume % of the gas products was calculated. To determine the response factors (RF) for each species in the standard gases, the area values recognised by the GC by converting the electrical signal from the detector were used as shown in Equation 3.2. This was done for each gas detected.

$$RF = \frac{\text{peak area of standard gas}}{\text{volume \% standard gas}}$$

(3.2)

Next, Equation 3.3 shows how the volume percentages of each of the species in the product gas obtained from the experiments is observed:

$$Vol\% \text{ of gas component} = \frac{\text{peak area of gas component}}{RF \text{ of standard gas}} \quad (3.3)$$

The mass yield of each gas was calculated using the volume percentage obtained from the GC and the ideal gas equation (Equation 3.4) (Razaq et al., 2021)

$$m = \frac{MPV}{RT} \quad (3.4)$$

Where P (Pa) is the pressure, V is the volume of reactor headspace (m<sup>3</sup>), m is the mass (g) of gas, R (8.314 J mol<sup>-1</sup> K<sup>-1</sup>) is the universal gas constant, T (K) is the absolute temperature, and M is the relative molecular mass of gas component (g/mol).

After obtaining the mass yield of each gas, the results are input into a spreadsheet on Microsoft excel. This spreadsheet was specifically developed to accommodate and calculate the large amount of data collected to generate useful results such as volumes, moles, and ratios of the different gases, as well as the moles and weight of the individual and total gases detected. The nitrogen gas initially loaded in the reactor was used to correct any errors with the pressure reading.

### 3.2.3.9 Analysis of liquid products by gas chromatography mass spectrometry (GC/MS)

The organic liquid products from this research were quantified using Shimadzu GC-2010 GC/MS. This method is commonly used for identification and quantification of organic compounds (Crawford et al., 2019; Sorigué et al., 2016; Neonufa et al., 2021; Moser et al., 2016; Dourado et al., 2022). The GC/MS uses the mass/charge ratios(m/z) of compounds to identify the components of a sample. This detector works by either ionising the original sample (molecular ion) or by splitting the ionised sample into smaller fragments (fragment ions). The ionisation of the sample is essential as the GC-MS carries out its reading based on the acceleration of the ions to the mass analyser per attraction or repulsion.

There are various ionisation techniques such as electron impact (EI) and chemical ionisation (CI). In this case EI is explored. EI is the oldest and most common ionisation technique used in GC/MS. Most data collected required electron beam of 70 eV on impact for ionisation. A heated filament discharges electron which accelerates towards the negatively charged

plate(anode) and the gaseous molecules for collision (Figure 3.23). The impact on collision results in the positive ionisation and fragmentation of the neutral gaseous sample molecules (Rockwood, Kushnir and Clarke, 2018).

Post-ionisation, the quadrupole separates the ionised molecules based on  $m/z$  ratio. Direct current (DC) voltage is applied to and rapidly reversed from all four hyperbolic rods in this mass analyser, creating an oscillating electric field permeable to selective ions with a certain  $m/z$  ratio. The abundance of each ion focused and accelerated towards the quadrupole mass analyser is measured by an electron multiplier and is determined in a mass spectrum (Figure 3.24).

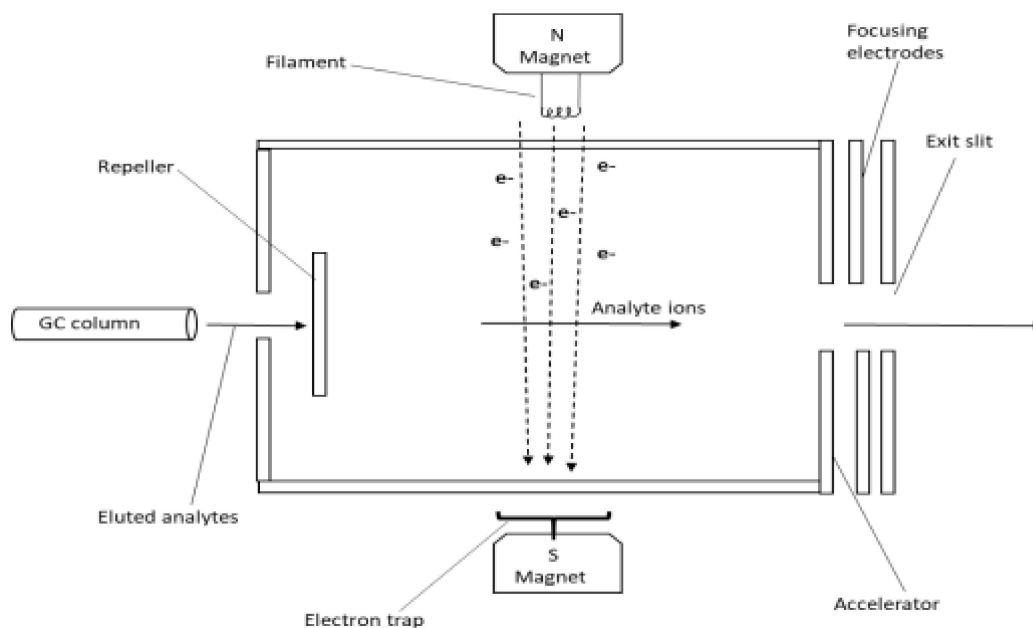


Figure 3.23: Schematic of electron Ionisation used in GC/MS (Rockwood, Kushnir and Clarke, 2018)

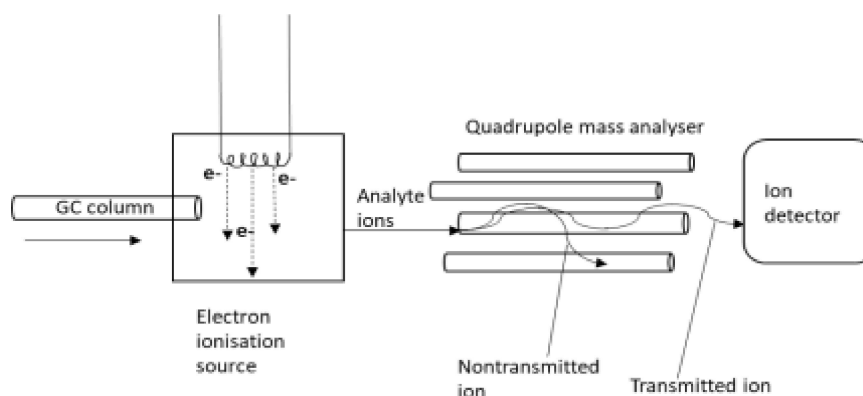


Figure 3.24: Pathway to detecting ions in a mass spectrometer (Domingues, García and Skrzydlewska, 2018)

This detector is three dimensional, it carries out compound identification using mass spectra, has the ability to determine the chemical and structural properties of the molecules and also produce a chromatogram for qualitative and quantitative analysis.

The GC/MS used for the analysis of this project is the Shimadzu GC-2010 GC/MS, combined with the Shimadzu GCMS-QP2010 SE (Figure 3.25).



Figure 3.25: Photo of Shimadzu GC-2010 GC/MS used for qualitative and quantitative analyses of liquid products

Typically, an autosampler vial is filled with a certain amount of the liquid to be analysed and placed in a vial slot of the GC/MS. Next, the autosampler injects 1  $\mu\text{L}$  of the sample liquid from the vial into the GC/MS. The heating up of the equipment causes the temperature to rise until the set point is reached. The mobile phase, helium in this case is vaporised and carried through the capillary column at a flowrate of 30 mL/min. The software database used to identify the molecules was National Institute of Standards and Technology (NIST).

After the run, the auto sampler was programmed to be cleaned with acetone to get rid of any contaminants. Purging is then carried out using 1 microlitre of the sample vaporised at 300  $^{\circ}\text{C}$  to ensure no acetone is left in the column (Rahman, El-Aty and Shim, 2015; Turner, 2020; Vetter, 2015).

### 3.2.3.9.1 GC/MS analysis of the liquid products from hydrolysis

The method for the analysis of FAMES started with oven temperature at 200 °C and held for 1 min, ramped at 5 °C/min to 250 °C, and then held for 9 mins to give a total of 20 min analysis time. The column used was an RTX-5ms capillary column (ID 0.25mm, 30 m in length) with carrier gas, helium at a flowrate of 15 mL/min. The components of the oils were identified using the NIST library that was installed on the GC.

### 3.2.3.9.2 Quantitative analysis of FAMES

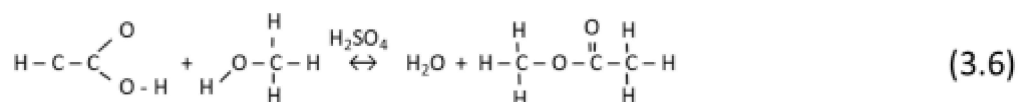
Quantitative analysis is carried out to determine the concentration of the compounds in the hydrolysis product. In order to quantify the fatty acids obtained after hydrolysis on the GC/MS, an external standard method was used with a standard mixture of FAMES. A calibration curve of 100, 250, 500, and 1,000 PPM of each FAME standard was plot against its corresponding peak area to obtain a slope and equation (Equation 3.5) that are used to calculate the unknown concentrations of the samples. The FAME standard compounds included: tridecanoic acid methyl ester, pentadecanoic acid, methyl ester heptadecanoic acid methyl ester, nonadecanoic acid methyl ester, and heneicosanoic acid methyl ester.

$$Y = mx + C \quad (3.5)$$

Where,

Y = concentration of compound; X = peak area; m = intercept; C = constant

### 3.2.3.9.3 Preparation of liquid products from hydrolysis stage by esterification of fatty acids to fatty acid methyl esters for GC/MS analysis



The chemical reaction of carboxylic acids and alcohols in the presence of a catalyst such as sulphuric acid to produce esters is called esterification. The FAMES were prepared based on the adapted method from Kostik at al., (2022). The setup used to achieve this is seen in Figure 3.26. The composition of fatty acid in the rapeseed oil and used cooking oils were identified as their corresponding methyl esters. The method started with dissolving 0.1 - 0.2 g of the oil in 0.2 mol/L H<sub>2</sub>SO<sub>4</sub> prepared in 10ml of anhydrous methanol. Esterification was carried out in a tightly sealed round bottom flask at 100°C for 30 minutes. After the refluxed

sample had cooled to room temperature, 10 ml of petroleum ether (40-60) was added. Next, 10 ml of deionised water was introduced, and gently mixed. The mixture was then allowed to settle until there are two distinct layers. The petroleum ether layer at the top, which contains the FAMES was decanted and analysed on the GC/MS (described in Section 3.2.5.1). The FAMES were compared with standards for identification and quantification.



Figure 3.26: Photo of reflux set up used for esterification

#### 3.2.3.9.3.1 Preliminary tests of GC/MS analysis and quantification method for hydrolysis stage

Preliminary tests were carried out using the methods and equations stated above to confirm the adopted methodology works. Table 3.4 shows the results obtained from analysing known concentrations of FAME standards, and Figure 3.27 shows the chromatogram obtained from the GC/MS. Using the derived equation from the calibration curves drawn, 300  $\mu\text{g}$  and 600  $\mu\text{g}$  of the known FAME standards were each analysed three times and their averages and standard deviations are stated in Table 3.4. The results show the method yielded approximately 2675  $\mu\text{g}$  and 5963  $\mu\text{g}$  in 10 ml from the analysis of the samples respectively. This implies reproducible results, and that the method is viable.

Table 3.4: Preliminary GC/MS analysis results of FAME standards

Retention time (min)	Name	Mass of each component ( $\mu\text{g}$ )	Mass of each component ( $\mu\text{g}$ )
	Nominal mass of FAMES in standard	3000	6000
22.52	Tridecanoic acid, methyl ester	$618.80 \pm 5.77\%$	$1295.78 \pm 5.52\%$
24.96	Pentadecanoic acid, methyl ester	$602.38 \pm 4.16\%$	$1326.61 \pm 6.72\%$
26.83	Heptadecanoic acid, methyl ester	$544.78 \pm 3.85\%$	$1250.25 \pm 7.34\%$
28.38	Nonadecanoic acid, methyl ester	$485.20 \pm 3.57\%$	$1124.53 \pm 8.68\%$
29.83	Heneicosanoic acid, methyl ester	$424.47 \pm 3.91\%$	$1101.39 \pm 9.15\%$
Total mass obtained from analysis		$2675.63 \pm 4.21\%$	$5963.58 \pm 6.86\%$

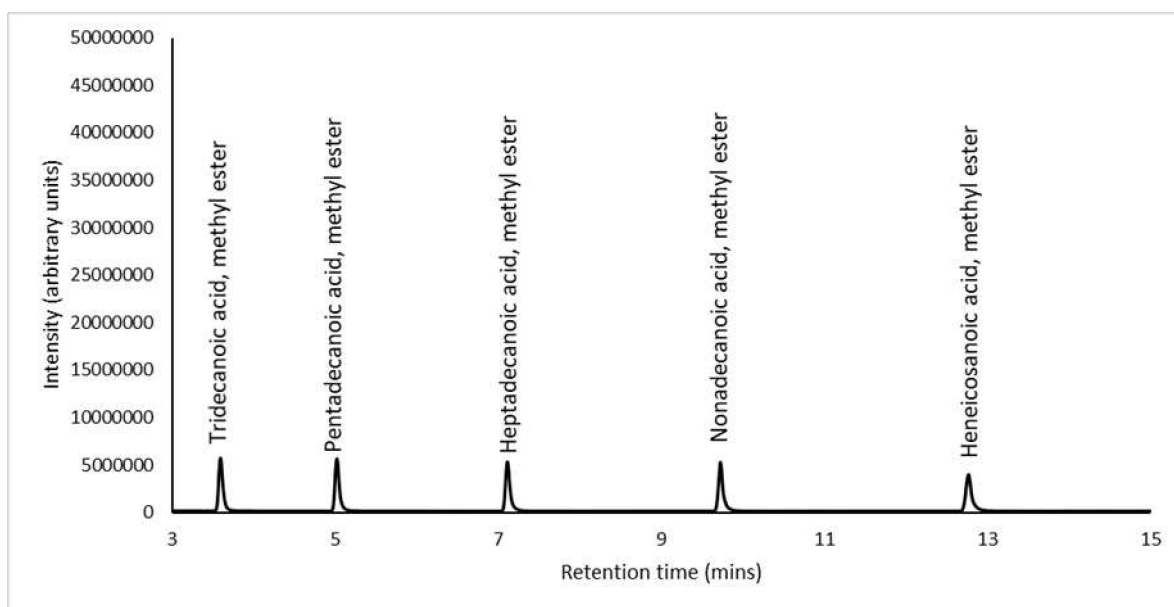


Figure 3.27: GC/MS chromatogram of FAMES standards

#### 3.2.3.9.4 GC/MS analysis of liquid products from decarboxylation and cracking

For the oil products from decarboxylation and cracking stages, the same GC/MS, column, carrier gas, NIST library decompiled in FAMES in Section 3.2.5.1 was used. A different temperature program was used; starting at 50 °C, held for 5 mins, ramped at 8 °C /min to 185 °C, held for 0 min, then ramped at 14 °C/min to 280 °C, and held for 2 mins to give a total of 30.66 min analysis time, as these oils contained lighter compounds that eluted faster. The products were quantified using the internal standard method, using diphenyl ether as the internal standard.



### 3.2.3.9.5 Quantitative analysis of hydrocarbons

For the decarboxylation and cracking stages, an internal standard method was used. This was done to provide improved results and minimise errors that could occur during sample preparation or injections. For the oil products obtained from the decarboxylation and cracking stages, in order to determine the ratio between the desired compound and the internal standard, calibration curves are drawn. A known amount of a standard compound (hexadecane and ortho-xylene in this case) detected in the samples and the internal standard were prepared at concentrations 250 mg/L, 500 mg/L, 750 mg/L, 1,000 mg/L and 2,500 mg/L, respectively. Diphenyl ether was the internal standard used in this research because it consisted of similar physicochemical characteristics as the expected hydrocarbon products but would not react with the compounds or solvent used. The concentration of the internal standard used for the analysis of all samples was 2,500 mg/L. Hexadecane and ortho-xylene were used as external standards as they constantly appeared in the samples. The prepared solutions were injected into the GC/MS. The slope of the peak area against concentration of both the external and internal standards are used to calculate the relative response factor (RRF).

First, a response factor (Equation 3.7), which is defined as the ratio between the peak area and the concentration of the analysed compound was obtained (Slemr et al., 2004).

$$\text{Response Factor} = \frac{\text{Peak area}}{\text{Concentration}} \quad (3.7)$$

This includes the use of another analyte, an internal standard to obtain a relative response factor between the compound in the sample, and the internal standard (Equation 3.8).

$$\text{Relative Response Factor (RRF)} = \frac{\text{Response Factor A}}{\text{Response Factor B}} \quad (3.8)$$

Where A is the known internal standard, and B is the unknown compound.

The conversion of the fatty acids was estimated from the amount of acid present in the sample. The method for calculating the acid yield is described below in Section 3.2.3.6. Therefore, the conversion was calculated from this equation (Equation 3.9):

$$\text{Fatty acid conversion} = \frac{(M_{hp} \times x_{hp}) - (M_{dp} \times x_{dp})}{M_{hp} \times x_{hp}} \quad (3.9)$$

Where:

$M_{hp}$  = mass of hydrolysis product used

$M_{dp}$  = mass of decarboxylated oil

$x_{hp}$  = acid content of hydrolysis product

$x_{dp}$  = acid content of decarboxylated product

The yields of the components in the products from decarboxylation and cracking (Equation 3.10) (Bayu et al., 2018) were calculated using the relative response factor (RRF) of ortho-xylene for compounds with unsaturated compounds and hexadecane for saturated compounds.

$$Yield = conversion \times selectivity$$

(3.10)

#### 3.2.3.9.6 Preparation of liquid products from cracking stage - distillation of cracked oil

The oil product from the cracking stage came out dark in colour, whereas the compounds identified in the GC/MS should be lighter in colour or colourless. Distillation, fractional distillation in particular, is a process commonly used in petroleum refining to obtain different fractions of petroleum according to their boiling points (Giordano et al., 2021). Based on the same principle, the oil product from cracking was distilled using the set-up shown in Figure 3.28 to obtain a clear liquid for further analysis.

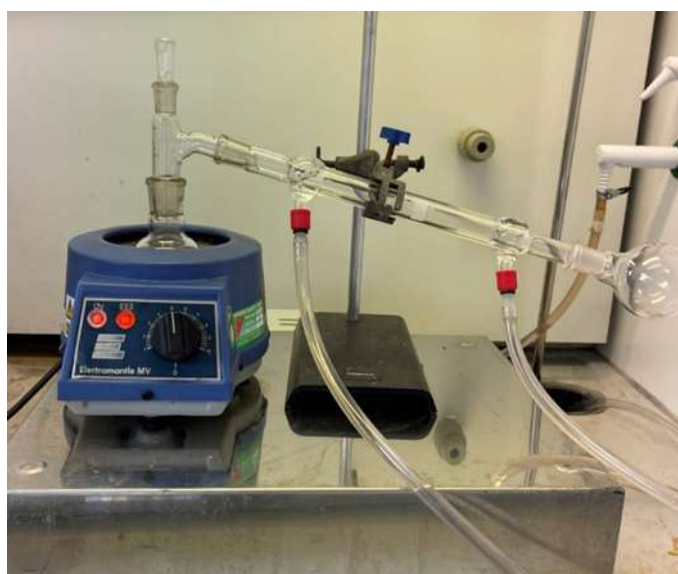


Figure 3.28: Photo of distillation set up

### 3.2.3.9.6.1 Preliminary tests of GC/MS analysis and quantification method for decarboxylation and cracking stages

Table 3.5 presents the results from running two standard samples containing 1500 ug and 3000 ug of each of o-xylene and heptadecane respectively. Figure 3.29 shows the GC/MS chromatogram obtained from this analysis. These samples were each injected three times, and their averages and standard deviations are shown in Table 3.5. The results suggest that the method was accurate in determining the concentrations of components in the prepared samples.

Table 3.5: Preliminary GC/MS analysis results of hydrocarbon standards

Retention time (min)	Name	Mass of each component ( $\mu\text{g}$ )	Mass of each component ( $\mu\text{g}$ )
Total mass obtained from analysis		$3089.55 \pm 3.34\%$	$5901.59 \pm 2.79\%$
Nominal mass of each compound in standard		1500	3000
7.43	o-Xylene	$1516.67 \pm 1.36\%$	$2910.94 \pm 3.15\%$
23.50	Heptadecane	$1572.88 \pm 5.26\%$	$2990.65 \pm 3.08\%$

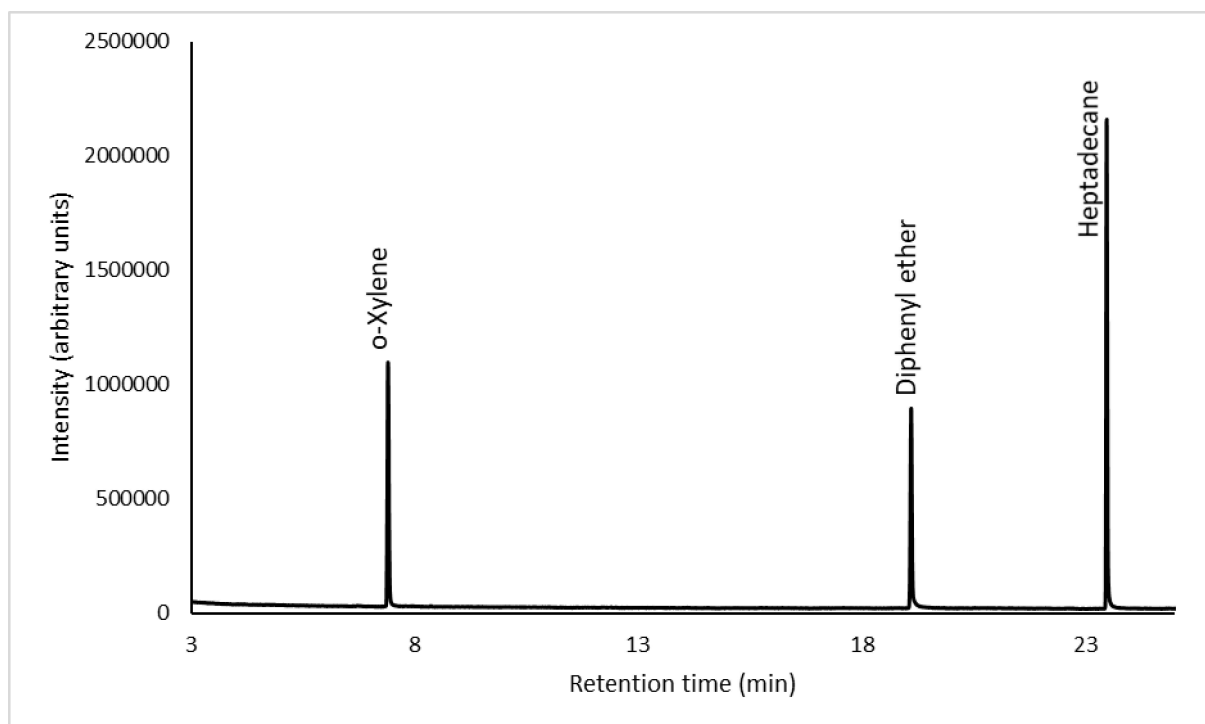


Figure 3.29: GC/MS chromatogram of hydrocarbon standards containing 3000 ug of each compound

### 3.2.3.10 Quantitation of fatty acids in hydrolysis and decarboxylation products by titration



Figure 3.30: Photo of titration setup used

Due to the formation of FFA during the hydrolysis step and the possibility of following the extent of FFA conversion at the decarboxylation stage, an acid-base titration method was developed and used in this work (Figure 3.30). This was a slight modification of the Official Method as described below (Analytical Methods, 1998; Commission Regulation (EEC) No 2568/91, 1991).

#### 3.2.3.10.1 Official method for fatty acid determination

AOCS: Cd-3a-63 (American Oil Chemists' Society) describes the standard procedure to determine the free fatty acid content in oil samples based on the acid-base titration technique. The sample dissolved in a given solvent is titrated against 0.1 N NaOH with phenolphthalein indicator.

The amount of FFA is calculated using Equation (3.11):

$$Fatty\ acid\ yield = \frac{(B-S) \times N \times M}{W}$$

(3.11)

Where,

S = base volume used in titration of sample (mL)

B = base volume used in titration of blank(mL)

N = normality(concentration) of base

W = weight of sample

M = molecular mass of fatty acid (282.5 g/mol for oleic acid)

#### 3.2.3.10.2 Modified fatty acid determination method

Due to the different fatty acids present after the hydrolysis of oil sample, the official method was modified to obtain results. The adjustment to this official method includes back titration with a known amount and concentration of acid, 0.1N hydrochloric acid is shown in Equation (3.12).

$$\text{Fatty acid yield: } \frac{(B - S) \times N \times M}{10 \times W}$$

(3.12)

Where,

B = volume of NaOH used in titration of blank (mL)

S = volume of NaOH used in titration of sample (mL)

N = concentration of NaOH used (mol/L)

W = weight of sample (g)

M = molecular mass of fatty acid (282.5 g/mol for oleic acid)

A blank titration was run initially to confirm the null effect of the solvent, DCM, and absence of fatty acids on the results. Following the titration run with blanks the procedure was repeated, with the hydrolysed sample.

#### 3.2.3.10.3 Validation of fatty acid contents by acid-base titration

The titration method developed for the analysis of fatty acids was tested on the vegetable oil and pure oleic acid to validate that it was fit for purpose. The titrations were carried out 3 times each, and averages reported. The standard deviation obtained for the titration of each

sample was less than 1 % (Table 3.6), showing the accuracy of the method to quantify fatty acids (Figure 3.31). Rapeseed oil was found to contain about 0.68 wt% free fatty acids by acid-base titration, whereas 100 wt% of oleic acid was accounted for.

The results of acid-base titration of the hydrothermal hydrolysis experiments carried out three times at 300 °C, are presented in Table 3.7. The results obtained through titration analysis represented the fatty acid yields. The highest yield obtained was 97.8% but the standard deviation being less than 1% implied the method used was repeatable and reliable giving very minimal systematic error. These results matched closely the results of GC/MS analysis FAMES that were prepared from the hydrolysis products in Section 3.2.3.9.1.

Table 3.6: Results from repeatability tests on the acid-base titration of hydrolysis products

	Test 1	Test 2	Test 3
Start	0.4	23.1	9.7
End	23.1	45.6	32.3
Titre (mL)	22.7	22.5	22.6

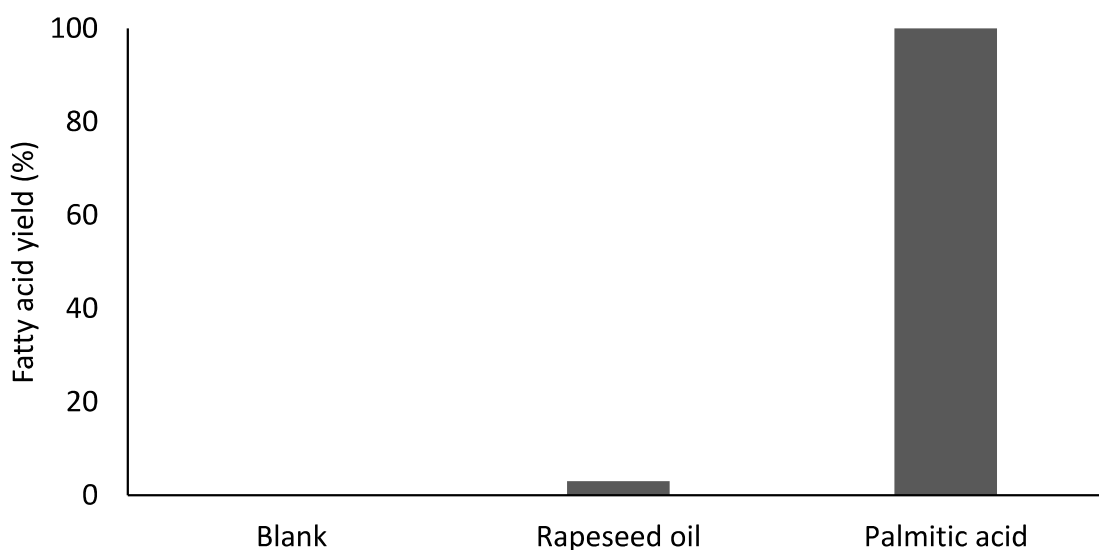


Figure 3.31: Results from fatty acid determination with acid-base titration method

Table 3.7: Reproducibility of acid-base titration using products from hydrolysis stage

Run	Mass of oil (g)	Mass of H <sub>2</sub> O (g)	Time of reaction (h)	FFA yield (%)
1	10	20	1	96.5
2	10	20	1	97.1
3	10	20	1	97.8
4	10	20	1	97.3
Average				97.18
SD %				±0.54

SD = Standard Deviation

Table 3.8: Reproducibility of acid-base titration using products from decarboxylation stage

Run	Mass of oil (g)	Mass of catalyst (g)	Time of reaction (h)	FFA yield (%)
1	10	2	1	2.06
2	10	2	1	2.44
3	10	2	1	2.74
4	10	2	1	2.33
Average				2.39
SD %				±0.28

SD = Standard Deviation

Repeatability of the acid-base determination of unconverted fatty acids during the decarboxylation stage was carried out using liquid samples obtained with Pt/C as catalyst at 400 °C. The titration was carried out four times and the results are presented in Table 3.8. The average yield obtained was 2.39%, and the standard deviation was less than 0.5%, which implied that the method was reliable to monitor the process of fatty acid conversion during decarboxylation. These results matched the GC/MS analysis results of the decarboxylated products which showed more than 97 wt% yields of hydrocarbons, thereby indicating that they contained low concentrations of unconverted fatty acids.

### 3.2.3.11 Elemental analysis of liquid products

#### 3.2.3.11.1 Elemental analysis by CHNS

A Flash 2000 Elemental analyser (Figure 3.32) was used to quantify the amount of carbon, hydrogen, nitrogen, sulphur, and oxygen (calculated by difference) in the main organic products obtained from hydrolysis, decarboxylation, and cracking tests. The same equipment was used for the feedstocks according to the ASTM D5291 Standard Method (ASTM D5291-21, 2021). In the procedure, sample masses used were within the range of 2-3 mg. The equipment was capable of analysing both semisolid and solid samples. The operating principle was adopted from the Pregl Dumas method which involved the combustion of the sample at about 1000 °C to gas (Shah, Pansare and Mulay, 1956). The combustion of carbon produced carbon dioxide, nitrogen converted to oxides of nitrogen, hydrogen to water, and sulphur to sulphur dioxide. Helium was used as the carrier gas to sweep the combustion gases into the chromatographic column for detection on the thermal conductivity detector.



Figure 3.32: Photo of CHNS equipment used

This detection occurred simultaneously with the determination of the CHNS compositions in the mixture being proportional to the output signal detected. The type of sample determined how the sample was prepared before being placed in the equipment. Liquid samples, used in this project, were adsorbed on an adsorbent pad (Figure 3.33a) then weighed out into tin crucibles (Figure 3.33b), while solid samples after being weighed were directly placed into the tin crucibles. Vanadium Pentoxide (Figure 3.33c) was added in both cases as a catalyst to help achieve complete combustion of the samples. To test the proper functioning of the equipment, a standard, sulphanilamide (Figure 3.33d), with known CHNS concentrations was analysed in triplicates (Table 3.9), and the results obtained correlated with the expected known CHNSO compositions.



(a)



(b)



(c)



(d)

Figure 3.33: Photos of materials used for CHNS analysis of oil products; (a) adsorbent pads b) tin crucibles c) vanadium pentoxide d) sulphanilamide



Table 3.9: Results of testing standard on CHNS equipment

Sample	Nitrogen (wt%)	Carbon (wt%)	Hydrogen (wt%)	Sulphur (wt%)	Oxygen (wt%)
Standard test 1	16.27	41.84	4.68	18.62	18.59
Standard test 2	16.27	41.84	4.68	18.62	18.59
Standard test 3	16.16	41.88	4.70	18.76	18.50

Dulong's formula was used to estimate the HHV of the oils (Equation 3.13) (Hosokai, Matsuoka, Kuramoto and Suzuki, 2016).

$$HHV (MJ/kg) = 0.3383C + 1.443(H - (O/8)) + 0.0942S \quad (3.13)$$

where C, H, O and S are the wt% composition of carbon, hydrogen, oxygen, and sulphur, respectively.

#### 3.2.3.11.2 Elemental analysis by GC/MS

Results from typical CHNS analyses of oil samples gave large variations in the elemental compositions. Indeed, results from analyses of cracking products still shown significant oxygen content, even though no oxygenated compounds were identified via GC/MS analysis. Hence, it was observed that the CHNS analyses were being affected by the volatility of the compounds in the liquid samples. Basically, the time lag between when the samples were weighed out and placed into the analyzer sample holder and the actual time when they were analysed, allowed significant amounts of volatile compounds to escape. However, there was no direct way of accounting for such losses given that the mass of the samples had already been recorded and entered into the software just after the samples were weighed. Hence, the software subsequently used the entered weights to calculate the CHNS compositions, which led to the significant errors observed.

To resolve this, a novel GC/MS method was developed in this project to give a better result for the elemental compositions of the oil products. To develop and validate this new method, three solvent-free mixtures of different hydrocarbons were prepared as shown in Table 3.10.

Six samples of each mixture were prepared and three samples of each used for elemental analyses with CHNS analyser (Method 1) and the GCMS analysis (Method 2), respectively. The GC/MS analyses were carried out by the internal standard method described in Section

3.2.3.9.5. The elemental compositions of the three mixtures via the GC/MS method were calculated using Equations 3.14 and 3.15.

Table 3.10: Solvent-free mixtures of hydrocarbons for elemental analysis by CHNS analyser and GC/MS method (0.1 g of each compound used in each mixture)

Heavy hydrocarbons (Mixture 1)	Light hydrocarbons (Mixture 2)	Combined light and heavy hydrocarbons (Mixture 3)
Hexadecane,	Ortho-xylene	Ortho-xylene
Heptadecane	Toluene	Toluene
Octadecane	Decane	Decane
		Hexadecane
		Heptadecane
		Octadecane

$$\text{Carbon composition, } C \text{ wt\%} = \sum \frac{M_{C,i} \times Y_i}{Mr_i} \quad (3.14)$$

$$\text{Hydrogen composition, } H \text{ wt\%} = \sum \frac{M_{H,i} \times Y_i}{Mr_i} \quad (3.15)$$

Where:

$M_{C,i}$  = number of carbon atoms in compound  $i$   $\times$  12.001

$M_{H,i}$  = number of hydrogen atoms in compound  $i$   $\times$  1.008

$Y_i$  = Yield of compound  $i$  in a given Mixture from GC/MS analysis

$Mr_i$  = Molecular mass of compound  $i$  in the given Mixture for GC/MS analysis

At the end of the two sets of analyses, the averages and standard deviations values were calculated and reported. In addition, the theoretical elemental compositions of each mixture were calculated (Method 3) based on the molecular formular of each compound and their mass fractions in the mixtures according to Equations 3.16 – 3.19.

$$\text{Theoretical carbon composition in a given Mixture} = \sum C \text{ wt\%}_i \times x_i \quad (3.16)$$

$$\text{Theoretical Hydrogen composition in a given Mixture} = \sum H \text{ wt}\%_i \times x_i \quad (3.17)$$

$$C \text{ wt}\%_i = \frac{\text{No. of carbon atoms in compound } i \times 12.001 \times 100}{\text{Mr of compound } i} \quad (3.18)$$

$$H \text{ wt}\%_i = \frac{\text{No. of hydrogen atoms in compound } i \times 1.008 \times 100}{\text{Mr of compound } i} \quad (3.19)$$

$x_i$  = mass fraction of compound  $i$  in a given Mixture

The results from the two analytical methods and the calculated values from Method 3 are presented in Table 3.11. The results show that the CHNS analyser generated unrealistic results. For instance, all the compounds used in the mixtures were hydrocarbons (made up of carbon and hydrogen atoms only) but the CHNS analyser (Method 1) reported high oxygen contents in mixtures containing lower molecular weight hydrocarbons (Mixture 2 and Mixture 3). Such default results occurred because oxygen is calculated by difference during standard CHNS analysis. Hence, the volatile losses led to lower carbon and hydrogen contents and the differences were reported as oxygen contents.

Table 3.11: Comparison between elemental analysis by CHNS and GC-MS

Standards	Analysis	Elemental composition				
		C (wt %)	H (wt %)	N (wt %)	S (wt %)	O (wt %)
Mixture 1	Method 1	84.02 ± 0.23	15.41 ± 0.02	0.20 ± 0.00	0	0.47 ± 0.22
	Method 2	86.05 ± 0.49	13.95 ± 0.21	0	0	0
	Theoretical	86.10	13.90	0	0	0
Mixture 2	Method 1	71.53 ± 14.76	11.89 ± 0.02	0.10 ± 0.02	0	16.48 ± 17.95
	Method 2	86.94 ± 0.80	13.06 ± 0.11	0	0	0
	Theoretical	88.79	11.21	0	0	0
Mixture 3	Method 1	64.20 ± 6.11	11.35 ± 1.02	0.11 ± 1.02	0	24.33 ± 7.10
	Method 2	85.73 ± 0.58	14.27 ± 0.15	0	0	0
	Theoretical	86.90	13.10	0	0	0

Interestingly, there were good matches between the elemental compositions of the Mixture 1, which contained long chain hydrocarbon from all three methods. Hence, due to their low-volatility, losses during waiting time for CHNS analyses were minimal, if at all. This confirmed

that the standard CHNS analyser was compatible with solid and non-volatile samples. In contrast, the results from the GC/MS gave very good similarities with those calculated using Method 3 for all three Mixtures. Hence, the GC/MS was able to produce representative elemental composition data for both volatile and semi-volatile hydrocarbons. Therefore, Method 2 was used to produce the CHNS data for samples deemed to contain volatile compounds, where the standard CHNS analyser failed to give realistic results.

#### 3.2.3.12 Analysis of liquid product by thermogravimetric analysis (TGA)

In a TGA analysis, a sample is heated incrementally in a furnace while its weight is recorded on an analytical balance that is kept outside the furnace. Figure 3.34 shows a schematic of the principle of operation of a TGA. The apparatus can measure a wide range of temperatures from 25 – 1200 °C. To depict thermal transitions in the material such as decomposition of the material, the sample weight is plotted versus time or temperature.

There are three variations of thermogravimetry. Dynamic TGA, a sample is heated linearly as the temperature rises and the change in mass recorded. Static TGA, at constant temperature, the sample weight is recorded as a function of time. While quasistatic TGA, temperature is elevated at intervals and the sample is heated to a constant weight. Even though TGA mostly accounts for losses in weight through kinetic processes like decomposition, evaporation, desorption, and reduction, there could also be weight gain through mechanisms like oxidation, absorption, and adsorption (Fedelich, 2019).



Figure 3.34: Photo of TGA used in this study

TGA analyses of the semi-solid product from hydrolysis stage was carried out using a Mettler Toledo Thermal Analysis TGA/DSC 2 Star System (Figure 3.34). The crucible that was used

to hold the sample was heated at heating rate of 10 °C/min from 25 °C to 1000 °C, using 30 mL/min of N<sub>2</sub> as a flow gas.

### 3.2.3.13 Characterisation of catalysts by nitrogen adsorption porosimetry

Nitrogen porosimetry can estimate the pore volumes by condensing nitrogen into the pores of the analyte and calculating the amount of gas used to fill the pores. At the boiling point of nitrogen (-196°C), the amount of gas that has been adsorbing onto the surface of the particles is measured. The amount of gas adsorbed is influenced by the exposed surface area as well as by temperature, gas pressure, and the degree of gas-solid interaction. The nitrogen gas condenses on the surface of the particles because it is below the critical temperature at this temperature (Westermarck, 2000). The quantity of gas adsorbed correlates with the entire surface area of the particles, including pores at the surfaces. Due to the known size of the molecule, it is assumed that the gas undergoes condensation at the surface in a monolayer (Bae, Yazaydin and Snurr, 2010; Brunauer, Emmett and Teller, 1938). This correlation between the adsorbed volume and the surface area is expressed in the BET equation (Equation 3.20).

$$\frac{p}{v(p_0 - p)} = \frac{1}{v_m c} + \left( \frac{c - 1}{v_m c} \right) X \left( \frac{p}{p_0} \right) \quad (3.20)$$

Where  $p$  is the pressure of the adsorbate,  $p_0$  is the saturation pressure,  $v$  is the quantity of adsorbed gas,  $v_m$  is the capacity of the monolayer, and  $c$  is the BET constant. BET is an extended version of the Langmuir model from monolayer adsorption to multilayer adsorption

To determine  $v_m$ , the BET equation is plotted against relative pressure ( $p/p_0$ ) in the range 0.025 - 0.30. The linear positive slope obtained when the graph is plotted in this range means the BET method was sufficient in obtaining the surface area. The  $v_m$  found from the gradient of the graph is then used to calculate the specific surface area (Equation 3.21)

$$SSA = \frac{v_m N_A S A_c}{V m} \quad (3.21)$$

Where  $N_A$  is Avogadro's number,  $S A_c$  is the adsorption cross section of the adsorbate (0.162 nm<sup>2</sup> for adsorbed nitrogen molecule),  $V$  is the molar volume of nitrogen, the adsorbate (22.4L), and  $m$ , the mass of the sample.

The use of nitrogen adsorption for pore size analysis is based on the Kelvin equation (Equation 3.22). Barrett, Joyner and Halenda (BJH) is the most common method used to obtain volume pore size distribution from an appropriate nitrogen isotherm. This method distinguishes pore size distribution irrespective of the exterior area due to the particle size of the sample (Barrett, Joyner and Halenda, 1951).

$$r_p = \frac{2\gamma V_{liq} \cos\theta}{RT \left( \ln \frac{p}{p_0} \right)} \quad (3.22)$$

Where  $r_p$  is the pore radius,  $\gamma$  is the surface tension of the liquid,  $V_{liq}$  is the molar volume of the liquid,  $\theta$  is the contact angle,  $R$  is the universal gas constant, and  $T$  is the absolute temperature.



Figure 3.35: Photo of nitrogen adsorption used

In this project, the measurements were performed on a Quantachrome NOVA 4000e surface area and pore size analyser, and the Quantachrome NovaWin software installed on the computer was used to collect the resulting data (Figure 3.35).

Prior to the analysis, but after weighing, the sample was degassed under vacuum at 120 °C for 5 - 6 h as pre-treatment to remove any contaminants. Pre-treatment settings must be tailored to the properties of the materials as using temperature too low or too high might significantly alter the BET surface area obtained from the following BET analysis. The sample was reweighed after cooling in order to account for any mass loss during degassing.

#### 3.2.3.14 Analysis of catalyst by x-ray diffraction

X-ray diffraction (XRD) is a method for determining the atomic and molecular structure of a substance. This non-destructive method functions best on fully or partially crystalline materials. The technique is frequently referred to as "X-ray powder diffraction" because the substance being examined is frequently uniformly processed to a fine powder. The bending of light upon striking an aperture, or the edge of an object is known as diffraction. The extent to which diffraction occurs is determined by the size of the wavelength in relation to the size of the aperture. A subset of the overall X-ray scattering phenomenon is the X-ray diffraction, which is essential to the XRD method. Wide-angle X-ray diffraction (WAXD) is one of numerous techniques that employ elastically scattered X-ray photons. Small angle X-ray scattering (SAXS) is another elastic scattering-based X-ray technique, where the X-rays are incident on the sample throughout the narrow angular range of generally 0.1-100, while beyond 100 angular range is covered by WAXD (Experimental studies of crystal structures. X-ray diffraction, 2004).



Figure 3.36: Photo of XRD used

The applications of XRD include measuring the thickness of thin films and multi-layers, identifying crystalline orientation, phases, and identifying the structural properties of the crystal such as epitaxy, grain size, lattice parameters, phase composition, preferred orientation, and strain (Banerjee, 2022).

The samples were loaded into a polymethyl methacrylate (PMMA) sample holder, with their surfaces flattened out using a glass microscope slide. They are analysed in a Bruker D8 Advance Bragg-Brentano, fitted with a Lynxeye P8D detector and CuK $\alpha$  radiation (40kV and 40mA, 0.2mm Nik $\beta$  absorber, 2.5° Soller slits, 10° - 80° 2 $\Theta$  range, virtual step scan of 0.02° 2 $\Theta$ , virtual time per step of 1 or 8s (Figure 3.36). Göbel mirror, 0.2mm and 2.5° Soller slits were in the parallel beam geometry and used to carry out XRD measurements, in-situ, with an Anton-Paar XRK-900 reaction chamber. A virtual step scan of 2 $\Theta$  = 0.02° and virtual per step of 2s in a flowing 20%H<sub>2</sub>/80%He atmosphere were used to collect the resulting diffractograms.

### 3.3 Computation of mass balances

The product distribution consisted of gas, solid, and liquid products from all the experiments (except for hydrolysis, which did not produce any gas). The solid was obtained after separation by filtration and dried as described in Section 3.2.3.1 and Section 3.2.3.2. The masses and yields of the solid products were calculated using Equations 3.24 and 3.25, assuming the mass of catalyst did not change.

$$\text{Mass of solid} = M_{cpp} - (M_c + M_{fp}) \quad (3.24)$$

$M_{cpp}$  = mass of dried catalyst and filter paper after reaction

$M_c$  = mass of catalyst used for reaction

$M_{fp}$  = mass of filter paper

$$\text{Yield of solid} = \frac{\text{mass of solid}}{\text{mass of feedstock}} \quad (3.25)$$

The liquid products obtained from hydrolysis was weighed after drying, and those from the decarboxylation and cracking stages were measured after driving of the solvent, DCM (Section 3.2.3.1.2). The masses and yields of the liquid products were calculated using Equations 3.26, 3.27, 3.28 and 3.29, respectively.



$$\text{Mass of hydrolysis product (fatty acids)} = M_{Lh} - (M_w + M_{sol}) \quad (3.26)$$

Where,

$M_L$  = total mass of hydrolysed liquid products and solvent collected from reactor

$M_w$  = mass of separated aqueous phase

$M_{sol}$  = mass of solvent used for extaction

$$\text{Mass of liquid product from decarboxylation} = M_{Ld} - M_{sol} \quad (3.27)$$

$$\text{Mass of liquid product from cracking} = M_{Lc} - M_{sol} \quad (3.28)$$

Where,

$M_{Ld}$  = total mass of liquid organic products and solvent from decarboxylation

$M_{Lc}$  = total mass of liquid organic products and solvent from cracking

$$\text{Yield of liquid} = \frac{\text{mass of liquid}}{\text{mass of feedstock}} \quad (3.29)$$

Note: feedstock for the hydrolysis stage was vegetable oil, decarboxylation was hydrolysis product (mostly fatty acids), and cracking was decarboxylation liquid product (mostly hydrocarbons).

The gas product was collected in a gas bag (Figure 3.13) and quantified using equations 3.2-3.4 in Section 3.2.3.4.4. The yields of the gases were calculated using Equation 3.30.

$$\text{Yield of gas} = \frac{\text{mass of gas}}{\text{mass of feedstock}} \quad (3.30)$$

Figure 3.37 presents the results of preliminary mass balances from each of the three stages used in the conversion of the RSO into fuel range liquid hydrocarbons. In each case, products were analysed three times using the respective analytical tools and techniques described in previous Sections. The results of the analysis were further used to compute mass balanced based on Equations 3.24 to 3.30. Figure 3.40 shows that all the experiments and calculations gave good mass balance closures with low standard deviations. While the mass balances of the products from hydrolysis approached 100%, those from decarboxylation and cracking were around 85%, due to the production of highly volatile light hydrocarbon compounds in the oil products. In addition, some larger gas compounds were observed in the GC chromatograms but could not be identified and quantified. However, the low standard deviations indicate that the results were repeatable and therefore acceptable for these types of analysis.

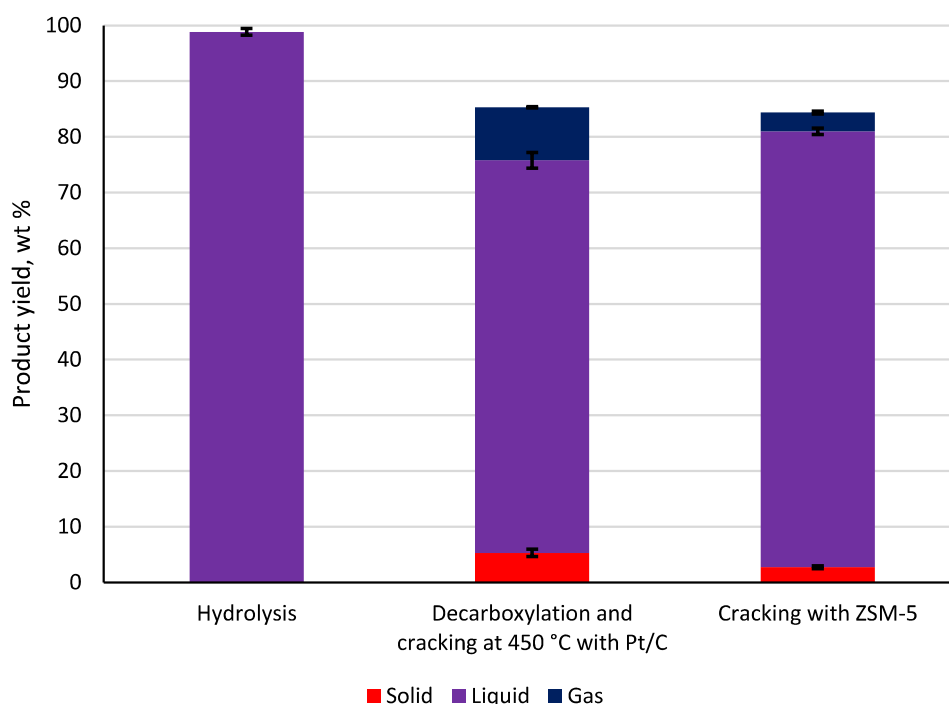


Figure 3.37: Repeatability results on yield of products from each process stage

Overall, the research methodology used in this work was carefully planned and implemented. The results produced were repeatable, reliable and acceptable. These results provided sufficient confidence in the analytical techniques and skills that were used throughout the research to produce the results presented in subsequent chapters.

### 3.4 References

- Alam, M. (2019) "Fat and oil (food)," AccessScience [Preprint]. Available at: <https://doi.org/10.1036/1097-8542.251400>.
- "Analytical Methods" (1998) *Fats and Oils Handbook*, pp. 803–808. Available at: <https://doi.org/10.1016/b978-0-9818936-0-0.50014-7>.
- ASTM D5291-21 (2021) "Test methods for instrumental determination of carbon, hydrogen, and nitrogen in petroleum products and Lubricants." Available at: <https://doi.org/10.1520/d5291-21>.
- ASTM D5355 – 95 (1995) "Standard Test Method for Specific Gravity of Oils and Liquid Fats." Available at: <https://allcivilstandard.com/wp-content/uploads/2018/12/D-5355.pdf>. Bae, Y.-S., Yazaydin, A.Ö. and Snurr, R.Q. (2010) "Evaluation of the BET Method for Determining Surface Areas of MOFs and Zeolites that Contain Ultra-Micropores," *Langmuir*, 26(8), pp. 5475–5483. Available at: <https://doi.org/10.1021/la100449z>.
- Banerjee, D. (2022) X-Ray Diffraction (XRD). Department of Chemical Engineering IIT Kanpur. Available at: <https://www.iitk.ac.in/che/pdf/resources/XRD-reading-material.pdf> (Accessed: 2022).
- Barrett, E.P., Joyner, L.G. and Halenda, P.P. (1951) "The Determination of Pore Volume and Area Distributions in Porous Substances. I. Computations from Nitrogen Isotherms," *Journal of the American Chemical Society*, 73(1), pp. 373–380. Available at: <https://doi.org/10.1021/ja01145a126>.
- Bayu, A., Yoshida, A., Karnjanakom, S., Kusakabe, K., Hao, X., Prakoso, T., Abudula, A., and Guan, G. (2018). Catalytic conversion of biomass derivatives to lactic acid with increased selectivity in an aqueous tin(ii) chloride/choline chloride system. *Green Chemistry*, 20(17), 4112–4119. <https://doi.org/10.1039/c8gc01022f>.
- Brunauer, S., Emmett, P.H. and Teller, E. (1938) "Adsorption of Gases in Multimolecular Layers," *Journal of the American Chemical Society*, 60(2), pp. 309–319. Available at: <https://doi.org/10.1021/ja01269a023>.
- "Commission Regulation (EEC) No 2568/91" (1991) EUR-Lex [Preprint]. Available at: <https://eur-lex.europa.eu/legal-content/EN/TXT/PDF/?uri=CELEX:01991R2568-20161204&from=IT> (Accessed: 2020).
- Control Tutorials for MATLAB and Simulink - Introduction: PID Controller Design (2020) [Ctms.engin.umich.edu](http://ctms.engin.umich.edu). Available at: <http://ctms.engin.umich.edu/CTMS/index.php?example=Introduction&ion=ControlPID#1> (Accessed: 2020).

- Crawford, J. M., Zaccarine, S. F., Kovach, N. C., Smoljan, C. S., Lucero, J., Trewyn, B. G., Pylypenko, S., and Carreon, M. A. (2019). Decarboxylation of stearic acid over Ni/MOR catalysts. *Journal of Chemical Technology and Biotechnology*, 95(1), 102–110. <https://doi.org/10.1002/jctb.6211>.
- Domingues, P.M.D.N., García, A.G. and Skrzydlewska, E. (2018) *Advanced analytical chemistry for life sciences*. [Białystok]: [Uniwersytet Medyczny].
- Dourado, M., Fonseca, N., Fréty, R., and Sales, E. (2022). Fast Catalytic Pyrolysis of Tetradecanoic Acid: Formation of Ketones as Intermediate Compounds in the Production of Hydrocarbons. *Journal of the Brazilian Chemical Society*. <https://doi.org/10.21577/0103-5053.20220056>.
- “Evaluation of analytical instrumentation. Part XIX CHNS elemental analysers” (2006) *Accreditation and Quality Assurance*, 11(11), pp. 569–576. Available at: <https://doi.org/10.1007/s00769-006-0185-x>.
- “Experimental studies of crystal structures. X-ray diffraction” (2004) *Minerals*, pp. 117–133. Available at: <https://doi.org/10.1017/cbo9780511811296.009>.
- Fedelich, N. (2019) “TGA-GC/MS,” *Evolved Gas Analysis*, pp. 31–39. Available at: <https://doi.org/10.3139/9781569908105.004>.
- Giordano, G. F., Vieira, L. C. S., Gomes, A. O., de Carvalho, R. M., Kubota, L. T., Fazzio, A., Schleder, G. R., Gobbi, A. L., and Lima, R. S. (2021). Distilling small volumes of crude oil. *Fuel*, 285, 119072. <https://doi.org/10.1016/j.fuel.2020.119072>.
- Gröger, T.M., Käfer, U. and Zimmermann, R. (2020) “Gas chromatography in combination with fast high-resolution time-of-flight mass spectrometry: Technical overview and perspectives for data visualization,” *TrAC Trends in Analytical Chemistry*, 122, p. 115677. Available at: <https://doi.org/10.1016/j.trac.2019.115677>.
- Hosokai, S., Matsuoka, K., Kuramoto, K., and Suzuki, Y. (2016). Modification of Dulong's formula to estimate heating value of gas, liquid and solid fuels. *Fuel Processing Technology*, 152, 399–405. <https://doi.org/10.1016/j.fuproc.2016.06.040>.
- Kostik, V., Memeti, S. and Bauer, B. (2022) “Fatty acid composition of edible oils and fats,” *Journal of Hygienic Engineering and Design* [Preprint].
- Kumar, R., Strezov, V., Kan, T., Weldekidan, H., He, J., and Jahan, S. (2019). Investigating the Effect of Mono- and Bimetallic/Zeolite Catalysts on Hydrocarbon Production during Bio-oil Upgrading from Ex Situ Pyrolysis of Biomass. *Energy and Fuels*, 34(1), 389–400. <https://doi.org/10.1021/acs.energyfuels.9b02724>.
- Moser, B. R., Knothe, G., Walter, E. L., Murray, R. E., Dunn, R. O., and Doll, K. M. (2016). Analysis and Properties of the Decarboxylation Products of Oleic Acid by Catalytic

Triruthenium Dodecacarbonyl. *Energy and Fuels*, 30(9), 7443–7451.

<https://doi.org/10.1021/acs.energyfuels.6b01728>.

Neonufa, G. F., Elizabeth, L., Puspawiningtiyas, E., Pratiwi, M., Istyami, A. N., Purwadi, R., and Soerawidjaja, T. H. (2021). Comparison of Liquid Product Characteristics of PFAD Metal Soap Decarboxylation by Batch and Continuous Process. *Journal of Engineering and Technological Sciences*, 53(3), 210311.

<https://doi.org/10.5614/j.eng.technol.sci.2021.53.3.11>.

Nitbani, F. O., Tjitda, P. J. P., Nurohmah, B. A., and Wogo, H. E. (2020). Preparation of Fatty Acid and Monoglyceride from Vegetable Oil. *Journal of Oleo Science*, 69(4), 277–295.

<https://doi.org/10.5650/jos.ess19168>

PID Controller (2020) EIProCus - Electronic Projects for Engineering Students. Available at: <https://www.elprocus.com/the-working-of-a-pid-controller/> (Accessed: 2020).

PID Theory Explained - National Instruments (2020) Ni.com. Available at:

<https://www.ni.com/en-gb/innovations/white-papers/06/pid-theory-explained.html> (Accessed: 2020).

Rahman, M.M., El-Aty, A.M.A. and Shim, J.-H. (2015) “Overview of Detectors in Gas Chromatography,” *Analytical Separation Science*, pp. 835–848. Available at:

<https://doi.org/10.1002/9783527678129.assep025>.

Razaq, I., Simons, K.E. and Onwudili, J.A. (2021) “Parametric study of PT/c-catalysed hydrothermal decarboxylation of butyric acid as a potential route for biopropane production,” *Energies*, 14(11), p. 3316. Available at: <https://doi.org/10.3390/en14113316>.

Rockwood, A.L., Kushnir, M.M. and Clarke, N.J. (2018) “Mass Spectrometry,” *Principles and Applications of Clinical Mass Spectrometry*, pp. 33–65. Available at:

<https://doi.org/10.1016/b978-0-12-816063-3.00002-5>.

Saitman, A. (2019) “Overview of Analytical Methods in Drugs of Abuse Analysis,” *Critical Issues in Alcohol and Drugs of Abuse Testing*, pp. 157–171. Available at:

<https://doi.org/10.1016/b978-0-12-815607-0.00013-7>.

Salimon, J., Abdullah, B. M., and Salih, N. (2011). Hydrolysis optimization and characterization study of preparing fatty acids from *Jatropha curcas* seed oil. *Chemistry Central Journal*, 5(1). <https://doi.org/10.1186/1752-153x-5-67>

Shah, G.D., Pansare, V.S. and Mulay, V.N. (1956) “A modified micro-dumas method for rapid determination of nitrogen,” *Mikrochimica Acta*, 44(7-8), pp. 1140–1143. Available at:

<https://doi.org/10.1007/bf01257446>.

Slemr, J., Slemr, F., D'Souza, H., and Partridge, R. (2004). Study of the relative response factors of various gas chromatograph–flame ionisation detector systems for measurement of

C2–C9 hydrocarbons in air. *Journal of Chromatography A*, 1061(1), 75–84.

<https://doi.org/10.1016/j.chroma.2004.10.037>.

Sorigué, D., Légeret, B., Cuiné, S., Morales, P., Mirabella, B., Guédeney, G., Li-Beisson, Y., Jetter, R., Peltier, G., and Beisson, F. (2016). Microalgae Synthesize Hydrocarbons from Long-Chain Fatty Acids via a Light-Dependent Pathway. *Plant Physiology*, 171(4), 2393–2405. <https://doi.org/10.1104/pp.16.00462>.

Spangler, G.E. (2015) “Gas Chromatography: Theory and Thermodynamics, and Selectivity,” *Analytical Separation Science*, pp. 775–806. Available at: <https://doi.org/10.1002/9783527678129.assep022>.

Specifications - Parr Instrument Company (n.d.) Parr Instrument Company. Available at: <https://www.parrinst.com/products/controllers/4848-reactor-controller/specifications/> (Accessed: 2020).

Stauffer, E., Dolan, J.A. and Newman, R. (2008) “Chemistry and physics of fire and liquid fuels,” *Fire Debris Analysis*, pp. 85–129. Available at: <https://doi.org/10.1016/b978-012663971-1.50008-7>.

Torres, D.J. (2016) *Carrying You Through Gas Chromatography*.

Turner, D.D. (2020) *Gas Chromatography – How a Gas Chromatography Machine Works, How To Read a Chromatograph and GCxGC*.

Vetter, W. (2015) “Gas Chromatography with Mass Spectrometry (GC-MS),” *Analytical Separation Science*, pp. 883–926. Available at: <https://doi.org/10.1002/9783527678129.assep027>.

Westermarck, S. (2000) *Use of mercury porosimetry and nitrogen adsorption in characterisation of the pore structure of mannitol and microcrystalline cellulose powders, granules and tablets dissertation*.

Zuo, H. L., Yang, F. Q., Huang, W. H., and Xia, Z. N. (2013). *Preparative Gas Chromatography and Its Applications*. *Journal of Chromatographic Science*, 51(7), 704–715. <https://doi.org/10.1093/chromsci/bmt040>.

## 4 Hydrothermal Hydrolysis of Rapeseed oil and WCOs

Hydrothermal hydrolysis was the first stage in the three-stage process to convert the lipid feedstocks to hydrocarbon. During this first stage, the lipids were hydrolysed to produce fatty acids (main product) and glycerol. The hydrothermal hydrolysis of rapeseed oil (RSO) and two waste cooking oils (WCO) samples were carried out without the need for external catalysts. Experiments were conducted to identify the optimum reaction conditions to generate the best yields of fatty acids from the lipids by examining the effects of temperature, time, oil-water mass ratio, and stirring speed. The product samples were quantified using analytical techniques such as CHNS, TGA, GC/MS, and acid-base titration, and the results discussed. The experimental procedure for the hydrolysis experiments is depicted in Figure 4.1.

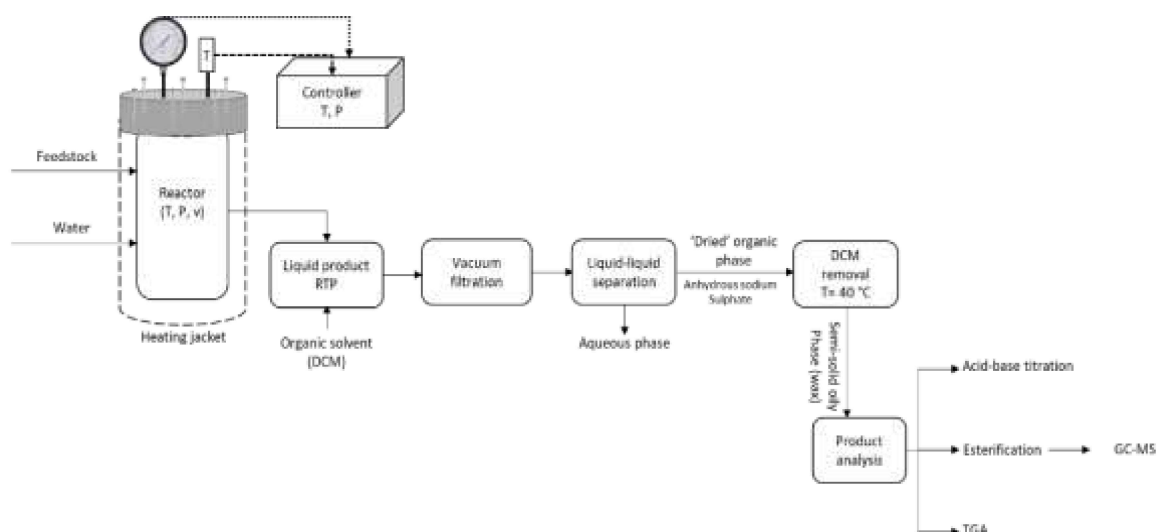


Figure 4.1: Schematic of hydrolysis experimental procedure

### 4.1 Selection of optimum conditions for hydrolysis experiments

Initial hydrolysis experiments were carried out with RSO as the model triglyceride to determine the optimum conditions to produce the highest yields of fatty acids. All reactions were carried out in a stirred 450 ml stainless steel batch reactor (Parr Instruments Co. Illinois, USA), with a maximum working temperature of 350 °C and a pressure of 345 bar. In these experiments, no added external catalyst was used. The mass of RSO was fixed at 10 g, while the other reaction parameters were varied. These included the water loading, the reaction temperature, the reaction time, and stirring speed. In addition, the effect of reactor wall on the hydrolysis process was investigated with and without the use of a quartz liner. The influence of reaction temperature was tested at 200 °C, 250 °C and 300 °C, with

corresponding autogenic pressures ranging from 9 bar to 51 bar. In addition, the effects of reaction time (10 min to 180 min) and oil – water mass ratios (1:0.1 to 1:3), stirring speeds and reactor wall on the yields of fatty acids from RSO oil were studied at set temperature of 300 °C. For the waste cooking oil samples, the reactions were carried out under the optimum conditions obtained for the hydrolysis of RSO, using 10 g of each sample and 20 g of deionised water.

## 4.2 Results and Discussions

The main objective is to understand the extent of hydrolysis, to determine the optimum conditions for complete hydrolysis of RSO through the characterisation of the hydrolysis product by the fatty acid yields. The standard method for quantifying fatty acids yields, titration, is employed with oleic acid as the reference standard compound. As the hydrolysed product would contain other fatty acids in addition to oleic acid, and could contribute to having some errors, other methods such as TGA, and GC-MS were used as well to help confirm the results obtained.

In this section, the results of the characterisation and compositions of the pure components (glycerol, oleic acid and methyl oleate), rapeseed oil and the two WCO samples will be discussed. Following this, the results of method development for hydrothermal hydrolysis of lipids, using rapeseed oil as model compound are presented. As no gas and mostly no solid residues were produced, the hydrolysis results have focused on the detailed characterisation of the organic-phase oil/wax products containing the fatty acids. Glycerol from the hydrolysis experiments were deemed to be in the aqueous phases and were not further analysed. Thereafter, the results of the hydrolysis of the WCO samples, using the developed set of optimum hydrothermal conditions are provided.

The elemental compositions of the rapeseed oil, oleic acid, glycerol and the WCOs are shown in Table 4.1. A Flash 2000 Elemental analyser was used to quantify the amount of carbon, hydrogen, nitrogen, sulphur, and oxygen (calculated by difference) (ASTM D5291), to provide an estimate for their relative HHVs based on Dulong's Formula stated in Section 3.2.9 (Castello et al., 2017). The table also shows their total acid numbers (TANs) (Zeleňáková et al., 2019; Sagan et al., 2019).



Table 4.1: Some physicochemical properties of the samples used in this present study

Sample	C (wt%)	H (wt%)	N (wt%)	S (wt%)	O (wt%)	HHV (MJ/kg)	TAN (mgKOH/g)	Ash (wt%)	Moisture (wt%)
RSO	77.0±1.02	11.0±0.15	0.13±0.01	nd	10.9±1.42	41.0±0.65	1.40±0.02	nd	0.03±0.00
WCO-A	75.7±2.47	12.54±0.61	0.22±0.03	nd	11.54±3.0 6	41.6±1.16	13.0±1.37	nd	0.12±0.00
WCO-B	76.03±1.29	12.37±0.12	0.18±0.05	nd	11.43±1.4 7	41.5±0.34	8.92±2.75	nd	0.11±0.00
Oleic acid	76.5±0.01	12.2±0.03	0.13±0.00	nd	11.3±0.31	41.4±0.34	198.6±1.20	nd	0.08±0.01
Glycerol	40.8±0.43	9.86±0.20	0.12±0.01	nd	49.3±0.62	19.1±0.54	5.44±1.30	nd	0.11±0.03

## 4.2.1 Results from TGA characterisation of samples

### 4.2.1.1 TGA characterisation of oleic acid, methyl oleate and rapeseed oil

The results from the thermogravimetric analyses of glycerol, oleic acid and methyl oleate are shown in Figure 4.2. The start and end temperatures for the degradation of these compounds are also shown in Figure 4.2. Glycerol, oleic acid and methyl oleate have been analysed using TGA to obtain their thermal degradation patterns and use these as signatures to determine their presence in the hydrolysis and esterification products of RSO oil and the WCOs. The temperature at which the maximum degradation temperature occurred (highest peak on the derivative-TGA plot) is regarded in this work as the  $T_{max}$ . According to the results, the thermal degradation of glycerol, oleic acid and methyl oleate show one distinct peak each with  $T_{max}$  of approximately, 218 °C, 267 °C and 415 °C, respectively.

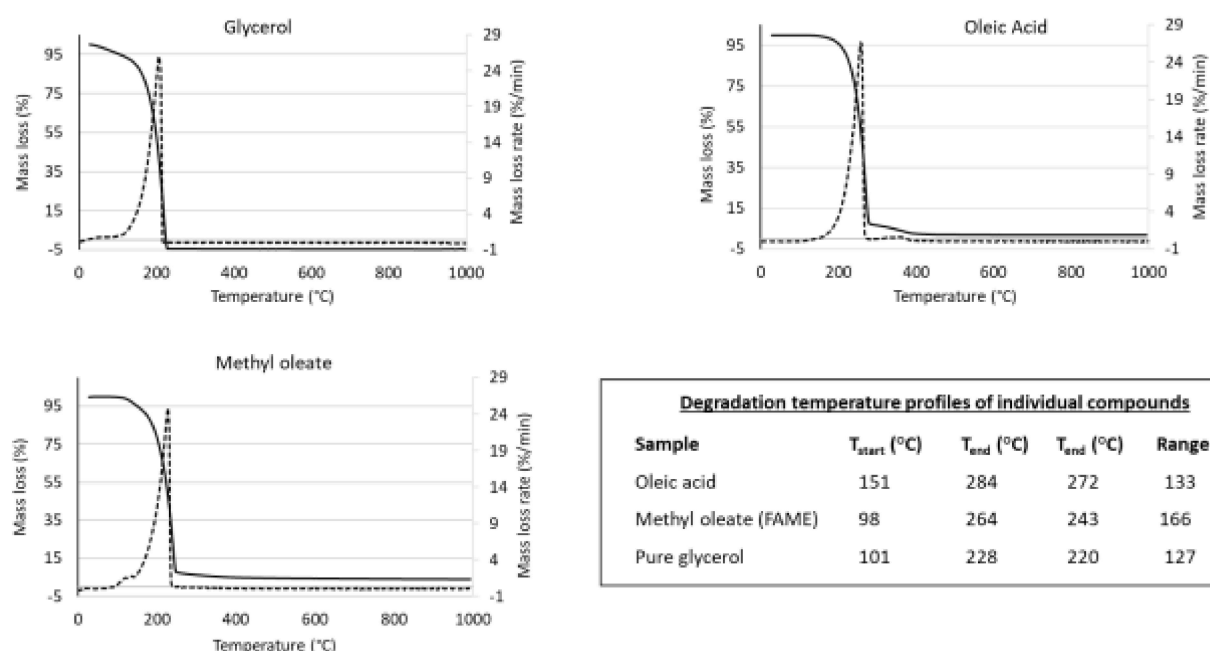


Figure 4.2: TGA thermograms and degradation temperature profiles of pure glycerol, oleic acid and methyl oleate

Oleic acid degradation occurred from 151 °C to 285 °C, which agrees with the range of 180 °C to 300 °C reported in literature (Niu et al., 2017, García-Zapateiro et al., 2013). In addition, the methyl oleate degradation occurred between 98 °C and 263 °C, which again coincides with the work of Pillar et al., who reported the range to be from 100 °C to 230 °C.

Finally, the degradation of glycerol started at 100 °C and ended at 228 °C, thereby agreeing with the work of Alsamad et al., (2018) who reported a degradation temperature range for glycerol as 77.5 °C – 240 °C. The slight differences in these reported temperature ranges would be due to differences in heating rates and carrier gas flow rates used in the different TGA studies.

#### 4.2.1.2 Estimation of major components in RSO and WCOs by TGA

The main components of RSO, WCO-A and WCO-B were determined from thermal degradation analysis using TGA. About 3.0 mg of each sample was used in the analyses and the mass losses corresponding to the pure components in Figure 4.2 (where applicable, glycerol and fatty acids (corresponding to oleic acid)) were used to estimate their compositions in the three lipid samples. In addition, the degradation pattern of RSO was also used to estimate the triglyceride contents of the WCOs. The results in Figure 4.3, and Table 4.2 present their estimated compositions according to their observed mass losses. Each thermogram was divided into the observed three stages of thermal degradation corresponding of free fatty acids in Stage I, some middle components in Stage II, which have been designated as mono- and diglycerides based on data from literature (de Lacerda et al., 2019) and triglycerides in Stage III. In addition, the thermograms could account for over 99 wt% of the three samples.

RSO showed a tiny peak starting from 179 °C to 289 °C, which corresponded to the oleic acid TGA pattern seen in Figure 4.2, hence this was taken as free fatty acids and the calculated mass loss was just 0.42 wt%. Then, there was a tailing shoulder before the main peak, which started around 290 °C and ending at 360 °C, which corresponded to the mono- and diglycerides (Alsamad et al., 2018) with a mass loss of 5.80 wt%. Furthermore, the largest degradation occurred between 360 °C and 504 °C, representing the triglycerides, with a mass loss of 93.5 wt%. Somé et al. reported a degradation temperature range of 220 °C to 450 °C for rapeseed oil, which seemingly covers the entire degradation pattern without identifying the distinction degradation stages. In addition, these differences could be due to the heating rates and/or carrier gas flow rates used in the reported work and this present study.

Figure 4.3 shows that the three stages of degradation of the WCOs are much more pronounced compared to RSO. For WCO-A, the Stage I mass loss was the highest of the three samples at 4.0%, then the Stage II loss accounted for 12.3 wt%, while the Stage III loss was 83.3 wt%. For WCO-B, apart from having a lower Stage I loss of 2.55 wt% compared to WCO-A, its Stage II and Stage III losses were similar to those of WCO-A. Essentially, the WCOs seemed to contain more free fatty acids and slightly more of the mono- and diglycerides than RSO. This should be expected from waste cooking oils. The different free

fatty acid contents in the two WCO samples could be due to the different types of vegetable oils used by the two kitchens from where they were sourced. It could also be due to differences in cooking practices in terms of length of use of the oils for cooking and length of storage of the used oils. These compositions could therefore influence their hydrolysis to fatty acids and their esterification to FAMEs. Acid-base titration was used to determine the fatty acid contents of the three samples (based on Equation 3.12, using oleic acid), giving yields of 0.68 wt% for RSO, 6.57 wt% for WCO-A and 4.27 wt% for WCO-B. These values are slightly higher than values obtained at the Stage 1 of the TGAs, and the differences could possibly be due to reactions of acid groups in the mono- and diglycerides observed in Stage II.

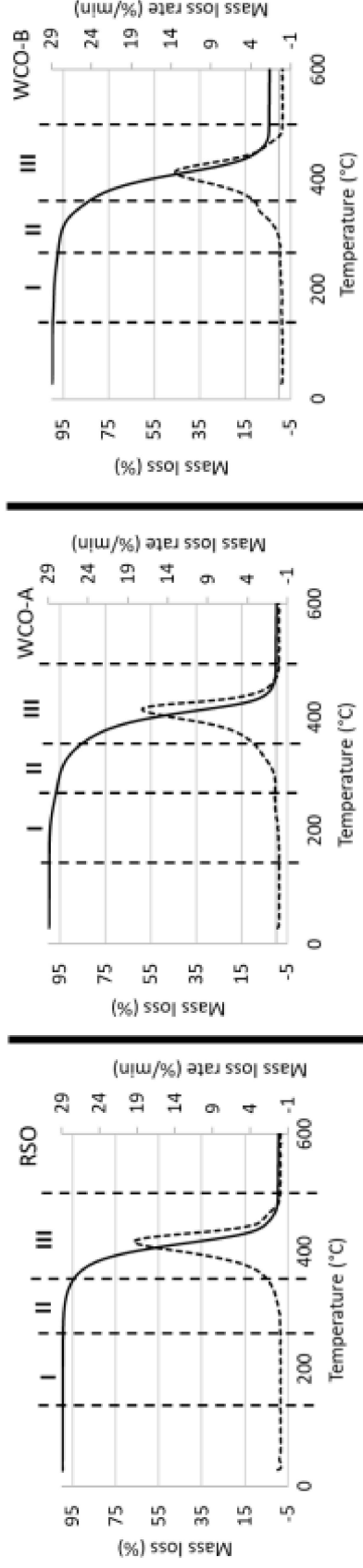


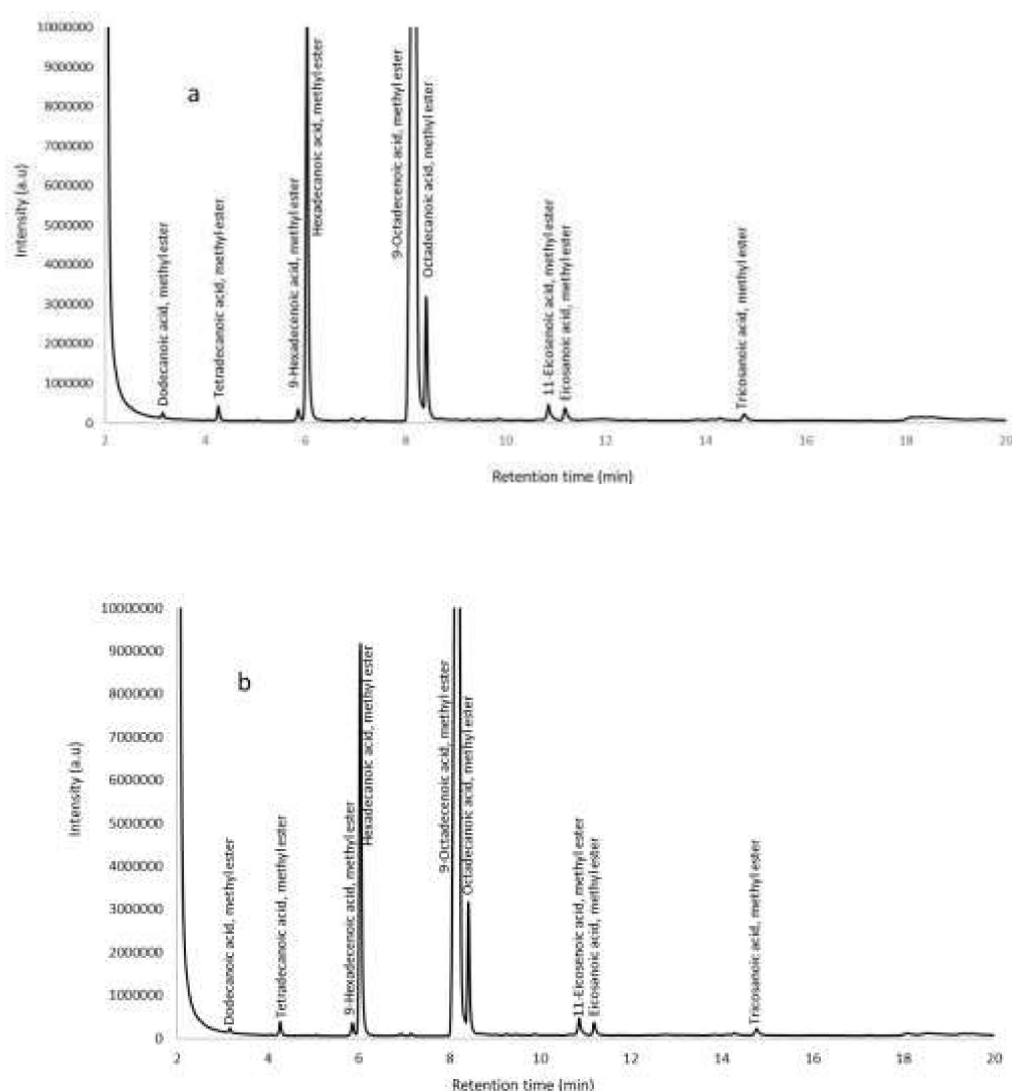
Figure 4.3: TGA thermograms of RSO, WCO-A and WCO-B, indicating the degradation profiles with Stage I (free fatty acids), Stage II (mono- & diglycerides) and Stage III (triglycerides)

Table 4.2: Temperature profiles and mass losses during the degradation of components of lipids samples in a TGA

	Stage I (free fatty acids)				Stage II (mono- & diglycerides+)				Stage III (triglycerides+)			
Sample	$T_{(start)}$ °C	$T_{(end)}$ °C	$T_{(range)}$ °C	Mass loss %	$T_{(start)}$ °C	$T_{(end)}$ °C	$T_{(range)}$ °C	Mass loss %	$T_{(start)}$ °C	$T_{(end)}$ °C	$T_{(range)}$ °C	Total mass loss %
RSO	179	289	110	0.55	290	360	70	5.80	360	504	144	99.9
WCO-A	180.4	288.9	108.5	4.01	290	359.3	69.5	12.3	360	509	149	99.6
WCO-B	181	289	108	2.55	290	356.9	66.9	12.0	357	512	155	99.3

#### 4.2.2 Characterisation of RSO, WCO-A and WCO-B by GC/MS after esterification

Table 4.3 shows compositions of the fatty acids present in the RSO and the two WCO samples from the kitchens of a pub and a cafeteria determined according to the method described by Luddy et al (1960). GC/MS have been used to identify the FAMES and hence the fatty acids in the three lipid samples (Figure 4.4). However, the results showed that the lipid samples did not undergo complete conversion as the yields of the FAMES were 21.4 wt% for RSO, 7.62 wt% for WCO-A and 18.9 wt% for WCO-B. Indeed, it is known that the esterification with methanol in the presence of sulfuric acid is more efficient in the conversion of free fatty acid groups in oils and fats than the triglyceride (Marchetti and Errazu, 2008; Kail et al., 2012). Hence, in biodiesel plants the sulphuric acid catalysed reaction is used for pre-treatment to remove free fatty acid groups by esterification to stop them from forming soaps during subsequent transesterification with methanol and sodium hydroxide (Ding et al., 2012).



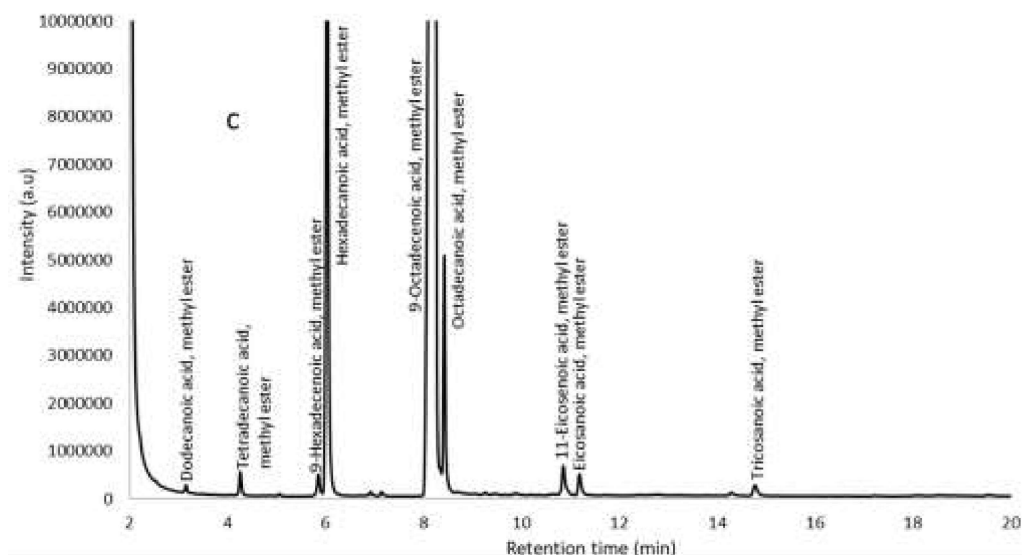


Figure 4.4: Compositions of fatty acids in the ‘as-received’ samples; (a) rapeseed oil, (b) WCO-A and (c) WCO-B

Clearly the RSO is apparently dominated by oleic acid (84.7 wt%), followed by palmitic acid (6.71 wt%) and linoleic acid at 2.18 wt%. However, the high content of oleic acid of 84.7 wt% was above the range of 50 to 75 wt% often reported in literature (Sagan et al., 2019; Matthaus et al., 2016; Kleyменова et al., 2021; Cristea et al., 2018), which may indicate its predominance in RSO (Sagan et al., 2019) and therefore occurred at enhanced levels among the free fatty acids that were esterified. Although, high oleic rapeseed oil cultivars have been developed (Long et al., 2018), it was unlikely that this result was conclusive, and would be checked after the subcritical water hydrolysis method in Section 4.3. In total however, the C18 fatty acids make up to 88 % of all the fatty acids found in the fresh RSO. This agrees with similar rapeseed oil characterisation data in literature (Sagan et al., 2019), which reported up to 92 % of C18 fatty acids in rapeseed oil with oleic acid being dominant at 64 wt%.

The WCOs were also dominated by both oleic acid (49 wt% for WCO-A and 65 wt% for WCO-B) along with strong presence of palmitic acid (31.4 wt% and 16.5 wt%). The higher amounts of palmitic acid in WCO-A and WCO-B compared to the fresh RSO, could be due to source and types of cooking oils used by the kitchens, with sunflower and rapeseed oil being common. The fatty acid contents of these WCOs samples can be used for the production of biodiesel, renewable hydrocarbon fuels and chemicals as well as important oleochemicals e.g., fatty alcohols. For instance, more than 80 wt% of the fatty acids in WCO samples could be further processed to make higher value oleochemicals. For example, they can undergo

mild reduction to produce detergent range fatty alcohols or used to produce cosmetic range methyl esters, such as Cetyl and Stearyl alcohols (Kreutzer, 1984).

Interestingly, for all three samples however, higher yields of fatty acids were obtained following the esterification process compared to the initial acid determination by TGA and acid-base titration methods. This indicated that some of the monoglycerides, diglycerides and possible triglycerides were also esterified alongside the free fatty acid present in the oils.

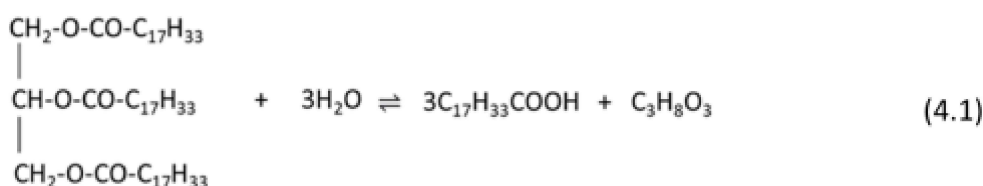
Table 4.3: Types and compositions of fatty acids in 'as-received' RSO, WCO-A and WCO-B

Scientific Name	Common Name	RSO (wt%)	WCO-A (wt%)	WCO-B (wt%)
Decanoic acid (C10:0)	Capric acid	nd	2.42	nd
Dodecanoic acid (C12:0)	Lauric acid	nd	3.43	1.03
Tetradecanoic acid (C14:0)	Myristic acid	0.98	3.39	1.12
9-Hexadecenoic acid (C16:1)	Palmitoleic acid	1.3	2.62	1.08
Hexadecanoic acid (C16:0)	Palmitic acid	6.71	31.4	16.5
Heptadecanoic acid (C17:0)	Margaric acid	nd	nd	1.01
9-Octadecenoic acid (C18:1)	Oleic acid	84.7	49.0	65.5
9,12-Octadecadienoic acid (C18:2)	Linoleic acid	2.18	nd	1.54
9,12,15-Octadecatrienoic acid (C18:3)	Linolenic acid	2.18	nd	nd
Octadecanoic acid (C18:0)	Stearic acid	1.02	7.72	8.58
cis-11-Eicosenoic acid (C20:1)	Gondoic acid	1.89	nd	1.22
Eicosanoic acid (C20:0)	Arachidic acid	1.22	nd	1.26

nd = not detected

### 4.3 Results from hydrothermal hydrolysis of RSO

Using RSO as a model triglyceride, experiments were carried out to investigate the influence of various parameters (temperature, vegetable oil – water mass ratio and reaction time) on the yields of fatty acids. All experiments were conducted under subcritical water conditions (hot water held under sufficient pressure to maintain its liquid state) without added catalysts. Each experiment was repeated two or three times and the error margins shown in the respective figures, with values of <2% indicating good reproducibility of experimental procedures. The main (reversible) reaction expected is shown in Equation 4.1, using oleic acid:





#### 4.3.1. Effect of temperature on hydrolysis of RSO

The first set of hydrolysis experiments were carried out to investigate the effect of temperature (Figure 4.5) on the yields of fatty acids under subcritical water conditions. The fatty acid yields were determined by acid-base titration method. Using a vegetable oil/water mass ratio of 1:2 (Mello et al., 2017). Experiments were carried out at temperatures of 200 °C, 250 °C and 300 °C, for 60 min reaction time each and a constant stirring speed of 50 rpm. The results presented in Figure 4.5 shows that the contents of fatty acids in the hydrolysis products increased drastically as temperature increased from 200 °C to 300 °C. At 200 °C, fatty acids accounted for only 8.3 wt% of the oil/wax product, but this increased to 89.3wt% at 250 °C and further to 97.2wt% at 300 °C. Although, 99.2 wt% of the oil/wax product was recovered after the reaction 200 °C, the low yield of fatty acids corresponded to the degree of hydrolysis achieved, indicating that just over 90 wt% of the oil/wax product remained as unreacted triglycerides.

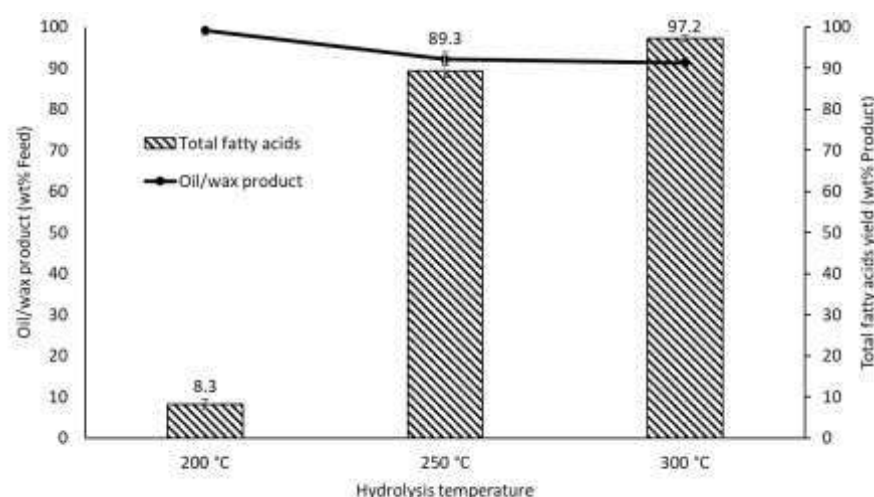


Figure 4.5: Influence of reaction temperature on yields of fatty acids from hydrolysis of RSO (vegetable oil – water mass ratio = 1:2; reaction time of 60 min and stirring speed of 50 rpm)

However, with increase in temperature, the degree of hydrolysis increased producing 82.2 wt% and 88.6 wt% of total fatty acids in relation to the RSO feed. Hydrolysis of triglycerides is a reversible endothermic reaction, so that an increase in temperature favoured the forward reaction leading to increased yields of fatty acids. In addition, under subcritical water conditions, increasing the temperature is known to increase the ionisation of water, lower its dielectric constant of water, and

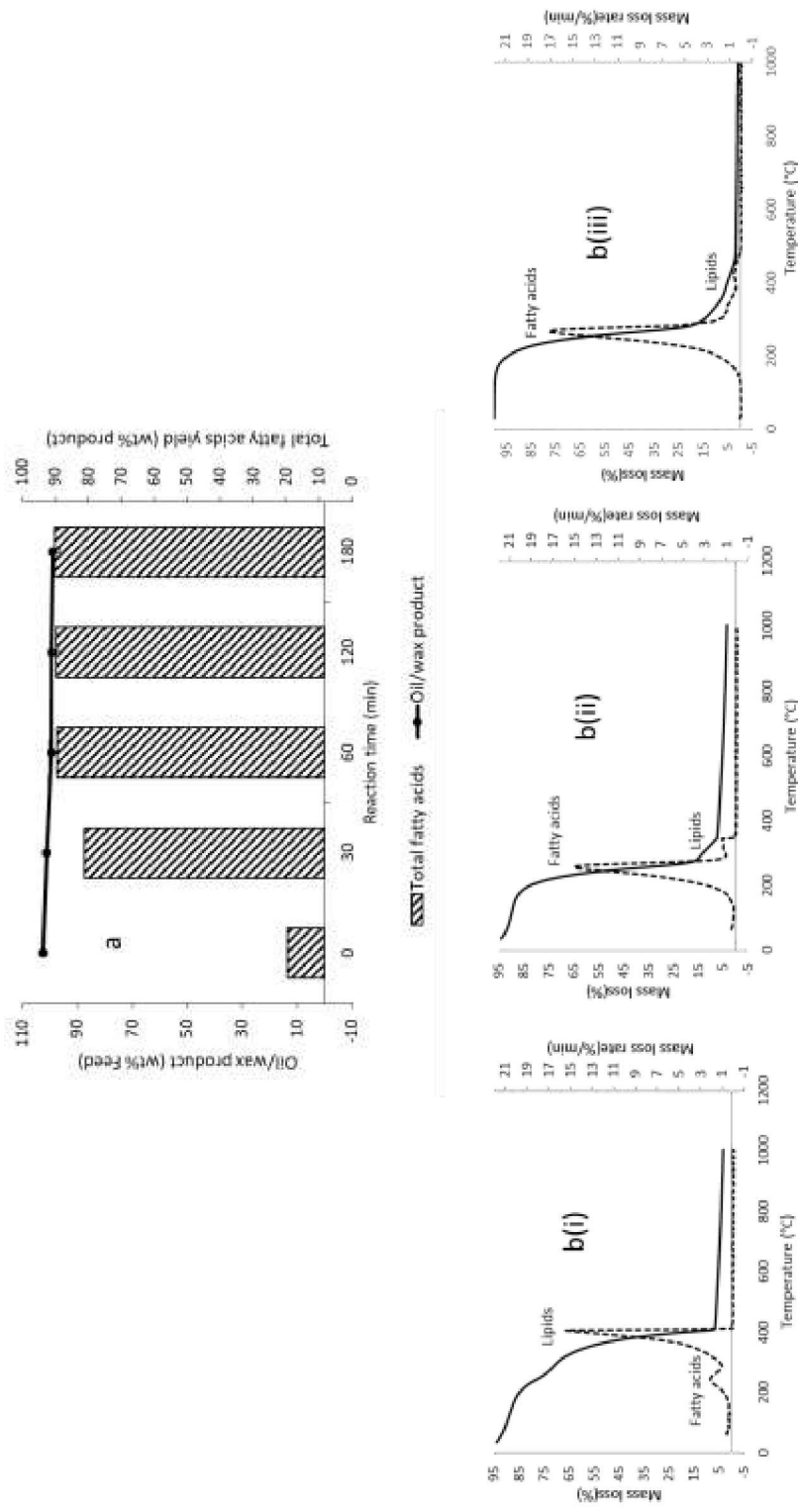


Figure 4.6: Influence of reaction time on conversion of RSO at 300 °C and vegetable oil – water mass ratio of 1:2 (stirring speed of 50 rpm); (a) yields of fatty acids; (b(i) – (iii)) TGA thermograms of hydrolysis products obtained at 0 min, 30 min and 60 min, respectively

provide more energy for molecular diffusions, thereby increasing the interactions between the triglycerides and water molecules (Pinto and Lanças, 2006; Patil et al., 1988). Under these conditions, and especially with the high concentrations of  $H^+$  and  $OH^-$  ions, the rate of hydrolysis would increase according to Equation 4.1 (based on oleic acid as the dominant fatty acid in RSO).

#### 4.3.2. Effect of reaction time

The effect of reaction time on the hydrothermal hydrolysis of rapeseed oil was investigated using an oil – water ratio of 1:2 at reaction times from 0 min to 180 min at a constant stirring speed of 50 rpm. The reaction time was measured once the reactor reached the set temperature of 300 °C and “0 min” experiment means that the experiment was stopped once the reactor reached this set temperature.

The results of these tests, determined by acid-base titration method, are presented in Figure 4.6a, which shows that reaction time was an important factor for the hydrolysis of rapeseed oil under the studied hydrothermal conditions. After 0 min, fatty acids accounted for 13.4 wt% of the oil/wax product and this increased dramatically to 87.5 wt% when the reaction time was increased to 30 min. After 60 min of reaction, the fatty acid yields increased to 97.2 wt%. Thereafter, there were only marginal increases to 97.6 wt% and 98.1 wt%, when the reaction time was extended to 120 min and 180 min, respectively. These values can also be used to represent the purity of fatty acids in the oil/wax products. Figure 4.6a also presents the yields of oil/wax products from the hydrolysis of RSO. Using the two sets of data in Figure 4.6a, then the yields of fatty acids, on RSO feed basis, with respect to time were 12.6 wt%, 81.174.2 wt%, 88.6 wt%, 89.0 wt% and 89.1 wt% at reaction times of 0 min, 30 min, 60 min, 120 min and 180 min, respectively. Hence, these results indicate that subcritical water hydrolysis of RSO could produce nearly the theoretical yields of fatty acids after 60 min of reaction.

Figures 4.6b(i - iii) show the corresponding TGA thermograms of the products oil/wax products obtained from the hydrolysis of RSO at 0 min, 30 min and 60 min, respectively. The thermograms are in agreement with the results of fatty acid yields obtained by acid-base titration, with the DTG peak corresponding to fatty acids getting larger with increase in reaction time. At the same time, the corresponding DTG peaks of lipids became smaller with the progress of hydrolysis in relation to time. Therefore, as shown in Figures 4.6b(i - iii), the TGA thermograms were able to indicate the extent of hydrolysis with respect to time. Thus, the TGA method can provide quick and reliable results for large scale applications such as monitoring the conversion of lipids during biodiesel production and for monitoring the quality of the final biodiesel product, including during storage.

#### 4.3.3. Effect of RSO – water mass ratio on hydrolysis of rapeseed oil

While the use of 300 °C, 60 min reaction time and RSO – water mass ratio of 1:2 was found to produce high yield of fatty acids, it was deemed necessary to further investigate the effect of water loading in this work. For instance, using excess water would ideally shift the position of equilibrium to produce more fatty acids. However, using too much water would also increase processing costs in terms of the energy required to heat and maintain the water at the reaction conditions. Figure 4.7 shows the effect of the rapeseed oil – water mass ratios on the yields of oil/wax products and their fatty acids at a temperature of 300 °C and constant stirring speed of 50 rpm. The fatty acid yields were obtained by acid-base titration method. Generally, the yields of oil/wax products decreased slightly due to the formation and transfer of glycerol into the aqueous phase whereas there was a steady rise in fatty acid contents in the oil/wax products with increased water loading at constant temperature.

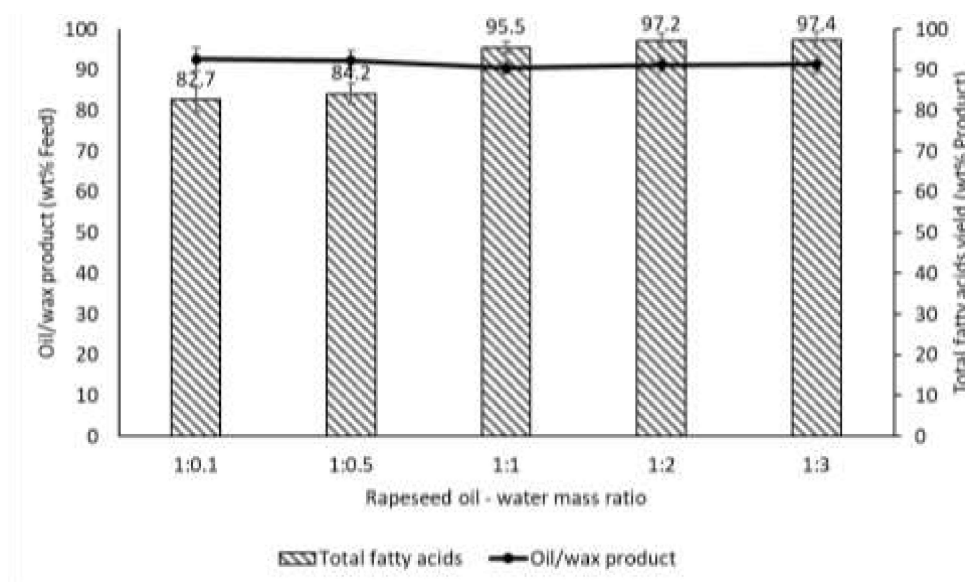


Figure 4.7: Influence of vegetable oil-water mass ratios on fatty acid yields from RSO at 300 °C and reaction time of 60 min (stirring speed of 50 rpm)

Although with the oil to water mass ratios at 1:0.1 and 1:0.5, the stoichiometric amounts of water were present in the reactor, but the amount fatty acids produced were 83 wt% and 84 wt% of the oil/wax products, respectively. However, it was only when the mass ratios were 1:1 and above that the amount of fatty acids in the oil/wax product increased dramatically to above 95 wt%, reaching the highest value of 97.4 wt% at oil – water ratio of 1:3.

Stoichiometrically, 10 g of vegetable oil (molecular mass of 882 g/mol, based on oleic acid chain as the dominant fatty acid) should require 0.61 g of water for hydrolysis, higher water loading should therefore shift the equilibrium towards the forward direction by the dissolution of the glycerol co-product (Anouti et al., 2015). In addition, fatty acids produced early in the

reaction have been reported to act as auto-catalysts during hydrolysis (Satyarthi et al., 2011). Hence, the observed results showed that increase in water loading led to increased yields of fatty acids to a possible combination of catalysis and favourable reaction equilibria. Giving that the yields of fatty acid were similar at 1:1, 1:2 and 1:3 oil to water mass ratios, respectively, any of these conditions could be deemed appropriate to use for the hydrolysis tests at 300 °C. In addition, considering that the stainless-steel vessel weighed much more than the quantities of water using in these tests, it took approximately about 40 min to reach 300 °C in each case, so that similar amounts of energy were required. However, in practice it was found that using 1:2 mass ratio made it easier to carry out separation of the aqueous phase (with glycerol) than 1:1 and was similar fatty acids to 1:3 mass ratio; hence it was decided to adopt the 1:2 mass ratio as the basis for further hydrolysis tests.

#### 4.3.4 Effect of stirring speed and reactor wall

Hydrolysis experiments were further carried out with RSO to monitor the effects of stirring speeds and reactor wall on the yields of fatty acids. The stirring speed was varied from 0 (no mechanical stirring) to 150 rpm, while a quartz liner was inserted into the reactor (Figure 4.8) to investigate the influence of reactor wall. The experiments were conducted at 300 °C, oil-water mass ratio of 1:2 and reaction time of 60 min. The fatty acid yields in Figure 8, determined by acid-base titration method showed that with no stirring at all (0 rpm), 93.8 wt% of total fatty acids was obtained in the oil/wax product from RSO. This increased to 97.2% when the stirring speed was increased to 50 rpm, and further increased to 98.9% at a stirring speed of 150 rpm. On RSO basis, these corresponded to 86.2 wt%, 88.6 wt% and 89.1 wt% of the original feed. Hence, the subcritical water medium could be said to have provided good mixing of the vegetable oil and reactant water molecules even without mechanical stirring.

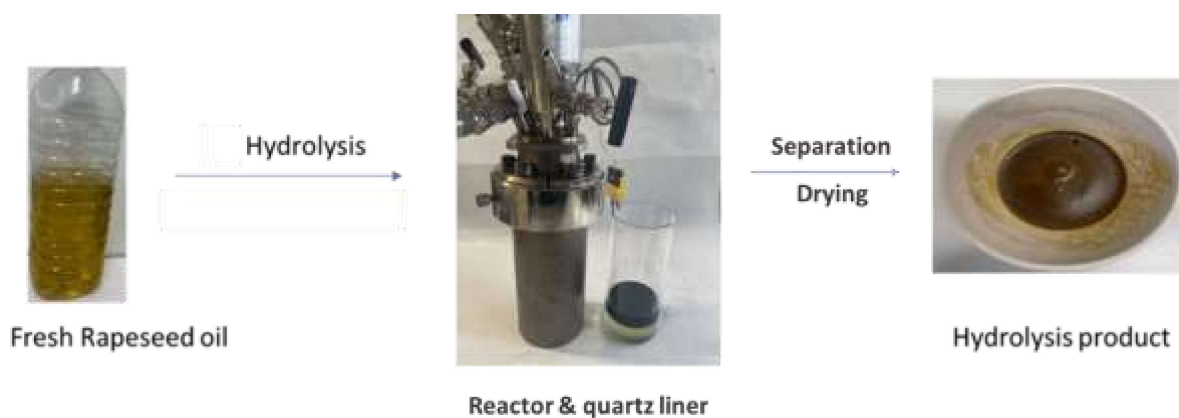


Figure 4.8: Images of rapeseed oil, reactor vessel/liner and hydrolysis product

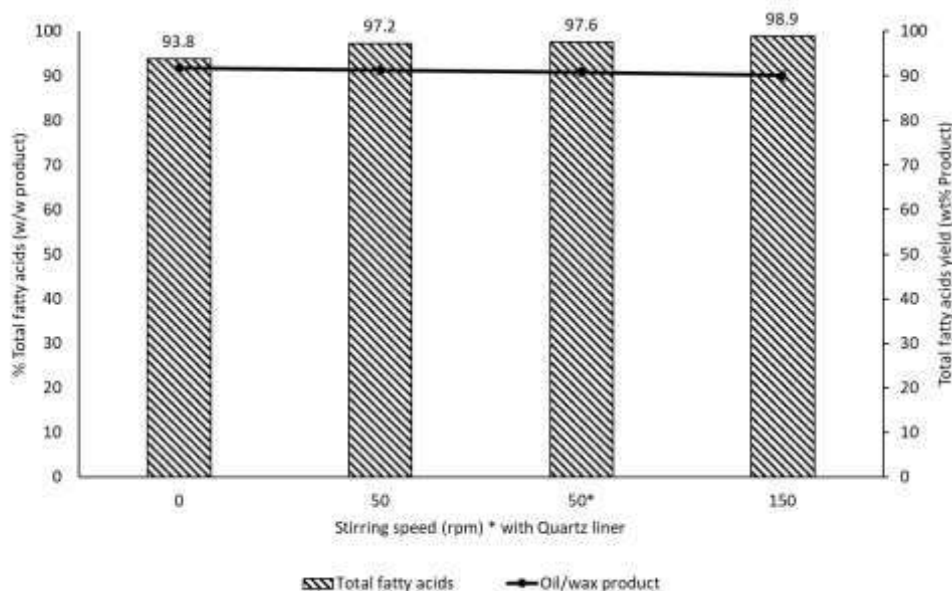


Figure 4.9: Influence of stirring speed on the yields of total fatty acids from the hydrolysis of RSO at 300 °C, reaction time of 60 min and vegetable oil – water mass ratio of 1:2

However, as Figure 4.9 shows, there was only marginal increase in actual fatty acid yields (2.9 wt%) when stirring speed was increased from 0 rpm to 150 rpm. Therefore, using 50 rpm could be considered more economically viable than 150 rpm. Additionally, the experiment with the quartz liner at a stirring speed of 50 rpm resulted in a 97.6% (88.5 wt%) yield of total fatty acids in the hydrolysis product, which is identical to the result obtained without the liner. This indicated that the reactor wall did not noticeably affect the hydrolysis reaction, neither acting as a catalyst nor an inhibitor for RSO hydrolysis. These results demonstrated that expansion of water under pressure, leading to significant autogenic pressure, clearly had more influence on the hydrolysis process than stirring the reaction mixture.

## 4.4 Results from hydrolysis of WCO samples

### 4.4.1 Fatty acid yields and mass balances from hydrolysis of WCO samples

Hydrothermal hydrolysis of the two cooking oil wastes samples was investigated at the selected optimum conditions of 300 °C, sample – water mass ratio of 1:2, reaction time of 60 min and stirring speed of 50 rpm. In these tests, about 10 g of each sample reacted with 20 g of water. Table 4.4 presents the mass balance closures and the yields of fatty acids from these tests as determined by acid-base titration method.



Table 4.4: Mass balance closures and fatty acids yields after hydrothermal hydrolysis of WCO

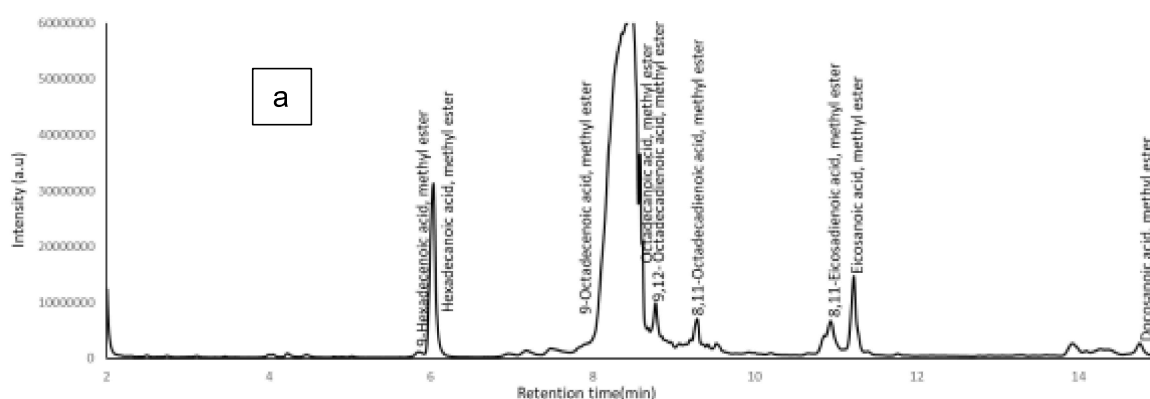
Sample	Sample (g)	Water (g)	Total (g)	Oil/wax Product (g)	Aqueous Phase (g)	Total (g)	Balance (%)	*FA yield (%)
WCO-A	10.0	20.0	30.0	9.21	20.65	29.86	99.5	99.6
WCO-B	9.99	20.0	29.99	9.27	20.61	29.88	99.6	100

FA = total fatty acids; \*based on oil/wax product via acid-base titration

In all cases, the main oil/wax phase deemed to comprise of the fatty acids remained the dominant organic product. Any glycerol product was deemed to be in the aqueous phase.

#### 4.4.2 Quantification of fatty acids in hydrolysed lipids as FAMES by GC/MS

The hydrolysis products obtained from RSO, WCO-A and WCO-B under the optimum conditions of 300 °C, 60 min reaction time, vegetable oil-water mass ratio of 1:2 and stirring speed of 50 rpm, were quantified using GC/MS after esterification with methanol. The fatty acids in the product were first converted into FAMES before the GC analysis by external standard method. The GC/MS chromatograms were used to identify the FAMES prior to quantification in Table 4.5. Clearly, the subcritical hydrolysis process led to near complete conversion of the lipid samples into fatty acids, which were esterified to FAMES (Figure 4.10).



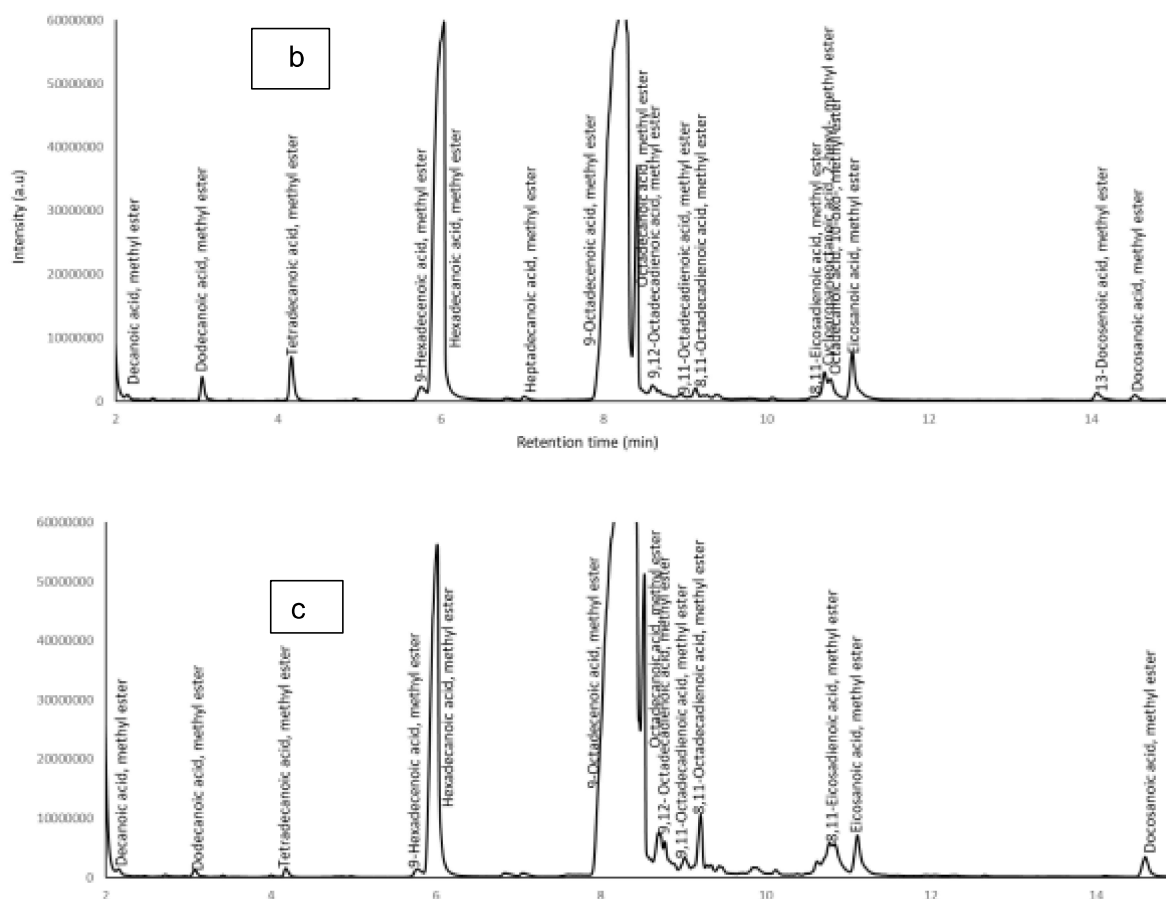


Figure 4.10: Annotated GC/MS chromatograms of the esterified hydrolysis products for (a) RSO, (b) WCO-A and (c) WCO-B

In this case, oleic acid content of RSO was found to be 74.4 wt% compared to 84.7 wt% in the esterified ‘as-received’ sample. Similarly, the oleic acid contents of WCO-A and WCO-B were also enhanced after the hydrolysis stage, with WCO-B giving identical yield to RSO, aligning with the source-kitchen confirmation of using mostly rapeseed oil for cooking. Based on the identified compounds by GC/MS (Figure 4.10), Table 4.5 shows that the WCOs contained more palmitic acid than RSO, particularly so for WCO-A. This was expected considering that restaurants may use different sources of oils for cooking and the waste generated are often combined, therefore the compositions of these waste cooking oils should be different from that of fresh rapeseed oil.

The percentage of individual FAMES among the identified and quantified compounds from the GC/MS are presented in Table 4.5. The total yields of FAMES were lower than 100 wt% in all three cases, with total yields of 88.6 wt%, 92.6 wt% and 84 wt% for RSO, WCO-A and WCO-B, respectively. Hence, a quick and more accurate method of determining fatty acids obtained from hydrolysis of lipids is needed for quick business decision making by relevant stakeholders without the use of expensive chemicals and extensive sample preparation protocols.



Table 4.5: Types and compositions of fatty acids in hydrolysed RSO

Name	Hydrolysed RSO (wt%)	Hydrolysed WCO-A (wt%)	Hydrolysed WCO-B (wt%)
Dodecanoic acid, methyl ester	nd	0.68	0.25
Tetradecanoic acid, methyl ester	nd	1.20	0.31
9-Hexadecenoic acid, methyl ester	0.36	0.70	0.37
Hexadecanoic acid, methyl ester	6.89	28.81	13.22
Heptadecanoic acid, methyl ester	nd	0.25	0.25
9-Octadecenoic acid, methyl ester	74.4	57.5	72.4
Octadecanoic acid, methyl ester	6.46	5.99	6.28
9,11-Octadecadienoic acid, methyl ester,	5.11	1.82	4.18
9,12,15-Octadecatrienoic acid, methyl ester	1.92	0.35	0.59
11-Eicosenoic acid, methyl ester	nd	1.07	0.87
Eicosanoic acid, methyl ester	2.55	0.99	0.72
13-Docosenoic acid, methyl ester, (Z)-	0.86	0.36	nd
Docosanoic acid, methyl ester	0.59	0.26	0.54

#### 4.4.3 TGA quantification of fatty acids and FAMEs obtained from hydrolysis of lipids

Figure 4.11 presents the TGA thermograms of the products of hydrothermal hydrolysis of RSO, WCO-A and WCO-B as well as those obtained after their subsequent esterification with methanol (FAMEs). Figure 4.11 shows two distinct groups of peaks for each of the samples after hydrolysis; the first peaks correlated with pattern observed for oleic acid in Figure 4.2, and the second peak is in the same range as the triglycerides in RSO seen in Figure 4.3. It can therefore be deduced that the small peaks in the triglyceride range seen in both samples implied incomplete hydrolysis of all triglycerides to fatty acids comprising of unreacted triglycerides or products of partial conversions to mono- and diglycerides. The thermograms of the FAMEs obtained from the hydrolysis products also showed two distinct groups of degradation peaks, with the first and second of these corresponding to FAMEs and non-FAMEs compounds (mono-, di- and triglycerides), respectively. In Figure 4.11, the second group of peaks for lipids appear to have substantially reduced after esterification (HYD WCO-A FAME and HYD WCO-B FAME). Hence, it could be inferred that the esterification converted not only the free fatty acids to FAMEs, but also partially converted the lipid-type compounds (incompletely converted and unreacted triglycerides).

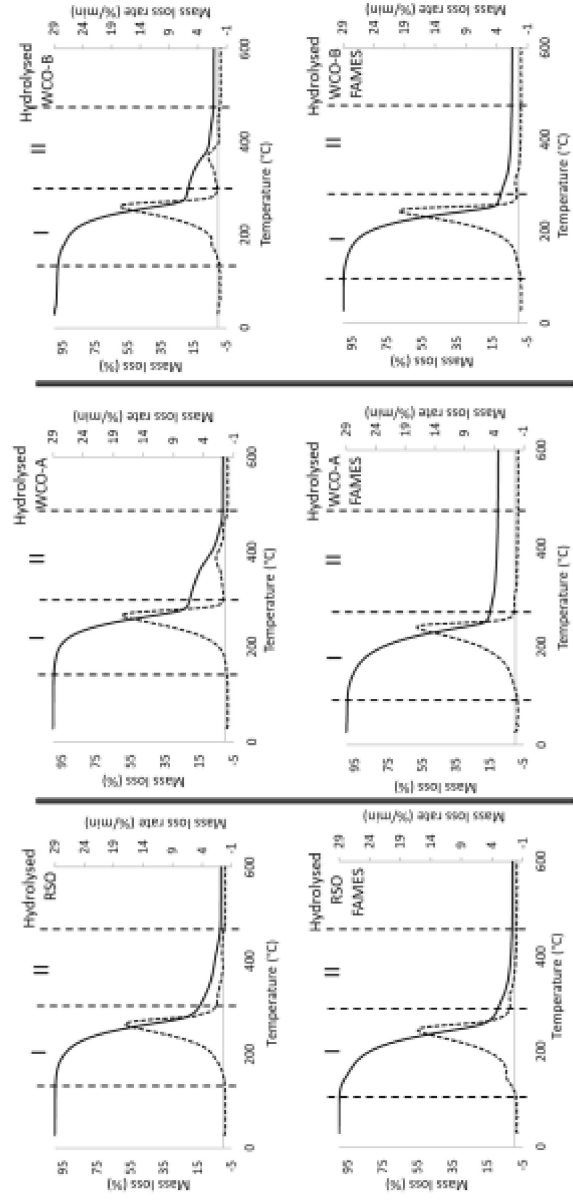


Figure 4.11: TGA thermograms of hydrolysis products of RSO, WCO-A and WCO-B before and after esterification with methanol, indicating their degradation profiles with Stage I (fatty acids/FAMES), Stage II (unreacted triglycerides and others)

The mass losses corresponding to the degradation peaks for both the fatty acids and FAMES are presented in Table 4.6. Compared to the TGA thermograms in Figure 4.3, the size of the peaks representing the degradation of triglycerides and hence the percentage mass losses decreased significantly after the hydrothermal hydrolysis. In contrast, there was huge increases in the size of the peaks corresponding to fatty acids (oleic acid in Figure 4.2).

Table 4.6: Temperature profiles and mass losses during the degradation of components of lipids samples in a TGA

A: Hydrolysis products							
Stage I (fatty acids)				Stage II (mono, -diglycerides & triglycerides+)			
Sample	T(start), °C	T(end), °C	Mass loss, %	T(start), °C	T(end), °C	Mass loss, %	Total mass loss, %
RSO	132	310	86.0	310	510	13.7	99.7
WCO-A	131	309	79.6	309	512	20.0	99.6
WCO-B	131	308	79.8	308	511	18.4	98.2

B: Esterification products							
Stage I (FAMES)				Stage II (mono-, diglycerides & triglycerides+)			
Sample	T(start), °C	T(end), °C	Mass loss, %	T(start), °C	T(end), °C	Mass loss, %	Total mass loss, %
RSO	90	290	91.0	290	360	8.90	99.9
WCO-A	88	280	90.0	280	354	9.60	99.6
WCO-B	88	280	85.2	280	355	14.1	99.3

The combination of these two observations confirmed the conversions of the lipid samples into fatty acids from the hydrolysis process. In addition, Table 4.6 also shows that mass losses occurred during the degradation of the esterified hydrolysis products. Clearly, the mass losses from the esterification products mirrored those of the hydrolysis products, showing that the fatty acids obtained from hydrolysis subsequently formed FAMES after esterification, which the degradation patterns closely matching those of methyl oleate in Figure 4.2. However, the mass losses due to degradation of FAME in both samples were much higher than the mass losses recorded for their corresponding fatty acids. Hence, the esterification process did not only convert the fatty acids to their methyl esters equivalent, but also led to the conversion of the heavier compounds in the products such as the incompletely mono- diglycerides and triglycerides.

The mass loss due to the combined glycerides in the hydrolysed RSO, reduced from 13.7 wt% to 8.90 wt% after esterification. For hydrolysed WCO-A sample, the mass loss due to incompletely converted compounds reduced from 20 wt% to 9.6 wt%, while for hydrolysed WCO-B, the reduction was from 18.4 wt% to 14.1 wt%. Hence, using TGA for the characterisation of esterified fatty acids or vegetable oils can be a simple and accurate technique to determine the purity of esterification products.

#### 4.4.4 Comparing quantification of fatty acids by titration, GC/MS and TGA

In this section, the comparative quantification of fatty acids in the hydrolysis products of RSO obtained with respect to effect of reaction time at 300 °C is presented. Considering that there were no significant differences between the fatty acid yields obtained after 60 min reaction time (Figure 4.6), only the results obtained at 0 min, 30 min and 60 min have been used for this comparison here. Figure 4.12 shows that the three methods gave similar results after 0 min, but differences can be seen after 30 min reaction times at 300 °C. After 60 min reaction time, the TGA result for fatty acids was much lower than those obtained by titration and GC/MS as shown in Figure 4.12.

Giving that RSO contains fatty acids with different chain lengths with different degrees of unsaturation, the use of oleic acid (C18:1) as the basis for calculation, has often been cited as the reason for over reporting the actual fatty acid yields (Jenkins, 2010). It is possible that such errors could become magnified at higher conversions of lipids during hydrolysis. In addition, the over expression of fatty acid yields by titration may be due to carboxylic acid groups that are not in the form of free fatty acids. For example, incomplete hydrolysis of the ester linkages in triglycerides may leave one or two -COOH groups as part of monoglycerides and diglycerides, respectively. Such compounds would not be seen within the free fatty acids range on TGA and may not elute from the GC/MS column but would react during acid-base titration. Figure 4.12 also shows that the fatty acid yields from GC/MS were higher than that of TGA.

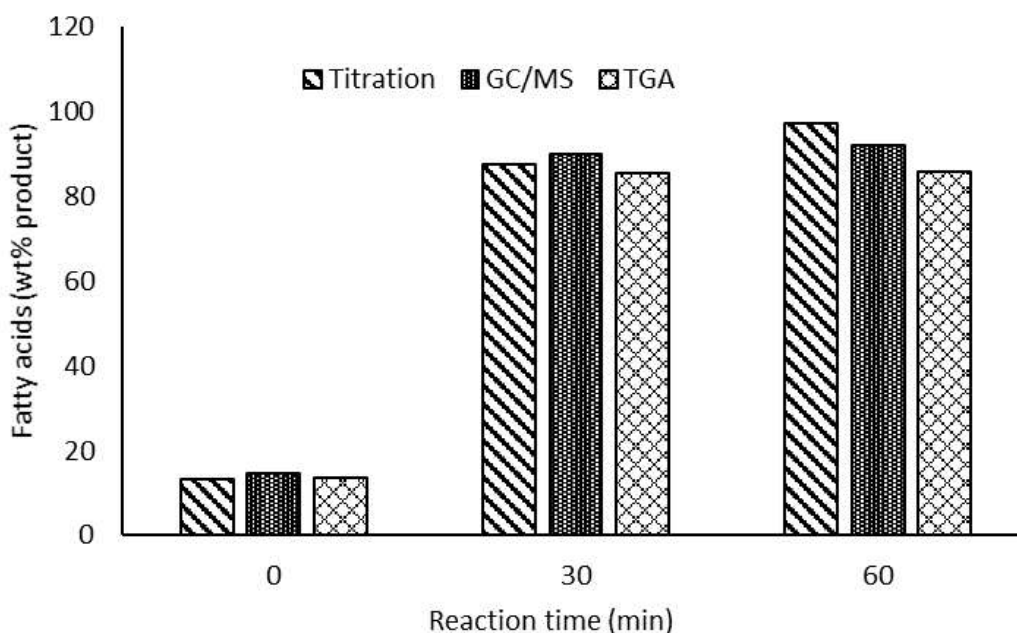


Figure 4.12: Results from comparative analysis studies; (a) quantification of fatty acid yields using the three different analytical methods

This could be explained by possible in situ transesterification of hydrolysis products, which has been reported to give higher free fatty acids contents in lipids during their conversion to methyl esters prior to GC/MS analysis (Martinez-Silveira et al., 2019). Therefore, by being able to use degradation patterns to differentiate fatty acids from higher molecular weight compounds (such as lipids, monoglycerides and diglycerides, the TGA may provide the most accurate results compared to titration and GC/MS methods.

In summary, three analytical methods, TGA, GC-MS, and acid-base titration, were explored and compared to analyse the fatty acids obtained from hydrolysing vegetable oil. The optimum operating condition determined for hydrolysing fresh rapeseed oil, and WCOs was 1:2 oil to water mass ratio for 1 h at 300 °C in the absence of catalysts with a 97.2% fatty acid yield. The comparative investigation explored the influence of reaction time (0 min, 30 min, and 60 min) on fatty acid quantification using three analytical techniques: titration, GC/MS, and TGA. Initially, results were comparable at 0 min, but disparities arose after 30 min, which notably showed lower fatty acid yields with TGA compared to titration and GC/MS at 60 min. Titration errors were noted, particularly the use of oleic acid in calculations, potentially leading to inflated yields, especially at higher lipid conversion rates. Overreported fatty acid yields in titration were linked to carboxylic acid groups not as free fatty acids, possibly due to incomplete hydrolysis. GC/MS demonstrated elevated yields, attributed to in situ transesterification during methyl ester conversion. TGA was identified as the most comprehensive method, proficient in analysing feedstocks, esterified, and hydrolysed products, while discerning fatty acids from higher molecular weight compounds.

Optimal conditions for hydrolysing rapeseed oil and waste cooking oils were established. In other words, the study highlighted the strengths and weaknesses of each method, positioning TGA as the most comprehensive, and emphasised the importance of thorough error consideration for precise fatty acid quantification during hydrolysis.

## 4.5 References

- Alsamad, T., Almazrouei, M., Hussain, M. and Janajreh, I. Modeling of Thermochemical Conversion of Glycerol: Pyrolysis and H<sub>2</sub>O and CO<sub>2</sub> Gasification. *Waste Biomass Valori*. 2018, 9(12), 2361-2371. DOI: 10.1007/s12649-018-0306-x
- Anouti, S., Haarlemmer, G., Deniel, M., Roubaud, A., Analysis of Physicochemical Properties of Bio-Oil from Hydrothermal Liquefaction of Blackcurrant Pomace. *Energy Fuels*, 2016, 30 (1), 398-406. <https://doi.org/10.1021/acs.energyfuels.5b02264>
- AOCS. Official methods and recommended practices of the American Oil Chemists' Society. 2004. Champaign, USA: AOCS Publishing
- ASTM D5291-ASTM International. Standard Test Methods for Instrumental Determination of Carbon, Hydrogen, and Nitrogen in Petroleum Products and Lubricants; ASTM D529, 2016.
- Castello, D., Rolli, B., Kruse, A. and Fiori, L. Supercritical Water Gasification of Biomass in a Ceramic Reactor: Long-Time Batch Experiments. *Energies*. 2017, 10(11), 1734. DOI: 10.3390/en10111734
- Cristea, G., Cazamir, D., Dima, D., Georgescu, C. and Deleanu, L. Influence of TiO<sub>2</sub> as nano additive in rapeseed oil. *IOP Conf. Ser.: Mater. Sci. Eng.* 2018, 444, 022011. DOI: 10.1088/1757-899X/444/2/022011
- de Lacerda, J.G.P., Candeia, R.A., de Moraes Sales, L.L., dos Santos, A., Portela da Cunha, A.F., Wanderley, A.F., Campos, A.F. Characterization of biodiesel from frying oil obtained by hydro-esterification using vermiculite as heterogeneous catalyst. *J. Therm. Anal. Calorim.* 2019, 137, 2045–2052. DOI: 10.1007/s10973-019-08092-0

Ding, J., Xia, Z. and Lu, J. Esterification and Deacidification of a Waste Cooking Oil (TAN 68.81 mg KOH/g) for Biodiesel Production. *Energies*. 2012, 5(8), 2683-2691. DOI: 10.3390/en5082683

Francis E. Luddy, R. A. Barford, R. W. Riemenschneider. Direct conversion of lipid components to their fatty acid methyl esters. *J. Am. Oil Chem. Soc.* 1960 37(9), 447-451. <https://doi.org/10.1007/BF02631205>

García-Zapateiro, L.A., Franco, J.M., Valencia, Delgado, M.A., Gallegos, C., Viscous, thermal and tribological characterization of oleic and ricinoleic acids-derived estolides and their blends with vegetable oils. *J. Ind. Eng. Chem*, 2013, 19(4), 1289–1298. <https://doi.org/10.1016/j.jiec.2012.12.030>.

Jenkins, T.C., Technical note: Common analytical errors yielding inaccurate results using analysis of fatty acids in feed and digesta samples. *J. Dairy Sci.* 2010, 93 :1170–1174. DOI: 10.3168/jds.2009-2509

Kail, B., Link, D. and Morreale, B. Determination of Free Fatty Acids and Triglycerides by Gas Chromatography Using Selective Esterification Reactions. *J. Chromatogr. Sci.* 2012, 50(10), 934-939. DOI: 10.1093/chromsci/bms093

Kleymentova, L. N., N Bolgova, I., V Kopylov, M. and Y Zheltoukhova, E. Study of the Qualitative Characteristics of Rapeseed Oil Obtained by Cold Pressing. *KnE Life Sciences*. 2021. DOI: 10.18502/kl.v0i0.8959

Kreutzer, U. Manufacture of fatty alcohols based on natural fats and oils. *J. Am. Oil Chem. Soc.* 1984, 61(2), 343-348. DOI: 10.1007/BF02678792

Long, W., Hu, M., Gao, J., Chen, S., Zhang, J., Cheng, L. and Pu, H. Identification and Functional Analysis of Two New Mutant BnFAD2 Alleles That Confer Elevated Oleic Acid Content in Rapeseed. *Front. Genet.* 2018, 9. DOI: 10.3389/fgene.2018.00399

Luddy, F.E., Barford, R.A. and Riemenschneider, R.W. (1960) "Direct conversion of lipid components to their fatty acid methyl esters," *Journal of the American Oil Chemists' Society*, 37(9), pp. 447–451. Available at: <https://doi.org/10.1007/bf02631205>.

Marchetti, J. and Errazu, A. Esterification of free fatty acids using sulfuric acid as catalyst in the presence of triglycerides. *Biomass Bioenergy*. 2008, 32(9), 892-895. DOI: 10.1016/j.biombioe.2008.01.001

Martinez-Silveira, A., Villarreal, R., Garmendia, G., Rufo, C., Vero, S., Process conditions for a rapid in situ transesterification for biodiesel production from oleaginous yeasts. *Electron. J. Biotechnol.*, 2019, 38, 1-9.

- Matthaus, B., Özcan, M. and Al Juhaimi, F. Some rape/canola seed oils: fatty acid composition and tocopherols. *Zeitschrift für Naturforschung C*. 2016, 71(3-4), 73-77. DOI: 10.1515/znc-2016-0003
- Mello, B., Zempulski, D., Cardozo-Filho, L. and Silva, C., 2017. Hydrolysis of Canola Oil Under Subcritical Conditions for Biodiesel Synthesis. *Asian J. Chem.* 2017, 29(2), 398-402. DOI: 10.14233/ajchem.2017.20217
- Niu, S., Zhou, Y., Yu, H., Lu, C. and Han, K. Investigation on thermal degradation properties of oleic acid and its methyl and ethyl esters through TG-FTIR. *Energy Convers. Manag.* 2017, 149, 495-504. DOI: 10.1016/j.enconman.2017.07.053
- Patil, T. A., Butala, D. N., Raghunathan, T. S., and Shankar, H. S. (1988). Thermal hydrolysis of vegetable oils and fats. 1. Reaction kinetics. *Industrial and Engineering Chemistry Research*, 27(5), 727–735. <https://doi.org/10.1021/ie00077a001>.
- Pillar, R., Ginic-Markovic, M., Clarke, S. and Matisons, J. Effect of Alkyl Chain Unsaturation on Methyl Ester Thermo-Oxidative Decomposition and Residue Formation. *J. Am. Oil Chem. Soc.* 2009, 86(4), 363-373. DOI: 10.1007/s11746-009-1358-7.
- Pinto, J.S. and Lanças, F.M. (2006) "Hydrolysis of corn oil using subcritical water," *Journal of the Brazilian Chemical Society*, 17(1), pp. 85–89. Available at: <https://doi.org/10.1590/s0103-50532006000100013>.
- Sagan, A., Blicharz-Kania, A., Szmigielski, M., Andrejko, D., Sobczak, P., Zawisłak, K. and Starek, A. Assessment of the Properties of Rapeseed Oil Enriched with Oils Characterized by High Content of  $\alpha$ -linolenic Acid. *Sustainability*. 2019, 11(20), 5638. DOI: 10.3390/su11205638
- Satyarthi, J., Srinivas, D. and Ratnasamy, P. Hydrolysis of vegetable oils and fats to fatty acids over solid acid catalysts. *Appl. Catal. A: Gen.* 2011, 391(1-2), 427-435. DOI: 10.1016/j.apcata.2010.03.047
- Somé, S., Pavoine, A. and Chailleux, E. Evaluation of the potential use of waste sunflower and rapeseed oils-modified natural bitumen as binders for asphalt pavement design. *Int. J. Pavement Res. Technol.* 2016, 9(5), 368-375. DOI: 10.1016/j.ijprt.2016.09.001
- Zeľeňáková, L., Angelovičová, M., Šnirc, M., Žiarovská, J., Kráčmar, S., Gálik, B. and Kunová, S. Thermo-degradative changes of rapeseed and sunflower oils during deep-frying French fries. *Potr. S. J. F. Sci.*. 2019, 13(1), 138-149. DOI: 10.5219/1080





## 5 Catalytic decarboxylation of hydrolysis product up to 400 °C

Deoxygenation reactions were carried out with the aim to convert the fatty acids produced from the hydrolysis of RSO and WCO samples (Chapter 4) to hydrocarbons. The targeted deoxygenation reaction was decarboxylation during which the -COO functional group of fatty acids was expelled as CO<sub>2</sub> (Equation 5.1). All experimental data are reported to 2 decimal places.



The methodology for this set of experiments has been described in Chapter 3, Section 3.2.2.2, but Figure 5.1 is the schematic of the experimental procedure.

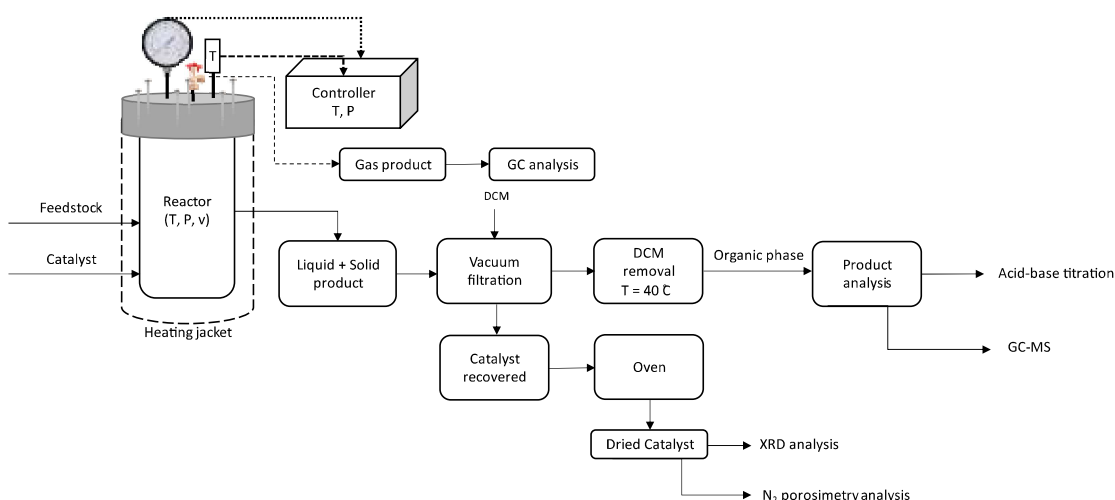


Figure 5.1: Schematic of decarboxylation experimental procedure

Majority of research that have been published in literature on the deoxygenation of vegetable oils or biomass were carried out under H<sub>2</sub> atmosphere to enhance the decarboxylation reaction, but this research has successfully been performed without any external addition of H<sub>2</sub>. For comparison, Jenišťová et al. (2017) obtained a 99% conversion from the deoxygenation of stearic acid with Ni-Al<sub>2</sub>O<sub>3</sub> catalyst but with 60 bar hydrogen pressure for 6 h, which required a relatively high amount of hydrogen to achieve similar results obtained in this research in the absence of hydrogen. On the other hand, Madsen et al. (2011) used relatively less hydrogen pressure of 20 bar and less reaction time of 5 h with Pt/ MgSiO<sub>3</sub>, and obtained 100% conversion of oleic acid. Both gave the highest conversions but the results obtained in this research in the absence of hydrogen are comparable. As Equation 5.1.

shows, hydrogen can be generated in situ in the reactor via a combination of reactions of carbon chains and the hydrogen used for hydrogenation of  $\text{-C=C-}$  bonds, leading to predominantly saturated compounds in the presence of Pt/C (Liu et al., 2021). The parametric experimental design for this chapter was used to assess the effects of temperature, time, catalyst type, and catalyst loading with the best potential to obtain the desired product, hydrocarbons. Deoxygenation leads to hydrocarbon-rich fuels, thereby avoiding the chemical and biochemical instability as well as possible polymerisation inherent in oxygenated fuels (Zheng et al., 2017).

In this present work, some experiments were more successful than others, in terms of the extent of decarboxylation, measured by acid-base titration to determine the concentration of carboxyl groups remaining at the end of the reactions. There was an inverse correlation between the fatty acid contents and the yields of hydrocarbons in relation to conversion. Therefore, experiments with low acid content and high hydrocarbon contents were deemed more successful in comparison to those with high acid contents and low hydrocarbon yields. Yields of the products were calculated as a weight percent of the hydrolysis product used as feedstock. The yield of the solid product (char) was calculated by deducting the mass of loaded catalyst from the mass of solid residues collected from the reactor after the reaction.

## 5.1 Catalyst characterisation

Seven different catalysts were used during the decarboxylation experiments in this work. The specific BET surface areas of the catalysts used for tests in this research project are shown in Table 5.1. The highest surface area of  $649 \text{ m}^2/\text{g}$  was observed for 5 % Pt/C, and the surface area of the other catalysts were similar, with 5 wt% Pd/MgSiO<sub>3</sub> having the lowest surface area of  $102 \text{ m}^2/\text{g}$ . The silica-based catalysts had the highest pore volumes, while the MgSiO<sub>3</sub> based catalysts had the highest pore diameters.

Table 5.1: Physical and morphological properties of the catalysts used in this study\*

Catalyst	Surface area ( $\text{m}^2 \text{ g}^{-1}$ )	Pore volume ( $\text{cc/g}$ )	Pore diameter (nm)
5 wt% Pt/C	648.68	0.26	3.84
1 wt% Pt/Silica	194.69	0.88	9.97
5 wt% Pt/Silica	208.38	0.97	16.09
10 wt% Ni-Cu/Al <sub>2</sub> O <sub>3</sub> (P)	108.91	0.27	6.69
5 wt% Pt/Al <sub>2</sub> O <sub>3</sub>	163.33	0.39	6.72

5 wt% Pt/MgSiO <sub>3</sub>	116.45	0.18	19.26
5 wt% Pd/MgSiO <sub>3</sub>	101.89	0.16	19.36

\*Surface area and pore volumes obtained from N<sub>2</sub> adsorption porosimetry

Figure 5.2 shows the powder XRD patterns of the catalysts used in this research. The Al<sub>2</sub>O<sub>3</sub> peaks identified at 43.1°, 45.9°, and 67.1° in NiCu Al<sub>2</sub>O<sub>3</sub> match with those reported by Suryawanshi et al. (2015) (JCPDS file No. 10-0425). The NiCu phase was observed at 48° and 76° (Jeong et al., 2012; He et al., 2019). The broad XRD peaks of SiO<sub>2</sub> were observed in the range 20-30° in both Pt/Silica catalysts (Pandya et al., 2018). The XRD diffraction peaks at 40°, 46°, and 68° identified in Pt/Al<sub>2</sub>O<sub>3</sub>, Pt/C, and Pt/SiO<sub>2</sub> correspond the (111), (200), and (220) characteristic planes of a typical face-centered structure of Pt (Zhang et al., 2007; Singh and Miyabayashi, 2020; Kishore et al., 2009). The peak observed for graphitic carbon on the XRD for Pt/C was the (002) at 26° (Pandya et al., 2018). The peak at 40° in the Pd/MgSiO<sub>3</sub> XRD pattern is assigned to Pd (Reddy et al., 2017). While the MgSiO<sub>3</sub> peaks were identified in Pt/MgSiO<sub>3</sub>, and Pd/MgSiO<sub>3</sub> (Bouaoun et al., 2017; Zhang et al., 2014).

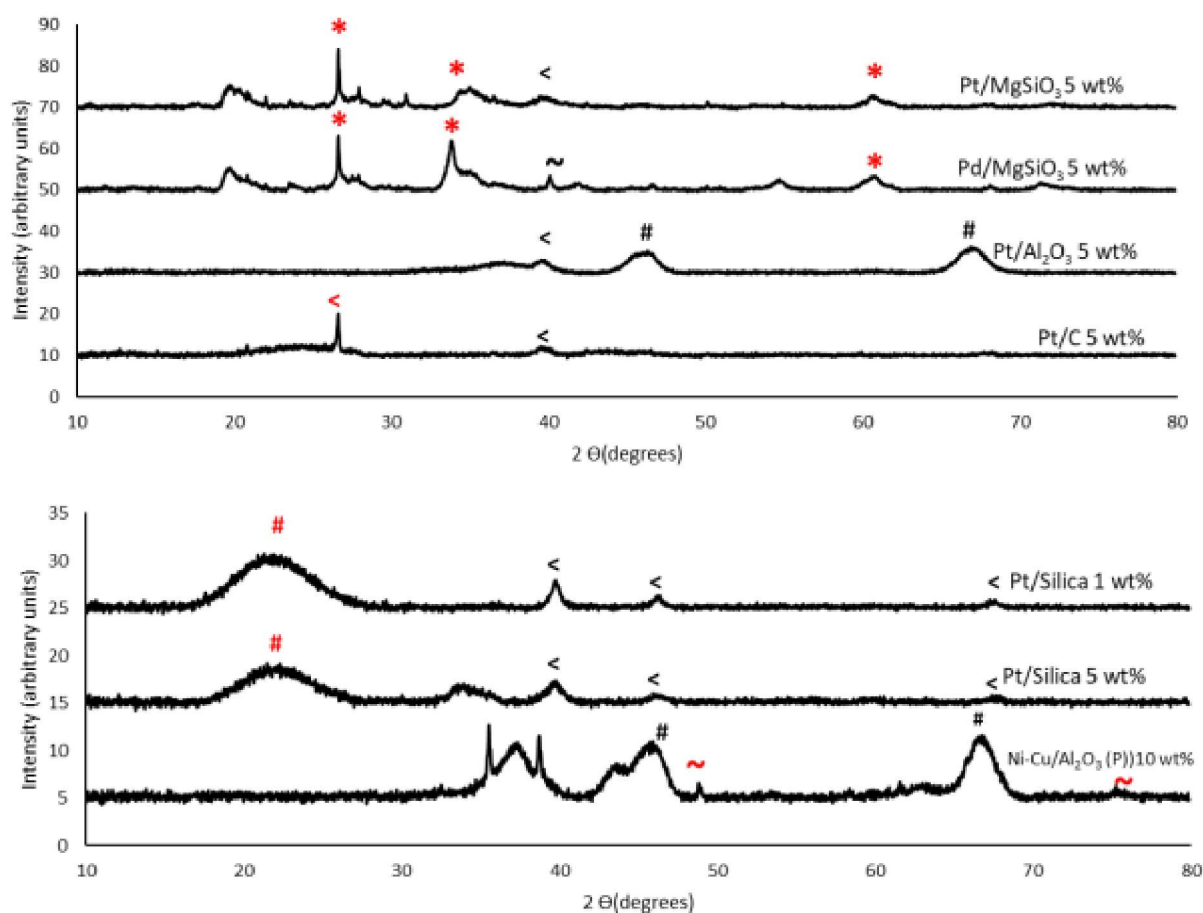


Figure 5.2: XRD patterns of fresh catalysts used (# Al<sub>2</sub>O<sub>3</sub>, # SiO<sub>2</sub>, < Pt, \* MgSilicate, < C, ~ NiCu, ~ Pd)

## 5.2 Influence of different reaction parameters on the decarboxylation of hydrolysis products

### 5.2.1 Screening of different catalysts for the decarboxylation of fatty acids from hydrolysis of RSO

This section explores the effect of various catalysts on the decarboxylation of hydrolysed RSO. The catalysts were characterised using N<sub>2</sub> adsorption porosimetry and XRD and have been previously discussed in Section 5.1. Minimising the impact of the other reaction parameters such as temperature or time are essential in order to emphasize the effect of the catalysts, which was the aim of this section. Therefore, to monitor decarboxylation and limit the effect of more severe reaction temperature that could cause cracking, 400 °C was used for the tests involving other catalysts. All reactions were carried out with 10 g hydrolysed oil at 400 °C for 2 hours under 5 bar N<sub>2</sub> pressure.

#### 5.2.1.1 Product yields and mass balance from tests with different catalysts

The product distributions and mass balances from the decarboxylation of the fatty acid products obtained from the hydrolysis stage are shown in Table 5.2. The catalytic decarboxylation results showed good mass balance closures of over 90 wt%. The mass loss could be attributed to the vaporisation of volatiles during transfer of samples. These reactions all yielded liquid product, the decarboxylated oil, as the main product from this stage, and accounted for at least 73% of the hydrolysed oil in each case. Ni-Cu powdered catalyst gave the highest liquid yield (87 wt%), Pd/MgSiO<sub>3</sub> produced the highest yield of solid residues product (12 wt%), and Pt/C, the highest gaseous product (7.95 wt%). It is also worthy of note that the liquid product obtained using 5 wt% Pt/C was the only product with a light-yellow colour, but this will be further discussed in Section 5.2.1.3 (Figure 5.3).

Figure 5.4 shows the yields of gas products on feedstock basis. CO<sub>2</sub> was produced in every reaction, and since this gas is a product of decarboxylation, this suggested all catalysts explored have the potential to deoxygenate fatty acids via this route. Gas products from this stage accounted for about 6 - 8 wt% on feed basis and consisted of > 45% CO<sub>2</sub>, some hydrogen and CH<sub>4</sub> with 10 wt% Ni-Cu/Al<sub>2</sub>O<sub>3</sub> (P)) producing the highest CO<sub>2</sub>. The degree of decarboxylation was really emphasised in these experiments with varying catalyst types because some liquid/wax products had little to no acid content and some still had over 50% of acid present post -reaction (Table 5.3).

Table 5.2: Mass balance for reaction products from decarboxylation of hydrolysed rapeseed oil at 400 °C, 2 h with various catalysts

Catalyst	Products			Balance (wt%)
	Solid (wt%)	Oil (wt%)	Gas (wt%)	
5 wt% Pt/C	8.35	73.76	7.95	90.05
5 wt% Pt/MgSiO <sub>3</sub>	3.78	84.18	6.97	94.89
5 wt% Pt/SiO <sub>2</sub>	4.98	82.57	6.18	93.73
5 wt% Pt/Al <sub>2</sub> O <sub>3</sub>	6.08	81.36	6.78	94.21
1 wt% Pt/SiO <sub>2</sub>	5.01	83.08	6.81	94.9
5 wt% Pd/MgSiO <sub>3</sub>	11.95	79.28	4.78	95.98
10 wt% Ni-Cu/Al <sub>2</sub> O <sub>3</sub> (P))	4.39	87.03	6.98	98.41
10 wt% Ni-Cu/Al <sub>2</sub> O <sub>3</sub> (S))	10.56	77.09	5.78	93.4

This implied that catalysts such as Pt/C, Pt/MgSiO<sub>3</sub>, Pt/SiO<sub>2</sub> had superior deoxygenation capabilities over catalysts such as Pd/MgSiO<sub>3</sub>, and Ni-Cu/Al<sub>2</sub>O<sub>3</sub>. The results from the two methods used for elemental analyses are shown in Table 5.3. Due to the low volatilities of the wax/oil samples, the two sets of elemental composition results were similar. The densities and calorific contents (HHV) of the oils ranged from 797 to 966 kg/m<sup>3</sup> and 42 - 48 MJ/kg respectively. The HHVs fall in the gasoline, kerosene, and diesel range of 45-47 MJ/kg (Strömberg, 2006).

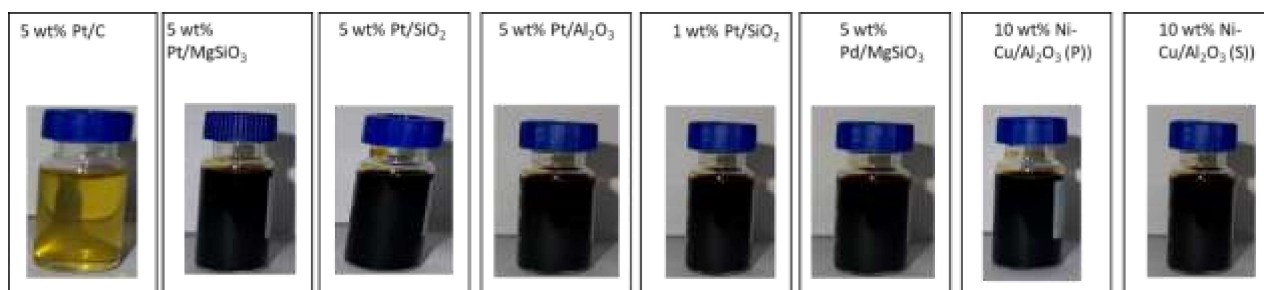


Figure 5.3: Appearance of products obtained from using different catalysts

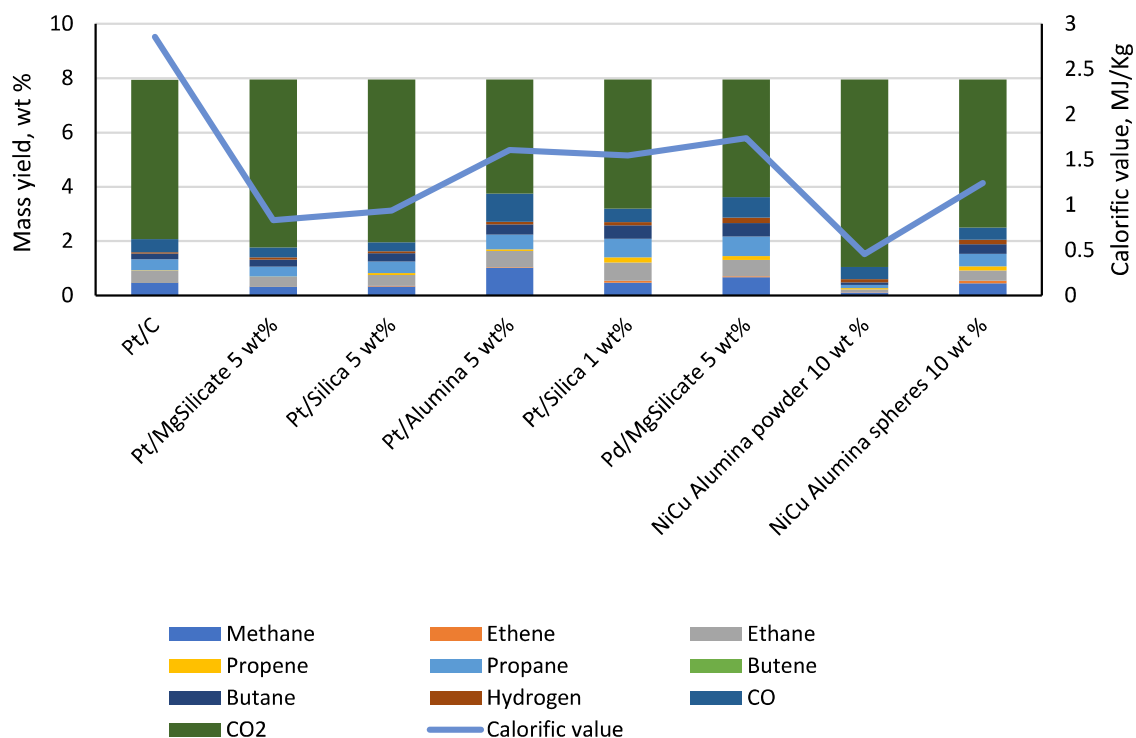


Figure 5.4: Mass yields of gas products obtained from decarboxylation of hydrolysed rapeseed oil at 400 °C, 2 h with various catalysts

#### 5.2.1.2 Gas composition in relation to decarboxylation with different catalysts

The feedstock being dominated by oleic acid (74.4% as reported in Section 4.4.2), the shorter chain alkane derivatives could be formed in one of two possible methods: the hydrocarbon derivatives can be formed from either the decarboxylation of the long-chain fatty acids, followed by cracking to produce shorter chain hydrocarbons, or cracking of long-chain fatty acids to shorter chain fatty acids, followed decarboxylation into hydrocarbons (Fu et al., 2011; Fu et al., 2010). In all cases, the supported Pt-based catalysts gave the highest conversions (Figure 5.5). Decarboxylation with PdMgSiO<sub>3</sub> gave the least alkane yields of about 46%, while Pt/MgSiO<sub>3</sub> in comparison, gave the highest alkane yields. This better activity of the Pt/MgSiO<sub>3</sub> over Pd/MgSiO<sub>3</sub> contradicted the findings reported by Snåre et al., (2006), which reported that Pd had better catalytic activity over Pt. However, the results from this present study agreed with the observations made by Na et al., (2012). The Ni-Cu catalysts had the same metal loadings, but the powdered form had 20% more yield of liquid products, possibly due to the increase in surface area when compared with the spheres.

### 5.2.1.3 Characterisation of liquid products obtained from different catalysts

Table 5.3: Physicochemical properties, density, acid content, elemental composition and calorific value obtained from varying catalyst types

Catalyst	Main organic product	Density (kg/m <sup>3</sup> )	Acid content (wt %)	Method	C (wt%)	H (wt%)	N (wt%)	S (wt%)	O (wt%)	HHV (MJ/kg)
5 wt% Pt/C	Yellow light oil	883	2.08	1	83.31 ± 3.20	13.93 ± 0.51	0.20 ± 0.00	0	2.56 ± 0.08	47.82
				2	84.92	14.84	0	0	0.24	50.1
5 wt% Pt/MgSiO <sub>3</sub>	Dark light oil	797	0	1	83.76 ± 0.40	13.13 ± 0.02	0.22 ± 0.03	0	2.89 ± 0.14	46.76
				2	84.95	15.05	0	0	0	50.43
5 wt% Pt/Silica	Dark light oil	899	17.66	1	82.28 ± 2.75	12.76 ± 0.30	0.20 ± 0.03	0	4.76 ± 0.21	45.39
				2	83.45	14.53	0	0	1.99	48.83
5 wt% Pt/Al <sub>2</sub> O <sub>3</sub>	Dark light oil	880	0	1	84.33 ± 2.13	13.22 ± 0.16	0.20 ± 0.03	0	2.25 ± 0.19	47.2
				2	84.86	14.94	0	0	0.2	50.24
1 wt% Pt/SiO <sub>2</sub>	Dark light oil	846	12.57	1	80.12 ± 2.31	12.15 ± 0.17	0.20 ± 0.02	0	7.53 ± 0.14	43.28
				2	83.53	14.8	0	0	1.67	49.31
5 wt% Pd/MgSiO <sub>3</sub>	Dark light oil	966	51.63	1	81.76 ± 0.85	12.04 ± 0.10	0.20 ± 0.02	0	6.00 ± 0.12	43.95
				2	80.29	13.81	0	0	5.89	46.03
10 wt% Ni-Cu/Al <sub>2</sub> O <sub>3</sub> (P))	Dark light oil	888	30.61	1	80.09 ± 2.54	11.82 ± 0.40	0.24 ± 0.02	0	7.85 ± 0.15	42.73
				2	82.15	14.3	0	0	3.55	47.79
10 wt% Ni-Cu/Al <sub>2</sub> O <sub>3</sub> (S))	Dark light oil	942	49.54	1	81.51 ± 1.13	12.10 ± 0.02	0.19 ± 0.03	0	6.20 ± 0.17	43.92
				2	80.48	13.86	0	0	5.66	46.2

1: CHNS analyser; 2: Calculated from GC-MS analysis



### 5.2.1.3.1 Chemical composition of liquid products in relation to catalyst types

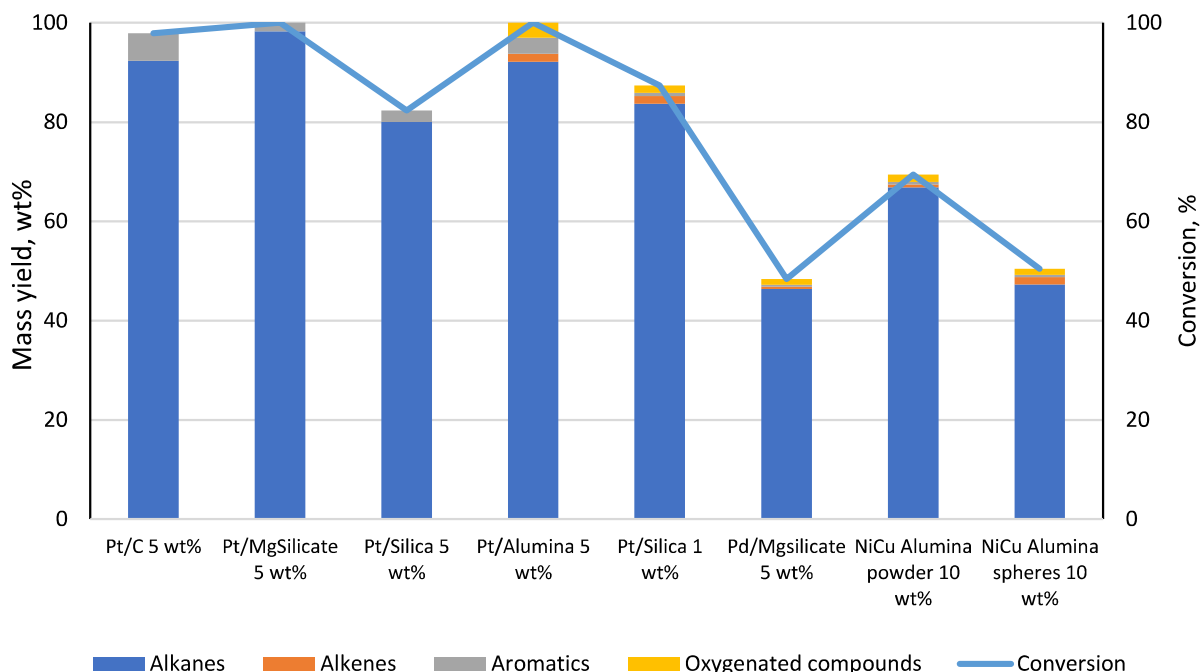


Figure 5.5: Mass yields of hydrocarbon products obtained from decarboxylation of hydrolysed RSO at 400 °C, 2 h with various catalysts based

Figure 5.6 shows the range of hydrocarbons obtained according to their carbon chain length. The hydrocarbons have been grouped into 3 groups. <C11 as potentially gasoline, C11-16 as potentially kerosene, and >C16 as potentially diesel. While the reaction with 1 wt % Pt/SiO<sub>2</sub> did not have the highest liquid hydrocarbons yield, it produced the highest yield of gasoline and kerosene range liquids (55.8%), which suggested the catalyst supports cracking. However, the relatively low yield obtained using this catalyst could not make it the most appropriate option. Supported Pt catalysts produced the largest proportion of fractions >C16. The 5 wt% Pt/C in particular produced the largest proportion of >C16. This could be because the presence of Pt promotes cracking, which leads to the formation of smaller radicals that interact with long chain fractions to yield products with larger molecular weights (Teeter et al., 1957). Overall, it was evident from the heptadecane yields obtained (22 wt% – 60 wt%) that all catalysts could catalyse fatty acid deoxygenation as this was relatively higher than that obtained from the non-catalysed reaction to be reported in Section 5.2.2.

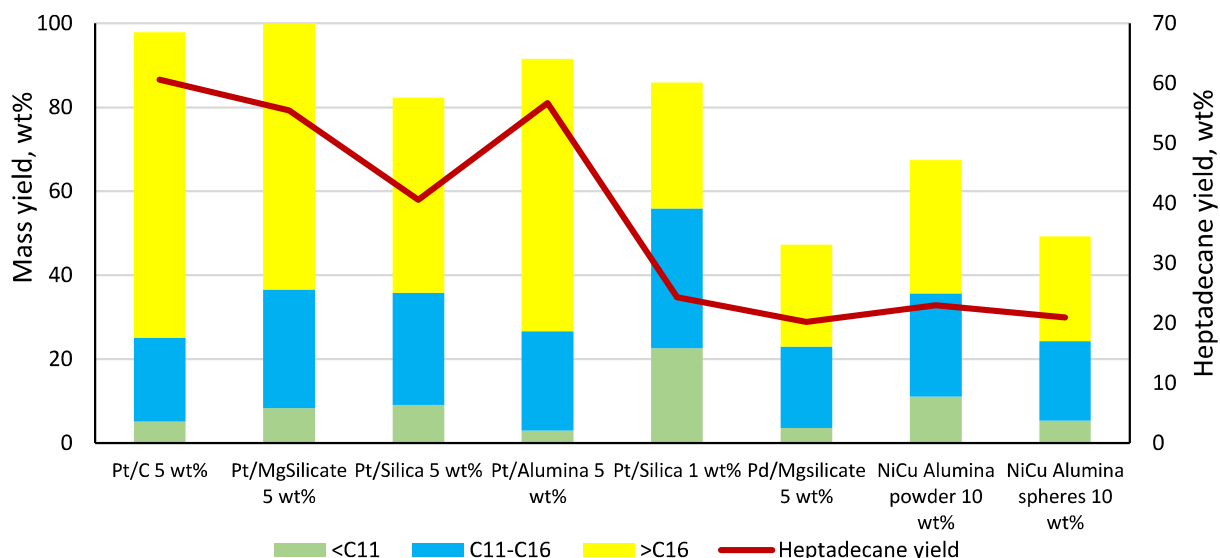


Figure 5.6: Mass yields of heptadecane and other hydrocarbon products obtained from decarboxylation of hydrolysed rapeseed oil at 400 °C, 2 h with various catalysts

In addition, all catalysts produced liquid products that had kerosene-diesel like odour but, the highest overall yields were obtained with Pt/C and Pt/MgSiO<sub>3</sub>. This indicated almost complete decarboxylation, and the absence of shorter chain hydrocarbons furthermore showed that decarboxylation was the dominant reaction step followed by the cracking of the hydrocarbons into shorter chains, as previously discussed in. Fu et al. (2011) reported a 9% heptadecane yield from the decarboxylation of oleic acid with Pt/C at 330 °C for 1.5 h, which was significantly less than the 60% heptadecane yield obtained in this present work when reaction was done at 400 °C for 2 h. Factors such as the increased time and temperature could have definitely contributed to the increase in yield, but contributions from other C<sub>18</sub> fatty acids present in the feedstock could not be ignored. Even though 5 wt% Pt/MgSiO<sub>3</sub> had a higher yield by 2%, Pt/C was chosen as the optimum catalyst because all other catalysts produced dark coloured liquids, which could cause issues with further processing and use of the products. The dark coloured liquids produced was probably due to the dissolution of high molecular weight carbon compounds in the oil. The formation of such compounds may be the onset of coke formation which can be promoted by the acidity of silica and alumina supports (Speight, 2013). The compounds present in these oils are presented in Table 5.4.

Table 5.4: List of compounds from decarboxylation of hydrolysed rapeseed oil at 400 °C, 2 h with various catalysts

Alkanes	Yield, wt %							
	5% Pt/C	5% Pt/MgSiO <sub>3</sub>	5% Pt/SiO <sub>2</sub>	5% Pt/Al <sub>2</sub> O <sub>3</sub>	1% Pt/SiO <sub>2</sub>	5% Pd/MgSiO <sub>3</sub>	10% P-NiCu/Al <sub>2</sub> O <sub>3</sub>	10% S-NiCu/Al <sub>2</sub> O <sub>3</sub>
Heptane	1.22	1.90	2.18	1.99	5.02	0.22	2.45	1.23
Octane	1.27	2.11	2.34	2.10	5.37	0.78	2.69	1.38
Nonane	1.30	2.15	2.24	2.12	5.10	1.18	2.60	1.32
Decane	1.30	2.19	2.34	2.25	5.35	1.46	2.81	1.40
Undecane	1.35	2.42	2.59	2.51	5.59	1.78	3.10	1.63
Dodecane	1.39	2.67	3.17	3.00	5.89	2.18	3.44	1.87
Tridecane	1.42	2.11	2.22	2.28	4.03	1.84	2.57	1.50
Tetradecane	1.45	1.70	1.62	1.96	3.03	1.28	1.94	1.06
Pentadecane	6.52	7.73	7.46	7.83	8.62	5.86	7.54	6.20
Hexadecane	1.43	2.02	1.59	1.92	2.30	1.47	1.72	1.12
Pentadecane, 7-methyl-	-	4.29	0.61	1.62	-	2.14	0.91	1.61
Cyclohexane, 1,5-diethyl-	-	-	0.42	-	0.31	-	-	-
2,3-dimethyl-	-	-	-	-	-	-	-	-
Cyclopentane, 1-pentyl-2-propyl-	-	-	0.69	0.51	0.54	0.35	0.60	0.36
Cyclodecane, octyl-	-	-	3.04	-	1.36	-	2.02	-
Cyclohexane, 1,2-dimethyl-3-pentyl-4-propyl-	-	-	1.50	-	-	-	-	-
Tetradecane, 5-methyl-	0.72	1.31	-	0.48	-	0.65	-	0.49
Tetradecane, 4-methyl-	0.86	1.06	-	-	-	0.53	-	0.37
Hexadecane, 2-methyl-	2.84	1.28	-	-	-	-	-	-
Tetradecane, 3-methyl-	1.76	1.54	-	-	-	-	-	-
Cyclohexadecane	-	0.74	-	-	0.69	-	1.05	0.61
2,6,10-Trimethyltridecane	2.07	-	-	-	0.79	-	-	-
Decane, 2,5-dimethyl-	0.75	-	-	-	-	-	-	-
Undecane, 6-methyl-	-	1.33	-	0.50	-	0.70	-	0.51
Dodecane, 4-methyl-	-	-	-	0.55	-	-	-	-
1,3-Dimethyl-(3,7-dimethyloctyl)cyclohexane	-	-	-	-	-	-	1.64	-
Heptadecane	60.63	55.49	40.56	56.72	24.30	20.21	22.97	20.94
Cyclopentane, decyl-	0.26	-	0.63	0.46	-	0.58	-	0.80
Cyclopentane, undecyl-	-	-	-	-	1.28	-	1.71	-
Cyclohexane, undecyl-	-	-	0.90	-	1.79	0.54	2.14	0.86
10-Methylnonadecane	-	-	-	-	-	-	0.51	-
Cyclopentane, 1-pentyl-2-propyl-	-	-	1.13	-	-	-	-	-
Octadecane	1.81	1.44	0.93	0.89	0.69	0.83	0.51	0.36
Nonadecane	1.54	2.19	1.38	1.85	1.17	1.28	1.35	1.18
Eicosane	0.41	0.65	0.51	0.64	0.50	0.48	0.55	0.45
<b>Total</b>	<b>92.35</b>	<b>98.32</b>	<b>80.04</b>	<b>92.18</b>	<b>83.71</b>	<b>46.3</b>	<b>66.82</b>	<b>47.24</b>

Alkenes	Yield, wt %							
1-Hexene	-	-	-	-	0.50	-	-	-
2-Heptene	-	-	-	-	1.09	-	0.44	-
9-Octadecene, (E)-	-	-	-	1.63	-	-	-	-
5-Octadecene, (E)-	-	-	-	-	-	0.94	-	-

5-Eicosene, (E)-	-	-	-	-	-	-	-	1.51
<b>Total</b>	<b>-</b>	<b>-</b>	<b>-</b>	<b>1.63</b>	<b>1.59</b>	<b>0.94</b>	<b>0.44</b>	<b>1.51</b>

<b>Aromatics</b>	<b>Yield, wt %</b>							
Toluene	-	-	-	-	-	-	0.15	-
Benzene, (1-methyldecyl)-	1.28	0.63	0.95	1.23	-	-	0.17	-
Benzene, (1,1-dimethylnonyl)-	1.81	-	-	1.37	-	-	-	-
Benzene, undecyl-	1.48	0.36	0.53	0.60	0.37	0.14	0.19	0.24
Benzene, dodecyl-	-	0.68	0.82	-	-	0.28	-	0.21
Benzene, 1,4-dimethyl-2-(2-methylpropyl)-	-	-	-	-	-	-	-	-
Benzene, (2-methyl-1-propenyl)-	-	-	-	-	0.22	-	-	-
<b>Total</b>	<b>5.57</b>	<b>1.67</b>	<b>2.3</b>	<b>3.20</b>	<b>0.59</b>	<b>0.42</b>	<b>0.51</b>	<b>0.45</b>

<b>Oxygenated compounds</b>	<b>Yield, wt %</b>							
1-Decanol, 2-hexyl-	-	-	-	3.00	-	1.16	1.50	1.25
1-Hexadecanol	-	-	-	-	1.54	-	-	-
<b>Total</b>	<b>-</b>	<b>-</b>	<b>-</b>	<b>3.00</b>	<b>1.54</b>	<b>1.16</b>	<b>1.50</b>	<b>1.25</b>

After further processing of the elemental compositions of the oils, the van Krevelen diagram was generated using the H/C and O/C molar ratios and comparing to those of common fuels (gasoline, kerosene and diesel). Figure 5.7 shows that the NiCu and Pd supported catalysts had the highest O/C ratios which correlates with their relatively high oxygen contents reported in Table 5.3. The oils produced over Pt/C, Pt/SiO<sub>2</sub>, and Pt/Al<sub>2</sub>O<sub>3</sub> had the greatest potential of comparison with the conventional fuels as they had the high H/C ratios, and the lowest O/C ratios.

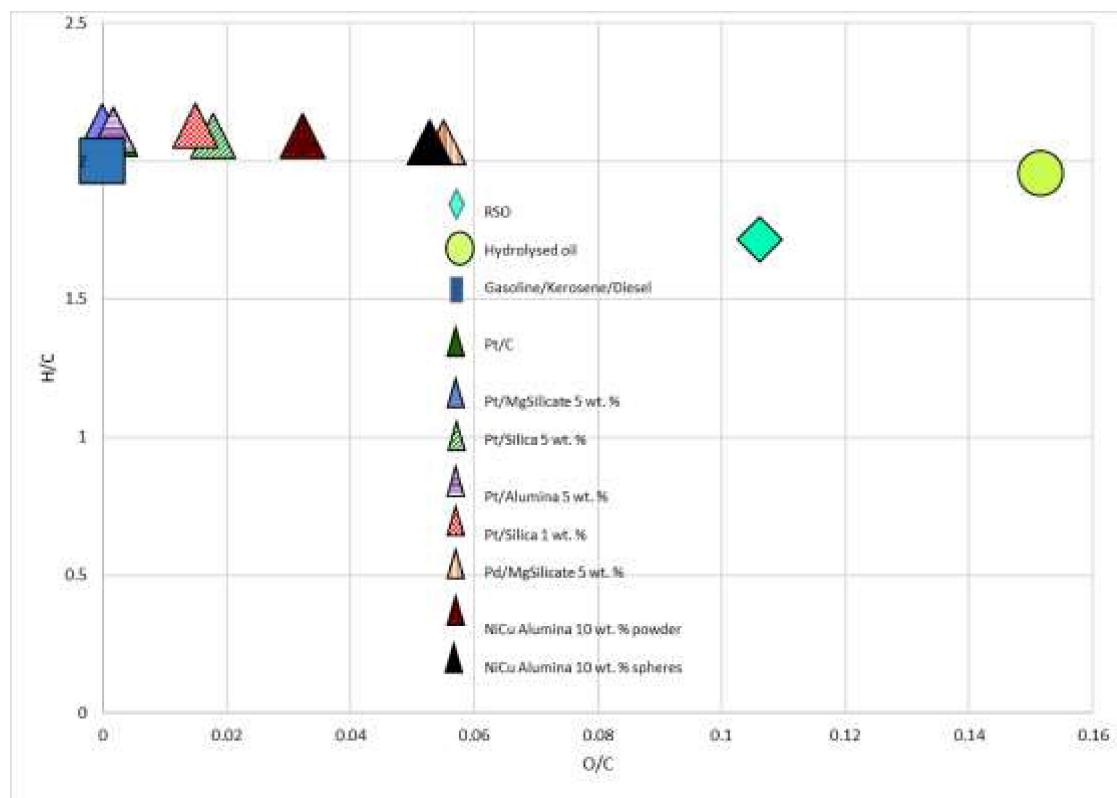


Figure 5.7: Liquid fuels characterisation from varying catalyst type by H/C and O/C molar ratios in Van Krevelen diagram

## 5.2.2 Effect of decarboxylation temperature

This section presents information on the effect of varying reaction temperature on the decarboxylation of fatty acids in hydrolysis products. The reactions were carried out for 1 hour from 350 °C – 400 °C, with and without a catalyst. 2 g of 5 wt% Pt/C was used in the reactions with a catalyst. Pt/C was chosen for these tests because it is commonly used for decarboxylation of fatty acid reactions and is known to give high lipids or fatty acids to liquid hydrocarbons conversion rates (Fu et al., 2011; Zhang et al., 2019).

### 5.2.2.1 Influence of temperature on product yields and mass balance

The liquid/wax products obtained were recovered using dichloromethane solvent, which was subsequently discharged by gentle evaporation as described in Section 3.2.3.1.2.2. The sums of wt% of products from each experiment in Table 5.5 were over 90 wt%, which shows good mass balance closures. This implied minimal formation of highly volatile components, which tend to be lost during sample handling, leading to poor mass balance closures. The detailed characterisation of the liquid products done in subsequent sections could help illustrate this further. Table 5.5 also shows the yields of the products obtained from changing

the reaction temperature. There was an increase in the gas and solid fractions, and a decrease in the liquid and wax products in the absence and presence of catalyst as temperature increased.

Table 5.5: Mass balance for reaction products from decarboxylation of hydrolysed rapeseed oil for 1 h at different temperatures (feed = 10 g)

Temperature (°C)	Catalyst	Products				Balance (wt %)
		Solid (wt%)	Oil (wt%)	Wax (wt%)	Gas (wt%)	
350	-	0.60	95.91	-	0.83	97.34
380	-	0.60	91.81	-	2.30	94.7
400	-	2.60	86.14	-	4.49	93.23
350*	Pt/C	7.21	-	84.28	4.70	96.19
400*	Pt/C	5.37	77.81	-	7.08	90.26

\*reactions with 5 wt% Pt/C catalyst

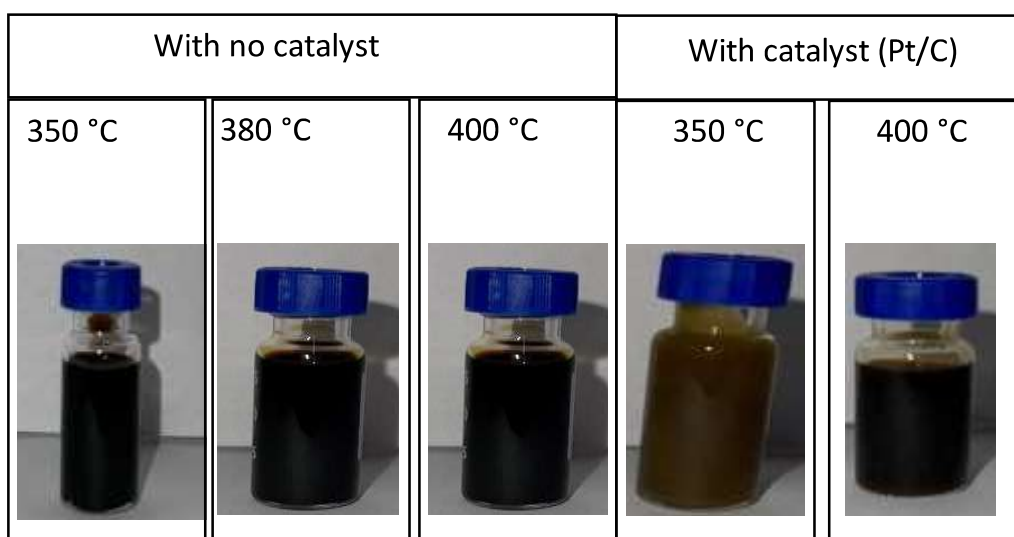


Figure 5.8: Appearance of liquid/wax products

Compared to the corresponding non-catalytic test, the formation of wax at 350 °C with Pt/C suggested the possible hydrogenation of the hydrocarbon chains to form long chain alkanes, which came out as wax at room temperature (Oliver-Tomas et al., 2017). Indeed, a significant amount of DCM-insoluble white solid particles were formed during the catalytic experiment at 350 °C, which melted after heating on a hot plate to 50 °C, showing that they were organic in nature and therefore could be solid hydrocarbons. This should be further clarified after the liquid/wax fractions were analysed on the GC/MS, in the results presented below in Section 5.2.2.3. Although liquid/wax products obtained in the absence of the catalyst looked similar in terms of their colours, the oil from the reaction at 350 °C was very viscous, and this viscosity reduced with the increase in temperature (Figure 5.8). Overall, all

oil/wax products obtained were relatively darker in colour compared to the feed (hydrolysis product). With the 5 wt% Pt/C catalysed reaction at 350 °C, it was impossible to separate the catalyst from white solid organic particles, hence higher (34%) solid yield was recorded during this test compared to the catalytic test at 400 °C. On the other hand, the solid fractions accounted for from the non-catalysed reactions at 350 °C, 380 °C, 400 °C were pure char because all the liquid product dissolved in the DCM and filtered off. All fractions except the solid products are further characterised and discussed in the following sections. This is because the yields of the solids were too low and considered negligible.

#### 5.2.2.2 Influence of decarboxylation temperature on gas composition

The composition of gases produced from varying the reaction temperature during decarboxylation is presented in Figure 5.8. There was a notable increase in the CO<sub>2</sub> produced with the rise in temperature in reactions carried out in the absence of a catalyst. As decarboxylation is achieved by the release of CO<sub>2</sub>, this could mean that deoxygenation occurred even without a catalyst. However, the yields of gas products indicated that gas formation in the absence of catalyst was a non-selective process, with seeming increases in the yields of different gas components. Hence, the effect of temperature alone was insufficient to make gas formation selective towards the target decarboxylation reaction. However, there was at least a nine-fold increase in CO<sub>2</sub> yields at temperatures 350 and 400 °C when reactions in the absence of catalyst are compared with those performed with catalyst, which showed the effect of the presence of Pt/C. The selectivity of the catalyst towards decarboxylation and hence, CO<sub>2</sub> production is clearly shown in Figure 5.9 between 350 and 400 °C. This may be the reason decarboxylation reactions are commonly carried out between 350 °C and 400 °C in literature (Jiraroj et al., 2021; Hossain et al., 2018) and Pt/C is well-known to promote decarboxylation of fatty acids. For example, Fu et al. (2011) reported over 90% selectivity towards hydrocarbons from the decarboxylation of C12, C16, and C18 saturated fatty acids. There is also an increase in the yield of hydrocarbon gases with the increase in temperature, with or without a catalyst. Cracking of C-C bonds in the fatty acids or products of their decarboxylation, is an endothermic process, which can be promoted at elevated temperatures (Hubesch et al., 2022). A potential contribution to these increased yields of C1-C4 gases, especially in the presence of Pt/C is the elevated H<sub>2</sub> yields detected with the increase in temperature. Vardon et al., (2014) reported that the presence of H<sub>2</sub> as a reducing gas helps to keep the active sites on the catalyst in reduced oxidation states and therefore, enhance the function of the catalyst to carry out the decarboxylation reaction and produce hydrocarbons. The gases obtained are just a by-product of this process, and not the goal. Nonetheless, they have calorific values ranging from 0.5 - 4 MJ/kg which could be utilised for process heat.

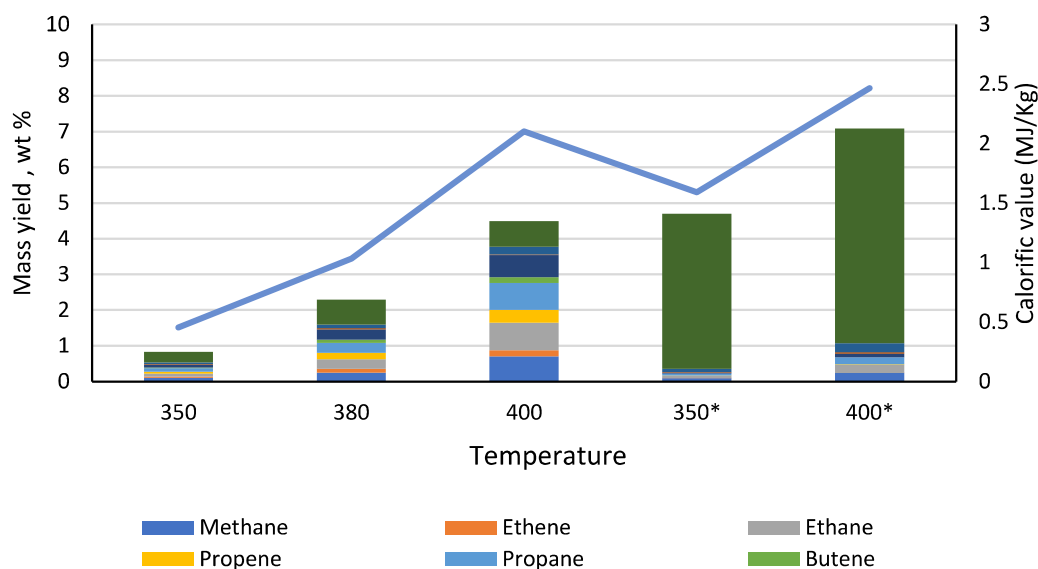


Figure 5.9: Mass yield, wt% of gases obtained from decarboxylation of hydrolysed RSO for 1 h at different temperatures (\*reactions with 5 wt% Pt/C catalyst)

The acid contents obtained by titration showed that increasing temperature aided decarboxylation because the acid yield can be seen to reduce in Table 5.6. The drop in acid content at same temperatures but with a catalyst further emphasised the effect of 5 wt% Pt/C. At 350 °C, the acid content was 75.16 wt% in the absence of catalyst, but this decreased by 47.7% in the presence of the Pt/C catalyst. Similar trends were observed at 400 °C, where the acid contents decreased by 79.8% when Pt/C catalyst was present compared to the test without the catalyst. Therefore, the oil/wax products with high acid content still contained significant amounts of unconverted fatty acids. The densities of the oils seemed to decrease with the increase in temperature, which was expected as the rise in reaction condition severity led to higher decarboxylation and production of lighter chain products in the oils. Commercial fuels such as gasoline, kerosene, and diesel have densities 715 – 780 kg/m<sup>3</sup> at 15 °C, 775 – 840 kg/m<sup>3</sup> at 15 °C and 820 – 959 kg/m<sup>3</sup> at 15 °C, respectively (Strömberg, 2006). The densities of the decarboxylated hydrolysed RSO obtained at this stage with varying temperature fell between those of kerosene and diesel fuels, even with their varying oxygen (acid) contents.



### 5.2.2.3 Influence of decarboxylation temperature on the characteristics of liquid products

#### 5.2.2.3.1 Physico-chemical properties of the liquid products

Table 5.6 also highlights the elemental composition and calorific values of the oil/wax products. In Table 5.6, the values obtained through Method 1 were those obtained from the CHNS elemental analyser, while values from Method 2 were those obtained using the composition and yields of compounds identified by the GC/MS (a new method described in Chapter 3). This was due to increased volatility of the oil products, meaning that a proportion of the weighted oils for CHNSO analysis were lost during the analytical procedure. There was only a slight difference in the expected and calculated values in the non-catalysed reactions which possibly had minimal decarboxylation (hence, little volatile compound contents) when compared to the reactions carried out with a catalyst. The calorific values of the oil/wax products were also a crucial characteristic to consider as this has an impact on the engine efficiency. An interesting trend can be observed in the calorific values of the oil/wax products in Table 5.6. The calorific values of the products obtained at lower decarboxylation temperatures were around 40 MJ/kg, similar to those reported for >C18 fatty acids by Demirbas (2016) to be between 39 – 42 MJ/kg. In contrast, as the reaction severity increased in terms of temperature and presence of 5 wt% Pt/C, the calorific values increased to between 45.8 and 49.5 MJ/kg, similar to those of diesel fuel (Strömberg, 2006). Hence, the trends in the densities, acid contents and calorific values of the oil/wax products in Table 5.6, could be used to indicate the degree of decarboxylation of the fatty acids.

Table 5.6: Density, acid content, elemental composition and calorific value obtained from varying reaction temperature

*Elemental composition											
Temperature (°C)	Catalyst	Main organic product	Density (kg/m <sup>3</sup> )	Acid content (%)	Method	C (wt%)	H (wt%)	N (wt%)	S (wt%)	O (wt%)	HHV (MJ/Kg)
350	-	Dark viscous oil	1001	75.16	1	76.32 ± 0.34	12.06 ± 0.23	0.11 ± 0.02	-	11.5 ± 0.21	41.15
					2	77.73	10.16	-	-	12.11	38.77
380	-	Dark viscous oil	930	45.81	1	77.69 ± 0.7	12.26 ± 0.02	0.11 ± 0.01	-	9.94 ± 0.10	42.18
					2	80.3	13.67	-	-	6.03	45.8
400	-	Dark heavy oil	937	37.1	1	77.04 ± 0.84	11.72 ± 0.09	0.09 ± 0.01	-	11.2 ± 0.13	40.95
					2	81.48	13.18	-	-	0.44	46.51
350	Pt/C	Dark wax	910	39.32	1	79.58 ± 0.64	12.74 ± 0.70	0.1 ± 0.01	-	7.59 ± 0.16	43.94
					2	81.84	13.66	-	-	4.5	46.59
400	Pt/C	Dark heavy oil	906	7.49	1	83 ± 0.1	13.9 ± 0.31	0.11 ± 0.01	-	2.99 ± 0.11	47.6
					2	84.55	14.61	-	-	0.84	49.53

1 = CHNS analyser; 2 = Calculated from GC-MS analysis

#### 5.2.2.3.2 Chemical composition of liquid/wax products in relation to reaction temperature

Figure 5.10 shows the yields of components in the oil/wax products derived from the decarboxylation of the rapeseed oil hydrolysate with and without 5 wt% Pt/C catalyst. Only the compounds that eluted from the column and seen in the GC/MS chromatograms were used to produce Figure 5.10. The heavier components such as unconverted fatty acids which did not elute from the GC/MS column were not considered. As expected, the conversion and yield of the liquid products were found to increase with temperature (Lestari et al., 2008; Simakova et al., 2009), leading to the formation of compounds that were more volatile than fatty acids and thus could be quantified by GC/MS. It is important to recall that determination of fatty acid by GC/MS was only possible after their esterification for fatty acid alkyl esters (Chapter 4). The GC/MS results showed that the oil/wax products obtained in the presence of catalyst contained higher proportions of GC/MS quantified components in the form of alkanes. Indeed, no oxygenated compounds were detected at 400 °C. However, at 350 °C in the presence of Pt/C, about 0.6 wt% oxygenates remained in the oil/wax product. Hence, the inability of the GC/MS to quantify the unconverted fatty acids is represented by the conversion data shown in Figure 5.10.

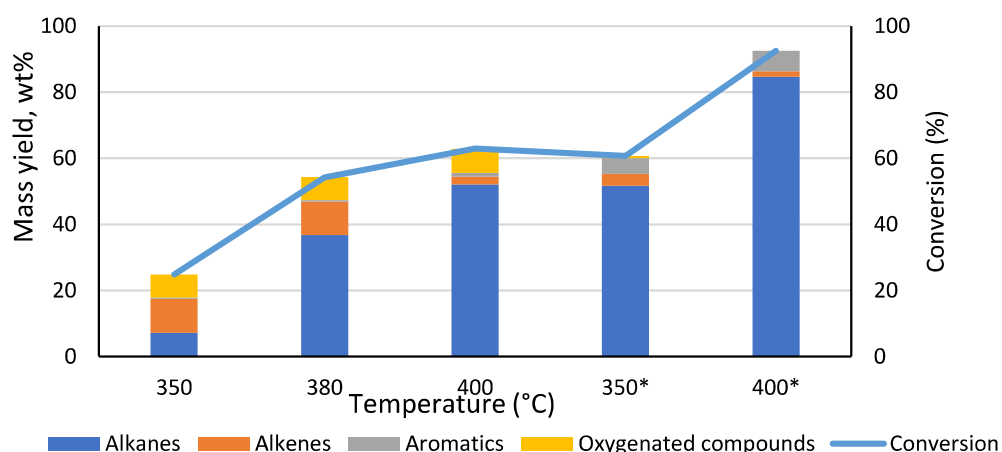


Figure 5.10: Mass yields of compounds groups obtained from decarboxylation of hydrolysed RSO for 1 h at different temperatures (\*with 5 wt% Pt/C catalyst)

Therefore, in the absence of 5 wt% Pt/C, the trend in the conversions of the hydrolysis products (fatty acids) to GC/MS elutable, identifiable and quantifiable components were as follows: 350 °C < (24.84 %) < 380 °C (54.19 %) < 400 °C (62.9 %). In the presence of the catalyst, conversion was still low at 350 °C (60.68 %) but increased dramatically to 92.5 % at 400 °C.

Results in Figure 5.10 shows that there was an increase in the yield of alkanes with increasing temperature with and without a catalyst, but the higher yields of alkanes were observed in the presence of 5 wt% Pt/C shows the selective effect of the catalyst towards decarboxylation as temperature

increased. In the presence of 5 wt% Pt/C, there is also an increase in the yield of aromatics. This could be linked to the increase in hydrogen yield observed with increased temperature reported in Section 5.2.2.2. As reported in literature, aromatics can be produced from the combined process of cyclisation and aromatisation of alkanes, with subsequent release of hydrogen gas (Ali et al., 2022). The presence of aromatics may be important for fuel properties, but the highest yield of aromatics was 6.20 wt% (at 400 °C), amounted to just 6.70% of the oil product. Hence, decarboxylation alone even at 400 °C, did not seem to produce the level and possibly types of aromatics to make the product comparable to Jet-A, which contains up to 25% aromatics.

The yield of GC/MS elutable, identifiable and quantifiable oil/wax products based on the carbon chain length from the decarboxylation of RSO-derived fatty acids with and without 5 wt% Pt/C over a range of temperatures (350 °C – 400 °C) are shown in Figure 5.11. The length of the carbon chains obtained was strongly influenced by reaction temperature. Increasing decarboxylation temperature led to a wide range of product distribution with both light and heavy hydrocarbons. The results in Figure 5.11 mirrored those in Figure 5.10, showing that the increase in process severity (temperature) and use of catalysts, led to increased decarboxylation and subsequently produced higher alkane yields.

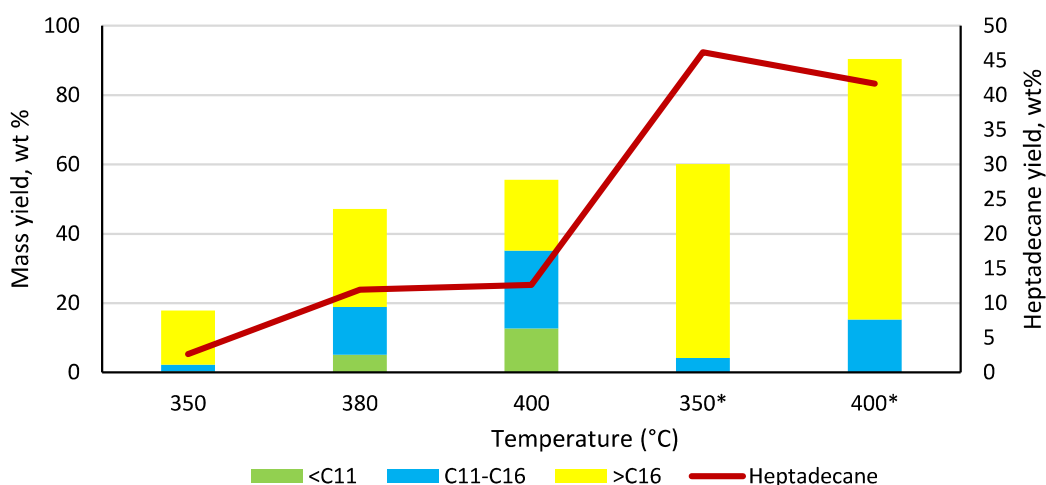


Figure 5.11: Mass yields of heptadecane and other hydrocarbon products obtained from decarboxylation of hydrolysed RSO for 1 h at different temperatures (\*with 5 wt% Pt/C catalyst)

In particular, the yield of heptadecane were a good indication of the decarboxylation selectivity of the reactions. The yields of quantifiable compounds from the GC/MS analysis aligned well with those of the acid contents of the processed samples as determined by acid-base titration in Table 5.6. This confirmed the obvious negative correlation between the acid contents (Table 5.6) and yields of alkanes (Figure 5.10). Considering that RSO was dominated by C<sub>18</sub> fatty acids and particularly oleic acid, the formation

of heptadecane should indicate the extent of decarboxylation of the fatty acids. Chapter 4 showed that RSO contained fatty acids with the C12 to C22 range, therefore, the formation of hydrocarbons with less than C12 chain lengths indicated that some C-C bond cracking occurred in addition to the main decarboxylation. It was also possible that this cracking contributed to the range of compounds with C12 – C16 chain lengths, as the yields of these compounds increased with increasing reaction temperature. With the 5 wt% Pt/C, there was over a two-fold increase of C11-C16 hydrocarbons from 350 °C, while a 36.36% increase in the >C16 fraction was observed as the temperature increased. The increase in <C11 and C11-C16 hydrocarbons as the temperature increased from 350 °C, may also indicate that the cracking reactions were favoured over isomerisation reactions. As indicated in Section 5.2.2.3.2, the presence of the catalyst proved to not only increase the conversion but also the selectivity of hydrocarbons produced. The experiment carried out at 400 °C with catalyst had the highest conversion, 92.5% (Section 5.2.2.3.2), which implied almost complete decarboxylation of the fatty acids. However, the product obtained at 400 °C was a dark heavy oil (Figure 5.8), which would not be directly suitable as a fuel substitute. The compounds obtained are displayed in Table 5.7. Figure 5.12 presents the H/C and O/C ratios of the oils produced from varying reaction temperature in a Van Krevelen diagram. The figure shows that the reactions carried out in the absence of the catalysts had the highest O/C ratios, which correlated with the conversion results reported in Table 5.6. The major findings from these tests varying temperature were that an increase in reaction severity in terms of temperature favoured the conversion of fatty acids to hydrocarbons. This is observed with the decrease in fatty acid yields and increase in hydrocarbon yields as temperature increased. This result also supports the expectation that increasing reaction temperature will cause an increase in the reaction rate due to the increase in kinetic energy which causes increased collision of molecules for there to be faster conversions in a certain time.

Table 5.7: List of compounds from decarboxylation of hydrolysed rapeseed oil for 1 h at different temperatures (feed = 10 g)

Alkanes	Yield, wt %				
	350 °C	380 °C	400 °C	350* °C	400* °C
Heptane	-	0.91	1.65	-	-
Cyclohexane, methyl-	-	-	-	-	-
Cyclopentane, ethyl-	-	-	-	-	-
Octane	-	1.1	2.73	-	-
Cyclohexane, ethyl-	-	-	-	-	-
Nonane	0.16	1.14	3.27	-	-
Decane	0.12	0.99	3.07	-	-
Cyclopentane, butyl-	-	-	-	-	-
Decane	-	-	-	-	-
Cyclohexane, butyl-	-	0.34	-	-	-
Cyclopentane, pentyl-	-	-	-	-	-

Undecane	0.14	1.18	-	-	0.3
Cycloheptane, methyl-	-	-	0.23	-	-
Octane, 2,4,6-trimethyl-	-	-	2.71	-	-
Cyclopentane, hexyl-	-	-	0.22	-	-
Cyclohexane, pentyl-	-	-	-	-	-
Dodecane	0.15	1.32	3	-	0.57
Cyclohexane, octyl-	-	0.16	0.26	-	-
Cyclopentane, 1-butyl-2-propyl-	-	-	0.22	-	-
Cyclohexane, hexyl-	-	-	-	-	-
Tridecane	-	0.66	1.63	-	0.73
Cyclopentane, 1-hexyl-3-methyl-	-	-	0.61	-	-
Tetradecane	-	-	1.29	-	0.86
Dodecane, 2-cyclohexyl-	-	-	0.4	-	-
Pentadecane	1.6	0.48	6.32	5.38	5.86
Cyclohexane, undecyl-	-	-	0.49	-	-
Hexadecane	-	4.88	1.13	0.57	1.19
2,6,10-Trimethyltridecane	-	-	-	-	1.73
Decane, 2,5-dimethyl-	-	-	-	-	0.65
Cyclododecane	-	0.16	-	-	-
Cyclohexane, undecyl-	-	0.23	-	-	-
Cyclohexadecane	-	0	-	1.02	-
Hexadecane	-	0.56	-	-	-
Decane, 4-cyclohexyl-	-	2.8	0.27	-	-
Cyclohexane, 1,5-diethyl-2,3-dimethyl-	-	-	0.66	-	-
Cyclopentane, 1-pentyl-2-propyl-	-	-	1.05	-	0.85
Cyclopentane, 1-butyl-2-pentyl-	-	-	0.84	-	-
Dodecane, 2-cyclohexyl-	-	-	-	-	-
Cyclohexane, nonadecyl-	-	-	-	-	-
1-Cyclopentyleicosane	-	-	1.13	-	-
Pentadecane, 4-methyl-	0.47	-	-	-	-
Hexadecane, 2-methyl-	1.14	-	-	-	-
Tetradecane, 5-methyl-	-	-	-	-	0.54
Tetradecane, 4-methyl-	-	-	-	-	0.66
Tetradecane, 3-methyl-	-	-	-	-	1.4
Hexadecane, 2-methyl-	-	-	-	-	2.11
Heptadecane	2.64	11.96	12.64	76.13	63.49
Cyclopentadecane	0.55	1.43	-	-	-
Cyclohexane, undecyl-	1.29	2.96	2.44	-	-
Cyclooctacosane	-	0.31	-	-	-
Cyclopentane, decyl-	-	1.53	-	-	-
Octadecane	0.54	0.85	-	2.08	1.53
Cyclopentane, 1-hexyl-3-methyl-	-	-	1.13	0	0
Cyclooctane, tetradecyl-	-	-	-	-	-
Heptadecane, 3-methyl-	-	-	-	-	-
Nonadecane	-	-	0.41	-	1.69
Eicosane	-	0.61	1.08	-	0.47
Heneicosane	-	0.21	0.25	-	-
Docosane	-	-	0.69	-	-

Tricosane	-	-	0.25	-	-
<b>Total</b>	<b>7.19</b>	<b>36.75</b>	<b>52.08</b>	<b>51.68</b>	<b>84.61</b>

<b>Alkene</b>	<b>Yield, wt %</b>				
	350 °C	380 °C	400 °C	350* °C	400* °C
2-Heptene, (E)-	-	0.25	0.33	-	-
2-Octene, (E)-	-	0.2	0.27	-	-
trans--4-Nonene	-	-	0.22	-	-
4-Nonene	-	-	0.37	-	-
(Z)-5-Decene	-	-	0.4	-	-
2-Decene, (E)-	-	0.19	0.23	-	-
4-Undecene, (E)-	-	0.2	0.53	-	-
2-Undecene, (E)-	-	0.24	-	-	-
3-Dodecene, (Z)-	-	0.16	-	-	-
5-Tetradecene, (E)-	-	0.16	-	-	-
1-Hexadecene	-	2.1	-	-	-
8-Heptadecene	-	1.57	-	0.94	1.13
5-Octadecene, (E)-	0.13	-	-	1.27	0.57
9-Octadecene, (E)-	-	-	-	3.67	-
9-Eicosene, (E)-	1.77	5.04	-	-	-
9-Eicosene, (E)-	5.44	-	-	-	-
5-Eicosene, (E)-	1.68	-	-	-	-
9-Eicosene, (E)-	0.81	-	-	-	-
5-Heptadecene, 1-bromo-	0.29	-	-	-	-
Cyclohexene, 1-decyl-	0.22	-	-	-	-
<b>Total</b>	<b>10.32</b>	<b>10.13</b>	<b>2.35</b>	<b>3.57</b>	<b>1.69</b>

<b>Aromatics</b>	<b>Yield, wt %</b>				
	350 °C	380 °C	400 °C	350* °C	400* °C
Toluene	-	-	0.12	-	-
1-Phenyl-1-butene	-	-	0.12	-	-
Benzene, hexyl-	-	-	0.17	-	-
Benzene, heptyl-	-	-	0.31	-	-
Benzene, (1-methyldecyl)-	0.12	0.13	0.2	3.41	3.07
Benzene, undecyl-	-	0.05	0.21	0.4	2.07
Benzene, (1,1-dimethylnonyl)-	-	-	-	1	1.06
<b>Total</b>	<b>0.12</b>	<b>0.18</b>	<b>1.13</b>	<b>4.81</b>	<b>6.2</b>

<b>Oxygenated compounds</b>	<b>Yield, wt %</b>				
	350 °C	380 °C	400 °C	350* °C	400* °C
2-Ethyl-oxetane	-	0.18	0.39	-	-
Octanoic acid	-	0.25	-	-	-
Nonanoic acid	0.12	0.39	-	-	-
n-Decanoic acid	0.13	0.36	-	-	-
Undecanoic acid	-	0.27	-	-	-
Acetic acid n-octadecyl ester	0.36	1.36	1.78	-	-

n-Nonadecanol-1	0.73	0	2.38	-	-
(3-Methylphenyl) methanol, 2-methylpropyl ether	-	0.35	-	-	-
1,3-Dimethyl-(3,7-dimethyloctyl), cyclohexane	-	0.99	-	-	-
1,3-Dimethyl-(3,7-dimethyloctyl), cyclohexane	-	0.87	-	-	-
Carbonic acid, decyl undecyl ester	0.13	0.54	1.17	-	-
Carbonic acid, octadecyl propyl ester	0.38	-	-	-	-
Oxalic acid, butyl 1-menthyl ester	0.12	0.58	-	-	-
n-Heptadecanol-1	-	1.59	-	-	-
Oxalic acid, cyclohexylmethyl octyl ester	0.18	0.21	-	-	-
Oxalic acid, cyclohexylmethyl nonyl ester	0.13	-	-	-	-
n-Pentadecanol	0.25	-	-	-	-
(3-Methylphenyl) methanol, 2-methylpropyl ether	0.2	-	-	-	-
Pentadecanoic acid	0.3	-	-	-	-
2-n-Heptylcyclopentanone	0.14	0.26	-	-	-
Phenol, 4-undecyl-	-	0.31	-	-	-
Octadecanoic acid	1.46	0.33	-	-	-
2(3H)-Furanone, dihydro-5-tetradecyl-	0.46	0.23	-	0.61	-
<b>Total</b>	<b>6.93</b>	<b>7.06</b>	<b>7.33</b>	<b>0.61</b>	<b>-</b>

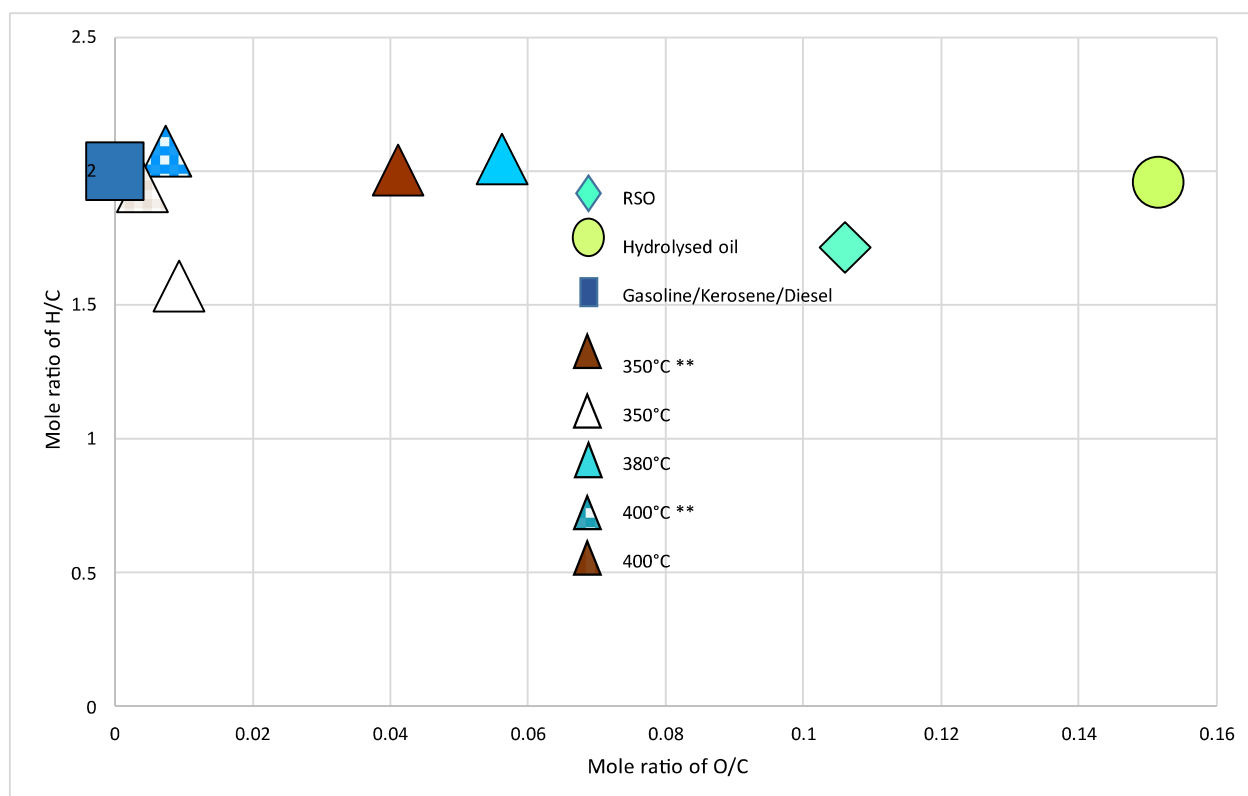


Figure 5.12: Liquid fuels characterisation from varying reaction temperature by H/C and O/C molar ratios in Van Krevelen diagram





### 5.2.3 Effect of 5 wt% Pt/C catalyst loading of the decarboxylation of fatty acids from hydrolysis stage

From the work conducted on effect of temperature, the reaction conditions of 400 °C, 1 h with 2 g Pt/C (catalyst/feed mass ratio of 0.2) seemed to produce the best results in terms of oil yield and composition. Therefore, experiments were carried out to test the effect of catalyst loading using identical conditions to investigate the possibility of achieving desirable results with lower catalyst loadings. Catalyst-to-feed mass ratios of 0.0, 0.05, 0.1 and the baseline 0.2 were explored. Catalyst loading referred to the mass of each catalyst formulation used during the reactions; e.g. 2 g of 5 wt% Pt/C.

#### 5.2.3.1 Effect of 5 wt% Pt/c catalyst/feed mass ratios loading on product yields and mass balance

Table 5.8 shows the yields of the different phases of products obtained, with mass balance closures over 90%. For a basis of comparison, an experiment was carried out in the absence of any catalyst, which produced a liquid with similar yields to the yields of oil/wax from the experiments with Pt/C (Table 5.8). The liquid/wax products from these reactions were dominant and followed the order of catalyst/feed ratios  $0 > 0.05 > 0.1 > 0.2$ . Solid product yields increased with increased catalyst/feed ratios and a similar trend was observed for the gas products. This non-catalysed reaction is the same as that reported and discussed in Section 5.2.2. The same results have been displayed in the following sections for ease of comparison, and discussion.

Table 5.8: Mass balance for reaction products from decarboxylation of hydrolysed rapeseed oil at 400 °C, 1 h with different 5 wt% Pt/C catalyst/feed mass ratios

Catalyst/ feed mass ratio	Products				Balance (wt%)
	Solid (wt%)	Oil (wt%)	Wax (wt%)	Gas (wt%)	
0	2.59	86.14	-	4.49	93.22
0.05	2.30	-	85.40	4.50	92.2
0.1	4.89	-	84.13	4.99	94.02
0.2	5.37	77.81	-	7.06	90.24

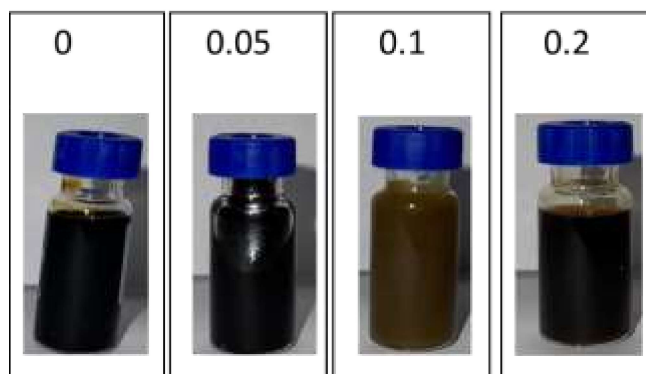


Figure 5.13: Appearance of products in relation to 5 wt% Pt/C catalyst/feed mass ratios from decarboxylation of hydrolysed RSO

These results showed that increased catalyst loading led to increased cracking to lower molecular weight compounds with higher volatility, hence leading to losses and lower mass balance closures. The formation of wax products with catalyst/feed ratios of 0.05 and 0.1 implied the formation of long-chain saturated hydrocarbons, while the liquid products formed with catalyst/feed ratios of 0 and 0.2 suggested the formation of shorter chain hydrocarbons providing a solvent effect for the longer chain hydrocarbons (Figure 5.13). However, the reaction carried out in the absence of a catalyst indicated the shorter chain hydrocarbons were produced more by cracking than decarboxylation, as discussed in Section 5.

#### 5.2.3.2 Gas composition in relation to 5 wt% Pt/C catalyst/feed ratio

The production and yield via decarboxylation of  $\text{CO}_2$  would be an indication of the degree of deoxygenation, by losing oxygen atoms as  $\text{CO}_2$ . Therefore, the least amount of  $\text{CO}_2$  (7.5%) produced in the absence of a catalyst showed the importance of the addition of a catalyst, which in comparison, was further emphasised by the 460% increase in the yield of  $\text{CO}_2$  in the reaction with catalyst/feed ratio of 0.2 (Figure 5.14).

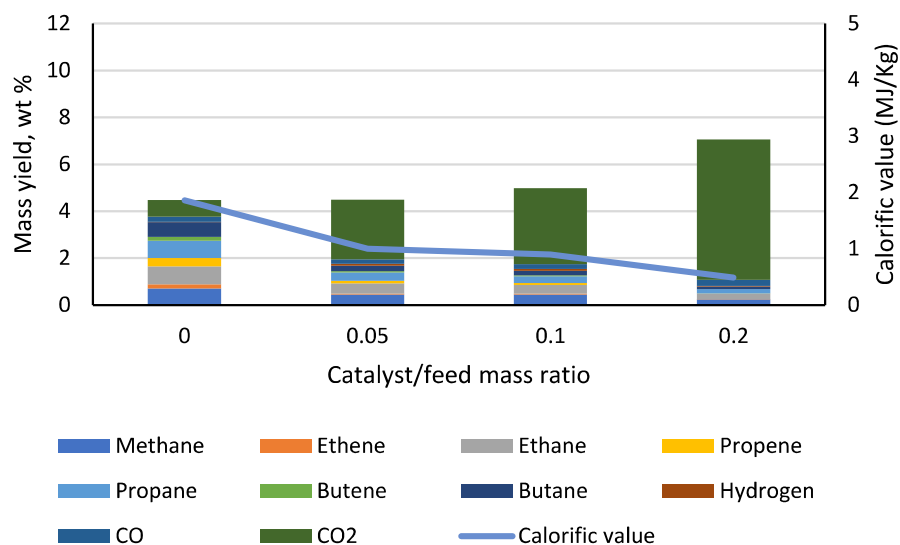


Figure 5.14: Mass yields and calorific values of gas products obtained from decarboxylation of hydrolysed RSO at 400 °C, 1 h with different 5 wt% Pt/C catalyst/feed mass ratios

The test without catalyst gave the highest mass yield of 3.6 wt% towards CH<sub>4</sub>, C<sub>2</sub>H<sub>4</sub>, and C<sub>2</sub>H<sub>6</sub>, which implied that thermal cracking occurred. As stated earlier, there was in situ H<sub>2</sub> production possibly due to the effect of the catalyst or cracking at high reaction temperatures (Liu et al., 2021). Nonetheless, the detection of H<sub>2</sub> in the gaseous products implied more than the stoichiometric minimum H<sub>2</sub> amount required for the hydrogenation of the unsaturated bonds was present. Since CO<sub>2</sub> has no calorific value, the gas obtained using catalyst/feed ratio of 0.2, which contained the highest CO<sub>2</sub> yield, gave the lowest calorific value (0.48 MJ/Kg).

### 5.2.3.3 Characterisation of liquid products in relation to varying 5 wt% Pt/C catalyst/feed mass ratios

#### 5.2.3.3.1 Liquid product properties in relation to varying 5 wt% Pt/C catalyst/feed mass ratios

Table 5.9: Density, acid content, elemental composition and calorific value obtained from varying 5 wt% Pt/C catalyst/feed mass ratios

*Elemental compositions										
Catalyst/feed mass ratio	Main organic product	Density (Kg/m <sup>3</sup> )	Acid content (wt%)	Method	C (wt%)	H (wt%)	N (wt%)	S (wt%)	O (wt%)	HHV (MJ/Kg)
0	Dark thick oil	923	37.1	1	77.04 ± 0.84	11.72 ± 0.09	0.09 ± 0.01	-	11.2 ± 0.13	40.95
				2	81.48	13.18	-	-	0.44	40.74
0.05	Dark wax	910	30.65	1	79.31 ± 0.03	13.14 ± 0.03	0.15 ± 0.06	-	7.39 ± 0.40	44.46
				2	81.85	13.85	-	-	3.56	47.03
0.1	Dark wax	907	24.98	1	80.90 ± 0.89	13.69 ± 0.11	0.12 ± 0.00	-	5.30 ± 0.02	46.17
				2	82.74	14.11	-	-	3.15	47.78
0.2	Dark heavy oil	906	7.49	1	83 ± 0.1	13.9 ± 0.31	0.11 ± 0.01	-	2.99 ± 0.11	47.6
				2	84.55	14.61	-	-	0.84	49.53

1: CHNS analyser; 2: Calculated from GC-MS analysis

The elemental compositions and calorific values of the product oils are presented in Table 5.9. As previously stated in Section 5.2.2.3.1, the values for Method 1 were obtained from the CHNS analyser and Method 2 from the GC-MS. The wax and heavy oil samples (from catalyst/feed ratios of 0.0, 0.05 and 0.1), which possibly contained heavier chain hydrocarbons had minimal differences between their values from the two methods in comparison with the product oil from the test with catalyst/feed ratio of 0.2. The acid content of the oils and densities decreased as the ratio of catalyst increased, while the HHVs also increased from 41 MJ/kg by 22% (Table 5.9). The HHV of the oils were in the range of existing fuels such as gasoline, kerosene, and diesel which ranges from 45-47 MJ/kg (Strömberg, 2006) highlighting the changes in the properties of the oil/wax products with both the presence of the catalyst and with increase catalyst/feed ratios.

#### 5.2.3.3.2 Chemical composition of liquid/wax products in relation to 5 wt% Pt/C catalyst/feed loading

There was an increase in conversion with increasing catalyst loading, which correlated with the gas yields results reported in Figure 5.14 due to the increasing CO<sub>2</sub> contents. As seen Figure 5.15, the yield of liquid alkanes increased with the increasing catalyst/feed mass ratios, suggesting the catalyst played a significant role in hydrogenation and possibly hydrogenolysis (Feng et al., 2016). All reactions with catalyst/feed mass ratio of lower than 0.2 showed the presence of oxygenated compounds and significantly lower overall yield of hydrocarbon products, which implied the inefficiency of the reaction system to achieve complete decarboxylation, (Snåre et al., 2006).

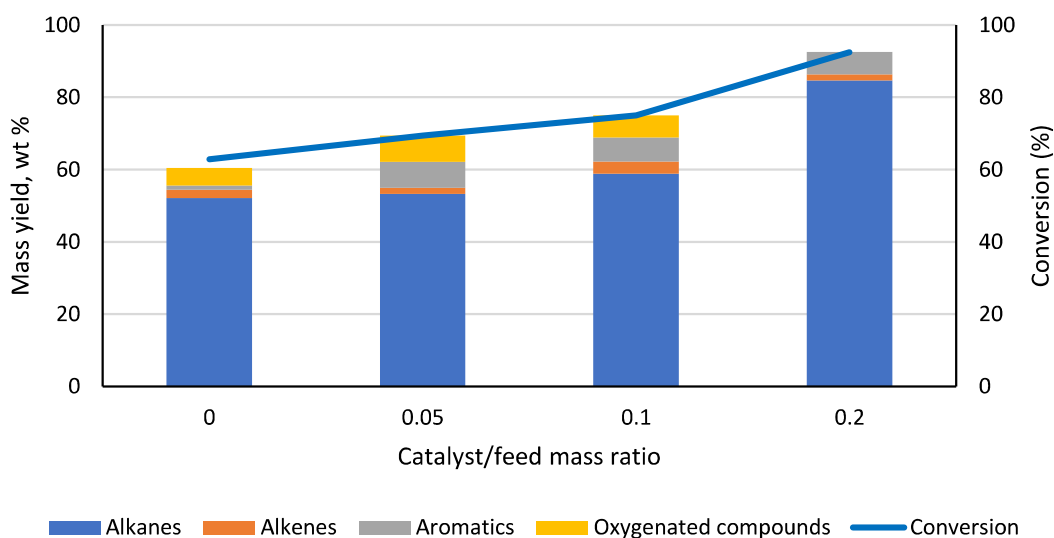


Figure 5.15: Conversion of fatty acids in hydrolysed RSO and mass yields of hydrocarbon products at 400 °C, 1 h with different 5 wt% Pt/C catalyst/feed mass ratios

The chain lengths of the components of the oil/wax product obtained from different catalyst to feed ratio are compared in Figure 5.16. Percentage yields of heptadecane at catalyst/feed ratios of 0.0, 0.05, 0.1 and 0.2 were found to be 12.64%, 36.62%, 42.21%, and 63.49% respectively. This means that in addition to the increasing conversion with catalyst loading reported in Figure 5.15, the catalyst also favoured selectivity to heptadecane from the decarboxylation of the dominant C18 fatty acids in RSO. The reaction carried out in the absence of catalyst also showed a range of product distribution, which implied thermal cracking occurred possibly due to the high reaction temperature used. Cracking can produce hydrogen, which can enhance decarboxylation reaction (Hossain et al., 2018). However, this could also lead to the generation of shorter chain hydrocarbons, consumption of energetic C-H bonds, and also coking of the catalyst surface (Snåre et al., 2006).

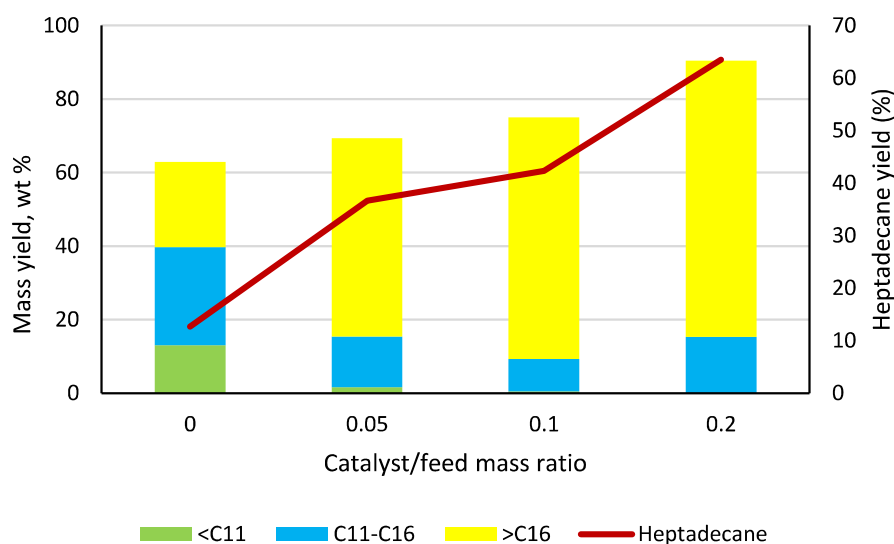


Figure 5.16: Mass yields of heptadecane and other hydrocarbon products from decarboxylation of hydrolysed RSO at 400 °C, 1 h with 5 wt% Pt/C catalyst/feed ratios

Nonetheless, the increase in catalyst/feed mass ratio produced longer chain hydrocarbons, which indicated decarboxylation reactions were favoured over cracking reactions. Overall, with a higher catalyst/feed mass ratio, higher yields of hydrocarbons were achieved, which agreed with findings by Simakova et al., (2010) and Mäki-Arvela et al., (2006). Yang et al., (2015) reported an 80.44% yield of heptadecane with Pt/Zelite as catalyst to feed ratio with 20 bar H<sub>2</sub>, which seemed attractive, but the high amount of catalyst and hydrogen required would only lead to higher production costs. Hence, the catalyst/feed mass ratio for maximum yield of hydrocarbons from the decarboxylation of fatty acids using 5 wt% Pt/C in this study

was limited to 0.2 in this present study. Table 5.10 shows the list of compounds obtained from varying the catalyst to feed mass ratios. Figure 5.17 presents the Van Krevelen diagram produced from the elemental compositions of the oils using their H/C and O/C ratios. Even though it might appear that the O/C ratios of the oils with 0.05 and 0.1 catalyst to feed mass ratios have relatively higher H/C ratios than the oil produced with no catalyst, this diagram has been obtained from the elemental composition obtained from the GC/MS. Therefore, even though the reaction carried out in the absence of catalyst had the lowest conversion (Table 5.9), its O/C ratio here shows up relatively lower because some of the oxygenated compounds did not show up on the GC/MS. Overall, the oil produced using 0.2 catalyst feed mass ratio had the highest H/C to O/C ratio was most comparable with the conventional fuels, gasoline, kerosene, and diesel.

Table 5.10: List of compounds from decarboxylation of hydrolysed rapeseed oil at 400 °C, 1 h with different 5 wt% Pt/C catalyst/feed mass ratios

Alkanes	Yield, wt %			
	0	0.05	0.1	0.2
Heptane	1.65	-	-	-
Octane	2.73	-	-	-
Nonane	3.27	0.57	0.14	-
Octane, 2,4,6-trimethyl-	3.07	0.81	-	-
Decane	-	-	0.33	-
Undecane	-	1.08	0.50	0.30
Cycloheptane, methyl-	0.23	-	-	-
Octane, 2,4,6-trimethyl-	2.71	-	-	-
Cyclopentane, hexyl-	0.22	-	-	-
Dodecane	3.00	1.44	0.66	0.57
Cyclohexane, octyl-	0.26	-	-	-
Cyclopentane, 1-butyl-2-propyl-	0.22	-	-	-
Tridecane	1.63	1.04	0.60	0.73
Cyclopentane, 1-hexyl-3-methyl-	0.61	-	-	-
Tetradecane	1.29	0.93	0.62	0.86
Pentadecane	6.32	4.75	4.00	5.86
Dodecane, 2-cyclohexyl-	0.40	-	-	-
Pentadecane, 7-methyl-	-	0.37	0.46	-
Cyclohexane, undecyl-	0.49	0.58	-	-
Hexadecane	1.13	1.05	0.76	1.19
Cyclohexane, 1,5-diethyl-2,3-dimethyl-	-	0.18	-	-
Cyclopentane, 1-pentyl-2-propyl-	1.05	0.57	-	0.85
2,6,10-Trimethyltridecane	-	-	-	1.73
Decane, 2,5-dimethyl-	-	-	-	0.65
Tetradecane, 5-methyl-	-	-	-	0.54
Cyclohexane, 1,5-diethyl-2,3-dimethyl-	0.66	-	-	-
Cyclopentane, decyl-	0.27	0.39	-	-
Heptane, 3-ethyl-2-methyl-	-	-	0.12	-
Tetradecane, 2,6,10-trimethyl-	-	-	0.11	-



Tetradecane, 4-methyl-	-	-	-	0.66
Hexadecane, 2-methyl-	-	-	-	2.11
Tetradecane, 3-methyl-	-	-	-	1.40
Cyclopentane, 1-butyl-2-pentyl-	0.84	-	-	-
Heptadecane	12.64	36.62	42.31	63.49
Cyclopentane, 1-hexyl-3-methyl-	1.13	-	0.27	-
Octadecane	-	0.36	0.30	1.53
1-Cyclopentyleicosane	1.13	-	-	-
Cyclohexane, undecyl-	2.44	-	-	-
Nonadecane	0.41	1.34	1.34	1.69
Eicosane	1.08	0.20	0.47	0.47
Heneicosane	0.25	0.60	0.38	-
Docosane	0.69	0.19	0.36	-
Tricosane	0.25	0.19	5.09	-
<b>Total</b>	<b>52.08</b>	<b>53.29</b>	<b>58.81</b>	<b>84.61</b>

<b>Alkenes</b>	<b>Yield, wt %</b>			
	0.00	0.05	0.10	0.20
2-Heptene, (E)-	0.33	-	-	-
2-Octene, (E)-	0.27	-	-	-
trans--4-Nonene	0.22	-	-	-
4-Nonene	0.37	-	-	-
(Z)-5-Decene	0.40	-	-	-
2-Decene, (E)-	0.23	-	-	-
4-Undecene, (E)-	0.53	-	-	-
3-Hexadecene, (Z)-	-	0.53	-	-
8-Heptadecene	-	1.13	0.47	1.13
3-Heptadecene, (Z)-	-	-	0.56	-
5-Octadecene, (E)-	-	-	-	0.57
9-Eicosene, (E)-	-	-	1.24	-
5-Eicosene, (E)-	-	-	1.09	-
<b>Total</b>	<b>2.35</b>	<b>1.66</b>	<b>3.37</b>	<b>1.69</b>

<b>Aromatics</b>	<b>Yield, wt %</b>			
	0.00	0.05	0.10	0.20
Toluene	0.12	-	-	-
1-Phenyl-1-butene	0.12	-	-	-
Benzene, hexyl-	0.17	-	-	-
Benzene, heptyl-	0.31	-	-	-
Benzene, (1-methyldecyl)-	0.20	-	-	-
Benzene, undecyl-	0.21	-	-	-
Benzene, 1-ethyl-2-methyl-	-	0.09	-	-
Benzene, 1-methyl-2-propyl-	-	0.12	0.06	-
Benzene, 1-methyl-4-butyl	-	0.11	0.07	-
Benzene, (1,3-dimethylbutyl)-	-	0.11	0.17	-
1-Methyl-2-n-hexylbenzene	-	0.14	0.08	-
Benzene, (1-methylheptyl)-	-	0.11	0.08	-
Benzene, nonyl-	-	0.10	-	-
Benzene, (1-methyldecyl)-	-	4.37	4.62	4.90
Benzene, (1,1-dimethylnonyl)-	-	0.90	0.90	0.83
Benzene, undecyl-	-	0.57	0.47	0.47

Benzene, 1,4-dimethyl-2-(2-methylpropyl)-	-	0.12	0.11	-
Benzene, (1-methylundecyl)-	-	-	0.09	-
Benzene, (2,3-dimethyldecyl)-	-	-	0.06	-
Benzene, dodecyl-	-	0.15	-	-
Benzene, (1-methyldodecyl)-	-	0.10	-	-
<b>Total</b>	<b>1.13</b>	<b>7.21</b>	<b>6.69</b>	<b>6.20</b>

Oxygenated compounds	Yield, wt %			
	0.00	0.05	0.10	0.2
2-Ethyl-oxetane	0.39	-	-	-
1-Decanol, 2-octyl-	1.78	-	0.56	-
n-Nonadecanol-1	2.38	-	-	-
(3-Methylphenyl) methanol, 2-methylpropyl ether	0.35	-	-	-
1,3-Dimethyl-(3,7-dimethyloctyl)cyclohexane	0.99	-	-	-
1,3-Dimethyl-(3,7-dimethyloctyl)cyclohexane	0.87	-	-	-
Carbonic acid, decyl undecyl ester	0.57	-	-	-
8-Octadecanone	-	-	0.33	-
(3-Methylphenyl) methanol, 2-methylpropyl ether	-	0.21	-	-
Androstane-3,17-diol, 17-methyl-, (3.alpha.,5.alpha.,17.beta.)-, 3-acetate	-	0.75	1.04	-
1-Hexadecanol	-	0.80	-	-
9-Octadecanone	-	0.20	-	-
Coprostanol	-	1.56	-	-
5.alpha.-Cholestane	-	3.43	-	-
10-Nonadecanone	-	0.26	-	-
1-Heptacosanol	-	-	4.22	-
<b>Total</b>	<b>4.89</b>	<b>7.19</b>	<b>6.15</b>	<b>-</b>

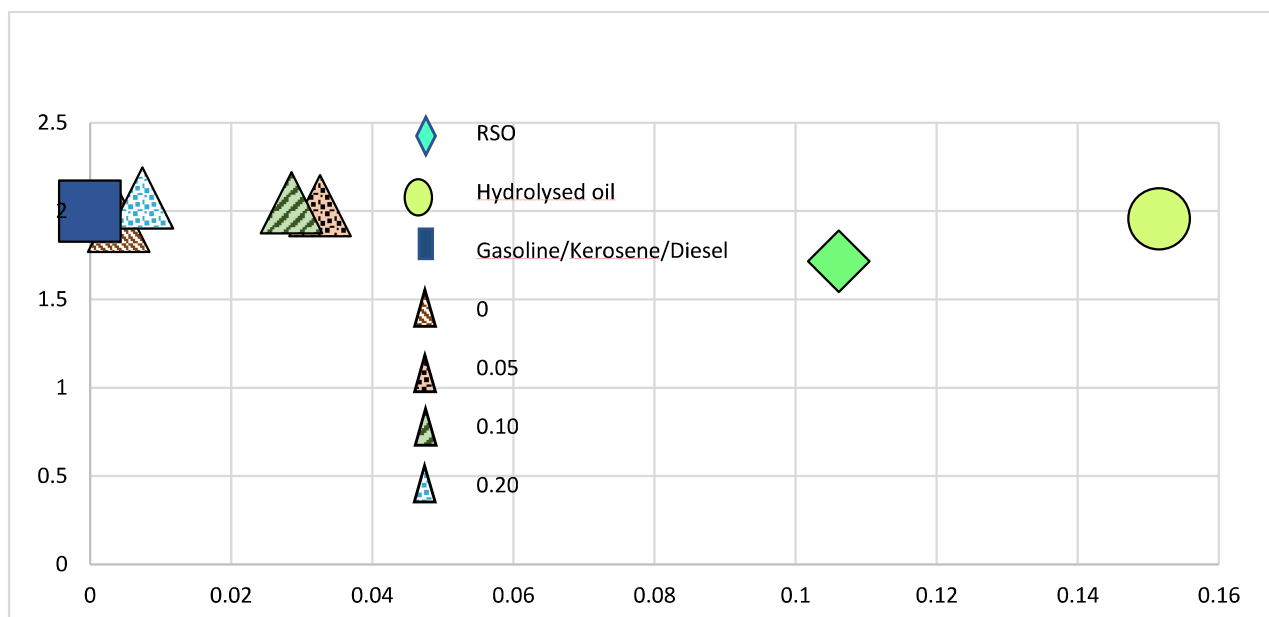


Figure 5.17: Van Krevelen diagram of liquid fuels characterisation from varying catalyst to feed mass ratios

In summary, the results emphasised the impact of catalyst loading on the product yield and product composition, and oil chemical composition. Fig 5.14, 5.15 and 5.16 showed that higher catalyst/feed mass ratios favoured decarboxylation over random cracking reactions. Even though the product composition of the non-catalysed reaction seen in Table 5.8 had the highest oil yield, and least gas and char fraction, which should make it the most attractive, further analysis of the gas product presented in Fig 5.14 showed its relatively low yield of  $\text{CO}_2$ . As the presence of  $\text{CO}_2$  is an indicator of the occurrence of decarboxylation, which is the goal of these tests, proved the presence of catalyst, Pt/C, was the more attractive condition. Furthermore, the significance of the catalyst was further demonstrated by the decrease in acid content (Table 5.9), the increase in hydrocarbon yield (Figs. 5.15 and 5.16), and the proximity of the oil in the Van Krevelen diagram (Fig. 5.17) when compared to conventional fuels. In particular, the effect of increasing as the loading of 0.2 catalyst/feed mass ratio produced the best results in all categories.

#### 5.2.4 Effect of reaction time on the decarboxylation of fatty acids from hydrolysis of RSO with 5 wt% Pt/C catalyst

To determine the reaction time to maximise the degree of decarboxylation, experiments were carried out in time range of 0 min - 180 min (i.e., up to 3 h). The reaction time here referred to the time the reaction was kept running once the reaction temperature was reached. Hence, the time of reaction “0 h” simply means the reaction was stopped once the set

reaction temperature was reached. These reactions were carried out at 400 °C, which gave the highest conversion reported in Section 5.2.2.3.2.

#### 5.2.4.1 Product yields and mass balance in relation to reaction time with 5 wt% Pt/C catalyst

All reactions yielded gas, liquid, and solid products. Table 5.11 shows the mass balance closures from the investigation of the effect of reaction time on the decarboxylation of hydrolysed RSO. The mass balance reduced from 96.64 wt% to 79.69 wt% as reaction time increased from 0 h to 3 h at 400 °C. This reduction in the mass balance closure can be attributed to increased volatile losses from the gas and liquid products obtained at longer reaction times. There was an increase in the yield of gas products with increased reaction time, which suggested the degradation of heavy compounds to lighter products. The reaction at 0 h gave the most solid residues (18.38%), and this was partly due to the presence of embedded unreacted feedstock with the catalyst. As explained earlier some heavy oil molecules formed white solids, which were insoluble in the dichloromethane solvent.

There was also a notable difference in the appearance of the liquid products (Figure 5.18). At 0 h, the product obtained is a semi-solid but as the severity of the reaction increased in terms of reaction time, the products were obtained in liquid forms, and become much lighter in colour as shown in Figure 5.18.

Table 5.11: Mass balance for reaction products from decarboxylation of hydrolysed rapeseed oil at 400 °C with different reaction times with 5 wt% Pt/C catalyst

Time (h)	Products				Balance (wt %)
	Solid (wt %)	Oil (wt %)	Wax (wt %)	Gas (wt %)	
0	18.38	-	76.79	1.46	96.64
1	5.37	77.81	-	7.08	90.26
2	8.35	73.76	-	7.94	90.05
3	6.73	64.66	-	8.30	79.69

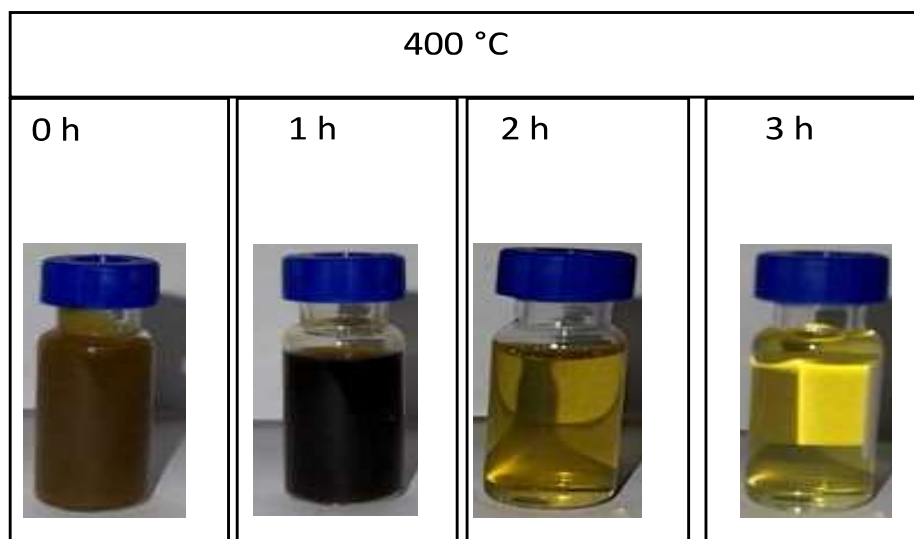


Figure 5.18: Appearance of products in relation to reaction time at 400 °C

#### 5.2.4.2 Gas composition in relation to reaction time

Figure 5.19 shows the yields of the components in the gas products obtained from the decarboxylation reactions done varying time. All reactions produced  $\text{CO}_2$ , which increased with increasing reaction time and implied increasing decarboxylation. The increasing  $\text{CO}_2$  yield corresponded to increase in the mass yield of gases produced with the increase in reaction time. In addition, there was an increase in the hydrocarbon

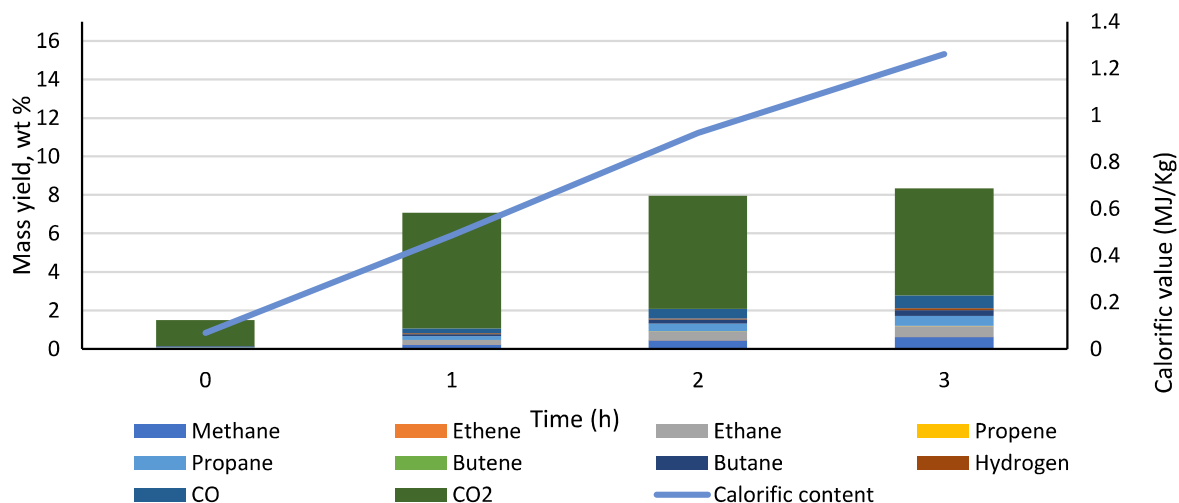


Figure 5.19: Mass yields and calorific values of gas products obtained from decarboxylation of hydrolysed RSO at 400 °C at different reaction times with 5 wt% Pt/C catalyst

### 5.2.4.3 Characterisation of liquid products in relation to reaction time in the presence of 5 wt% Pt/C catalyst

#### 5.2.4.3.1 Liquid product properties

Table 5.12: Density, acid content, elemental composition and calorific value obtained of oil/wax products obtained from RSO in relation to reaction time in the presence of 5 wt% Pt/C catalyst

Time (h)	Main organic product	Density (kg/m <sup>3</sup> )	Acid content (wt %)	Elemental composition						HHV (MJ/Kg)
				Method	C (wt %)	H (wt %)	N (wt %)	S (wt %)	O (wt %)	
0	Dark wax	923	85.43	1	75.08 ± 1.63	12.00 ± 0.24	0.27 ± 0.00	-	12.66 ± 0.04	40.43
				2	77.73	12.38	-	-	9.89	42.38
1	Dark heavy oil	906	7.49	1	83 ± 0.1	13.9 ± 0.31	0.11 ± 0.01	-	2.99 ± 0.11	47.6
				2	84.55	14.61	-	-	0.84	49.53
2	Yellow light oil	883	2.08	1	83.31 ± 3.20	13.93 ± 0.51	0.20 ± 0.00	-	2.56 ± 0.08	47.82
				2	84.92	14.84	-	-	0.24	50.1
3	Yellow light oil	879	1.15	1	82.40 ± 3.83	13.60 ± 0.63	0.14 ± 0.01	-	3.86 ± 0.16	46.8
				2	85.01	14.84	-	-	0.13	50.15

1: CHNS analyser; 2: Calculated from GC-MS analysis

gases from 0 – 3 h, but the increase in CO<sub>2</sub> was more dramatic when reaction time increased from 0 -1 h. From reaction time 1 h, the yield of CO<sub>2</sub> stayed fairly constant, while the yields of hydrogen and other hydrocarbon gases became more significant, suggesting that increased cracking reactions occurred with longer reaction time. The calorific values of the gas products reflected their compositions. The increase in the yields of hydrogen and the hydrocarbon gases at more severe reaction conditions, led to higher calorific value of the gas products by seventeen-folds from 0 h to 2 h. The high calorific gases can be used for process heating.

The acid content obtained from varying reaction time follows a similar trend as that seen in varying temperature in Section 5.2.2.3 (Table 5.6). There was a consistent decrease in acid contents with increase in time (Table 5.12). From 0 h, the acid content was reduced by approximately 99% as reaction condition became more severe at 3 h. This increase in the severity of reaction conditions also contributed to the state of the obtained organic product, with higher reaction times producing light-coloured oils. The densities of the oils also reduced with the increase in reaction time as the rise in reaction condition severity will probably lead to the production of smaller chain compounds. The densities and the HHVs of the decarboxylated hydrolysed RSO obtained at this stage were similar to those of gasoline, kerosene and diesel, ranging from 45–47 MJ/kg (Strömberg, 2006). As mentioned previously, both the experimental and calculated HHVs are presented in Table 5.12, and a similar trend was observed, with greater difference in the experimental and calculated calorific values as reaction time increased, for reasons of incompatibility of the CHNSO analysis method with highly volatile samples that was previously adduced.

#### 5.2.4.3.2 Chemical composition of liquid/wax products in relation to reaction time

Figure 5.20 shows the results of the analysis of liquid products based on the group of compounds obtained from the decarboxylation reactions carried out at different reaction times. These were limited to only the eluted and quantifiable components of the oil/wax products. Oxygenated compounds only appeared at 0h. In addition to the increase in conversion with the increased reaction time, the yield of alkanes, which was only 8.44% at 0 h, reached 93.08% at 3 h. The yield of aromatics remained at approximately 6% at reaction times 1-3 h. This implied there was little to no effect on the aromatisation of the compounds as reaction time increased. A few alkenes were present at 0 h (2.97 wt%) and 1 h (1.69 wt%) but none was detected at longer reaction times, which showed that increasing the reaction time minimised the production of olefins, possibly via catalytic hydrogenation. This is advantageous as alkenes can be reactive and have an adverse effect on stability of the fuel (Na et al., 2010). As reaction time increased from 2 to 3 h at 400 °C, there was very little

change in the conversion as well as the profile of compounds produced. Therefore, choosing reaction time at 400 °C for 2 h could be more beneficial as the energy consumed in extending the reaction time would only translate to the minor differences observed.

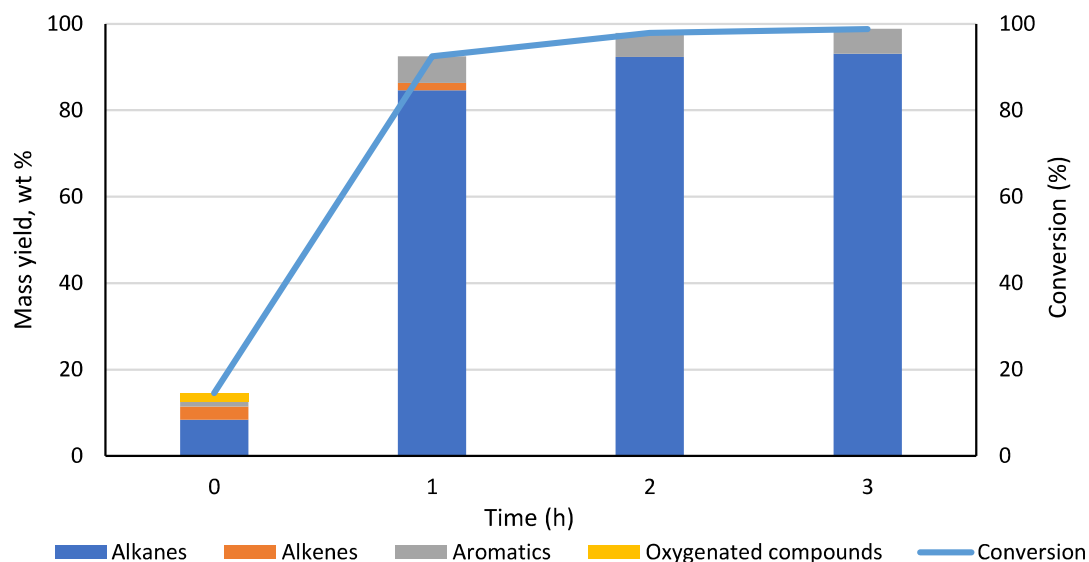


Figure 5.20: Mass yields of groups of hydrocarbon products obtained from decarboxylation of hydrolysed RSO at 400 °C with different reaction times with 5 wt% Pt/C catalyst

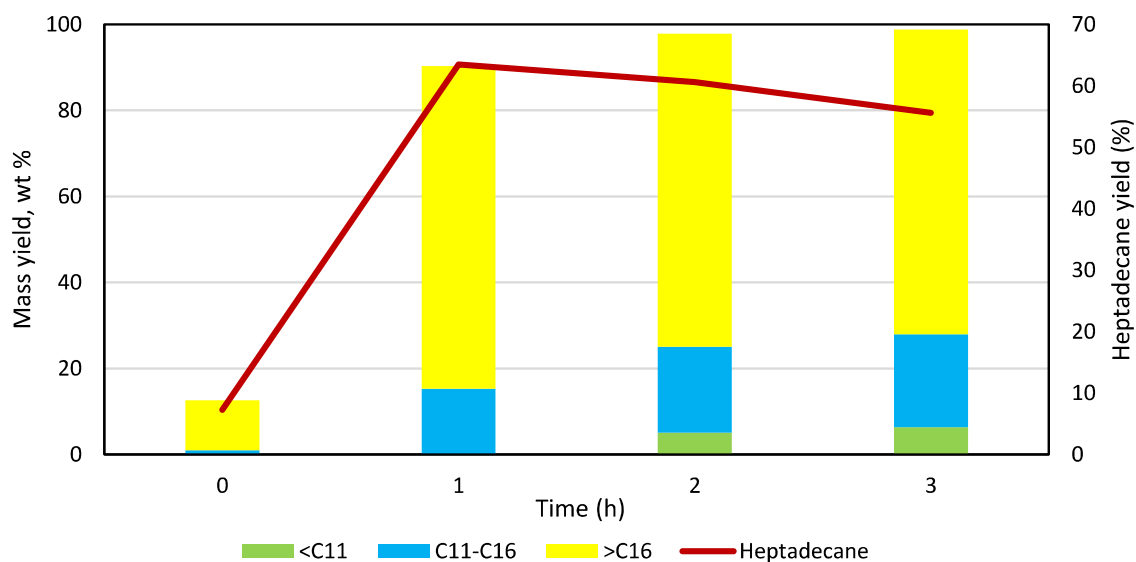


Figure 5.21: Mass yields of heptadecane and other hydrocarbons from decarboxylation of hydrolysed RSO at 400 °C with different reaction times with 5 wt% Pt/C catalyst



Figure 5.21 shows the GC/MS elutable, identifiable, and quantifiable compounds obtained from the decarboxylation reactions at different reaction times according to carbon number ranges. Hydrocarbons in the carbon range <C11 were formed and increased by 25.29% from reaction times 2 - 3 h. Also, C11-C16 hydrocarbons increased by over twenty-folds 0 - 3 h, and the >C16 fraction reduced by 5.6 wt% from 1 - 3 h. In addition to this, the highest yield of heptadecane was observed at 1 h (63.49 wt%) but reduced as reaction time increased. These suggested that the increase in the time of reaction caused cracking, which led to the shift of product distribution from long-chain into short-chain hydrocarbon molecules. Wu et al. (2016) reported a 91 wt% heptadecane yield from stearic acid using Ni/C as catalyst at 330 °C after 5 h, which is significantly higher than the highest yield obtained in this research (63.49 wt%), but the substantial difference in reaction temperature (330 °C vs 400 °C) would explain the differences. In addition to this, the authors also used pure stearic acid, whereas these experiments carried out in this study used oil containing a mixture of fatty acids with various carbon chain lengths. Therefore, reducing the maximum yield of heptadecane possible. Table 4.5 showed the yield of oleic acid present in the oil after hydrolysis was 74.4%, which is 16.43 wt% higher than the highest heptadecane yield reported at 1 h. This suggests that indeed cracking occurred at reaction times 1 -3 h as previously implied. At 400 °C, the reaction carried out for 3 h had slightly higher yields of hydrocarbon products than the one that lasted for 3 h. However, working at 400 °C for 2 h was chosen as the more favourable reaction condition because of the similarity in yields and distributions of products. Indeed, the difference in the yields of products obtained was negligible when compared to the energy consumed during the extra hour in both cases. The list of compounds obtained are presented in Table 5.13. The elemental compositions of the oils have been used to generate a Van Krevelen diagram considering the H/C and O/C ratios of the oils in Figure 5.22. The reaction at 0 h had the highest O/C ratio which implied relatively low conversion as reported earlier in Table 5.12. The figure shows that the oils obtained under more severe reaction conditions have higher H/C ratios, lower O/C ratios and are most comparable to conventional fuels.

Table 5.13: List of compounds from decarboxylation of hydrolysed rapeseed oil at 400 °C with different reaction times with 5 wt% Pt/C catalyst

Alkanes	Yield, wt%			
	0 h	1 h	2 h	3 h
Hexane, 2-methyl-	-	-	-	0.22
Heptane	-	-	1.22	1.26
Octane	-	-	1.27	1.36
Nonane	-	-	1.30	1.39
Decane	-	-	1.30	1.39
Undecane	-	0.30	1.35	1.41
Dodecane	-	0.57	1.39	1.42
Tridecane	-	0.73	1.42	1.42
Tetradecane	-	0.86	1.45	1.45
Tetradecane, 2-methyl-	-	-	-	0.28
Pentadecane	1.40	5.86	6.52	6.24
Cyclohexadecane	1.38	-	-	-
Hexadecane	-	1.19	1.43	1.48
2,6,10-Trimethyltridecane	-	1.73	2.07	2.75
Decane, 2,5-dimethyl-	-	0.65	0.75	0.95
Tetradecane, 4-methyl-	-	0.54	0.72	1.17
Tetradecane, 5-methyl-	-	0.66	0.86	-
Hexadecane, 2-methyl-	-	2.11	2.84	3.27
Tetradecane, 3-methyl-	-	1.40	1.76	2.17
Heptadecane	4.90	63.49	60.63	56.25
Cyclopentane, 1-pentyl-2-propyl-	-	0.85	-	-
Cyclopentane, decyl-	-	-	0.26	-
Octadecane	-	1.53	1.81	1.60
Nonadecane	0.76	1.69	1.54	1.49
Eicosane	-	0.47	0.41	0.38
<b>Total</b>	<b>8.44</b>	<b>84.61</b>	<b>92.36</b>	<b>93.09</b>

Alkenes	Yield, wt%			
	0 h	1 h	2 h	3 h
8-Heptadecene	-	1.13	-	-
9-Octadecene, (E)-	1.81	-	-	-
5-Octadecene, (E)-	0.75	0.56	-	-
5-Eicosene, (E)-	0.41	-	-	-
<b>Total</b>	<b>2.97</b>	<b>1.69</b>	<b>-</b>	<b>-</b>

Aromatics	Yield, wt%			
	0 h	1 h	2 h	3 h
o-Xylene	-	-	-	0.15
Benzene, 1-ethyl-3-methyl-	-	-	-	0.21
Benzene, 1-methyl-2-propyl-	-	-	-	0.16
Benzene, (1-methyldecyl)-	4.41	4.90	4.27	2.85
Benzene, undecyl-	0.51	0.47	0.48	0.44
Benzene, 1,3-didecyl-	2.16	-	-	-
Benzene, (1,1-dimethylnonyl)-	0.96	0.83	0.82	0.76
<b>Total</b>	<b>1.17</b>	<b>6.20</b>	<b>5.57</b>	<b>5.76</b>

Oxygenated compounds	Yield, wt%			
	0 h	1 h	2 h	3 h
cis-7-Hexadecenoic acid	0.56	-	-	-
Octadecanoic acid	0.76	-	-	-
2(3H)-Furanone, dihydro-5-tetradecyl-	0.67	-	-	-
<b>Total</b>	<b>1.99</b>	<b>-</b>	<b>-</b>	<b>-</b>

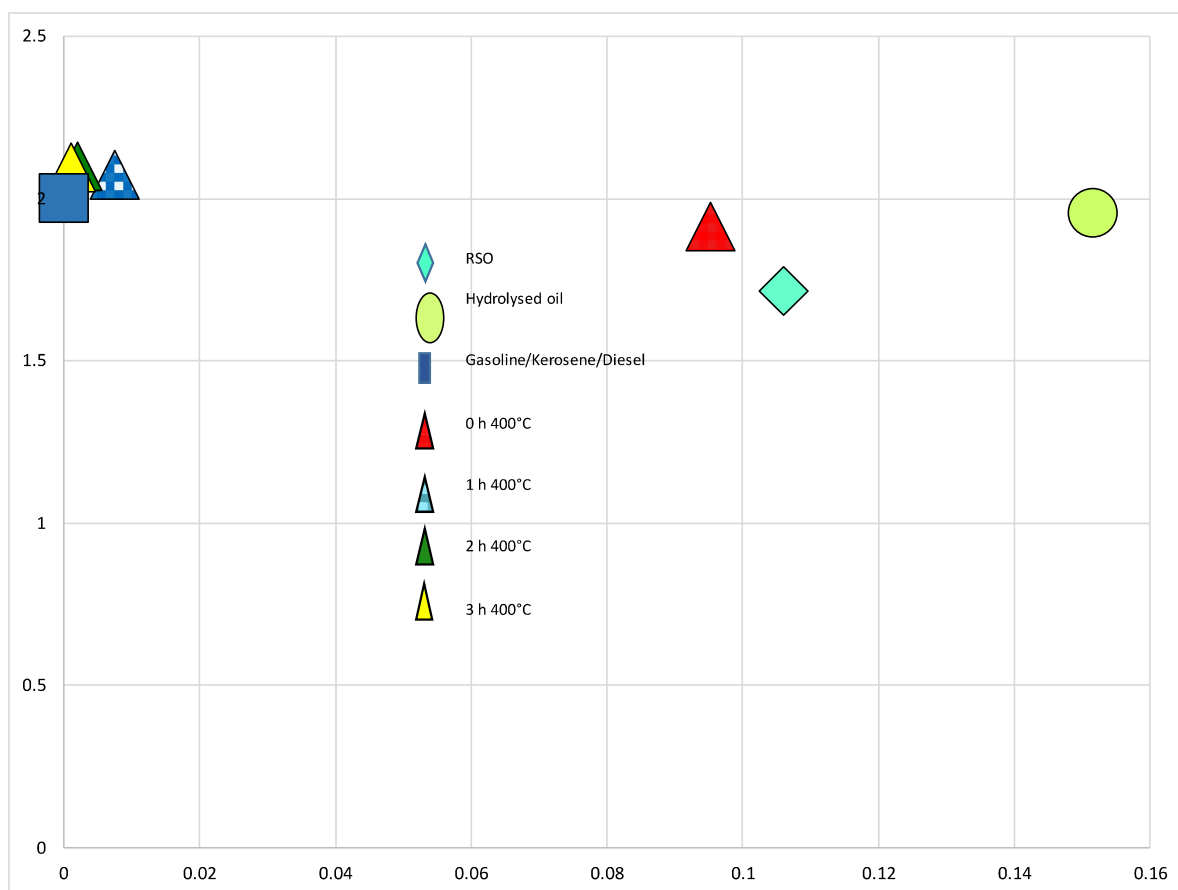


Figure 5.22: Liquid fuels characterisation from varying reaction time by H/C and O/C molar ratios in Van Krevelen diagram

Comprehensive results were obtained from the study of how reaction time affected the decarboxylation of hydrolysed rapeseed oil at 400 °C using a 5 wt% Pt/C catalyst. The mass balance closure decreased from 96.64% to 79.69% as reaction time rose from 0 to 3 hours. This decrease was ascribed to volatile losses from gas and liquid products. With time, gas yields and CO<sub>2</sub> generation rose, indicating that heavy molecules broke down into lighter ones. With increased reaction intensity, liquid products changed from semi-solid to lighter liquid forms. The potential of the obtained for usage as conventional fuels was demonstrated by their lowering acid content and density along with their increasing calorific values. Alkanes

were the most dominant hydrocarbons, but aromatics and alkenes declined with longer reaction periods, according to a chemical composition analysis. The yield of heptadecane significantly dropped, indicating that cracking happened. The Van Krevelen diagram showed how, in harsher circumstances, oils evolved to take on properties similar to conventional fuels. Overall, the study provides insights for optimising reaction conditions and tailoring product characteristics in the decarboxylation process.

Table 5.14: Summary table showing compiled results of decarboxylation experiments

Parameter	Dependent variables tested	Independent variables	Summary of main findings
Catalyst type	5 wt% Pt/C 5 wt% Pt/MgSiO <sub>3</sub> 5 wt% Pt/SiO <sub>2</sub> 5 wt% Pt/Al <sub>2</sub> O <sub>3</sub> 1 wt% Pt/SiO <sub>2</sub> 5 wt% Pd/MgSiO <sub>3</sub> 10 wt% Ni-Cu/Al <sub>2</sub> O <sub>3</sub> (P)) 10 wt% Ni-Cu/Al <sub>2</sub> O <sub>3</sub> (S))	Feed: 10 g oil Temperature: 400 °C Reaction time: 2 h Catalyst: 2 g	<p>This study showed the catalyst choice has a significant impact on not only the yield of the target product, the decarboxylated oil, but also the composition of the oils. Mass balance results showed that even though all catalyst yielded all three phase products, powdered 10 wt% Ni-Cu/Al<sub>2</sub>O<sub>3</sub> gave the highest liquid yield of 87% (Table 5.2). Further analysis of their gas products showed that all catalysts produced CO<sub>2</sub>, which is an indicator of the occurrence of decarboxylation with powdered 10 wt% Ni-Cu/Al<sub>2</sub>O<sub>3</sub> producing the highest yield of CO<sub>2</sub>, which accounted for 99% of its gas yield (Fig 5.4). However, following the analysis of the oils, even though 5 wt% Pt/MgSiO<sub>3</sub> had the highest conversion of 100%, Pt/C with 97.9% conversion was chosen to be the optimum catalyst as its conversion rate was not far from completion, and the oil colour came out the lightest (Fig 5.3, Fig 5.5). This colour factor was prioritised because the comparable fossil fuels have clear colours, and this will also ease challenges in subsequent processing and the practical application of the produced materials.</p>
Temperature	350 °C (no catalyst) 380 °C (no catalyst) 400 °C (no catalyst) 350 °C (with 2 g Pt/C) 400 °C (with 2 g Pt/C)	Feed: 10 g oil Reaction time: 1 h	<p>Following the decision from the previous tests to use Pt/C as the optimum catalyst, reaction temperature was varied. The effect of the presence of the catalyst was also examined simultaneously. The results post analysis of the gas phase implied not only the significant impact of the catalyst in regard to promoting decarboxylation as there was a 93% increase in CO<sub>2</sub> when catalyst was added at 350 °C, and 88% at 400 °C, but also the impact of temperature there was an 88% increase as temperature increased even without catalyst (Fig 5.9). The analysis of the oil products also showed a similar trend with 400°C in</p>

			the presence of catalyst giving the highest conversion of 92.5%, making it the optimum operating condition in this set of tests (Fig 5.10).
Catalyst/feed mass ratio (Pt metal/Feed ratio)	0, 0.05, 0.1, 0.2 (0, 0.0025, 0.005, 0.01)	Feed: 10 g oil Reaction time: 1 h Temperature: 400 °C  Catalyst: Pt/C	Even though prior tests had proved the significance of the presence of the catalyst, the catalyst of choice, Pt/C is expensive because of the metal Pt. Therefore, this set of tests were essential to examine the amount of the catalyst that could give the highest conversion. It was discovered that increasing the quantity of the catalyst promoted the increase in CO <sub>2</sub> yield (Fig 5.14), which could indicate degree of deoxygenation. The GC/MS analysis of the oils also correlated with the trend from the gas results. Catalyst/feed mass ratio was the optimum condition because it had a 92.5% conversion and no oxygenates seen on the chromatogram unlike the lower catalyst/feed mass ratios of 0 - 0.1 (Fig 5.15).
Time (h)	0, 1, 2, 3	Feed: 10 g oil Temperature: 400 °C Catalyst: 2 g Pt/C	Similarly, to the tests carried out varying temperature, it was discovered that increasing reaction severity in terms of time also promoted decarboxylation reactions. Fig 5.18 showed clear oil was obtained after 2 h but the analysis of the gas product presented in Fig 5.19 showed a plateau in the yield of CO <sub>2</sub> at about 6% after 1 h, which implied negligible impact on decarboxylation after an hour. This flat line trend is also seen in the analysis of the oil product after 1 h. However, 2 h was chosen as the optimum condition for these tests because it gave a 97.2% conversion, which was 5% more than that obtained at 1 h (Fig 5.20).

To conclude this chapter, the aim to carry out decarboxylation of fatty acids was achieved (Table 5.14).

The product of the previous stage, hydrolysis, was used as feedstock and a series of tests varying catalyst type, catalyst loading, reaction time, and temperature were carried out. The results showed that increasing reaction severity favoured conversion. Pt/C was found to be the catalyst with the most potential for conversion at 97.9%, and the optimum reaction conditions to achieve this high conversion was 400 °C for 2 h with 2 g catalyst. Even though the oil produced was clear and did smell like the conventional fuels, more tests were carried out in the following chapter to increase the aromatic yield of the oils produced to that comparable with the aromatic content of Jet-A kerosene.

### 5.3 References

- Ali, S. A., Alshareef, A. H., Theravalappil, R., Alasiri, H. S., and Hossain, M. M. (2022). Molecular Kinetic Modeling of Catalytic Naphtha Reforming: A Review of Complexities and Solutions. *Catalysis Reviews*, 1–54.  
<https://doi.org/10.1080/01614940.2021.2008622>.
- Ayhan Demirbas (2016) Calculation of higher heating values of fatty acids, *Energy Sources, Part A: Recovery, Utilization, and Environmental Effects*, 38:18, 2693-2697, DOI: 10.1080/15567036.2015.1115924
- Bouaoun, I., Hammi, H., Aït-Mokhtar, A., El Amine Hamami, A., & M'nif, A. (2017). Effect of calcination temperature of magnesium silicate on the properties of magnesium phosphate cement. *Journal of the Australian Ceramic Society*, 53(2), 351–359.  
<https://doi.org/10.1007/s41779-017-0044-8>.
- Feng, J., Xiong, W., Ding, H., and He, B. (2016). Hydrogenolysis of glycerol over Pt/C catalyst in combination with alkali metal hydroxides. *Open Chemistry*, 14(1), 279–286. <https://doi.org/10.1515/chem-2016-0030>.
- Fu, J., Lu, X. and Savage, P.E. (2010) “Catalytic hydrothermal deoxygenation of palmitic acid,” *Energy and Environmental Science*, 3(3), p. 311. Available at:  
<https://doi.org/10.1039/b923198f>.
- Fu, J., Lu, X. and Savage, P.E. (2011) “Hydrothermal decarboxylation and hydrogenation of fatty acids over PT/C,” *ChemSusChem*, 4(4), pp. 481–486. Available at:  
<https://doi.org/10.1002/cssc.201000370>.
- He, J., Zu, L., Liu, X., Zhang, L., & Duan, B. (2019). Porous NiCu alloy cathode with oriented pore structure for hydrogen evolution reaction by freeze casting. *Journal of Porous Materials*, 26(5), 1533–1539. <https://doi.org/10.1007/s10934-019-00751-9>.
- Hossain, M. Z., Chowdhury, M. B. I., Jhawar, A. K., Xu, W. Z., and Charpentier, P. A. (2018). Continuous low pressure decarboxylation of fatty acids to fuel-range hydrocarbons with in situ hydrogen production. *Fuel*, 212, 470–478.  
<https://doi.org/10.1016/j.fuel.2017.09.092>.
- Hubesch, R., Mazur, M., Selvakannan, P. R., Föger, K., Lee, A. F., Wilson, K., and Bhargava, S. (2022). Endothermic catalytic cracking of liquid hydrocarbons for thermal management of high-speed flight vehicles. *Sustainable Energy and Fuels*, 6(7), 1664–1686. <https://doi.org/10.1039/d1se01999f>.
- Jenišťová, K., Hachemi, I., Mäki-Arvela, P., Kumar, N., Peurla, M., Čapek, L., Wärnå, J., and Murzin, D. Y. (2017). Hydrodeoxygenation of stearic acid and tall oil fatty acids over



Ni-alumina catalysts: Influence of reaction parameters and kinetic modelling. *Chemical Engineering Journal*, 316, 401–409. <https://doi.org/10.1016/j.cej.2017.01.117>

Jeong, M.-G., Zhuo, K., Cherevko, S., & Chung, C.-H. (2012). Formation of nanoporous nickel oxides for supercapacitors prepared by electrodeposition with hydrogen evolution reaction and electrochemical dealloying. *Korean Journal of Chemical Engineering*, 29(12), 1802–1805. <https://doi.org/10.1007/s11814-012-0097-x>.

Jiraroj, D., Jirarattanapochai, O., Anutrasakda, W., Samec, J. S. M., and Tungasmita, D. N. (2021). Selective decarboxylation of biobased fatty acids using a Ni-FSM-16 catalyst. *Applied Catalysis B: Environmental*, 291, 120050. <https://doi.org/10.1016/j.apcatb.2021.120050>.

Kishore, P.S., Viswanathan, B. and Varadarajan, T.K. (2009) “Electrochemical oxygen reduction reaction by PT nanoparticles on carbon support stabilized by polyoxometalates,” *Journal of Nanoscience and Nanotechnology*, 9(9), pp. 5188–5197. Available at: <https://doi.org/10.1166/jnn.2009.1175>.

Lestari, S., Simakova, I., Tokarev, A., Mäki-Arvela, P., Eränen, K., and Murzin, D. Y. (2008). Synthesis of Biodiesel via Deoxygenation of Stearic Acid over Supported Pd/C Catalyst. *Catalysis Letters*, 122(3-4), 247–251. <https://doi.org/10.1007/s10562-008-9457-x>.

Liu, X., Yang, M., Deng, Z., Dasgupta, A., & Guo, Y. (2021). Hydrothermal hydrodeoxygenation of palmitic acid over Pt/C catalyst: Mechanism and kinetic modeling. *Chemical Engineering Journal*, 407, 126332. <https://doi.org/10.1016/j.cej.2020.126332>.

Madsen, A.T. *et al.* (2011) ‘Hydrodeoxygenation of waste fat for diesel production: Study on model feed with PT/alumina catalyst’, *Fuel*, 90(11), pp. 3433–3438. doi:10.1016/j.fuel.2011.06.005.

Mäki-Arvela, P., Kubickova, I., Snåre, M., Eränen, K., and Murzin, D. Y. (2007). Catalytic Deoxygenation of Fatty Acids and Their Derivatives. *Energy and Fuels*, 21(1), 30–41. <https://doi.org/10.1021/ef060455v>.

Oliver-Tomas, B., Renz, M. and Corma, A. (2017) “High quality biowaxes from fatty acids and fatty esters: Catalyst and reaction mechanism for accompanying reactions,” *Industrial & Engineering Chemistry Research*, 56(45), pp. 12870–12877. Available at: <https://doi.org/10.1021/acs.iecr.7b01794>.

Pandya, R., Mane, R. and Rode, C.V. (2018) “Cascade dehydrative amination of glycerol to oxazoline,” *Catalysis Science and Technology*, 8(11), pp. 2954–2965. Available at: <https://doi.org/10.1039/c8cy00185e>.

Reddy, G. K., Ling, C., Peck, T. C., & Jia, H. (2017). Understanding the chemical state of palladium during the direct NO decomposition – influence of pretreatment environment and reaction temperature. *RSC Advances*, 7(32), 19645–19655.  
<https://doi.org/10.1039/c7ra00836h>.

Simakova, I., Simakova, O., Mäki-Arvela, P., Simakov, A., Estrada, M., and Murzin, D. Y. (2009). Deoxygenation of palmitic and stearic acid over supported Pd catalysts: Effect of metal dispersion. *Applied Catalysis A: General*, 355(1-2), 100–108.  
<https://doi.org/10.1016/j.apcata.2008.12.001>.

Simakova, I., Simakova, O., Mäki-Arvela, P., and Murzin, D. Y. (2010). Decarboxylation of fatty acids over Pd supported on mesoporous carbon. *Catalysis Today*, 150(1-2), 28–31. <https://doi.org/10.1016/j.cattod.2009.07.064>.

Singh, A. and Miyabayashi, K. (2020) “Novel continuous flow synthesis of PT NPS with narrow size distribution for pt@carbon catalysts,” *RSC Advances*, 10(1), pp. 362–366. Available at: <https://doi.org/10.1039/c9ra08762a>.

Snåre, M., Kubičková, I., Mäki-Arvela, P., Eränen, K., and Murzin, D. Y. (2006). Heterogeneous Catalytic Deoxygenation of Stearic Acid for Production of Biodiesel. *Industrial and Engineering Chemistry Research*, 45(16), 5708–5715.  
<https://doi.org/10.1021/ie060334i>.

Speight, J.G. (2013) “Catalytic cracking,” *Heavy and Extra-heavy Oil Upgrading Technologies*, pp. 39–67. Available at: <https://doi.org/10.1016/b978-0-12-404570-5.00003-x>.

Strömberg, B. (2006) *Fuel Handbook*. Stockholm: VÄRMEFORSK.

Suryawanshi, Y. R., Chakraborty, M., Jauhari, S., Mukhopadhyay, S., Shenoy, K. T., and Sen, D. (2015). Selective hydrogenation of Dibenzo-18-crown-6 ether over highly active monodisperse Ru/γ-Al<sub>2</sub>O<sub>3</sub> nanocatalyst. *Bulletin of Chemical Reaction Engineering and Catalysis*, 10(1). <https://doi.org/10.9767/bcrec.10.1.7141.23-29>.

Teeter, H. M., O'Donnell, J. L., Schneider, W. J., Gast, L. E., and Danzig, M. J. (1957). Reactions of Conjugated Fatty Acids. IV. Diels-Alder Adducts of 9,11-Octadecadienoic Acid1. *The Journal of Organic Chemistry*, 22(5), 512–514.  
<https://doi.org/10.1021/jo01356a010>.

Vardon, D. R., Sharma, B. K., Jaramillo, H., Kim, D., Choe, J. K., Ciesielski, P. N., and Strathmann, T. J. (2014). Hydrothermal catalytic processing of saturated and unsaturated fatty acids to hydrocarbons with glycerol for in situ hydrogen production. *Green Chemistry*, 16(3), 1507. <https://doi.org/10.1039/c3gc41798k>.

- Wu, J., Shi, J., Fu, J., Leidl, J. A., Hou, Z., and Lu, X. (2016). Catalytic Decarboxylation of Fatty Acids to Aviation Fuels over Nickel Supported on Activated Carbon. *Scientific Reports*, 6(1). <https://doi.org/10.1038/srep27820>.
- Yang, L., Tate, K. L., Jasinski, J. B., and Carreon, M. A. (2015). Decarboxylation of Oleic Acid to Heptadecane over Pt Supported on Zeolite 5A Beads. *ACS Catalysis*, 5(11), 6497–6502. <https://doi.org/10.1021/acscatal.5b01913>.
- Zhang, J., Huo, X., Li, Y., and Strathmann, T. J. (2019). Catalytic Hydrothermal Decarboxylation and Cracking of Fatty Acids and Lipids over Ru/C. *ACS Sustainable Chemistry and Engineering*, 7(17), 14400–14410. <https://doi.org/10.1021/acssuschemeng.9b00215>.
- Zhang, T., Vandeperre, L. J., & Cheeseman, C. R. (2014). Formation of magnesium silicate hydrate (M-S-H) cement pastes using sodium hexametaphosphate. *Cement and Concrete Research*, 65, 8–14. <https://doi.org/10.1016/j.cemconres.2014.07.001>.
- Zheng, Y., Wang, F., Yang, X., Huang, Y., Liu, C., Zheng, Z., and Gu, J. (2017). Study on aromatics production via the catalytic pyrolysis vapor upgrading of biomass using metal-loaded modified H-ZSM-5. *Journal of Analytical and Applied Pyrolysis*, 126, 169–179. <https://doi.org/10.1016/j.jaap.2017.06.011>.

## 6 Catalytic decarboxylation and cracking of hydrolysis product up to 450 °C

The results from the previous chapters showed that as reaction severity increased in terms of reaction time and temperature, the formation of products arising from cracking was observed. Indeed, results in Chapter 5 showed that the different catalysts used were active towards selective decarboxylation of the fatty acids. However, the 5 wt% Pt/C catalyst clearly stood out as the best performing catalyst, considering the yield, composition and appearance of the oil products obtained at 400 °C. In addition, the oil products obtained at temperatures up to 400 °C contained heptadecane as the major component. This would mean that the oil would be more useful as green diesel. Therefore, to produce other fuel fractions, especially biojet fuel, cracking would be required to reduce heptadecane yield and increase the yield of <C16 hydrocarbons. For this reason, experiments were designed to investigate the possibility of simultaneous decarboxylation and cracking of the RSO hydrolysis products (fatty acids) at temperatures above 400 °C. To do this, the three Pt-based catalysts that produced light oils at 400 °C in Chapter 5 were selected. These included 5 wt% Pt/C, 5 wt% Pt/Al<sub>2</sub>O<sub>3</sub> and 5 wt% Pt/MgSiO<sub>3</sub>. Some of the relevant properties of these catalysts have been given in Table 5.1 of Chapter 5. In addition, a set of optimum reaction conditions for the hydrolysed RSO was used to convert the hydrolysis products from two waste cooking oil (WCOs) samples. The experimental procedure followed was the same as that shown in Figure 5.1 of Chapter 5. All data obtained were reported in 2 decimal places. First, the effect of increasing temperature beyond 400 °C to 420 °C and 450 °C was investigated; thereafter, the effect of reaction time at 450 °C was tested and finally, the reusability and properties of the 5 wt% Pt/C catalyst over three reaction cycles was tested. All catalytic experiments were carried out under nitrogen atmosphere and involved 2 g of catalysts and 10 g of hydrolysed RSO (catalyst/feed ratio of 0.2 from Chapter 5).

### 6.1 Effect of reaction temperature

This section presents information on the effect of varying temperature on the combined decarboxylation and cracking of fatty acids. The reactions were carried out for 1 hour from 420 °C – 450 °C, with and without 5 wt% Pt/C catalyst, which gave the overall best result in Chapter 5, confirming its superior activity towards decarboxylation of fatty acids as reported in several literature (Fu et al., 2011; Zhang et al., 2019).

### 6.1.1 Product yields and mass balance

The mass balance closures presented in Table 6.1 for this set of experiments ranged between 83 and 91%. The loss of volatile shorter chain hydrocarbons was arguably responsible for the lower mass balances, which became lower as temperature increased. Table 6.1 shows as temperature increased from 420 °C to 450 °C, there is a notable decrease in the oil product yield, while the yields of gaseous and solid products increased in the non-catalysed reactions. In contrast, the presence of 5 wt% Pt/C gave a 7.05% increase in the oil yield when compared to the reaction without a catalyst at 450 °C. Even though all reactions yielded liquid oils, suggesting the production of short-chain hydrocarbons, there was an observable change in the colours of the oil products upon addition of the catalyst at 450 °C (Figure 6.1). The possible reason for the dark colours seen in these non-catalysed tests is due to the decomposition of higher molecular weight compounds. Cracking without hydrogen may lead to the formation of higher molecular weight compounds, which is one of the challenges faced in this project as mentioned earlier. As previously discussed in Section 5, the presence of Pt in these catalysts provided in situ hydrogen production, which possibly contributed to the formation of lighter molecular weight compounds and minimising the chances of decomposition reactions occurring and producing dark coloured oils. Moreover, the GC/MS results should provide more clarity on the compositions of the oil products.

Table 6.1: Mass balance for reaction products from decarboxylation of hydrolysed rapeseed oil for 1 h at different temperatures

Temperature (°C)	Catalyst	Products			Balance (wt %)
		Solid (wt %)	Oil (wt %)	Gas (wt %)	
420	-	1.20	84.22	5.59	90.98
450	-	5.97	67.76	9.45	83.14
450*	Pt/C	4.69	72.68	9.61	86.98

\*reactions with Pt/C catalyst

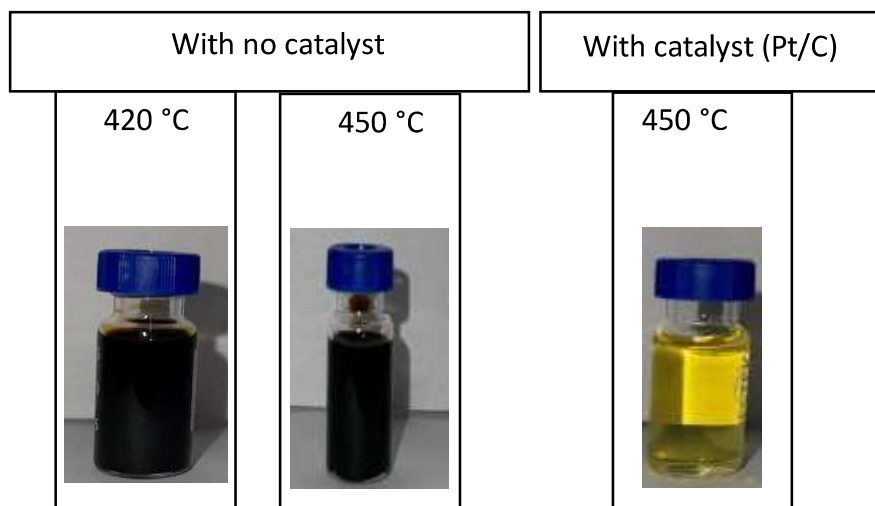


Figure 0.1: Appearance of liquid products obtained from high temperature decarboxylation and cracking tests

### 6.1.2 Gas composition

Figure 6.2 displays the composition of the gases obtained as temperature changes. The production of  $\text{CO}_2$  from the non-catalysed reactions indicates that decarboxylation occurred. There was 71.34% increase in  $\text{CO}_2$  yield as temperature increased from 420 °C to 450 °C. However, the addition of the Pt/C catalyst at 450 °C resulted in an almost four-fold yield of  $\text{CO}_2$ , with hydrocarbon gases produced. This suggested that even though a quantifiable amount of  $\text{CO}_2$  was produced in the absence of the catalyst, the reaction conditions employed led to unselective side reactions like cracking, occurring simultaneously in competition with the main decarboxylation reaction. Nonetheless, the formation of hydrocarbon gases in the presence of Pt/C implied that the combination of reaction conditions used was capable of achieving both decarboxylation and cracking reactions. Despite the production of gases not being the target for this research project, the calorific value of the gases obtained ranged from 2.58 MJ/kg to 4.00 MJ/kg, and may be useful for process heating.

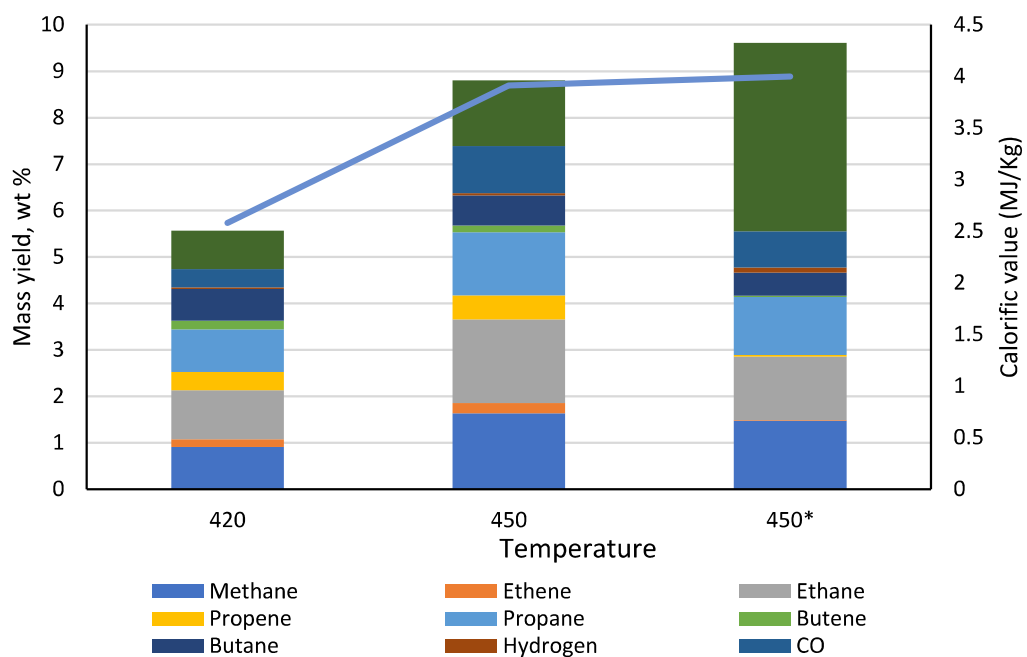


Figure 0.2: Mass yields of gas products and their calorific values obtained from decarboxylation and cracking of hydrolysed RSO for 1 h at different temperatures without and with 5 wt% Pt/C catalyst

### 6.1.3 Characterisation of liquid products obtained from combined decarboxylation and cracking at higher temperatures

#### 6.1.3.1 Properties of liquid products

Table 0.2: Density, acid content, elemental composition and calorific value obtained combined decarboxylation and cracking at higher temperatures

Temperature (°C)	Catalyst	Main organic product	Density (kg/m <sup>3</sup> )	Acid content (%)	Elemental composition						
					Method <sup>a</sup>	C (wt %)	H (wt %)	N (wt %)	S (wt %)	O (wt %)	HHV (MJ/kg)
420	-	Dark heavy oil	923	25.8	1	79.22 ± 0.09	11 ± 0.09	0.06 ± 0.01	0	15.71 ± 0.18	39.53
					2	81.92	14.19	0	0	3.89	47.49
450	-	Dark light oil	920	22.61	1	81.09 ± 1.11	10.96 ± 0.37	0.1 ± 0.01	0	7.84 ± 0.15	41.83
					2	83.3	14.1	0	0	2.59	48.07
450*	Pt/C	Yellow light oil	828	2.34	1	81.38 ± 1.07	12.63 ± 0.02	0.19 ± 0.02	0	5.8 ± 0.12	44.71
					2	85.18	14.56	0	0	0.26	49.78

<sup>a</sup>Method 1: CHNS analyser; Method 2: Calculated from GC-MS analysis



Table 6.2 shows that in the absence of the catalyst, the increase in temperature from 420 °C to 450 °C did not significantly change the acid contents of the oil products. However, when Pt/C was used at 450 °C, the acid contents in the oil product reduced to 2.34 wt%, which was nearly 90% decrease compared to the no-catalytic reaction at the same temperature. This suggested that 5 wt% Pt/C had a major effect on deoxygenation by the removal of CO<sub>2</sub>. Similarly, this trend was also observed in the densities of the oil products. The oils became less dense as temperature increased, and upon addition of Pt/C. This was possibly due to the removal of more dense oxygenated compounds as well as the formation of lighter chain hydrocarbon compounds. In contrast to this, there was an increase in the calorific value of the oils with temperature and catalyst addition.

As previously stated in Chapter 5, the effect of increase in temperature promoted the formation of volatiles, which presented a challenge in accurately analysing the oils on the elemental analyser (Method 1). Therefore, the GC/MS method (Method 2) was used to estimate the elemental composition as well as the HHVs of the oils. Again, a good match was found between the elemental compositions obtained between the heavy oils than with the light oil obtained at 450 °C with the Pt/C catalyst. Hence, the GC/MS method was found to be more accurate than Method 1. The calorific values (47 – 50 MJ/kg) obtained based on Method 2, showed that the oils contained high hydrocarbon contents similar to conventional fuels (Strömberg, 2006).

#### 6.1.3.2 Chemical composition of liquid products in relation to combined high temperature decarboxylation and cracking

The yields of the oil products obtained from the combined decarboxylation and cracking of hydrolysed RSO at temperatures > 400 °C are presented in Figure 6.3. There was a slight increase in the conversion of fatty acids to hydrocarbons as temperature increased but this was more emphasised as catalyst was added (Lestari et al., 2008; Simakova et al., 2009). The conversion increased by 31.62 wt% from the non-catalysed reaction at 420 °C to the catalysed reaction at 450 °C. This trend was similarly observed in the increase of aliphatic and aromatic compounds. The reactions carried out in the absence of catalyst showed the presence of oxygenated compounds in addition to the incomplete conversion of fatty acids (based on the relatively high acid contents). Interestingly, the two non-catalysed reactions gave similar conversion of fatty acids, but the contents of oxygenates decreased with increasing temperature. This may indicate that the increase in temperature did not promote more decarboxylation, but rather increased the transformation of already converted fatty acids to hydrocarbons. This was supported by the much reduced contents of oxygenates in going from 420 °C to 450 °C in Figure 6.3. Furthermore, the increase in temperature proved

to contribute to the formation of hydrocarbons even without a catalyst as the yield of oxygenated compounds dropped by 88.8%. However, the notable increase in conversion, and formation of hydrocarbons were strong indicators that Pt/C had a stronger activity to achieve decarboxylation reactions as suggested in Sections 6.1.2 and 6.1.3.1. In addition to this, the reduction in the alkene content in the Pt/C catalysed oil product also implies that the catalyst does provide in situ hydrogenation, as mentioned in previous sections.

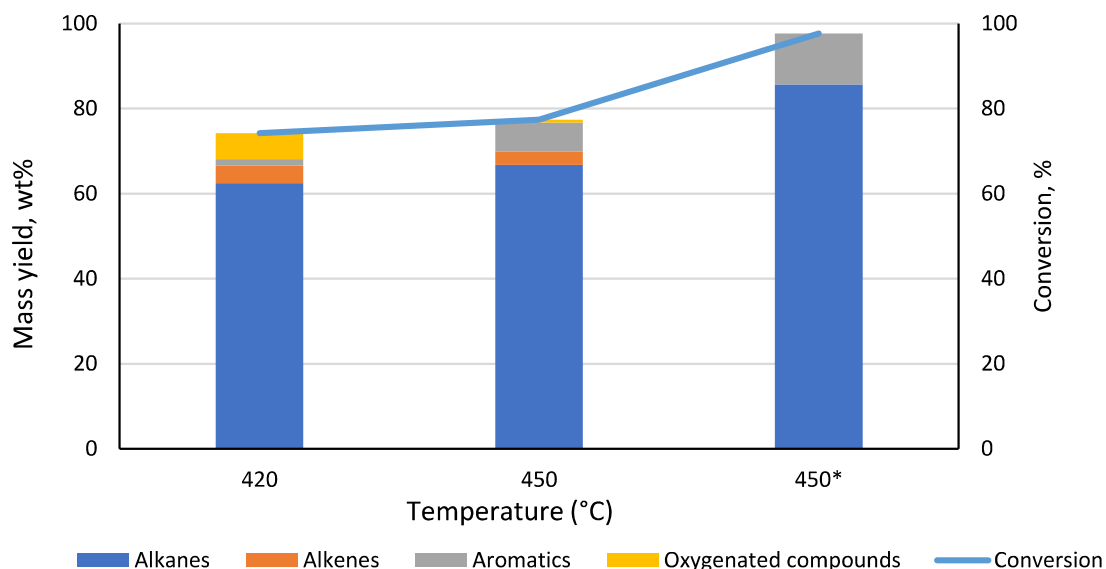


Figure 0.3: Mass yields of groups of compounds in liquid products and conversion of hydrolysed RSO during simultaneous decarboxylation and cracking at 450 °C (\* reaction with 5 wt% Pt/C)

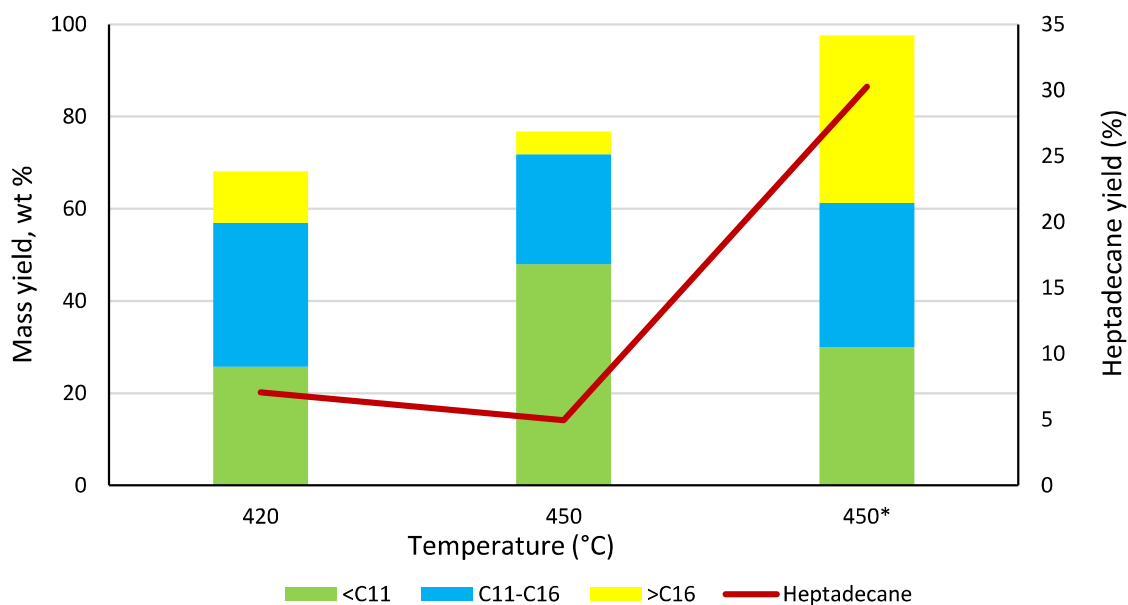
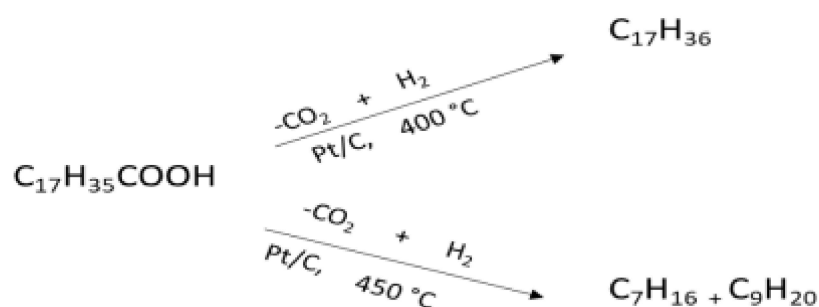


Figure 0.4: Mass yields of heptadecane and other hydrocarbon products from combined decarboxylation and cracking of hydrolysed RSO for 1 h at different temperatures (\*reaction with 5 wt% Pt/C catalyst)

Figure 6.4 shows the yields of hydrocarbons in the liquid products derived from the combined decarboxylation and cracking of hydrolysed RSO as temperature increased. In the absence of 5 wt% Pt/C, there was a reduction in the longer chain fractions, >C16 and C11-16, as well as the heptadecane yield, which reduced by almost 30%. While the shorter chain hydrocarbons fraction, <C11, increased by nearly twice with temperature in the absence of the catalyst. These suggested that increasing reaction temperature supported cracking reactions. However, upon addition of the Pt/C, there was six-fold increase in the heptadecane yield, which showed the selective nature of the catalyst towards decarboxylation. In addition to this, a more even distribution of the three fractions in the oils was observed with the Pt/C catalysed reaction, suggesting that in addition to the decarboxylation reaction, cracking also occurred as seen in the reaction without the Pt/C. Hence, results in Figure 6.4 showed that at 450 °C, Pt/C was capable of achieving the deoxygenation of fatty acids, cracking of hydrocarbons (Equation 6.1) as well as producing light coloured oil, which make these reaction conditions favourable for producing alternative liquid hydrocarbon fuels. The reaction carried out at 450 °C in the presence of the catalyst produced the diesel range (>C16) as the largest fraction in the oil. Therefore, it was inferred that a similar result would be obtained at 420 °C with catalyst; hence, not particularly promising for biojet production.



(6.1)

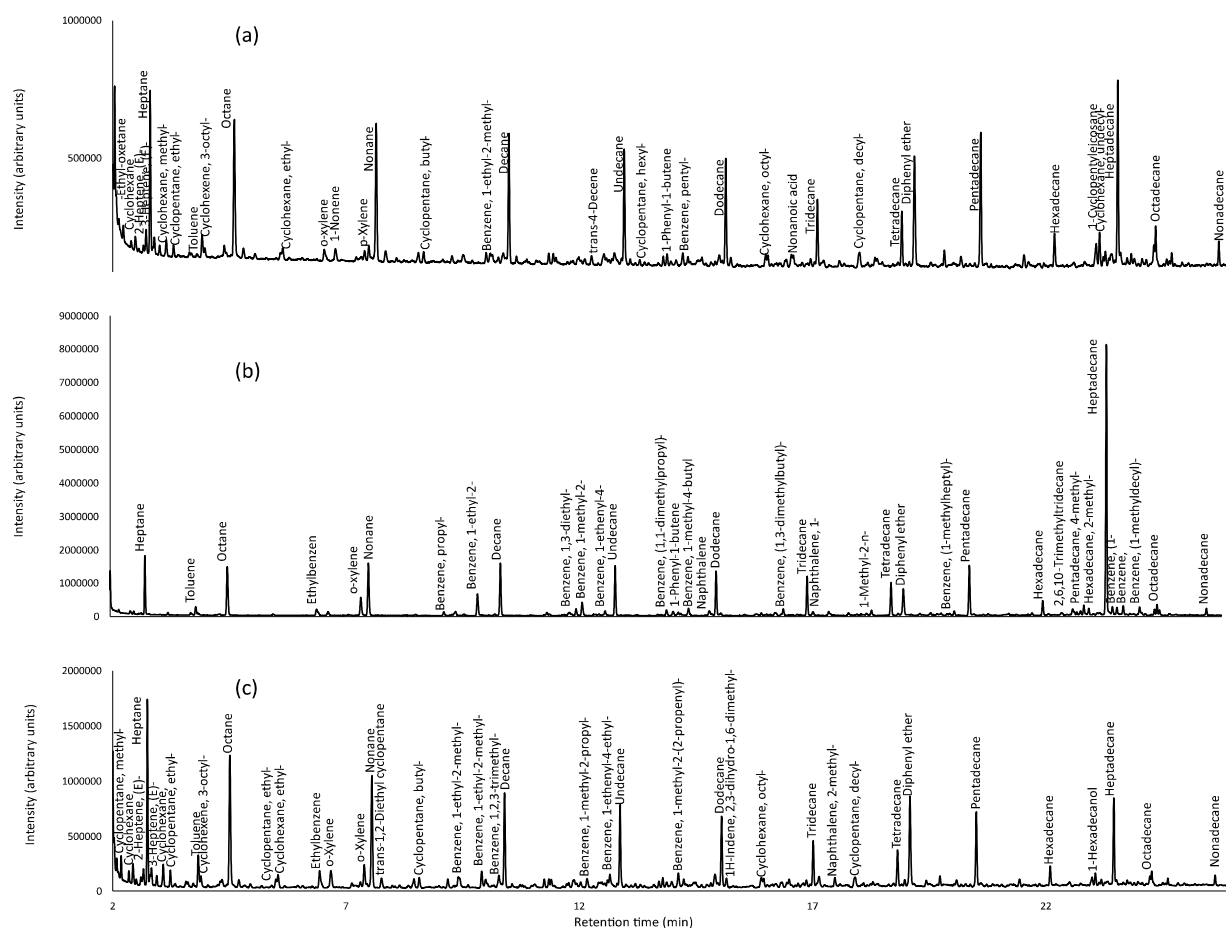


Figure 0.5: GC/MS chromatograms of combined decarboxylation and cracking of hydrolysed RSO for 1 h: (a) reaction at 420 °C without catalyst (b) reaction at 450 °C without catalyst (b) reaction at 450 °C in the presence of 5 wt% Pt/C

Figure 6.5 presents the chromatograms obtained from the GC/MS analysis of the product oils. This provides more insights into the exact compounds that made up the mass yields of the oils reported in Figures 6.3 and 6.4. Figure 6.5 clearly shows a reduction in the peak area of  $\geq C_{17}$  hydrocarbons upon increasing reaction temperature, and addition of the catalyst. Furthermore, there is an increase in the peak areas of the lighter chain hydrocarbons as reaction severity increases as well. Table 6.3 is an extract of these chromatograms, but the results have been classified into hydrocarbon groups, just as Figure 6.3 but also highlighting the quantity of each identified compound. Table 6.3 shows the presence of naphthenes at 420 °C, in the absence of Pt/C. However, there is a reduction in the yield of the cycloalkanes, and an increase in the yield of aromatics as temperature increases. This suggests that increasing reaction severity can cause cracking of naphthenes into aromatics (Sadeghbeigi, 2012). Figure 6.6 shows the H/C and O/C ratios of the oils based on their elemental compositions in a Van Krevelen diagram. The non-catalysed reactions had relatively higher O/C ratios than the catalysed reaction which emphasises the impact of the catalyst, Pt/C, on

the degree of decarboxylation. The reaction at 450 °C in the presence of catalyst had H/C to O/C ratios most comparable to conventional fuels.

Table 6.3: List of compounds in the oil products obtained from combined decarboxylation and cracking of hydrolysed RSO for 1 h at different temperatures (\*reaction with 5 wt% Pt/C catalyst)

Alkanes	Yield, wt %		
	420 °C	450 °C	450 °C *
Cyclopentane, methyl-	0.36	0.97	0.00
Cyclohexane	0.51	1.14	0.00
Heptane	5.25	9.03	5.15
Cyclohexane, methyl-	0.58	1.29	-
Cyclopentane, ethyl-	0.42	0.90	-
Octane	6.17	9.25	6.28
Cyclopentane, ethyl-	0.22	0.64	-
Cyclohexane, ethyl-	0.31	0.90	-
Nonane	6.2	7.54	6.58
trans-1,2-Diethyl cyclopentane	-	0.76	-
Cyclopentane, butyl-	0.46	0.63	-
Decane	4.8	6.15	6.09
Cyclohexane, pentyl-	0.81	-	-
Undecane	4.29	4.99	5.63
Cyclopentane, hexyl-	0.48	-	-
Dodecane	3.98	4.63	5.23
Cyclohexane, octyl-	1.00	1.15	-
Tridecane	2.40	2.75	4.51
Cyclopentane, decyl-	0.95	0.95	-
Tetradecane	2.03	2.27	3.93
Dodecane, 2-cyclohexyl-	0.6	-	-
Pentadecane	5.38	4.66	6.07
Hexadecane	1.34	1.21	1.71
Cyclohexane, nonadecyl-	1.81	-	-
2,6,10-Trimethyltridecane	-	-	0.76
Pentadecane, 4-methyl-	-	-	0.47
Hexadecane, 2-methyl-	-	-	1.14
Heptadecane, 3-methyl-	-	-	0.81
Heptadecane	7.06	4.95	30.19
Cyclohexane, undecyl-	1.52	-	-
Cyclooctane, tetradecyl-	0.23	-	-
1-Cyclopentyleicosane	0.64	-	-
Octadecane	0.39	-	0.50
Nonadecane	0.57	-	0.62
1-Cyclopentyleicosane	-	-	-
<b>Total</b>	<b>62.49</b>	<b>66.75</b>	<b>85.69</b>

#### Alkenes

#### Yield, wt %

	420 °C	450 °C	450 °C *
1-Heptene	-	0.89	-
3-Heptene, (E)-	-	0.62	-
2-Heptene, (E)-	-	0.92	-
Cyclohexene, 3-methyl-	1.39	-	-
Cyclohexene, 3-octyl-	-	0.71	-
1-Octene	.37	-	-
1-Nonene	0.54	-	-
trans-4-Decene	1.67	-	-
1-Phenyl-1-butene	0.48	-	-
<b>Total</b>	<b>4.15</b>	<b>3.14</b>	<b>-</b>

<b>Aromatics</b>	<b>Yield, wt %</b>		
	420 °C	450 °C	450 °C *
Toluene	0.52	1.13	0.46
Ethylbenzene	-	0.83	0.67
p-Xylene	0.31	0.74	1.36
o-Xylene	0.35	0.72	0.25
Benzene, 1-ethyl-2-methyl-	0.21	1.15	1.51
Benzene, pentyl-	0.12	-	-
Benzene, (1-methyldecyl)-	-	-	2.41
Benzene, (1,1-dimethylnonyl)-	-	-	0.37
Benzene, undecyl-	-	-	0.35
Benzene, 1-methyl-2-propyl-	-	0.34	0.96
Benzene, 1-ethenyl-4-ethyl-	-	0.35	0.25
Benzene, 1,2,3-trimethyl-	-	0.38	-
Benzene, 1,3-diethyl-	-	-	0.45
Benzene, (1,1-dimethylpropyl)-	-	-	0.40
1-Phenyl-1-butene	-	-	0.32
Benzene, 1-methyl-4-butyl	-	-	0.56
Naphthalene	-	-	0.39
Benzene, (1,3-dimethylbutyl)-	-	-	0.37
Naphthalene, 1-methyl-	-	-	0.31
1-Methyl-2-n-hexylbenzene	-	-	0.31
Benzene, (1-methylheptyl)-	-	-	0.29
Benzene, 1-methyl-2-(2-propenyl)-	-	0.50	-
1H-Indene, 2,3-dihydro-1,6-dimethyl-	-	0.35	-
Naphthalene, 2-methyl-	-	0.33	-
<b>Total</b>	<b>1.51</b>	<b>6.82</b>	<b>11.97</b>

<b>Oxygenated compounds</b>	<b>Yield, wt %</b>		
	420 °C	450 °C	450 °C *
2-Ethyl-oxetane	3.07	-	-
Nonanoic acid	0.83	-	-
Acetic acid n-octadecyl ester	-	-	-
n-Nonadecanol-1	1.32	-	-
n-Tridecan-1-ol	0.83	-	-

1-Hexadecanol	-	0.68	-
<b>Total</b>	<b>6.06</b>	<b>0.68</b>	<b>-</b>

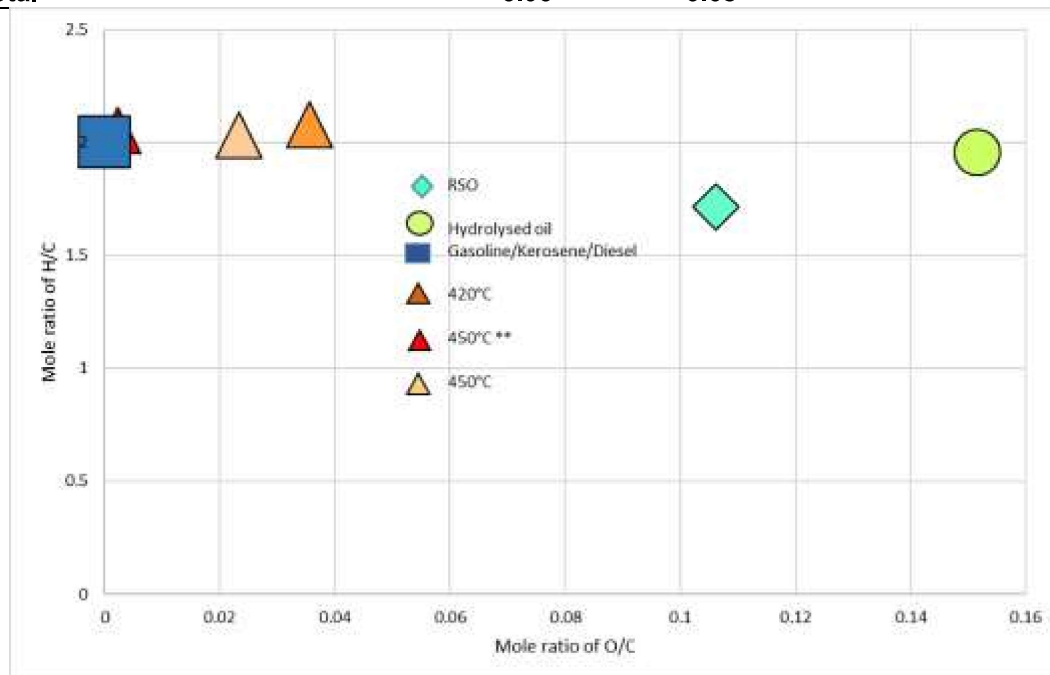


Figure 0.6: Liquid fuels characterisation from varying reaction temperature by H/C and O/C molar ratios in Van Krevelen diagram

## 6.2 Effect of different catalysts on combined decarboxylation and cracking of hydrolysed RSO at 450 °C

The conversion and yield of product distribution obtained for decarboxylation with Pt/C, Pt/MgSiO<sub>3</sub>, and Pt/Al<sub>2</sub>O<sub>3</sub> were found to be the highest and most selective towards liquid hydrocarbons in Chapter 5. Therefore, these catalysts were selected to explore their potential for possible combined (simultaneous) decarboxylation and cracking of hydrolysed RSO to give more jet fuel range liquid hydrocarbons. Each reaction was carried out at 450 °C for 1 h reaction time.

### 6.2.1 Product yields and mass balance

The mass balance closures of these experiments with different catalysts were relatively low at between 81.5 wt% and 87 wt% (Table 6.4). The Pt/Al<sub>2</sub>O<sub>3</sub> gave the lowest mass balance of 81.5 wt%, possible due to the acidic nature of alumina. There were no significant differences in the yields of gas and liquid products from these catalysts, however Pt/C produced the highest solid product (> three times compared to the two other catalysts). Hence, the lower mass balance closures obtained for Pt/Al<sub>2</sub>O<sub>3</sub> and Pt/MgSiO<sub>3</sub>, could be due to enhanced

losses of volatile compounds in the oil and gas products. The catalysts and high temperature conditions must have led to more extensive cracking, hence producing more volatile compounds, which were probably lost during the handling of samples during collection from the reactor, and during separation and analyses. For instance, some unidentified and unquantified gas components with retention time above butane, were also observed during the analysis of the gas products. Such gas components were thus not accounted for in the mass balance. All oil products obtained were in the liquid phase and categorised as light oils. However, Figure 6.7 shows that Pt/C had the lightest colour (light yellow), while the Pt/Al<sub>2</sub>O<sub>3</sub> was darker, and Pt/MgSiO<sub>3</sub>, the darkest. The results displayed as “no catalyst” is the same reported in Section 6.1 as the non-catalysed 450 °C reaction. The results have simply been reported here to aid comparison and discussion.

Table 6.4: Mass balance for reaction products from decarboxylation of hydrolysed RSO at 450 °C, 1 h with different catalysts

Catalyst	Products			Balance (wt%)
	Solid (wt%)	Oil product (wt%)	Gas phase (wt%)	
No catalyst	5.97	67.76	9.45	83.14
Pt/C	4.69	72.68	9.61	86.98
Pt/MgSiO <sub>3</sub>	1.69	75.67	8.10	85.47
Pt/Al <sub>2</sub> O <sub>3</sub>	1.89	69.76	9.84	81.50

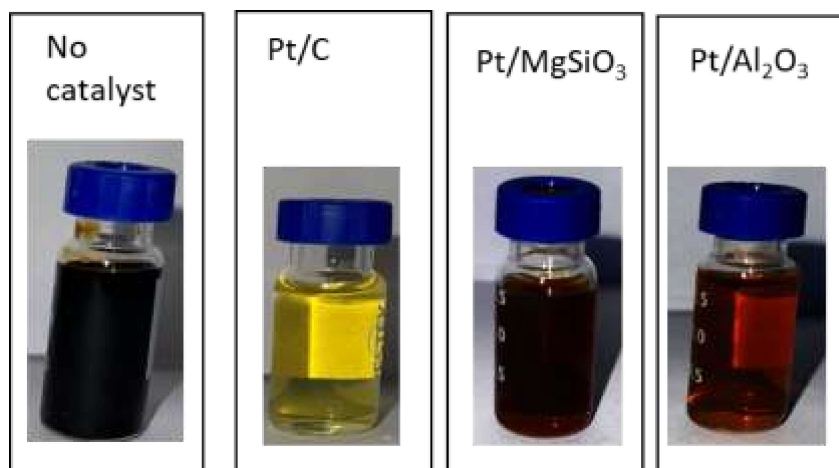


Figure 0.7: Appearance of the liquid products obtained from different catalysts during combined decarboxylation and cracking of hydrolysed RSO at 450 °C for 1 h



## 6.2.2 Gas composition

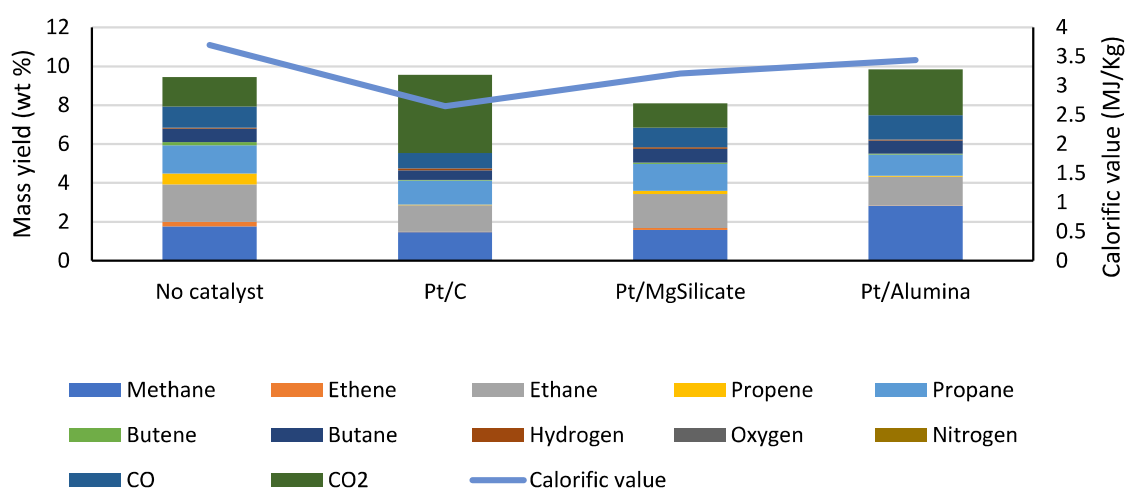


Figure 0.8: Mass yield of gas products and their calorific values during combined decarboxylation and cracking of hydrolysed RSO at 450 °C, 1 h with different catalysts

Results in Figure 6.8 show that Pt/C produced 41.75 wt% and 68.49 wt% more CO<sub>2</sub> yield than Pt/Al<sub>2</sub>O<sub>3</sub> and Pt/MgSiO<sub>3</sub>, respectively, implying less decarboxylation activity with these non-carbon support catalysts. In addition, Pt/MgSiO<sub>3</sub> and Pt/Al<sub>2</sub>O<sub>3</sub> produced more alkanes gases than Pt/C, which also indicated their poorer selectivity towards decarboxylation compared to their enhanced influence on cracking reactions. Furthermore, these results also indicate that even though they all had the same 5 wt% of Pt metal, their supports also played a role in the overall activity of the catalysts. Another interesting point to note is the reactions carried out with Pt/MgSiO<sub>3</sub> and no catalyst show similar gaseous products profiles, which could imply the minor impact of the addition of the catalyst Pt/MgSiO<sub>3</sub>. The enhanced yields of hydrocarbon gases from Pt/MgSiO<sub>3</sub> and Pt/Al<sub>2</sub>O<sub>3</sub> catalysts gave their gas products higher calorific values than that from Pt/C. While these gas products may be useful for process heating, the objective of the work was to keep as much of the hydrolysed RSO in the liquid form as liquid hydrocarbon fuels.

### 6.2.3 Characterisation of liquid products from combined decarboxylation and cracking of hydrolysed RSO at 450° C with different catalysts

#### 6.2.3.1 Physico-chemical properties of the liquid products

Table 6.5: Density, acid content, elemental composition and calorific value obtained from varying select catalyst types

Elemental composition										
Catalyst	Main organic product	Density (kg/m <sup>3</sup> )	Acid content (%)	Method <sup>a</sup>	C (wt%)	H (wt%)	N (wt%)	S (wt%)	O (wt%)	HHV (MJ/kg)
No catalyst	Dark light oil	920	22.61	1	81.09 ± 1.11	10.96 ± 0.37	0.1 ± 0.01	0	7.84 ± 0.15	41.83
				2	81.92	14.19	0	0	3.89	47.49
Pt/C	Yellow light oil	828	2.34	1	81.38 ± 1.07	12.63 ± 0.02	0.19 ± 0.02	0	5.8 ± 0.12	44.71
				2	85.18	14.56	0	0	0.26	49.78
Pt/MgSiO <sub>3</sub>	Dark light oil	800	2.98	1	68.58 ± 0.52	11.80 ± 0.16	0.13 ± 0.02	0	19.49 ± 0.13	36.71
				2	84.52	14.95	0	0	0.53	50.07
Pt/Al <sub>2</sub> O <sub>3</sub>	Dark light oil	800	6.63	1	59.24 ± 0.62	9.04 ± 0.08	0.13 ± 0.01	0	31.59 ± 0.14	27.39
				2	84.87	13.6	0	0	1.53	48.06

<sup>a</sup> Method 1: CHNS analyser; Method 2: Calculated from GC-MS analysis

Table 6.5 shows the results of the physico-chemical properties analysis. The acid-base titration results show that Pt/C and Pt/MgSiO<sub>3</sub> produced oils the least acid content, meaning they achieved the highest degree of decarboxylation. Both the Pt/MgSiO<sub>3</sub> and Pt/Al<sub>2</sub>O<sub>3</sub> catalysts produced dark coloured oils, but these had slightly lower densities compared to the oil obtained with Pt/C, possibly due to the presence of lighter chain hydrocarbons in the oils. All catalysed reactions had at least ten times less acid content in comparison with the non-catalysed reaction, which debunks the suggestion made in Section 6.2.2. The significantly reduced acid content implies the catalysts are playing a substantial role in the conversion of fatty acids to hydrocarbons. As shown in Table 6.5, the densities of the oils also agreed with the elemental compositions of the oil as there were greater discrepancies between the results from both methods with less dense oils. Where the CHNS analyser (Method 1) gave inaccurate results due to the loss of volatile components during the elemental analysis with the standard equipment. Hence, elemental compositions obtained from GC/MS (Method 2) were deemed more accurate, considering the low acid contents of the oils. Therefore, the calculated HHVs estimated from the GC/MS results indicated that the calorific values of the oils ranged from 48MJ/kg to 50 MJ/kg, which are similar to those of commercial fossil fuels (45-47 MJ/Kg) (Strömberg, 2006).

#### 6.2.3.2 Chemical composition of liquid/wax products

Figure 6.9 presents the conversion of the hydrolysed RSO to hydrocarbons followed the trend; Pt/C > Pt/MgSiO<sub>3</sub> > Pt/Al<sub>2</sub>O<sub>3</sub>. The oil from Pt/Al<sub>2</sub>O<sub>3</sub> contained the most oxygenated compounds, while Pt/C produced an oil with virtually no oxygenates, implying that the Pt/C had the highest decarboxylation activity as previously stated in Section 6.2.2. Even though the non-catalysed reaction had the least oxygenated compounds observed, its relatively low conversion still makes it the least efficient reaction. The Pt/MgSiO<sub>3</sub> produced the highest yield of alkanes but also yielded alkenes, which suggested the relatively lower hydrogenating capability of this catalyst when compared to the others. Interestingly, the Pt/MgSiO<sub>3</sub> catalyst also produced the lowest yield of aromatic hydrocarbons, indicating that it was also poor in aromatisation reactions. Although, all three catalysts produced different amounts of aromatic hydrocarbons, with Pt/Al<sub>2</sub>O<sub>3</sub> producing the highest (20.1 wt%), which may be attributed to it having the most acidic support, Pt/C produced nearly 12 wt% aromatics while Pt/MgSiO<sub>3</sub> produced only 1.76 wt%. This is possibly due to it being the catalyst with the most basic support. Hence, the absence of alkenes in the oils could be linked to the ability of the respective catalysts to promote both hydrogenation and aromatisation reactions. While Pt/C produced only alkanes and aromatics, the aromatic content from this catalyst was still lower than that required in commercial jet fuels. In contrast, the Pt/Al<sub>2</sub>O<sub>3</sub> produced an oil that seemed to be close enough to meet aromatic content requirement for jet fuel but still

contained over 6.6 % acid content. Therefore, the Pt/C appeared to be the best catalyst for producing hydrocarbons from decarboxylation of RSO, but further catalytic cracking may be needed to obtain sufficient aromatics in the final fuel to be used as jet fuel.

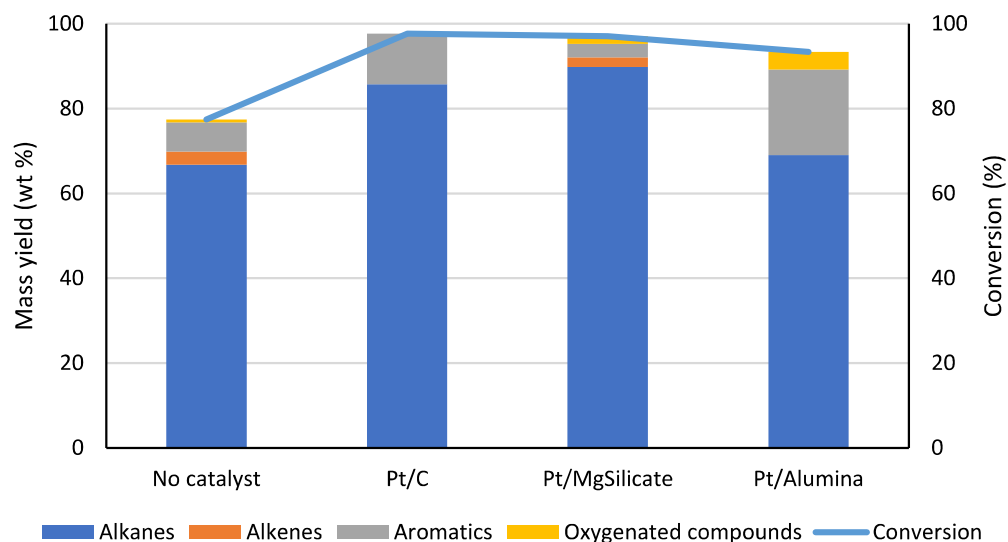


Figure 0.9: Mass yields of groups of compounds in the oil products and the conversion of hydrolysed RSO at 450 °C after 1 h with different catalysts

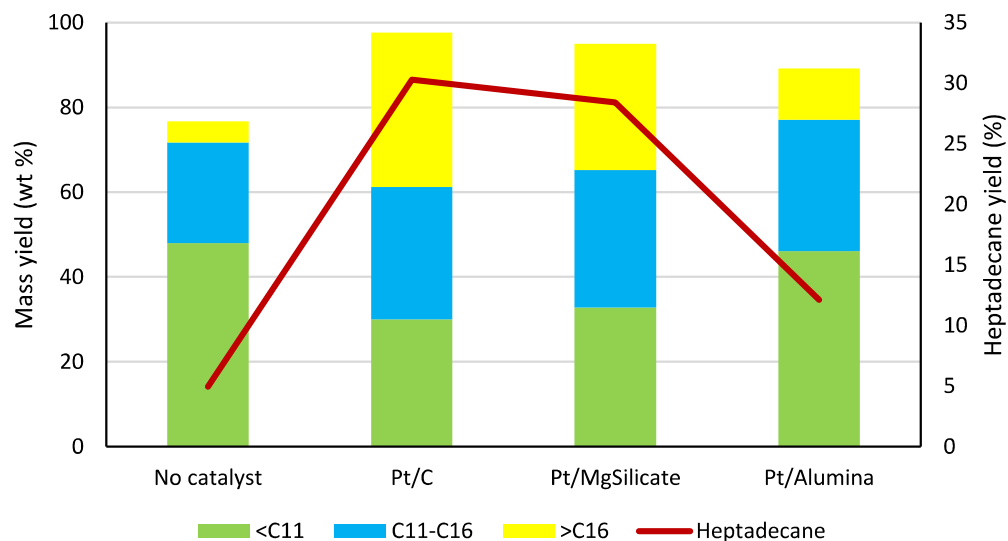


Figure 0.10: Mass yields of heptadecane and other hydrocarbon products obtained from combined decarboxylation and cracking of hydrolysed RSO at 450 °C, 1 h with different catalysts

Figure 6.10 shows the yields of compounds produced from the simultaneous decarboxylation and cracking of hydrolysed RSO using Pt/C, Pt/MgSiO<sub>3</sub>, and Pt/Al<sub>2</sub>O<sub>3</sub> based on their carbon chain lengths. There was an increase in the yields of <C11 compounds and a decrease in >C16 compounds in the order: Pt/Al<sub>2</sub>O<sub>3</sub> > Pt/MgSiO<sub>3</sub> > Pt/C, confirming the lower volatility and higher density of the oil obtained with Pt/C compared to the other two catalysts (Table 6.5). The GC/MS analyses results also showed that the degree of cracking by these catalysts reflected the changes in the yield of heptadecane in the oils. With Pt/C, heptadecane yield was 30.3 wt% and reduced slightly to 28.4 wt% with Pt/MgSiO<sub>3</sub>, however with Pt/Al<sub>2</sub>O<sub>3</sub>, the heptadecane yield was only 12.1 wt%. All three catalysts produced similar yields of C12-C16 hydrocarbons of between 30 wt% and 32 wt%, so that they only differed mainly around the gasoline and diesel range of hydrocarbons. Among the three catalyst, Pt/C was deemed the best as it produced light coloured oil that could be viable as fuel substitute (Figure 6.7), and still promoted cracking reactions to yield a good distribution of compounds with different chain lengths (Figure 6.10). The list of compounds present in the oils is presented in Table 6.6. The Van Krevelen diagram presented in Figure 6.11 shows the H/C to O/C ratios of the oils. The oil produced with Pt/MgSiO<sub>3</sub> had the highest O/C ratio while that with Pt/C was the most comparable with conventional fuels.

Table 6.6: List of compounds in the oil products obtained from combined decarboxylation and cracking of hydrolysed RSO for 1 h varying catalyst types

Alkanes	Yield, wt %		
	Pt /C 5 wt%	Pt/MgSiO <sub>3</sub> 5 wt%	Pt /Al <sub>2</sub> O <sub>3</sub> 5 wt%
Cyclopentane, methyl-	-	-	0.64
n-Hexane	-	2.33	-
Cyclopentane, 1,2-dimethyl-	-	-	0.44
Hexane, 2-methyl-	-	0.49	-
Heptane	5.15	4.78	7.05
Heptane, 2-methyl-	-	0.38	-
Heptane, 3-methyl-	-	0.35	-
Cyclohexane, methyl-	-	-	0.42
Cyclopentane, ethyl-	-	-	0.62
Heptane, 2,4-dimethyl-	-	5.89	7.77
Octane	6.28	-	-
Nonane	6.58	6.63	7.55
Cyclopentane, propyl-	-	-	0.37
Nonane, 3-methyl-	-	0.24	-
trans-1,2-Diethyl cyclopentane	-	-	0.45
Decane	6.09	6.58	6.99
Decane, 2-methyl-	-	0.46	-
Undecane	5.63	6.04	6.01
Undecane, 3-methyl-	-	0.26	-
Dodecane	5.23	5.60	-
Dodecane, 4-methyl-	-	0.33	-

Tridecane	4.51	4.35	9.82
Tridecane, 2-methyl-	-	0.24	-
Tetradecane	3.93	3.60	3.04
Pentadecane	6.07	6.03	4.35
Hexadecane	1.71	1.69	1.43
Heptadecane	30.19	28.40	12.09
2,6,10-Trimethyltridecane	0.76	2.33	-
Pentadecane, 4-methyl-	0.47	-	-
Tetradecane, 5-methyl-	-	0.60	-
Dodecane, 4-methyl-	-	0.34	-
Hexadecane, 2-methyl-	1.14	-	-
Heptadecane, 2-methyl-	0.81	0.46	-
Heptadecane, 3-methyl-	0.50	-	-
Octadecane	0.62	0.44	-
Nonadecane	-	0.45	-
2-Methylhexacosane	-	0.52	-
<b>Total</b>	<b>85.69</b>	<b>89.82</b>	<b>69.04</b>

<b>Alkenes</b>	<b>Yield, wt %</b>		
	Pt / C 5 wt%	Pt/MgSiO <sub>3</sub> 5 wt%	Pt / Al <sub>2</sub> O <sub>3</sub> 5 wt%
1-Heptene	-	0.39	-
2-Heptene, €-	-	0.44	-
1-Octene	-	0.26	-
2-Octene, €-	-	0.25	-
1-Nonene	-	0.29	-
2-Nonene, €-	-	0.39	-
2-Decene, €-	-	0.27	-
<b>Total</b>	-	<b>2.27</b>	-

<b>Aromatics</b>	<b>Yield, wt %</b>		
	Pt / C 5 wt%	Pt/MgSiO <sub>3</sub> 5 wt%	Pt / Al <sub>2</sub> O <sub>3</sub> 5 wt%
Toluene	0.46	0.41	2.5
Benzene	-	-	1.1
Ethylbenzene	0.67	0.56	1.3
p-Xylene	1.36	-	0.9
o-Xylene	0.25	0.30	1.6
Benzene, (3,3-dimethylbutyl)-	-	0.37	-
Benzene, 1-ethyl-2-methyl-	1.51	0.27	1.8
Benzene, propyl-	-	0.16	0.5
Benzene, 1-ethyl-3-methyl-	-	-	0.3
Mesitylene	-	0.27	1.0
Indane	-	-	0.6
Benzene, n-butyl-	-	-	0.7
Benzene, 1,3-diethyl-	-	-	0.3
Benzene, 1-methyl-2-propyl-	-	-	0.6
Benzene, 1-methyl-3-(1-methylethyl)-	-	-	0.2
Indan, 1-methyl-	-	-	0.4
Benzene, (1,3,3-trimethylnonyl)-	-	0.30	-
Benzene, (1,1-dimethylpropyl)-	-	0.21	0.4
Benzene, pentyl-	-	0.17	0.5

Naphthalene, 2-methyl-	-	0.17	-
p-Cymene	-	-	0.2
1H-Indene, 2,3-dihydro-5-methyl-	-	-	0.3
Benzene, 1-methyl-2-(2-propenyl)-	-	-	0.7
Benzene, (1-methyldecyl)-	2.41	-	-
Benzene, (1,1-dimethylnonyl)-	0.37	-	-
Benzene, 1-methyl-4-butyl	0.56	-	0.35
Naphthalene	0.39	-	1.10
1H-Indene, 2,3-dihydro-1,6-dimethyl-	-	-	0.38
Benzene, hexyl-	-	-	0.40
Benzene, (1,3-dimethylbutyl)-	-	-	0.36
Naphthalene, 1-methyl-	0.31	-	-
Naphthalene, 2-methyl-	-	-	0.73
Naphthalene, 2-ethyl-	-	-	0.23
Naphthalene, 1,4-dimethyl-	-	-	0.21
Benzene, undecyl-	0.35	-	-
Benzene, 1-methyl-2-propyl-	0.96	-	-
Benzene, 1-ethenyl-4-ethyl-	0.25	-	-
Benzene, 1,2,3-trimethyl-	0.00	-	-
Benzene, 1,3-diethyl-	0.45	-	-
Benzene, (1,1-dimethylpropyl)-	0.40	-	-
1-Phenyl-1-butene	0.32	-	-
Benzene, (1,3-dimethylbutyl)-	0.37	-	-
1-Methyl-2-n-hexylbenzene	0.31	-	-
Benzene, (1-methylheptyl)-	0.29	-	-
<b>Total</b>	<b>11.97</b>	<b>3.18</b>	<b>20.13</b>

Oxygenated compounds	Yield, wt %		
	Pt /C 5 wt%	Pt/MgSiO <sub>3</sub> 5 wt%	Pt / Al <sub>2</sub> O <sub>3</sub> 5 wt%
2-Ethyl-oxetane	-	-	4.2
Hydratropic acid, isohexyl ester	-	0.65	-
4-Methyl-3-heptanol, pentafluoropropionate	-	0.33	-
Hexanoic acid, octadecyl ester	-	0.47	-
1-Decanol, 2-hexyl-	-	0.31	-
<b>Total</b>	<b>-</b>	<b>1.76</b>	<b>4.2</b>

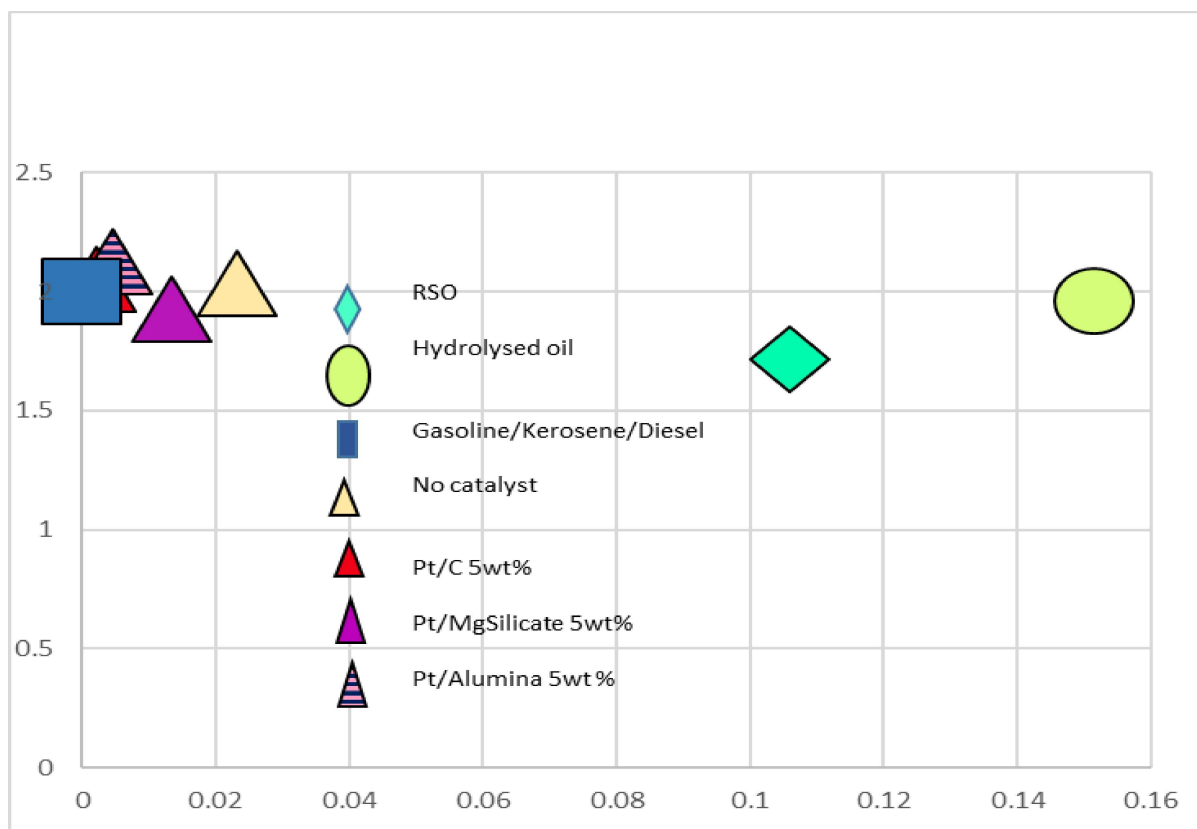


Figure 0.11: Liquid fuels characterisation from varying catalyst type by H/C and O/C molar ratios in Van Krevelen diagram

The investigation compared the performance of Pt/C, Pt/MgSiO<sub>3</sub>, and Pt/Al<sub>2</sub>O<sub>3</sub> catalysts in the simultaneous decarboxylation and cracking of hydrolysed rapeseed oil (RSO) at 450 °C for 1 h. The mass balance closures for these experiments ranged from 81.5% to 87%, with Pt/Al<sub>2</sub>O<sub>3</sub> exhibiting the lowest closure, likely due to its acidic nature. While there were no significant differences in gas and liquid product yields, Pt/C produced the highest solid product. The lower mass balance closures for Pt/Al<sub>2</sub>O<sub>3</sub> and Pt/MgSiO<sub>3</sub> were attributed to increased losses of volatile compounds. Gas composition analysis revealed that Pt/C exhibited higher CO<sub>2</sub> yields, indicating less decarboxylation activity with non-carbon support catalysts. Pt/MgSiO<sub>3</sub> and Pt/Al<sub>2</sub>O<sub>3</sub> produced more alkane gases, suggesting poorer selectivity toward decarboxylation and enhanced influence on cracking reactions. The physico-chemical properties of the liquid products showed that Pt/C and Pt/MgSiO<sub>3</sub> had the least acid content, signifying higher decarboxylation efficiency. Density, elemental composition, and calorific values suggested the potential use of these oils as conventional fuels. Chemical composition analysis indicated that Pt/C had the highest decarboxylation activity, producing oils with virtually no oxygenates. Pt/MgSiO<sub>3</sub> yielded the most alkanes, while Pt/Al<sub>2</sub>O<sub>3</sub> produced oils with higher aromatic content. Pt/C was considered the most suitable catalyst for producing hydrocarbons from RSO decarboxylation, with further catalytic cracking potentially needed to achieve the required aromatic content for jet fuel. The study



provided a comprehensive understanding of catalyst performance and product characteristics in the decarboxylation process.

### 6.3 Effect of reaction time on the simultaneous decarboxylation and cracking of hydrolysed RSO

From the previous sections, Pt/C showed the best activity towards decarboxylation and cracking of hydrolysed RSO to yield almost 100% hydrocarbon liquids using 1 h reaction time and 450 °C as fixed variables. In addition, in this section, the reaction time was varied from 0 h – 2 h to optimise the degree of simultaneous decarboxylation and cracking at 450 °C.

#### 6.3.1 Product yields and mass balance

Table 6.7 presents the mass balance closures for calculating the effect of changing reaction time on the decarboxylation of hydrolysed rapeseed oil. There was a decline in the mass balance from 93.26% to 85.64% with increased reaction time from 0 to 2 h at 450 °C. This was possibly due to the loss of shorter chain hydrocarbons in the form of volatiles that were produced by increasing reaction severity with time.

Table 6.7: Mass balance for reaction products from simultaneous decarboxylation and cracking of hydrolysed RSO at 450 °C with different reaction times

Time (h)	Products				Balance (wt%)
	Solid (wt%)	Oil (wt%)	Wax (wt%)	Gas (wt%)	
0	3.49	-	85.23	4.54	93.26
1	4.68	72.68	-	9.61	86.98
2	8.69	61.34	-	15.61	85.64

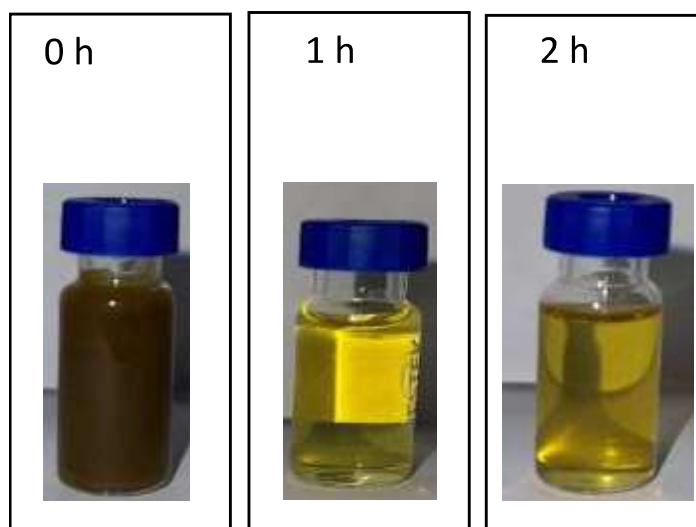


Figure 0.12: Appearance of products from simultaneous decarboxylation and cracking of hydrolysed RSO in relation to reaction time at 450 °C

The experiments at each reaction time yielded products in all three phases, gas, wax/oil, and solid. As stated earlier in Section 5.3.1, the reaction time denoted as “0 h” means the reaction was stopped upon reaching set temperature. Unlike the reaction at 0 h that produced wax, the experiments at 1 h and 2 h reaction times produced light coloured oil products (Figure 6.12). The wax product obtained was probably due to the presence of long chain alkanes, and not necessarily an indication of the absence of decarboxylation. However, this would be further clarified following the characterisation of the oil/wax products by GC/MS in subsequent sections.

### 6.3.2 Gas composition in relation to reaction times at 450 °C

Figure 6.13 shows the composition of the gas products obtained when reaction time was increased from 0 h to 2 h at 450 °C. The production of CO<sub>2</sub> from all experiments was an indication that decarboxylation occurred. It was observed that at 0 h, there was a notable yield of CO<sub>2</sub>, which indicated that temperature and the presence of Pt/C did play major roles in achieving decarboxylation, possibly even more than reaction time. Furthermore, besides the increase in CO<sub>2</sub>, there was also an increase in the yields of C1 – C4 hydrocarbon gases and hydrogen. This implied that increasing reaction time at 450 °C also promoted cracking reactions. Even with the dominant CO<sub>2</sub>, Figure 6.13 showed an increase in the calorific values of the gas products with reaction time increase due to the increased formation of the hydrocarbon gases and hydrogen produced. The calorific value of the gases obtained ranged from 0.99 MJ/kg to 5.13 MJ/kg and could be useful for process heating.

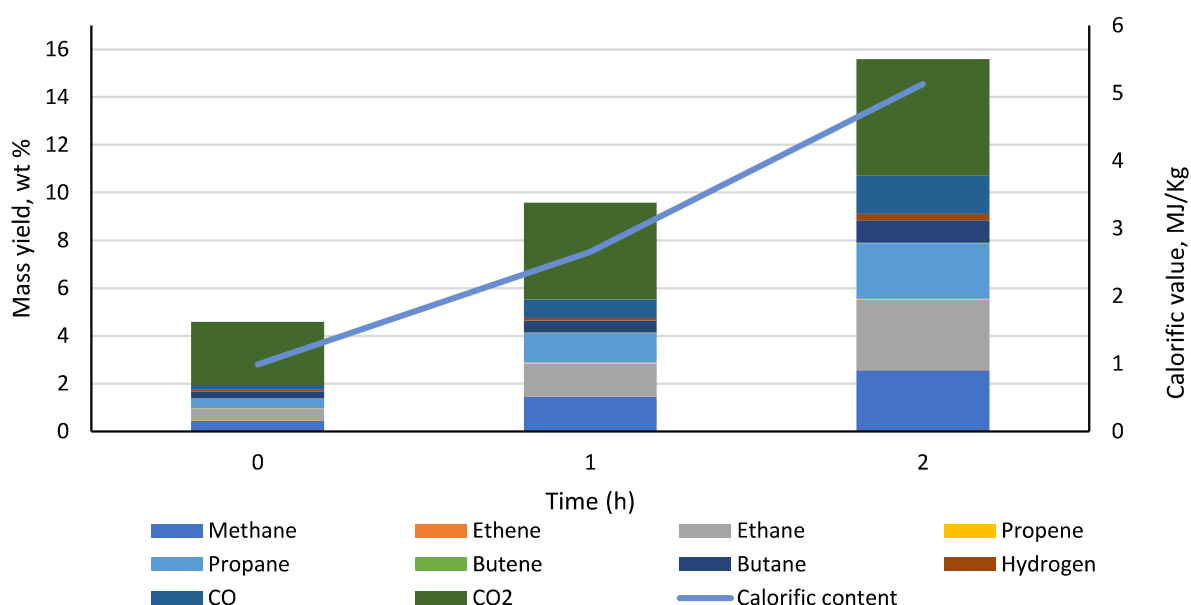


Figure 0.13: Mass yields of gas products and their calorific values from simultaneous cracking and decarboxylation of hydrolysed RSO at 450 °C at different reaction times

Table 6.8 shows that the acid contents in the oil products decreased dramatically as reaction severity increased from 0 h to 2 h reaction time. The same trend was also observed in their relative densities, possibly due to the formation of shorter chain hydrocarbons as cracking increased. The HHVs of all the wax/oil products were high, ranging from 45 MJ/kg to 47 MJ/kg, as evidence of enhanced hydrocarbon contents similar to those of conventional liquid fuels (Strömberg, 2006).

### 6.3.3 Characterisation of liquid products obtained in relation to reaction time at 450 °C in the presence of 5 wt% Pt/C catalyst

#### 6.3.3.1 Physico-chemical properties of liquid products

Table 6.8: Density, acid content, elemental composition and calorific value of liquid products in relation to reaction time at 450 °C with 5 wt% Pt/C catalyst

Elemental composition										
Time (h)	Main organic product	Density (Kg/m <sup>3</sup> )	Acid content (%)	Method <sup>a</sup>	C (wt %)	H (wt %)	N (wt %)	S (wt %)	O (wt %)	HHV (MJ/kg)
0	Dark wax	845	31.8	1	80.15 ± 0.54	13.54 ± 0.06	0.12 ± 0.00	-	6.18 ± 0.60	45.54
				2	82.34	13.94	-	-	3.72	47.30
1	Yellow light oil	828	2.34	1	81.38 ± 1.07	12.63 ± 0.02	0.19 ± 0.02	-	5.8 ± 1.12	44.71
				2	85.18	14.56	-	-	0.26	49.78
2	Yellow light oil	825	1.98	1	82.22 ± 3.37	12.92 ± 0.38	0.13 ± 0.00	-	4.73 ± 0.07	45.61
				2	86.47	16.27	-	-	1.26	50.84

<sup>a</sup> Method 1: CHNS analyser; Method 2: Calculated from GC-MS analysis

### 6.3.3.2 Chemical composition of liquid/wax products in relation to reaction time at 450 °C with 5 wt% Pt/C catalyst

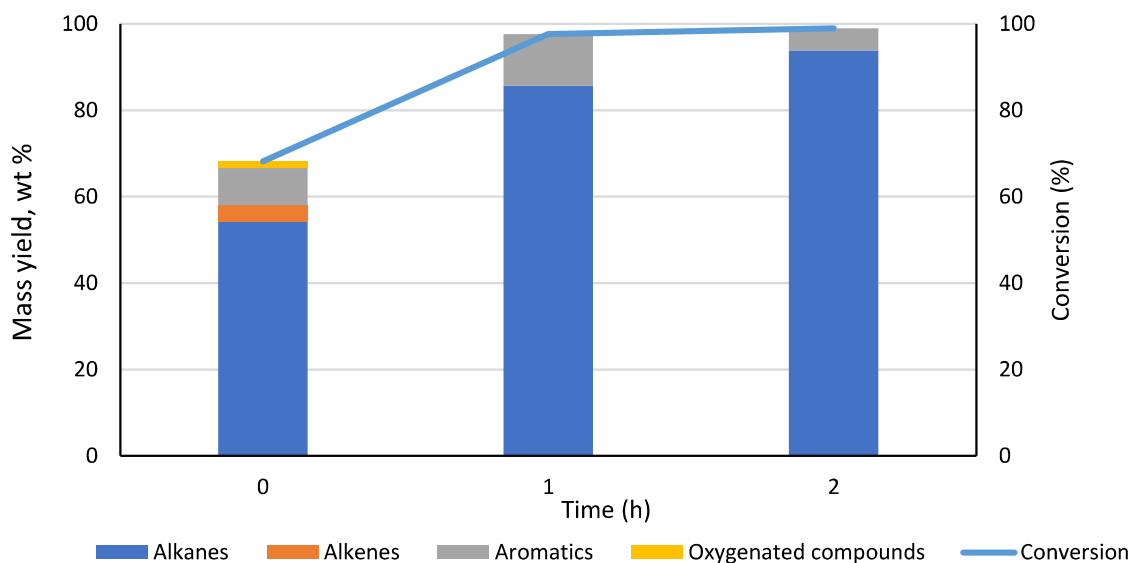


Figure 0.14: Mass yields of groups of hydrocarbon products and conversion of hydrolysed RSO during simultaneous decarboxylation and cracking at 450 °C and different reaction times

Figure 6.14 shows the results of analysis of the liquid hydrocarbons based on the group of compounds obtained from the combined decarboxylation and cracking reactions carried out varying time at 450 °C. There was a direct correlation between the increase in conversion and reaction severity. Clearly, alkenes and oxygenated compounds were only observed at 0 h reaction time. From 1 h reaction time and above, the only compounds found in the oil by GC/MS analyses were alkanes and aromatics. Furthermore, there was a 72.93% increase in the alkane yield, and a 40.26% decrease in aromatics from 0 - 2h. This suggested that increasing reaction severity promoted the production of saturated hydrocarbons from both alkenes and aromatics via hydrogenation, possibly catalysed by 5 wt% Pt/C (Ahmadi et al., 2015). Even though, there is an overall increase in conversion with time, there was plateau after the first hour. Hence, beyond 1 h, the increase in reaction severity had minimal effect on the conversion but influenced the ratio of aromatics and alkanes in the oil product.

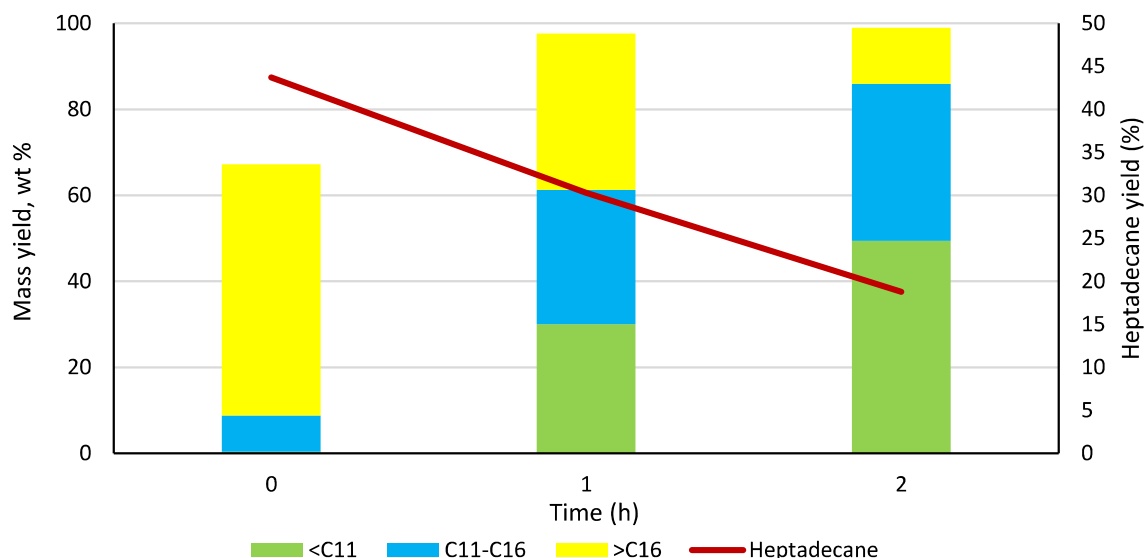


Figure 0.15: Mass yields of heptadecane and other hydrocarbon products from the simultaneous decarboxylation and cracking of hydrolysed RSO at 450 °C and different reaction times

Figure 6.15 shows the hydrocarbon contents of the oil products obtained from the Pt/C-catalysed combined decarboxylation and cracking reactions of hydrolysed RSO at 450 °C in relation to time. As reaction severity increased, there was an increase in the formation of the shorter chain hydrocarbons from long chain hydrocarbons. Specifically, there were no  $<C_{11}$  hydrocarbons identified at 0 h, but the yield of this range of hydrocarbon increased by 30% after 1 h and increased by 64.67% after 2 h reaction. Similarly, the C11-C16 hydrocarbons increased by almost three-folds from 0 h to 2 h. In contrast to these, the  $>C_{16}$  fraction decreased by 37.64% from 0 h to 1 h, and even more by 64.15% from 1 h to 2 h. This same trend was observed in the yield of heptadecane that decreased with increase in reaction time. These all suggested that in addition to the almost complete decarboxylation achieved by the increase in reaction severity, the 5 wt% Pt/C catalyst promoted cracking reactions to give higher yields of liquid hydrocarbons within the jet fuel and gasoline ranges. These results showed that changing the reaction times between 1 h and 2 h, the distribution of hydrocarbon fuels could be altered. Essentially, carrying out simultaneous decarboxylation and cracking reactions in 1 h would yield a fairly equal distribution of gasoline, jet fuel and diesel range liquid hydrocarbons. Moreover, increasing the reaction time to 2 h would give higher yields of gasoline range (49.4 wt%), moderately high jet fuel range (36.6 wt%) and much lower diesel range (13.0 wt%). Hence the fuel composition obtained was tuneable by reaction time, but the aromatic yield still remained lower than those required in gasoline and jet fuels. Figure 6.16 shows the Van Krevelen diagram produced based on the H/C to O/C

ratios of the oils. The reaction at 0 h had the highest oxygen content while the oil produced with highest reaction severity yielded the highest hydrocarbon content.

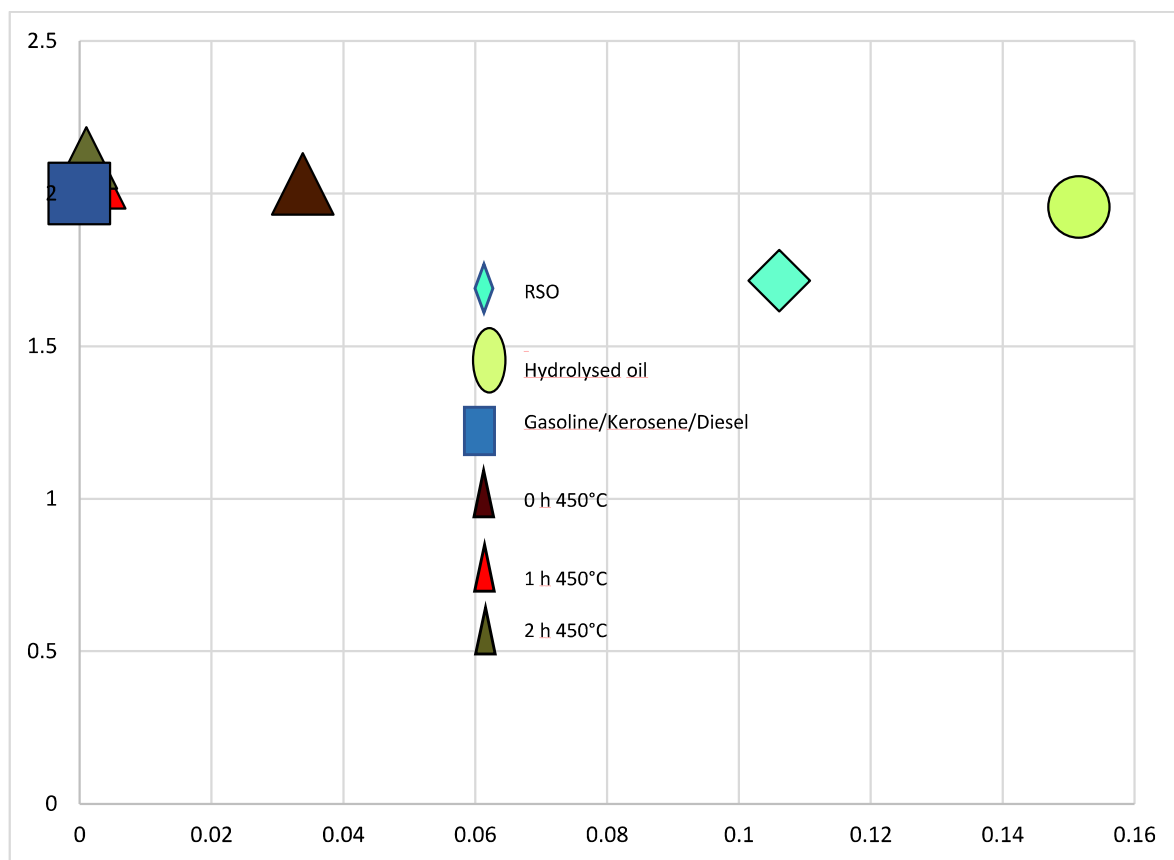


Figure 0.16: Liquid fuels characterisation from varying reaction time by H/C and O/C molar ratios in Van Krevelen diagram

The impact of reaction time on the simultaneous decarboxylation and cracking of hydrolysed rapeseed oil (RSO) at 450 °C with a 5 wt% Pt/C catalyst is explored in Table 6.7 and subsequent analyses. The mass balance closures (Table 6.7) indicate a decline from 93.26% to 85.64% as the reaction time increases from 0 to 2 h, attributed to the potential loss of shorter-chain hydrocarbons in volatile form with increased reaction severity. The appearance of products (Figure 6.12) shifts from dark wax at 0 h to light-coloured oil at 1 and 2 h. Gas composition analysis (Figure 6.13) reveals increased yields of CO<sub>2</sub> and C1-C4 hydrocarbon gases with extended reaction time, indicating enhanced decarboxylation and cracking reactions. Furthermore, the calorific values of the gas products increase, ranging from 0.99 MJ/kg to 5.13 MJ/kg. The characterisation of liquid products (Table 6.8) shows a dramatic decrease in acid content and relative densities as reaction severity increases. The calorific values of the wax/oil products remain high, ranging from 45 MJ/kg to 47 MJ/kg. GC/MS analysis (Figures 6.14 and 6.15) illustrates a correlation between increased conversion and

reaction severity, with alkanes and aromatics dominating the oil products at 1 and 2 h. The yield of heptadecane decreases with longer reaction times. Overall, increasing reaction severity influences hydrocarbon distribution, with 2 h resulting in higher yields of gasoline and jet fuel range liquid hydrocarbons. The Van Krevelen diagram (Figure 6.16) further highlights the impact of reaction time on the H/C to O/C molar ratios, indicating the highest oxygen content at 0 h and the highest hydrocarbon content with the most extended reaction severity. The results suggest that reaction time is a crucial parameter in tuning the composition of liquid fuels produced from simultaneous decarboxylation and cracking of hydrolysed RSO.

## 6.4 Reusability of 5 wt% Pt/C for combined decarboxylation and cracking at 450 °C

Experiments in this Chapter 6 have so far confirmed the superiority of 5 wt% Pt/C to promote decarboxylation of fatty acids in hydrolysed RSO. In addition, the reaction temperature of 450 °C and reaction time of 1 h, have been found to be sufficient to achieve near total decarboxylation as well as extensive cracking to produce light-coloured oils with a good distribution of commercial fuel ranges. In this Section, further experiments were carried out on the stability of the catalyst over three repeated cycles. Catalyst deactivation is a major cost factor in the development of catalytic processes to pilot and commercial scales. Given the high cost and increasing demand for platinum, especially for hydrogen fuel cells (Rasmussen et al., 2019), reducing the demand for Pt catalyst in this process would make economic sense and enhance its environmental sustainability. In this study, three experimental reaction cycles were conducted using the same Pt/C catalyst at 450 °C for 1 h under 5 bar N<sub>2</sub>. Following each run, the solid residue containing the used catalyst was washed with DCM, and dried at 40 °C. After this, the catalyst was used again in the next reaction cycle. Three repeats of the first and second cycles were carried out to ensure there was 10 g of oil to run the full cycle.

### 6.4.1 Product yields and mass balance

Table 6.9: Mass balance for reaction products from decarboxylation of hydrolysed rapeseed oil at 450 °C for 1 h assessing repeatability of results

Run	Products			Balance (wt%)
	Solid (wt%)	Oil (wt%)	Gas (wt%)	
1st cycle	4.69	72.68	9.61	86.98



2nd cycle	7.00	72.00	8.49	87.49
3rd cycle	6.10	72.70	8.62	87.42

The mass balance closures obtained from reusing the catalyst over 3 cycles all turned out to be approximately 87 wt% (Table 6.9). There are minor differences in the yields of solid, liquid and gas products obtained. This also applies to their appearances. All 3 reactions produced light oils, but the colour of the oil produced got slightly darker after each cycle (Figure 6.17).

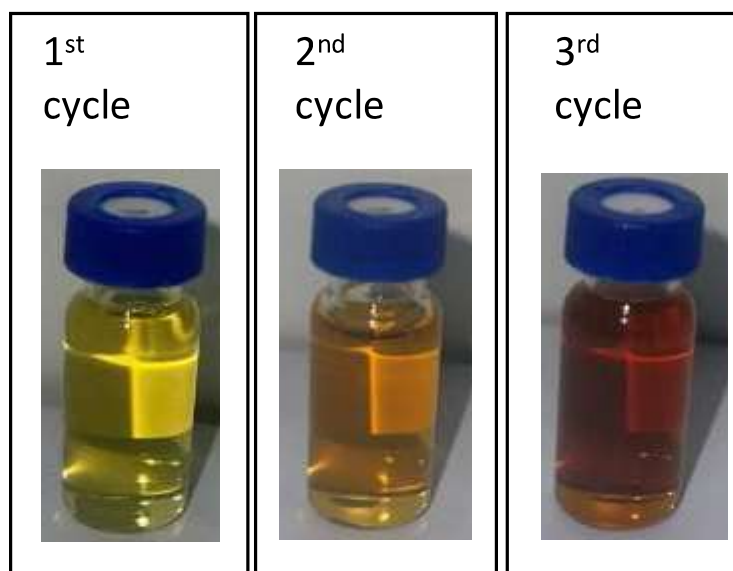


Figure 0.17: Appearance of oil products obtained from reusing the Pt/C catalysts over 3 reaction cycles

#### 6.4.2 Gas composition

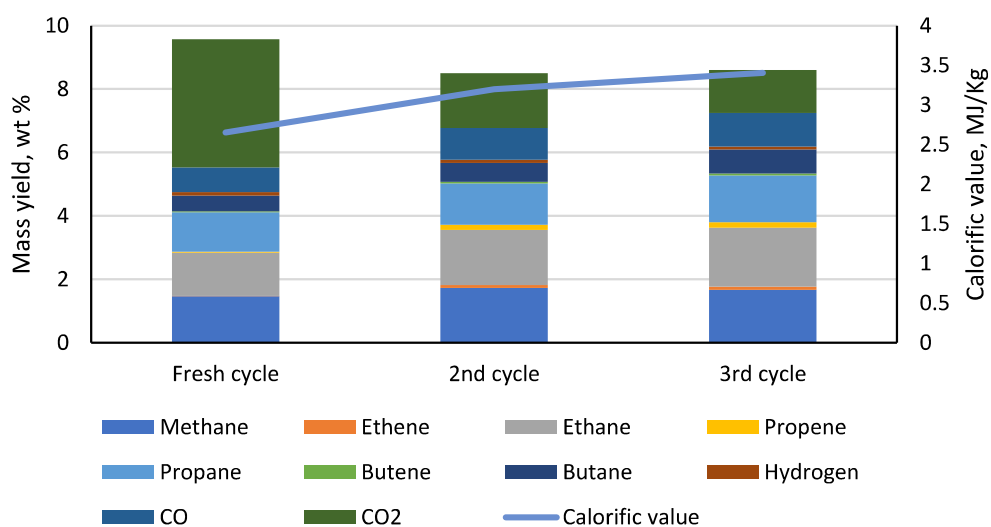


Figure 0.18: Mass yields of gas products obtained from reusing catalyst at decarboxylation stage

Decarboxylation produces  $\text{CO}_2$  and therefore its yield can be used to measure the extent and selectivity of this reaction. Therefore, the significant decrease in the  $\text{CO}_2$  gas volume from the first experiment with the fresh catalyst (19 wt%) to that from the third cycle (6.43 wt%), was an indicator of reduced catalyst activity toward decarboxylation (Figure 6.18). In addition, the enhanced yields of the hydrocarbon gases over subsequent cycles indicated that random cracking was more dominant than decarboxylation. Indeed, the yield of hydrocarbon gases were similar to those obtained without catalyst at 450 °C (Figure 6.2), implying reduction in catalytic activity. This also correlated with the increasing calorific value of the gases after each cycle, as less  $\text{CO}_2$  and more hydrocarbons were obtained. Pt/C being a metal-supported catalyst has the tendency to be poisoned from coke deposition on its surface, impurities from the feed, phase transformation or blockage of the pores leading to reduced surface area when exposed to harsh reaction conditions (Santillan-Jimenez and Crocker, 2012). Hence, any of these could be responsible for the loss in catalytic activity observed in this work.

6.4.3 Characterisation of liquid products obtained from reusing Pt/C catalyst over three reaction cycles

6.4.3.1 Physico-chemical properties of liquid products

Table 6.10: Density, acid content, elemental composition and calorific value obtained from reusing catalyst

Elemental composition										
Run	Main organic product	Density (Kg/m <sup>3</sup> )	Acid content (%)	Method <sup>a</sup>	C (wt%)	H (wt%)	N (wt%)	S (wt%)	O (wt%)	HHV (MJ/kg)
1st cycle	Yellow thin oil	828	2.34	1	81.38 ± 1.07	12.63 ± 0.02	0.19 ± 0.02	-	5.8 ± 0.12	44.71
				2	85.18	14.56	-	-	0.26	49.78
2nd cycle	Orange thin oil	853	8.22	1	77.76 ± 0.18	12.28 ± 0.10	0.15 ± 0.09	-	9.81 ± 0.61	42.26
				2	84.4	14.48	-	-	0.11	48.08
3rd cycle	Red thin oil	878	10.28	1	74.13 ± 1.08	11.86 ± 0.14	0.17 ± 0.07	-	13.84 ± 0.44	39.7
				2	83.57	14.35	-	-	1.2	48.77

<sup>a</sup> Method 1: CHNS analyser; Method 2: Calculated from GC-MS analysis

Table 6.10 shows that both the densities and acid contents of the oils increased with repeated use of the catalyst, which agreed with the reduction in the degree of deoxygenation by decarboxylation. However, the oil products still had better fuel properties than the oil obtained with no catalyst in Table 6.2 and Table 6.5. Indeed, the oil product from the third catalyst cycled contained slightly less than half of the acid content of the no-catalytic test. Hence, the spent catalyst, still had more potential decarboxylation activity than without the catalyst at all. Again, the elemental compositions obtained from GC/MS analyses (Method 2) gave results that aligned well with the other properties of the liquid products in terms of degree of decarboxylation and hydrocarbon contents. Hence, calorific values of the oils were all greater than >47 MJ/kg, indicating high hydrocarbon contents similar to commercial fuels (Strömberg, 2006).

#### 6.4.3.2 Chemical composition of liquid products obtained from reusing of 5 wt% Pt/C catalyst at 450 °C

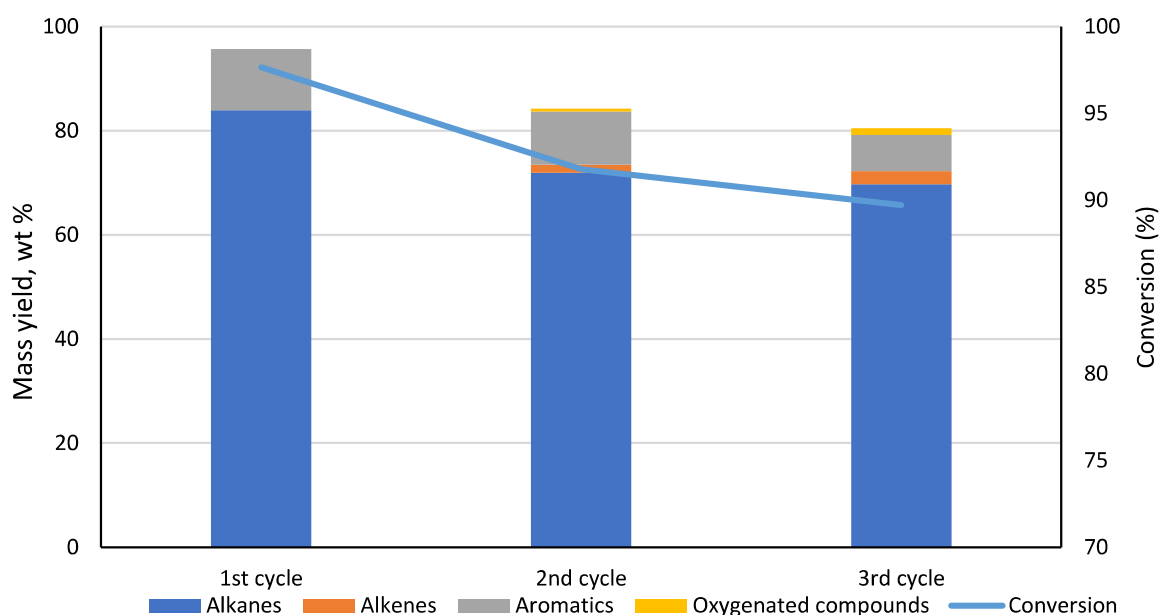


Figure 0.19: Mass yields of groups of products obtained from reusing Pt/C catalyst for simultaneous decarboxylation and cracking

The results of the analysis of the fresh and reused 5 wt% Pt/C catalyst are shown in Figure 6.19. The conversion and yield of alkanes decreased after each cycle, which reflected the reduced activity of the catalyst and agreed with the reduced yield of CO<sub>2</sub> in Figure 6.18. Hence, the overall reduction in conversion of the fatty acids with repeated catalyst reuse also matched with the acid contents in Table 6.10. The presence of oxygenated compounds in the

2<sup>nd</sup> and 3<sup>rd</sup> cycles can also be attributed to a reduction in catalyst activity when compared to that of the fresh cycle.

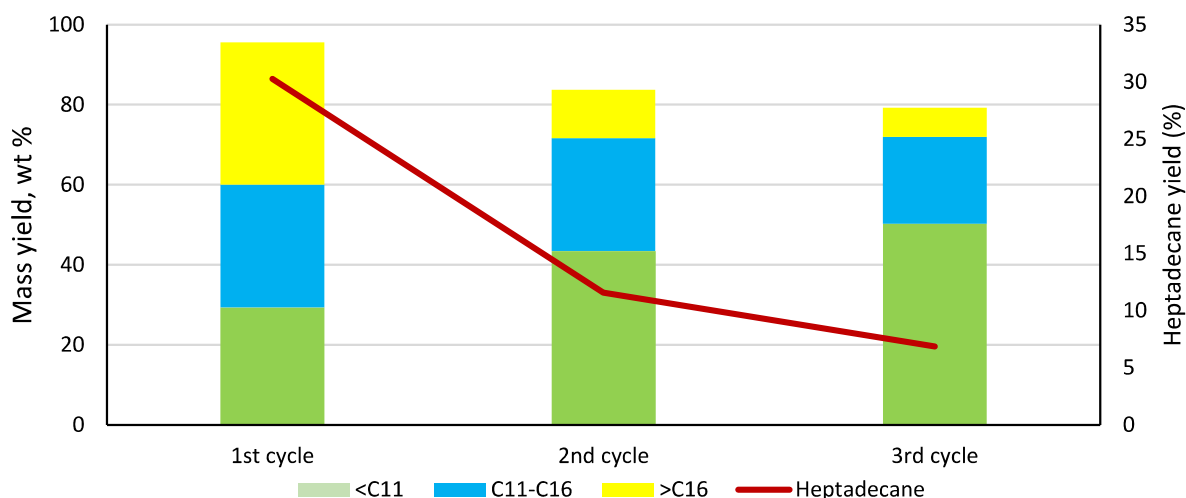


Figure 0.20: Mass yields of heptadecane and hydrocarbon products obtained from reusing Pt/C catalyst for simultaneous decarboxylation and cracking at 450 °C for 1 h

Figure 6.20 provides the distribution of liquid products according to the length of the carbon chain during the reusability test of the Pt/C catalyst at 450 °C for a reaction time of 1 h. Clearly, the yields of heptadecane decreased after each cycle and there was an increase in the yields of <C11 hydrocarbons with increasing reuse of the catalyst. However, the results were not too different from those obtained without catalyst in Figure 6.10. Hence, the reactions were less selective towards decarboxylation and instead more random cracking occurred with each subsequent cycle. These could be due to the saturation of the active sites and deactivation of the catalyst. One of the major challenges of using carbon-supported catalyst is that they cannot be easily regenerated by calcination or carbon-burn-off as this would lead to loss of the support. Instead, such catalyst would be generated by free metal recovery and subsequent fresh catalyst synthesis. The reusability potential of the Pt/C catalyst in this work was found to be constrained by the build-up of carbon deposits after each cycle of use as shown by increased char formation in Table 6.9. The list of compounds present is shown in Table 6.11. Figure 6.21 shows the Van Krevelen diagram used to estimate the H/C to O/C ratios of the oils. The figure shows a shift to the right, which signifies increase in oxygen content as catalyst is reused. This implies decrease in degree of decarboxylation and therefore deactivation of catalyst as suggested previously.

Table 6.11: List of compounds in the oil products obtained from combined decarboxylation and cracking of hydrolysed RSO for 1 h repeating catalyst

Alkanes	Yield, wt %		
	1st cycle	2nd cycle	3rd cycle
Cyclopentane, methyl-	-	-	0.88
Hexane, 3-methyl-	-	-	0.38
Heptane	5.15	7.86	11.25
Cyclopentane, ethyl-	-	0.59	0.84
Octane	6.28	10.02	11.66
Nonane	6.58	9.35	9.54
Cyclohexane, methyl-	-	-	0.86
Cyclohexane, ethyl-	-	-	1.33
Cyclopentane, butyl-	-	0.49	0.56
Decane	6.09	8.83	8.27
Undecane	5.63	7.04	6.35
Cyclopentane, hexyl-	-	-	0.53
Dodecane	5.23	6.37	5.43
Tridecane	4.51	4.14	3.20
Tetradecane	3.93	3.21	2.34
Pentadecane	6.07	5.89	4.91
Hexadecane	1.71	1.43	0.94
Heptadecane	30.19	11.58	6.85
2,6,10-Trimethyltridecane	0.76	-	-
Pentadecane, 4-methyl-	0.47	-	-
Hexadecane, 2-methyl-	1.14	-	-
Heptadecane, 2-methyl-	0.81	-	-
Heptadecane, 3-methyl-	0.50	-	-
Cyclopentane, decyl-	-	0.49	0.47
Cyclohexane, undecyl-	-	0.52	0.44
Nonadecane	0.62	0.55	0.36
<b>Total</b>	<b>85.69</b>	<b>71.91</b>	<b>69.70</b>
Alkenes	Yield, wt %		
	1st cycle	2nd cycle	3rd cycle
3-Hexene, (Z)-	-	-	0.39
3-Methyl-3-hexene	-	-	0.79
2-Heptene, (E)-	-	0.72	1.67
3-Heptene, (E)-	-	0.98	-
<b>Total</b>	<b>-</b>	<b>1.56</b>	<b>2.56</b>
Aromatics	Yield, wt %		
	1st cycle	2nd cycle	3rd cycle
Toluene	0.46	0.97	1.38
Ethylbenzene	0.67	1.13	1.09
p-Xylene	1.36	0.85	0.91
o-Xylene	0.25	0.98	0.80
1-Nonyne	-	-	0.33

Benzene, propyl-	-	0.44	0.39
Benzene, 1-ethyl-3-methyl-	-	0.90	0.80
Benzene, 1-ethyl-2-methyl-	1.51	1.06	0.72
Benzene, 1,2,3-trimethyl-	-	0.83	0.84
Benzene, n-butyl-	-	0.46	-
Benzene, 1,3-diethyl-	-	0.28	-
Benzene, 1-methyl-2-propyl-	-	0.62	0.48
Benzene, 1-methyl-2-(2-propenyl)-	-	0.56	-
Benzene, pentyl-	-	0.30	-
Benzene, (1-methyldecyl)-	2.41	-	-
Benzene, (1,1-dimethylnonyl)-	0.37	-	-
Benzene, 1-methyl-4-butyl	0.56	-	-
Naphthalene	0.39	0.61	-
Benzene, (1,3-dimethylbutyl)-	-	0.23	-
Naphthalene, 1-methyl-	0.31	0.55	-
Naphthalene, 2-methyl-	-	0.37	-
Benzene, undecyl-	0.35	-	-
Benzene, 1-methyl-2-propyl-	0.96	-	-
Benzene, 1-ethenyl-4-ethyl-	0.25	-	-
Benzene, 1,3-diethyl-	0.45	-	-
Benzene, (1,1-dimethylpropyl)-	0.40	-	-
1-Phenyl-1-butene	0.32	-	-
Benzene, (1,3-dimethylbutyl)-	0.37	-	-
1-Methyl-2-n-hexylbenzene	0.31	-	-
Benzene, (1-methylheptyl)-	0.29	-	-
<b>Total</b>	<b>11.97</b>	<b>10.21</b>	<b>6.94</b>

Oxygenated compounds	Yield, wt%		
	1st cycle	2nd cycle	3rd cycle
N-Methyl-9-aza-tricyclo[6.2.2.0(2,7)] dodec-2,4,6,11-tetraene-10-one	-	-	0.73
1-Hexadecanol	-	0.55	0.57
<b>Total</b>	<b>-</b>	<b>0.55</b>	<b>1.30</b>

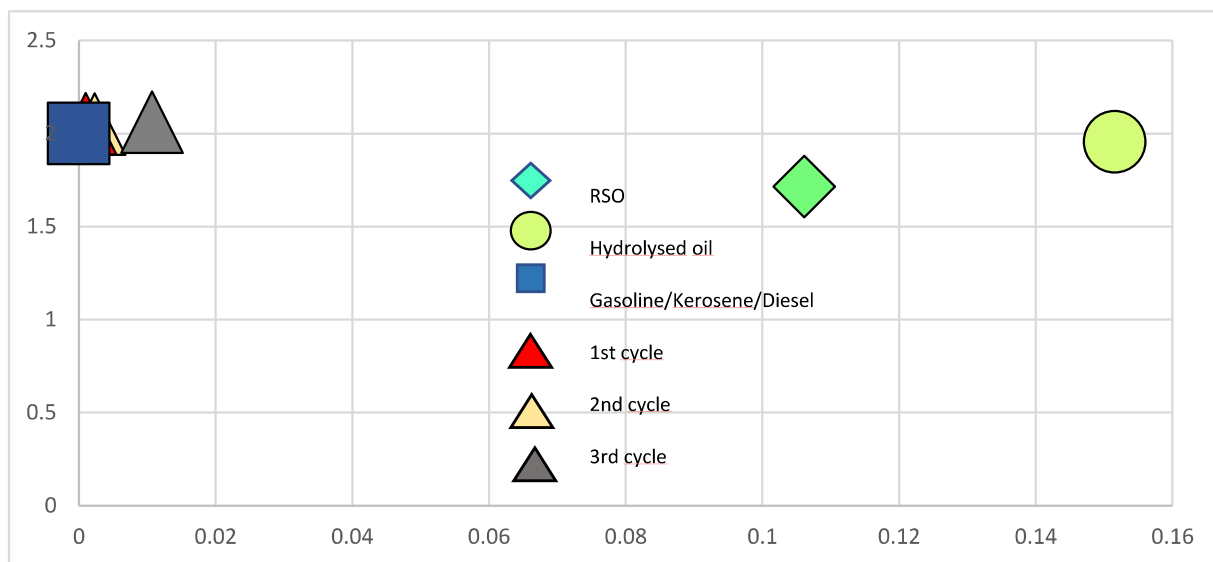


Figure 0.21: Liquid fuels characterisation from reusing Pt/C catalyst by H/C and O/C molar ratios in Van Krevelen diagram

The reusability of a 5 wt% Pt/C catalyst for the combined decarboxylation and cracking of hydrolysed rapeseed oil (RSO) at 450 °C was investigated in this study. Three consecutive reaction cycles were conducted, with each cycle involving the use of the same Pt/C catalyst. The mass balance closures for the reaction products over the three cycles were consistently around 87 wt%, with minor variations in the yields of solid, liquid, and gas products. The appearance of the oil products became slightly darker after each cycle. Gas composition analysis indicated a significant decrease in CO<sub>2</sub> volume from the first to the third cycle, suggesting reduced catalyst activity toward decarboxylation. The increased yields of hydrocarbon gases over subsequent cycles indicated a shift towards more dominant random cracking than decarboxylation. The physico-chemical properties of the liquid products, including density, acid content, elemental composition, and calorific value, changed with repeated use of the catalyst. The density and acid content of the oils increased, aligning with a reduction in the degree of deoxygenation by decarboxylation. Despite these changes, the oil products maintained better fuel properties than those obtained without the catalyst. The chemical composition analysis revealed a decrease in the yield of alkanes, an increase in oxygenated compounds, and a reduction in the selectivity towards decarboxylation with each subsequent cycle. The reusability potential of the Pt/C catalyst was found to be constrained by the build-up of carbon deposits after each cycle, leading to reduced catalytic activity. The results emphasise the challenges associated with catalyst deactivation and the importance of considering catalyst stability and regeneration in catalytic processes for the production of liquid fuels.



#### 6.4.4 Characterisation of the used Pt/C catalysts by x-ray diffraction (XRD) spectroscopy

The characterisation of the catalyst over three cycles using XRD is seen in Figure 6.22. The broad hump seen around  $26^\circ$  corresponds to the carbon support (Pandya et al., 2018), while that around  $39^\circ$  corresponds to the plane (111) of the face centred cubic(fcc) Pt lattice (Xiong and Manthiram, 2004; Xing et al., 2013). By applying the Scherrer equation, and the full width half maximum (FWHM), the crystallite sizes of the fresh catalyst, and reused are:  $64.7\text{\AA}$   $55.7\text{\AA}$ , and  $50.8\text{\AA}$  consecutively. Interestingly, two peaks appeared on the reused catalyst at around  $44^\circ$  and  $52^\circ$ , which grew in intensity with repeated reuse. These peaks could be due to the formation of graphitic carbons or due to the formation of new metal phases. Chowdhury et al. (2011) reported the XRD peaks of coke on used  $\text{Ni}/\text{Al}_2\text{O}_3$  catalyst surface at  $29.84^\circ$  and  $61.92^\circ$ , and when exposed to high temperatures. Although, the peaks observed in the reused catalyst were at different  $2\theta$  values, there was a strong possibility that these were graphitic carbon peaks due to the increased char formation. Also, no corresponding platinum metal phase was found in literature for these peaks.

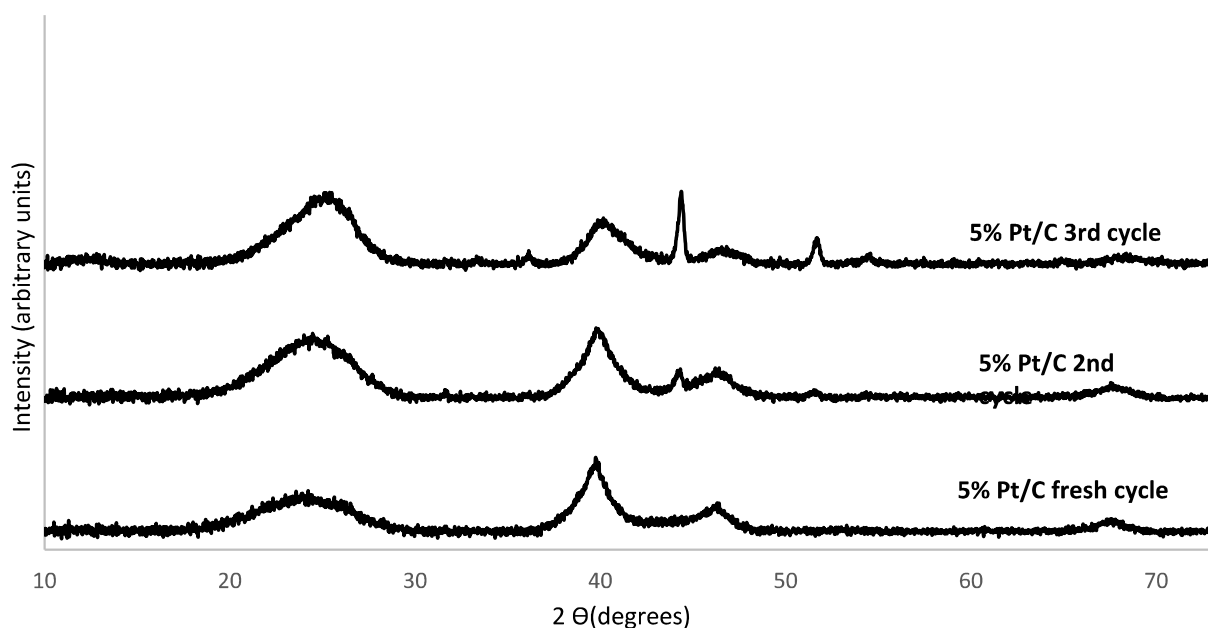


Figure 0.22: XRD diffractograms of fresh and spent Pt/C catalyst from the simultaneous decarboxylation and cracking of hydrolysed RSO

The diffraction peak associated with Pt (111) at  $2\theta$  value of  $39^\circ$  was visible in all cycles, and there was not much difference between the fresh and the reused catalysts except that the intensity decreased, which might be due to the accumulation of char produced from the

decarboxylation and cracking reactions. This also suggests the crystalline structure and therefore the catalyst function is impaired to a degree after each cycle. Hence, the decrease in yields reported in Section 6.4.3.2.

## 6.5 Simultaneous decarboxylation and cracking of hydrolysed waste cooking oils (WCOs)

### 6.5.1 Product yields and mass balance

Based on the results obtained from the simultaneous decarboxylation and cracking of RSO at 450 °C and 1 h which gave high degree of decarboxylation and extensive cracking, the products of hydrolysis of the two waste cooking oils (WCOs), were subjected to the same set reaction conditions. The mass balance closures shown in Table 6.12 for these experiments were approximately between 87 wt% and 88 wt%. The yields of oil products from the WCOs were similar to those from RSO, however, WCO-B generated much larger solid products. All the liquid products obtained were in light oils, with similar shades of yellow (Figure 6.23).

Table 6.12: Mass balance for reaction products from decarboxylation of hydrolysed WCOs at 450 °C for 1 h

Sample	Product			Balance (wt%)
	Solid (wt%)	Oil (wt%)	Gas phase (wt%)	
RSO	4.69	72.68	9.61	86.98
WCO-A	5.29	71.93	10.69	87.91
WCO-B	8.30	70.80	8.59	87.69

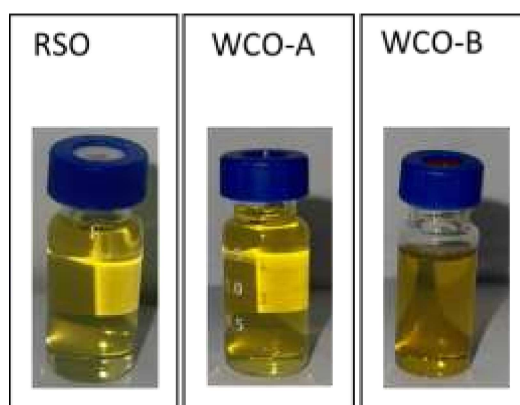


Figure 0.23: Appearance of liquid products from the simultaneous decarboxylation and cracking of hydrolysed vegetable oils

### 6.5.2 Gas composition

The gaseous products obtained from the decarboxylation of the hydrolysed WCO samples are presented in Figure 6.24. The yields of CO<sub>2</sub> obtained from WCO-A and WCO-B at optimum conditions were 1.3% more and 30.52% less than the CO<sub>2</sub> obtained from RSO. The RSO, WCO-A, and WCO-B samples produced 4.64 wt%, 5.60 wt%, and 4.16 wt% of hydrocarbon gases respectively. This implies WCO-A contained compounds that were even more susceptible to cracking than the fresh RSO. Even though WCO-A yielded the highest amount of CO<sub>2</sub>, it also produced the most hydrocarbon gases which resulted in this sample producing gases with the highest calorific content.

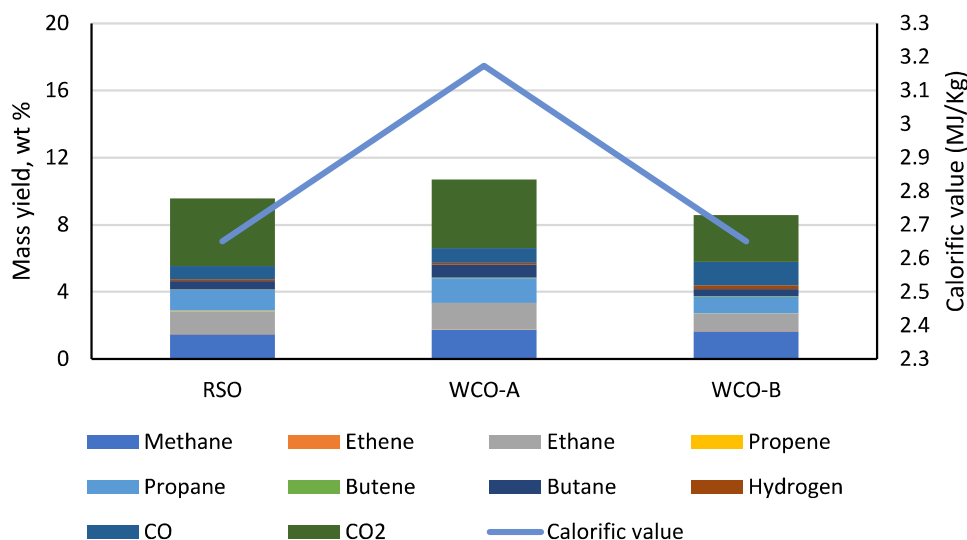


Figure 0.24: Mass yield, wt % of gases obtained from decarboxylation of hydrolysed WCOs at 450 °C for 1 h

Table 6.13 shows that acid contents of the oils derived from the WCOs were similar to or lower than that of the RSO-derived oil under the same set of reaction conditions. Hence, the results showed that the hydrolysis products (fatty acids) from the three samples of vegetable oils could be equally deoxygenated to the same extent via the decarboxylation. However, results showed that WCO-A had much lower acid contents, which may be linked to its higher reactivity after repeated use for cooking. The density of the oil from WCO-A was similar to that obtained from RSO, which corresponded to the similarity in compositions of the oil samples, confirming that WCO-B was mostly from used rapeseed oil (personal communication with kitchen staff). However, the oil products still had better fuel properties than the oil obtained with no catalyst in Table 6.2 above. Interestingly, according to the elemental analysis data, the oil products were composed of mainly of carbon and hydrogen, indicating their richness in hydrocarbon compounds. The elemental analysis with the CHNS analyser (Method 1) again threw up the challenge of inaccurate determination due to volatile losses. Hence, the GC/MS method (Method 2) was used to estimate the elemental composition, which aligned well with the other properties of the liquid products in terms of degree of decarboxylation and hydrocarbon contents. Hence, calorific values of the oils ranged from 46 MJ/kg to 51 MJ/kg, indicating high hydrocarbon contents similar to commercial fuels (Strömberg, 2006).

6.5.3 Characterisation of liquid products

6.5.3.1 Liquid product properties

Table 6.13: Physicochemical properties, density, acid content, elemental composition and calorific value obtained from using different feedstock sources

Elemental composition										
Sample	Main organic product	Density (kg/m <sup>3</sup> )	Acid content (%)	Method <sup>a</sup>	C (wt%)	H (wt%)	N (wt%)	S (wt%)	O (wt%)	HHV (MJ/kg)
RSO	Yellow light oil	828	2.34	1	81.38 ± 1.07	12.63 ± 0.02	0.19 ± 0.02	-	5.8 ± 0.12	44.71
				2	85.18	14.56	-	-	0.26	49.78
WCO-A	Yellow light oil	867	0.1	1	78.05 ± 0.29	13.46 ± 0.05	0.26 ± 0.00	-	8.23 ± 0.01	44.34
				2	82.93	14.94	-	-	-	50.95
WCO-B	Yellow light oil	823	1.68	1	77.67 ± 1.04	11.87 ± 0.20	0.28 ± 0.01	-	10.18 ± 0.07	41.57
				2	81.38	13.05	-	-	-	46.84

<sup>a</sup> Method 1: CHNS analyser; Method 2: Calculated from GC-MS analysis

### 6.5.3.2 Chemical composition of liquid products from the simultaneous decarboxylation and cracking of hydrolysed WCOs

Figure 6.25 shows that the set optimum reaction conditions were able to achieve complete conversion of the fatty acids obtained from the hydrolysed WCOs. Considering that all operating parameters were the same for both reactions, the difference in the yields of compound groups obtained will be due to the difference in the composition of the original vegetable oil feedstock. Indeed, Figure 6.25 shows that only alkanes and aromatic hydrocarbons were identified from the GC/MS analysis of the oil products. The absence of olefins and oxygenated compounds showed that the hydrolysed WCOs were similarly reacted as the hydrolysed RSO. However, WCO-B produced higher yields of aromatics and lower yields of alkanes compared to RSO and WCO-A. This result was a bit intriguing giving that WCO-B was mostly from rapeseed oil. However, the extent of use of the oil for cooking may be responsible for this. Degradation of vegetable oils occur during repeated heating and cooling when cooking and may lead to the formation of compounds that are more reactive than fresh oils (Warner, 1999).

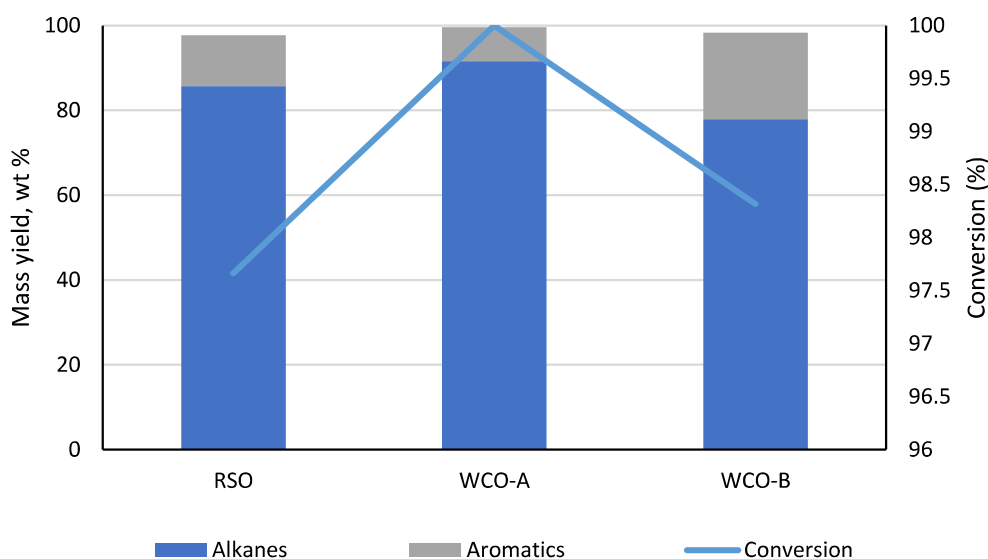


Figure 6.25: Mass yield, wt % of groups of hydrocarbon products obtained from decarboxylation of hydrolysed WCOs at 450 °C for 1 h

Just as stated in Section 6.5.3.2 above, the observed differences between both WCO samples presented in Figure 6.26 in the groups of compounds produced could be most likely due to the composition of the original vegetable oil feedstock. The <C11 hydrocarbons obtained from WCO-B (38.3 wt%), mirrored that from the fresh RSO. This similarity is also seen in the total yields of C11-16 and >C16 (approximately 67 wt%) with RSO and WCO-B

(66%). These similarities are consistent with the information obtained from the source kitchen WCO-B was collected from that they mainly used RSO (see Chapter 4, Section 4.2.7).

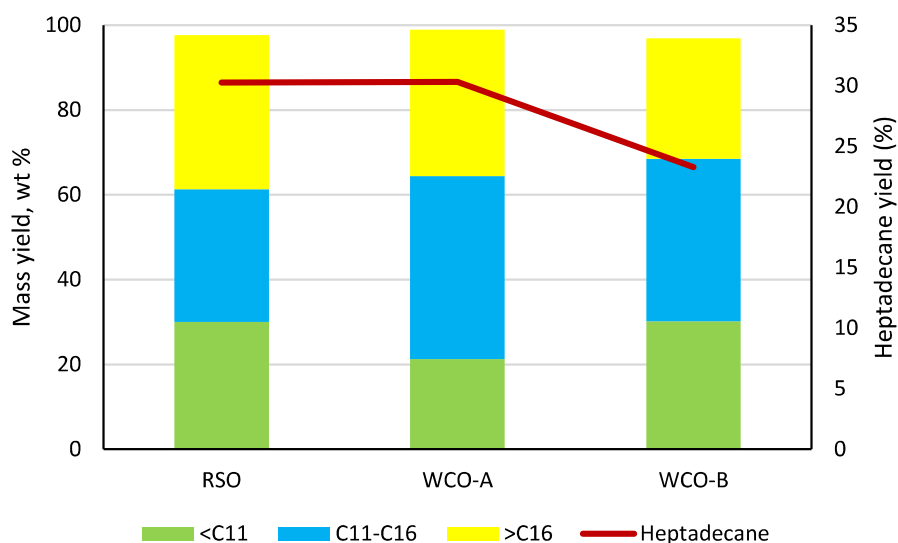


Figure 0.26: Mass yields of heptadecane and other hydrocarbon products obtained from simultaneous decarboxylation and cracking of hydrolysed WCOs at 450 °C for 1 h

However, it can be seen from Figure 6.26, that RSO produced 30% more heptadecane than WCO-B, which could be explained by the C18 fatty acid contents of both feedstocks. For instance, RSO contained only 5% more C18 fatty acids than WCO-B. A plausible explanation may be derived from the compositions of other classes of compounds found in the two oil products. Figure 6.25 shows that WCO-B produced nearly twice the yield of aromatic compounds compared to RSO. This may imply a shift from straight chain alkanes to aromatics in WCO-B, indicating that its fatty acids were more reactive in terms of cyclisation and aromatisation reactions. Such increased reactivity of WCO-B may therefore be attributed to its state before the hydrolysis stage. Oils are known to gradually denature during cooking from a variety of reactions between the oil molecules and extract chemicals from the food been cooked. Example reactions have been reported to include hydrolysis, oxidation and polymerisation (Warner, 1999). The list of compounds present in the different oils is presented in Table 6.14. Figure 6.21 presents the Van Krevelen diagram generated from the elemental compositions of the oils, comparing their H/C to O/C ratios. The figure shows an overlap of all three feedstock sources as they all yielded oil products with very low oxygen content and their very close proximity to the conventional fuels, gasoline, and kerosene show their comparable potential.

Table 6.14: List of compounds in the oil products obtained from combined decarboxylation and cracking of hydrolysed RSO for 1 h repeating catalyst

<b>Alkanes</b>	<b>Yield, wt %</b>		
	RSO	WCO-A	WCO-B
n-Hexane	-	1.17	0.70
Heptane	5.15	3.69	3.47
Heptane, 2,4-dimethyl-	-	-	4.99
Octane	6.28	4.24	
Nonane	6.58	4.45	5.70
Decane	6.09	4.48	5.41
Undecane	5.63	4.88	5.32
Dodecane	5.23	4.58	5.11
Tridecane	4.51	4.17	4.19
Dodecane, 2-methyl-	-	-	0.61
Tetradecane	3.93	3.23	3.31
Tetradecane, 4-methyl-	-	0.36	-
Tetradecane, 2-methyl-	-	0.65	0.91
Tetradecane, 3-methyl-	-	0.33	-
Pentadecane	6.07	20.90	9.48
Hexadecane	1.71	0.98	1.05
2,6,10-Trimethyltridecane	0.76	0.56	1.23
Tetradecane, 4-methyl-	-	-	0.75
Pentadecane, 4-methyl-	0.47	-	
Heptadecane	30.19	30.31	23.27
Hexadecane, 2-methyl-	1.14	0.87	1.26
Hexadecane, 4-methyl-	-	0.50	
Heptadecane, 2-methyl-	0.81	0.57	1.15
Heptadecane, 3-methyl-	0.50	-	-
Cyclopentane, undecyl-	-	0.31	-
Nonadecane	0.62	0.39	-
<b>Total</b>	<b>85.69</b>	<b>91.60</b>	<b>77.90</b>

<b>Aromatics</b>	<b>Yield, wt %</b>		
	1st cycle	2nd cycle	3rd cycle
Toluene	0.46	0.26	0.73
Benzene	-	0.15	-
Ethylbenzene	0.67	0.34	0.94
p-Xylene	1.36	-	-
o-Xylene	0.25	0.62	2.01
Benzene, (3,3-dimethylbutyl)-	-	-	0.43
Benzene, 1-ethyl-2-methyl-	1.51	0.88	2.34
Benzene, 1,2-diethyl-	-	0.24	-
Benzene, 1-methyl-2-propyl-	-	0.45	1.50
Indan, 1-methyl-	-	0.26	0.40
Benzene, 1-methyl-4-(1-methylpropyl)-	-	0.22	0.58
Benzene, 1-methyl-2-(2-propenyl)-	-	0.26	0.40
Benzene, 1-methyl-4-butyl	0.56	0.29	0.92
Benzene, propyl-	-	-	0.33
Benzene, n-butyl-	-	-	0.53



Benzene, 1,2-diethyl-	-	-	0.68
Benzene, (1-methyldecyl)-	2.41	-	-
Benzene, (1,1-dimethylnonyl)-	0.37	-	-
Naphthalene	0.39	0.26	0.79
Benzene, (1,3-dimethylbutyl)-	-	0.21	0.59
Naphthalene, 1-methyl-	0.31	0.23	1.40
1-Methyl-2-n-hexylbenzene	-	0.21	0.49
Benzene, 1-(1,5-dimethylhexyl)-4-methyl-	-	0.18	-
Benzene, (1,3-dimethylbutyl)-	-	0.24	-
Benzene, (1-methyldecyl)-	-	1.42	1.86
Benzene, undecyl-	0.35	0.19	-
Benzene, 1-methyl-2-propyl-	0.96	-	-
Benzene, 1-ethenyl-4-ethyl-	0.25	-	-
Benzene, 1,3-diethyl-	0.45	-	-
Benzene, (1-methylheptyl)-	0.29	-	0.37
Fluorene	-	-	0.32
9H-Fluorene, 9-methyl-	-	-	0.50
Benzene, (1,1-dimethylnonyl)-	-	-	0.62
Benzene, undecyl-	-	-	0.31
Benzene, (1,1-dimethylpropyl)-	0.40	-	-
1-Phenyl-1-butene	0.32	-	-
Benzene, (1,3-dimethylbutyl)-	0.37	-	-
1-Methyl-2-n-hexylbenzene	0.31	-	-
<b>Total</b>	<b>11.97</b>	<b>7.96</b>	<b>20.41</b>

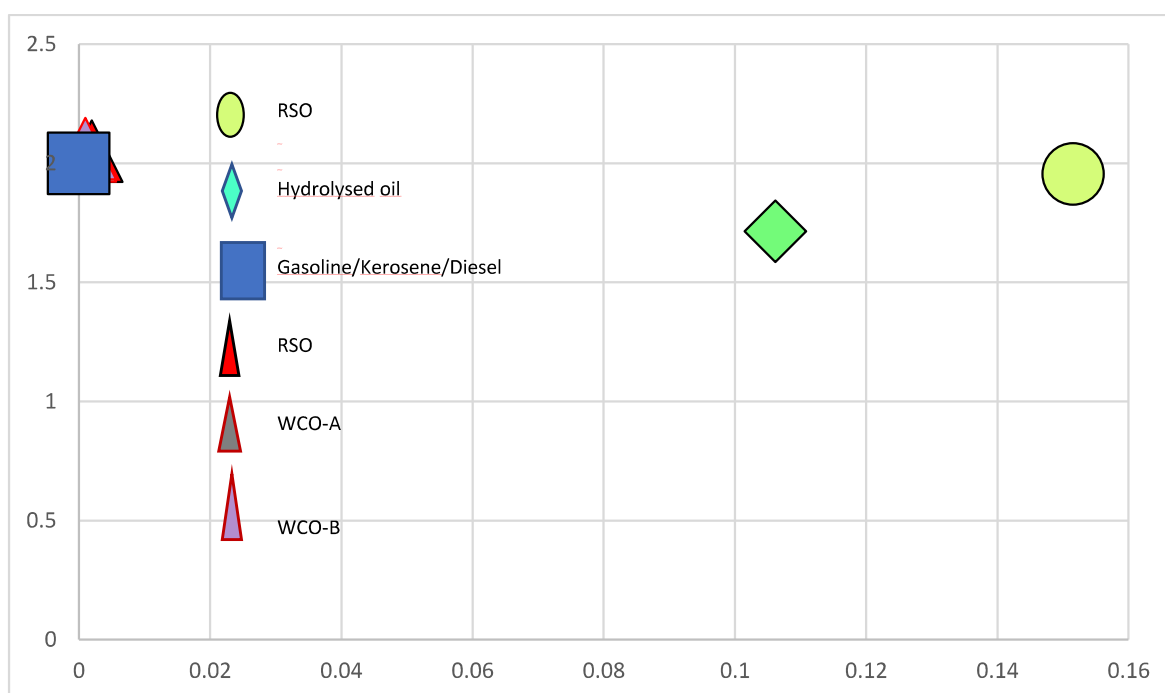


Figure 0.27: Liquid fuels characterisation from varying feedstock sources by H/C and O/C molar ratios in Van Krevelen diagram

Table 0.15: Summary table showing compiled results of decarboxylation and cracking experiments

Parameter	Dependent variables tested	Independent variables	Summary of main findings
Temperature	420 °C (no catalyst) 450 °C (no catalyst) 450 °C (with Pt/C)	Feed: 10 g oil Reaction time: 1 h Catalyst: 2 g	The mass balance closures for the experiments ranged between 83% and 91%, with lower closures at higher temperatures attributed to the loss of volatile shorter chain hydrocarbons (Table 6.1). The addition of 5 wt% Pt/C catalyst led to a 7.05% increase in oil yield at 450 °C compared to the non-catalysed reaction (Table 6.1). The colour change in oil products with catalyst addition suggested a reduction in higher molecular weight compounds (Fig 6.1). Gas composition analysis revealed that the Pt/C catalyst promoted both decarboxylation and cracking reactions, resulting in increased CO <sub>2</sub> yield and hydrocarbon gases (Fig 6.2). GC/MS analysis provided insights into the chemical composition of liquid products, showing increased conversion of fatty acids to hydrocarbons with temperature and catalyst addition (Fig 6.3). The presence of Pt/C facilitated deoxygenation, reduced acid content, and improved oil density. The yields of hydrocarbons, particularly heptadecane, increased with Pt/C, indicating the catalyst's selectivity towards decarboxylation (Fig 6.4). Considering the 97.7% conversion obtained, the study demonstrated the potential of Pt/C-catalysed reactions at 450 °C for producing alternative liquid hydrocarbon fuels.
Catalyst type	Pt/C Pt/MgSiO <sub>3</sub> Pt/Al <sub>2</sub> O <sub>3</sub>	Feed: 10 g oil Temperature: 450 °C	The study compared the performance of different catalysts in the decarboxylation of hydrolysed rapeseed oil at 450 °C. Mass balance showed Pt/Al <sub>2</sub> O <sub>3</sub> yielding the lowest closure at 81.5% and highest gas yield of 9.8%, potentially due to alumina's acidic nature. Pt/C produced the highest solid product, suggesting enhanced cracking and volatile compound losses. Gas and liquid

		<p>Reaction time: 1 h Catalyst: 2 g</p>	<p>product yields (Table 6.4) were comparable among catalysts, but Pt/C had the lightest-coloured oil (Fig 6.7). Gas composition analysis indicated differences in decarboxylation activity and selectivity among catalysts with Pt/C yielding the highest amount of CO<sub>2</sub> (Fig 6.8), which accounted for 42% of its gas product. Chemical composition analysis showed Pt/Al<sub>2</sub>O<sub>3</sub> produced oil with higher aromatics, making it closer to jet fuel requirements, Pt/MgSiO<sub>3</sub> exhibited relatively lower hydrogenation capability due to the presence of alkenes that was not found the oils produced from the other catalysts, and Pt/C achieved the highest degree of decarboxylation, with 97.7% conversion and producing oil with no oxygenates(Fig 6.9). Overall, Pt/C was identified as the most effective catalyst, potentially requiring further catalytic cracking for optimal jet fuel production.</p>
Time	0, 1, 2	<p>Feed: 10 g oil Temperature: 450 °C Catalyst: 2 g Pt/C</p>	<p>Pt/C exhibited optimal activity for simultaneous decarboxylation and cracking of hydrolysed rapeseed oil (RSO) at 450 °C, resulting in nearly 100% hydrocarbon liquid yield within a 1 h reaction time. Therefore, further tests were carried out to examine the influence of reducing and increasing reaction time. Increasing the reaction time from 0 to 2 h led to a decline in mass balance closures by 8.2%, attributed to the loss of shorter-chain hydrocarbons as volatiles (Table 6.7) but lighter coloured oils were produced with increased reaction severity (Fig 6.12). Gas composition analysis indicated enhanced CO<sub>2</sub> production and increased yields of C<sub>1</sub>–C<sub>4</sub> hydrocarbon gases and hydrogen with extended reaction time, resulting in higher calorific values from 0.99 MJ/kg to 5.13 MJ/kg (Fig 6.13). GC/MS analysis of the oils revealed a shift from alkenes and oxygenated compounds at 0 h to alkanes and aromatics at 1 h and beyond. Increasing reaction severity promoted hydrogenation, leading to higher yields of saturated hydrocarbons even though there was a plateau in conversion after 1 h (Fig 6.14). The</p>

			hydrocarbon distribution in the oil product could be tuned by adjusting the reaction time, with 1 h providing a balanced distribution of gasoline, jet fuel, and diesel range hydrocarbons, while 2 h favored higher gasoline and jet fuel yields (Fig 6.15). Therefore, this study demonstrated the tunability of fuel composition by adjusting reaction time during simultaneous decarboxylation and cracking using Pt/C as a catalyst.
Catalyst reusability	First cycle Second cycle Third cycle	Feed: 10 g oil Reaction time: 1 h Temperature: 450 °C Catalyst: 2 g Pt/C	<p>This set of tests, reaffirms the effectiveness of 5 wt% Pt/C catalyst for the simultaneous decarboxylation and cracking of hydrolysed rapeseed oil (RSO). The results confirmed the catalyst's superiority in achieving near-total decarboxylation and extensive cracking, producing light-coloured oils with favourable distributions across commercial fuel ranges. The experiments explored the catalyst's stability over three repeated cycles, revealing consistent mass balance closures around 87 wt% (Table 6.9) but the colour of the oils got darker after each cycle, and this pre-analysis suggested a decrease in catalyst activity, possibly due to coke deposition, impurities, or pore blockage. The reduced yield of CO<sub>2</sub> by 66.6% from the first to the third cycle also supported the notion of a decline in the activity of the catalyst (Fig 6.18). The chemical composition of the oils also revealed a similar trend with an 8.2% decrease in conversion by the third cycle as well as an increase in alkene and oxygenate contents(Fig 6.19). Overall, the study highlighted constraints on the reusability potential of the Pt/C catalyst, emphasizing the challenge of catalyst deactivation over multiple cycles and the need for strategies to address this limitation for sustained and economically viable processes.</p>
Feed source		Feed: 10 g oil Reaction time: 1 h	The investigation into simultaneous decarboxylation and cracking of hydrolysed rapeseed oil (RSO) at 450 °C and 1 h demonstrated significant success in achieving high degrees of

	<p>RSO WCO-A WCO-B</p>	<p>Temperature: 450 °C Catalyst: 2 g Pt/C</p>	<p>decarboxylation and extensive cracking, producing light-coloured oils across various feedstock sources (Fig 6.23). The mass balance closures for the reaction products from decarboxylation of hydrolysed waste cooking oils (WCOs), particularly WCO-A and WCO-B, were consistently around 87–88 wt% (Table 6.12). Gas composition analysis indicated variations in CO<sub>2</sub> and hydrocarbon gas yields among the different feedstocks, with WCO-A exhibiting higher reactivity and producing gases with the highest calorific content (Figure 6.24). The chemical composition of liquid products from hydrolysed WCOs, as depicted in Figure 6.25 and Figure 6.26, revealed distinct yields of alkanes, aromatics, and other hydrocarbon groups, providing insights into the reactivity and composition of different feedstocks during the process. The study emphasized the potential of hydrolysed waste cooking oils as viable feedstocks for the production of high-quality liquid fuels, despite variations in composition and reactivity arising from cooking-related degradation.</p>
--	--------------------------------	---	---

In summary, tests were carried out on the decarboxylation and cracking of fatty acids to hydrocarbons varying temperature, time, and Pt-based catalyst types (Table 6.15). Even though there was an increase in conversion as time of reaction increased, the minimal increase as well as the decrease in aromatics suggested that running reaction at 1 h was more beneficial than at 2 h. Analysis were carried out using GC/MS, CHNS, and titration to quantify as well as to understand the compositions of the oil products. The effect of the catalyst was emphasised when the acid yield of the non-catalysed reaction was almost 10 folds more than that carried out in the presence of Pt/C. The other catalysts, Pt/MgSiO<sub>3</sub> and Pt/Al<sub>2</sub>O<sub>3</sub> also showed great potential with high conversions, however, Pt/C produced oil with the highest degree of decarboxylation. Therefore, the optimum reaction conditions found to achieve nearly complete decarboxylation were 450 °C for 1 h with 2 g of Pt/C as catalyst. This set of operating conditions were applied to WCOs, and their relatively high conversion and hydrocarbon compositions proved that the process can also be applied to real world samples.

## 6.6 References

- Ahmadi, M., Nambo, A., Jasinski, J. B., Ratnasamy, P., and Carreon, M. A. (2015). Decarboxylation of oleic acid over Pt catalysts supported on small-pore zeolites and hydrotalcite. *Catalysis Science and Technology*, 5(1), 380–388. <https://doi.org/10.1039/c4cy00661e>.
- Ali, S. A., Alshareef, A. H., Theravalappil, R., Alasiri, H. S., and Hossain, M. M. (2022). Molecular Kinetic Modeling of Catalytic Naphtha Reforming: A Review of Complexities and Solutions. *Catalysis Reviews*, 1–54. <https://doi.org/10.1080/01614940.2021.2008622>.
- Chowdhury, M.B.I., Hossain, M.M. and Charpentier, P.A. (2011) “Effect of supercritical water gasification treatment on Ni/La<sub>2</sub>O<sub>3</sub>-Al<sub>2</sub>O<sub>3</sub>-based catalysts,” *Applied Catalysis A: General*, 405(1-2), pp. 84–92. Available at: <https://doi.org/10.1016/j.apcata.2011.07.031>.
- Fu, J., Lu, X. and Savage, P.E. (2011) “Hydrothermal decarboxylation and hydrogenation of fatty acids over PT/C,” *ChemSusChem*, 4(4), pp. 481–486. Available at: <https://doi.org/10.1002/cssc.201000370>.
- Fuel gases - heating values Engineering ToolBox. Available at: [https://www.engineeringtoolbox.com/heating-values-fuel-gases-d\\_823.html](https://www.engineeringtoolbox.com/heating-values-fuel-gases-d_823.html).
- Fuels - densities and specific volumes Engineering ToolBox. Available at: [https://www.engineeringtoolbox.com/fuels-densities-specific-volumes-d\\_166.html](https://www.engineeringtoolbox.com/fuels-densities-specific-volumes-d_166.html).
- Fuels - higher and lower calorific values Engineering ToolBox. Available at: [https://www.engineeringtoolbox.com/fuels-higher-calorific-values-d\\_169.html](https://www.engineeringtoolbox.com/fuels-higher-calorific-values-d_169.html).
- Lestari, S., Simakova, I., Tokarev, A., Mäki-Arvela, P., Eränen, K., and Murzin, D. Y. (2008). Synthesis of Biodiesel via Deoxygenation of Stearic Acid over Supported Pd/C Catalyst. *Catalysis Letters*, 122(3-4), 247–251. <https://doi.org/10.1007/s10562-008-9457-x>.
- Pandya, R., Mane, R. and Rode, C.V. (2018) “Cascade dehydrative amination of glycerol to oxazoline,” *Catalysis Science and Technology*, 8(11), pp. 2954–2965. Available at: <https://doi.org/10.1039/c8cy00185e>.
- Rasmussen, K.D. et al. (2019) “Platinum demand and potential bottlenecks in the global green transition: A dynamic material flow analysis,” *Environmental Science and Technology*, 53(19), pp. 11541–11551. Available at: <https://doi.org/10.1021/acs.est.9b01912>.
- Sadeghbeigi, R. (2012) “Fluid catalytic cracking handbook.” Available at: <https://doi.org/10.1016/c2010-0-67291-9>.

- Santillan-Jimenez, E. and Crocker, M. (2012) "Catalytic deoxygenation of fatty acids and their derivatives to hydrocarbon fuels via decarboxylation/decarbonylation," *Journal of Chemical Technology and Biotechnology*, 87(8), pp. 1041–1050. Available at: <https://doi.org/10.1002/jctb.3775>.
- Simakova, I., Simakova, O., Mäki-Arvela, P., Simakov, A., Estrada, M., and Murzin, D. Y. (2009). Deoxygenation of palmitic and stearic acid over supported Pd catalysts: Effect of metal dispersion. *Applied Catalysis A: General*, 355(1-2), 100–108. <https://doi.org/10.1016/j.apcata.2008.12.001>.
- Simakova, I., Simakova, O., Mäki-Arvela, P., and Murzin, D. Y. (2010). Decarboxylation of fatty acids over Pd supported on mesoporous carbon. *Catalysis Today*, 150(1-2), 28–31. <https://doi.org/10.1016/j.cattod.2009.07.064>.
- Strömberg, B. (2006) *Fuel Handbook*. Stockholm: VÄRMEFORSK.
- Warner, K. (1999) "Impact of high-temperature food processing on fats and oils," *Advances in Experimental Medicine and Biology*, pp. 67–77. Available at: [https://doi.org/10.1007/978-1-4615-4853-9\\_5](https://doi.org/10.1007/978-1-4615-4853-9_5).
- Xing, X., Zhang, G., Rogers, H., Zulli, P., and Ostrovski, O. (2013). Effects of Annealing on Microstructure and Microstrength of Metallurgical Coke. *Metallurgical and Materials Transactions B*, 45(1), 106–112. <https://doi.org/10.1007/s11663-013-0002-y>.
- Xiong, L. and Manthiram, A. (2004) "Influence of atomic ordering on the electrocatalytic activity of Pt–Co alloys in alkaline electrolyte and proton exchange membrane fuel cells," *J. Mater. Chem.*, 14(9), pp. 1454–1460. Available at: <https://doi.org/10.1039/b400968c>.
- Yang, L., Tate, K. L., Jasinski, J. B., and Carreon, M. A. (2015). Decarboxylation of Oleic Acid to Heptadecane over Pt Supported on Zeolite 5A Beads. *ACS Catalysis*, 5(11), 6497–6502. <https://doi.org/10.1021/acscatal.5b01913>.
- Zhang, C., Kwak, G., Park, H.-G., Jun, K.-W., Lee, Y.-J., Kang, S. C., and Kim, S. (2019). Light hydrocarbons to BTEX aromatics over hierarchical HZSM-5: Effects of alkali treatment on catalytic performance. *Microporous and Mesoporous Materials*, 276, 292–301. <https://doi.org/10.1016/j.micromeso.2018.10.005>.



## 7 Cracking

Cracking reactions are widely used in the petrochemical industry to convert or breakdown heavy oils with higher boiling points into light and valuable products with the right chemical compositions. This can be achieved thermally or catalytically but catalytic cracking is better adapted for selective processes with specific target products, and also helps to minimise the energy consumed during reaction by using lower reaction temperatures. Similarly, to the reactions carried out in Sections 5 and 6, the catalytic cracking experiments were also carried out without any additional hydrogen, adding to the novelty of this research project. Nearly complete deoxygenation (>97 %) of the hydrolysed RSO was achieved in the previous stage. This stage was designed to focus on the selective yields of the hydrocarbons, especially to improve the yields of aromatic hydrocarbons. Light aromatic hydrocarbons such as benzene, toluene, ethylbenzene and xylene (BTEX) are present at certain quantities in fossil gasoline and jet fuels. Moreover, they are also useful chemicals for industry and therefore can be isolated and used as raw materials or building blocks to produce other chemicals (de Jong and Gosselink, 2014). Therefore, producing 'green' BTEX from renewable lipids offers a route to sustainable organic chemical products. There are various factors that influence the degree of catalytic cracking of hydrocarbons, which include catalyst type, reaction time and reaction temperature. These parameters have been investigated in this Chapter to determine reaction conditions with the optimum potential to obtain the composition and yields of the target oil product. As discussed in Chapter 6, the elemental compositions all the oil products were determined using the GC/MS method (Method 2), which gave more accurate data than the standard CHNS analyser due to the presence of highly volatile components. All data obtained have been reported to 2 decimal places. The experimental method followed for these tests has been discussed in Chapter 3, Section 3.2.2, and Figure 7.1 shows a detailed schematic of the procedure.

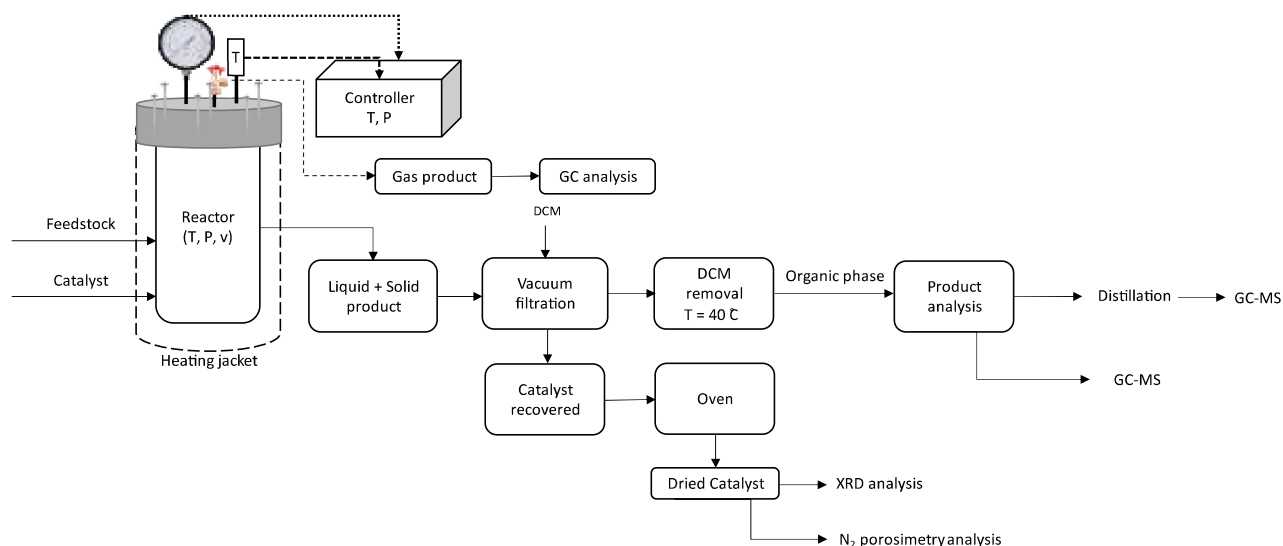


Figure 7.1: Schematic of procedure used for catalytic cracking experiments

## 7.1 Selection of optimum condition for preparation of feedstock for cracking

The results obtained from reactions performed at 400 °C and 450 °C in Chapter 6 were quite similar in terms of conversion, 97.9% and 97.7% respectively, as well as appearance and chemical compositions of both gas and liquid products. These experiments also produced substantial amounts of compounds up to C17. These results are in consideration as either one is to be used as the feedstock for the reactions that will be carried out in this chapter. Therefore, a combination of these factors; time, temperature, and energy balance were used to determine the optimum condition. The idea is to prioritise the oil that was produced with higher energy efficiency. Efficiency is known as the ratio of output to input, and in this case, the output is the total heat energy, depicted as  $Q_{\text{total}}$ .  $Q_{\text{total}}$  is an addition of the heat energy of all thermally conductive components involved in the reaction such as, the reactor, the oil, that is the feedstock, and the gas which was used to pressurise the reactor. While the input is the electrical energy turned into heat energy used to heat up the system, which is depicted as  $E$ . This  $E$  took into consideration the amount of energy generated by the heater to heat up the reaction to its set point ( $E_o$ ), and then to hold the reaction at that set temperature ( $E_{\text{st}}$ ) depending on the reaction condition.

$$Q = m C \Delta T \quad (7.1)$$

Where

$Q$  = heat energy (J)

$$m = \text{mass (Kg)}$$

$$C_p = \text{specific heat capacity (J kg}^{-1}\text{°C}^{-1}\text{)}$$

$$C_p \text{ of the reactor, stainless steel} = 460 \text{ J kg}^{-1} \text{°C}^{-1} \text{ (Hagmann \& Richards, 1995)}$$

$$C_p \text{ of the oil, Rapeseed oil} = 1.833 \text{ J kg}^{-1} \text{°C}^{-1} \text{ (Santos et al., 2005)}$$

$$C_p \text{ of Nitrogen} = 1.04 \text{ J kg}^{-1} \text{°C}^{-1} \text{ (NIST Office of Data and Informatics)}$$

$$\Delta T = \text{change in temperature (°C)}$$

$$E = P \Delta t$$

(7.2)

$$E_{total} = E_o + E_{st}$$

(7.3)

Where

$$E = \text{energy (J)}$$

$$P = \text{heater power (W)}$$

$$\Delta t = \text{change in time (s)}$$

$$E_o = \text{energy to heat up reactor}$$

$$E_{st} = \text{energy for reaction at set temperature}$$

$$E_{total} = \text{energy for total reaction}$$

$$H_{eff} = \frac{Q_{total}}{E_{total}}$$

(7.4)

Where

$$H_{eff} = \text{Heating efficiency}$$

$$Q_{total} = Q_{oil} + Q_{reactor} + Q_{nitrogen}$$

(7.5)

Table 7.1: Energy efficiency optimisation for cracking feedstock

	Reaction: 400 °C, 2 h	Reaction: 450 °C, 1 h
$Q_{\text{reactor}}$	0.269 MJ = 0.075 KWh	0.306 MJ = 0.085 KWh
$Q_{\text{total}}$	0.277 MJ = 0.077 KWh	0.313 MJ = 0.087 KWh
$E_o$	0.76 MJ = 0.021 KWh	0.84 MJ = 0.027 KWh
$E_{\text{st}}$	5.04 MJ = 1.4 KWh	2.52 MJ = 0.7 KWh
$E_{\text{total}}$	5.8 MJ = 1.61 KWh	3.36 MJ = 0.97 KWh
$H_{\text{eff}}$	47.83%	89.7%

After energy balance calculations (Table 7.1) using Equations 7.1 – 7.5, there is an 87.54% increase in energy efficiency at 400 °C for 2 h when compared with the reaction at 450 °C for 1 h. Therefore, 450 °C 1 h was prioritised as the optimum reaction condition and used as the set operating condition used to obtain the batch of decarboxylated hydrolysed RSO used for the catalytic cracking tests in this section.

## 7.2 Characteristics of the fresh catalysts used for cracking of decarboxylated oil from RSO.

The surface areas, pore volumes and pore diameters of the fresh catalysts used in the cracking process described in Chapter 3 are presented in Table 7.2.

Table 7.2: Some properties of the catalysts used in the cracking reactions

Catalyst	Surface area (m <sup>2</sup> g <sup>-1</sup> )	Pore volume (cc/g)	Pore diameter (nm)
ZSM-5	306.98	0.19	3.89
Zeolite Y	534.91	0.19	3.83
MCM-41	627.26	0.24	3.43
Ru/Al <sub>2</sub> O <sub>3</sub>	154.92	0.4	8.11

The highest surface area of 627.26 m<sup>2</sup> g<sup>-1</sup> was observed for MCM-41, while Ru/Al<sub>2</sub>O<sub>3</sub> had the lowest surface area of 154.92 m<sup>2</sup> g<sup>-1</sup>. Even though the three zeolite type catalysts used; ZSM-5, Zeolite Y, and MCM-41, had relatively similar pore volumes and pore diameters, their surface areas and XRD patterns were substantially different, which may affect their catalytic activities during the cracking reactions.

### 7.3 Effect of reaction temperature with and without catalyst

This section presents the results from varying temperature on the cracking of hydrocarbons. As stated earlier, these cracking reactions are endothermic, and are influenced by reaction temperatures and catalyst types. In this work, the cracking reactions were carried out for 1 h at 400 °C and 450 °C, respectively, with and without a catalyst. When required, 1 g of ZSM-5 was used as catalyst and reacted with 10 g of decarboxylated oils obtained at 450 °C for 1 h. The zeolite catalyst, ZSM-5 was chosen for these tests as it is commonly used in petrochemical industry for cracking of long-chain hydrocarbons, and it is also known to give high conversion rates.

#### 7.3.1 Product yields and mass balance

Table 7.3 presents the mass balance closures obtained from cracking reactions with and without ZSM-5 (1 g) at 400 °C and 450 °C, respectively for 1 h reaction time. Lower mass balance closures were obtained in the presence of the catalyst compared to the non-catalytic reactions, due to the loss of volatile components during product handling. As shown in Table 7.3, the increase in temperature and the use of the catalyst led to increase in gas products as well as solid products, with corresponding reduction in the yields of oil products. Without ZSM-5 catalyst, the increase in temperature led to an approximately three-fold increase in gas yield and an 5.18% decrease in oil yield, indicating that the loss in oil yield could be due to the formation of gases. Indeed, no solid products were formed when the reactions were carried out without catalyst. A similar observation was reported by Isa et al. (2016) when they carried out cracking of pyrolysis oil without catalysts. Therefore, the lower mass balance closure obtained at 450 °C compared to 400 °C from the non-catalytic tests, also indicate that the oil obtained at 450 °C contained more volatile components due to thermal cracking. With ZSM-5, 1.98 wt% of solid was formed at 400 °C, and this increased dramatically to 8.10 wt% when the cracking was carried out at 450 °C. Hence, between 400 °C and 450 °C, gas yield increased by 75%, while solid yield increased by 56% in the presence of the catalyst. In their work, Rahimi and Karimzadeh (2011) reported that the use of ZSM-5 also produced significant yields of gas due to the conversion of the liquid phase. Zeolites are known to promote C-C bond cleavage in hydrocarbons often resulting in high yields of gas phase products. In all four tests, liquid product remained dominant, and all these were light oils but with dark colours (Figure 7.2).

Table 7.3: Mass balance for reaction products from cracking of hydrocarbons for 1 h at different temperatures

Temperature (°C)	Catalyst	Solid (wt%)	Oil product (wt%)	Gas (wt%)	Balance (wt%)
400	-	0.00	97.70	0.44	98.14
450	-	0.00	92.64	1.70	94.31
400**	ZSM-5	1.98	82.55	2.59	87.18
450**	ZSM-5	8.10	67.30	6.00	81.37

\*\* indicates reactions carried out with catalyst, ZSM-5

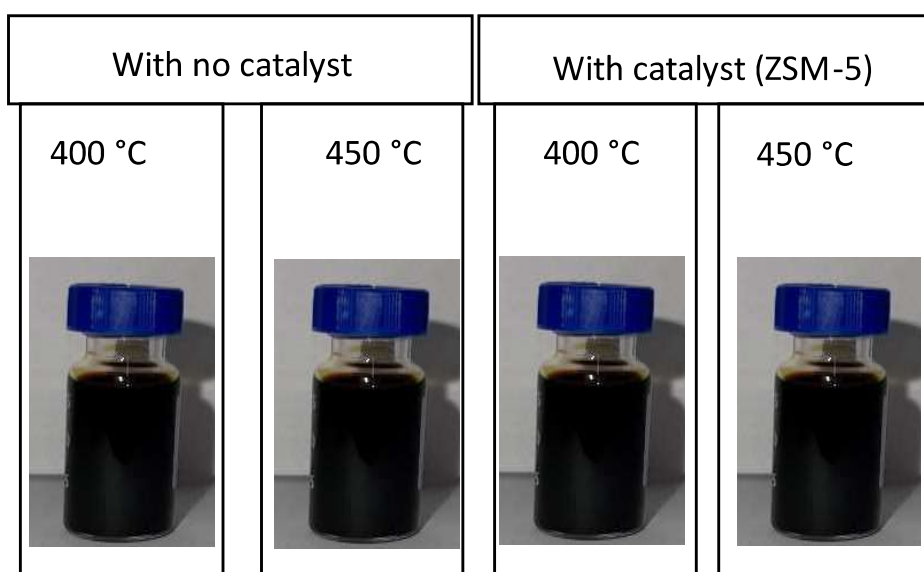


Figure 7.2: Appearance of oil products from catalytic and non-catalytic cracking of decarboxylated oil at different temperatures

### 7.3.2 Composition of gas products

Figure 7.3 shows that the composition of gas products follow the same trend at both temperatures for the catalytic and non-catalytic tests. However, the use of ZSM-5 influenced the formation of hydrocarbon gases, particularly C3 – C4 including propene, propane, butane and butene, which together accounted for at least 82% of total gas yields at both temperatures. Hence, the increased yields of these gas components in the presence of ZSM-5 implied that the effect of the catalyst was superior to the effect of temperature increase in these tests. For instance, between the catalytic and non-catalytic reactions at 400 °C, propane yield was 0.086 wt% without catalyst but increased by over fifteen folds in the presence of ZSM-5. Also, for the experiments at 450 °C, propane yield was only 0.28 wt% without the catalyst but increased by approximately eleven folds with ZSM-5. The increase in

the yields of the hydrocarbon gases in the presence of the catalyst influenced the increase in the calorific values of the gas products, which can be used for process energy.

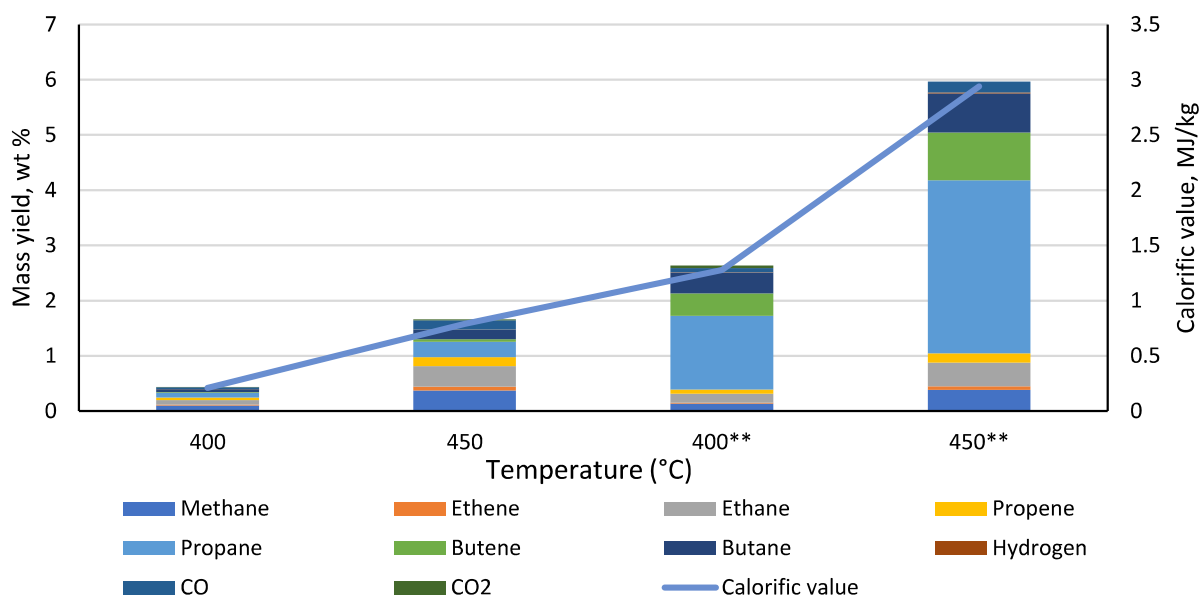


Figure 7.3: Mass yield % of gases obtained from cracking of decarboxylated oil for 1 h at different temperatures (\*\* indicates reactions carried out with catalyst, ZSM-5)

### 7.3.3. Characteristics of liquid products in relation to cracking temperature and catalyst

#### 7.3.3.1 Physico-chemical properties of liquid products

Table 7.4: Colour, elemental composition and calorific value of oil products in relation to cracking temperature

Temperature (°C)	Catalyst	Main organic product	C (wt%)	H (wt%)	N (wt%)	S (wt%)	O (wt%)	HHV (MJ/Kg)
400	-	Dark light oil	85.98	14.02	nd	nd	nd	49.32
450	-	Dark light oil	85.96	14.04	nd	nd	nd	49.34
400**	ZSM-5	Dark light oil	88.46	11.54	0.09	nd	nd	46.58
450**	ZSM-5	Dark light oil	90.90	9.070	0.10	nd	nd	43.83

\*\* indicates reactions carried out with catalyst, ZSM-5; nd = not detected

Table 7.4 shows the result of the elemental analysis of the oil products obtained in relation to cracking temperature using the GC/MS method (Method 2) temperature. Initial results from GC/MS analysis of the oils confirmed that they contained high proportions of lighter hydrocarbons, which will be discussed in detail in Section 7.3.3.2. The use of the GC/MS method for elemental composition determination was even more critical for the work reported

in this chapter due to their obvious volatile nature, leading to massive inaccuracies from the standard CHNS analyser (Method 1). The calorific values of the oils decreased with the introduction of ZSM-5, which was possibly due to cracking and hence, the production of lighter compounds. Overall, the calorific values indicated that the oils had fuel properties as with the range of conventional gasoline, kerosene and diesel fuels (Staffell, 2011). The oils also had similar odour as these fuels.

### 7.3.3.2 Chemical compositions of liquid products

#### 7.3.3.2.1 Composition of oil products by compound groups

Figure 7.4 shows the yields of compound groups the oil products derived from the cracking of decarboxylated oils from RSO with and without ZSM-5 catalyst. Unlike the decarboxylation and combined decarboxylation and cracking attempted in Chapter 5 and Chapter 6, respectively, alkanes and aromatics were the only two groups of compounds identified and quantified in these oils after the cracking process by the GC/MS. Indeed, both the catalytic and non-catalytic reactions produced the same two types of compound groups. The lower percentage yields of the oil products from the catalytic tests were simply due to volatile losses during analysis rather than the actual yields. Compared to decarboxylated oil feedstocks, the non-catalytic cracking at 400 °C, produced similar yields of oil but with 66.2% increase in aromatic compounds. Essentially the aromatic content of the oil increased from 12.3% in the decarboxylated oil to 20.4% in the oil obtained at 400 °C and then slightly to 19.4% at 450 °C, which are close to the 25% aromatic content in conventional jet fuel. However, the types of aromatic compounds present will be important for combustion efficiency, engine performance and emission of pollutants (Tree and Svensson, 2007; Abu-Jrai et al., 2009; Reijnders et al., 2016). The aromatic compositions of these oils are discussed in Section 7.3.3.2.2.

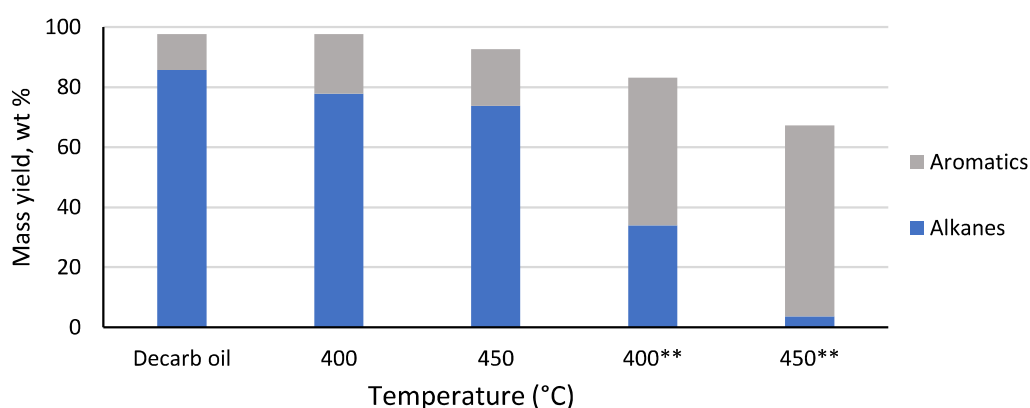




Figure 7.4: Mass yields of groups of compounds obtained from catalytic and non-catalytic cracking of decarboxylated oil for 1 h at different temperatures (\*\* indicates reactions carried out with catalyst, ZSM-5)

The non-catalytic test at 450 °C gave a similar aromatic content compared to the results from the corresponding reaction at 400 °C; so that in both non-catalytic tests, alkanes remained dominant. However, in the presence of ZSM-S at 400 °C, a dramatic increase in aromatic content was observed, so that the aromatic hydrocarbons became the dominant compounds in the oil, with 49 wt% yield compared to nearly 34 wt% of alkanes (aromatics to alkanes ratio of 1.45 or aromatic content of 59%). When the catalytic reaction was carried out at 450 °C, a much more dramatic increase in aromatic yields occurred, reaching 63.6 wt% compared to only 3.67 wt% of alkanes were identified and quantified (aromatics to alkanes ratio of 9.97; aromatic content of 94.5%). Clearly, the use of ZSM-5 favoured aromatisation reactions (Pan et al., 2022; Qian et al., 2022; Yuan et al., 2023; Zhang et al., 2023) and even more so at the higher temperature. Comparing the product profiles from the catalytic and non-catalytic tests, showed that the catalyst obviously had more influence than temperature in product distribution. However, there was also a strong synergy between the effects of both temperature and catalyst as evidenced by the differences between the product profiles from the catalytic tests. By increasing the temperature from 400 °C to 450 °C, the aromatics to alkanes ratio increased by a factor of 7.

According to Maher and Bressler (2007), during the direct non-catalytic cracking of vegetable oils, a liquid phase was produced comprising of oxygenated compounds as well as aromatic and aliphatic hydrocarbons. Recently, Buzetzki et al. (2011) carried out direct catalytic cracking of rapeseed oil (RSO) with a zeolite catalyst at temperatures between 350 and 440 °C and obtained average yields of liquid condensate of 87.5 wt%, which still contained a variety of oxygenated compounds. These authors found that oxygenated compounds (stearic acid, oleic acid, lauric acid, butyric acid) were the dominant organics the liquid phase product. Hence, the staged conversion used in this present study was successful in generating a final oil product with 100% hydrocarbon content.

### 7.3.3.2.2 Compositions of oil products in relation to reaction temperatures and catalysts

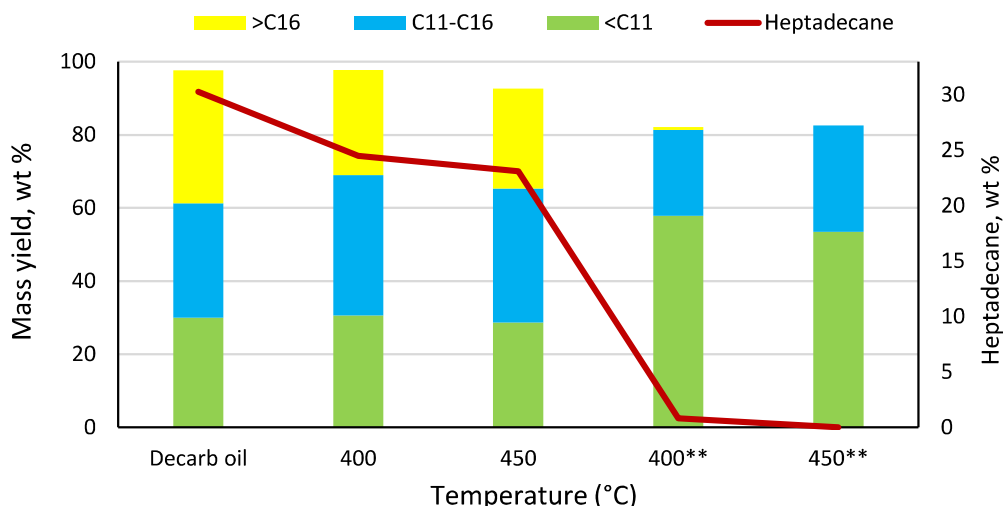


Figure 7.5: Mass yields of heptadecane and other hydrocarbons (aliphatics and aromatics) in the oil products obtained from cracking of decarboxylated oil for 1 h at different temperatures (\*\* indicates reactions carried out with catalyst, ZSM-5)

Figure 7.5 shows the yields of heptadecane (the dominant alkane from the decarboxylation of hydrolysed RSO) and the different fractions of the oils obtained during the cracking reaction with and without ZSM-5 at 400 °C and 450 °C. The hydrocarbons have been grouped according to the carbon numbers, with >C11 representing gasoline range, C12 – C16 representing kerosene range and >C16 for diesel range compounds. The oil products from the non-catalytic tests contained similar yields of gasoline range compared to the decarboxylated oil, but there was a noticeable increase in the kerosene and decrease in diesel range compounds, respectively over the two temperatures. Noticeably, however, the presence of ZSM-5 led to a 97.4 % decrease in >C16 hydrocarbons and 96.8% decrease in heptadecane yield when cracking at 400 °C when compared to the decarboxylated RSO. Indeed, at 450 °C, there was a complete loss of heptadecane and other diesel range compounds, so that the oil product contained only gasoline and kerosene compounds. Interestingly, the cracking at 450 °C produced 23.3% more kerosene range compounds than the corresponding reaction at 400 °C, which possibly the cracked >C16 fraction. Table 7.5 shows the list of compounds that make up the aliphatic and aromatic groups reported in Figures 7.4 and 7.5. The table highlights the presence of branched alkanes and isomers of some aromatic compounds. The compositional data of the oils showed that the reaction with ZSM-5 at 400 °C, produced the lowest yield (24.76 wt%) of <C<sub>11</sub> alkanes, with using the same catalyst at 450 °C produced the lowest yield (3.67 wt%) of this carbon number range. Table 7.5 also reveals that the types of aromatic hydrocarbons differed significantly in relation to temperature, with or without ZSM-5. The aromatics were dominated by

alkylbenzenes, with benzene itself only found in the oil produced with ZSM-5 at both temperatures. Detailed analysis of the results in Table 7.3 showed that the non-catalytic tests produced oils with about 9.6 wt% of light aromatics (with carbon numbers <C11), whereas at 400 °C, ZSM-5 tripled the production of these group of compounds to 33 wt%. Furthermore, increasing the temperature to 450 °C also increased the yield of the <C11 aromatics to 39.4 wt%. In addition, Table 7.5 clearly shows that the oils from the no-catalytic tests (both temperatures), and test with the ZSM-5 at 450 °C, contained the highest yields of heavier aromatics such as naphthalene and alkyl naphthalenes. Naphthalenes are known to produce significant amount of soot and harmful chemicals including polyaromatic hydrocarbons (PAHs) during combustion in engines and their contents in fuels are normally limited (Hasan et al., 2022). Hence, based on the lower content of heavy aromatics, total yields of <C11 alkanes and aromatics (57.8 wt%), the oil obtained at 400 °C with ZSM-5 could be adjudged to be the best for use as fuel in conventional engines. Moreover, the heavy aromatics could be separated by distillation to further improve the fuel properties of the oil products.

Table 7.5: List of compounds obtained from cracking of decarboxylated oil for 1 h at different temperatures (\*\* indicates reactions carried out with catalyst, ZSM-5)

Alkanes	Yield, wt %			
	400 °C	400 °C**	450 °C	450 °C**
n-Hexane	1.21	-	1.19	-
Hexane, 3-methyl-	0.38	0.76	-	0.52
Heptane	2.88	4.19	2.71	1.25
Heptane, 2-methyl-	4.53	0.65	4.26	-
Heptane, 3-methyl-	-	0.72	-	-
Heptane, 2,4-dimethyl-	-	-	-	1.18
Octane	-	6.41	-	-
Nonane	5.86	6.50	5.58	0.72
Nonane, 3-methyl-	-	0.64	-	-
Decane	6.11	4.89	5.77	-
Undecane	6.33	3.32	6.02	-
Dodecane	6.52	2.70	6.21	-
Dodecane, 4-methyl-	-	-	-	-
Tridecane	5.13	1.29	4.91	-
Tetradecane	4.34	0.62	4.18	-
Tetradecane, 2-methyl-	-	-	-	-
Pentadecane	5.71	0.48	5.46	-
Hexadecane	1.37	-	1.29	-
Pentadecane, 7-methyl-	0.53	-	0.50	-
Pentadecane, 4-methyl-	0.42	-	0.34	-
Heptadecane	24.51	0.81	23.29	-
Heptadecane, 3-methyl-	1.53	-	1.44	-
Octadecane	-	-	0.20	-
Nonadecane	0.44	-	0.42	-

<b>Total</b>	<b>77.80</b>	<b>33.99</b>	<b>73.76</b>	<b>3.67</b>
--------------	--------------	--------------	--------------	-------------

<b>Aromatics</b>	<b>Yield, wt %</b>			
	400 °C	400 °C**	450 °C	450 °C**
Benzene	-	1.48	-	1.82
Toluene	0.51	4.16	0.54	7.31
Ethylbenzene	0.74	2.63	0.75	2.68
p-Xylene	0.34	4.64	0.32	7.36
o-Xylene	2.07	2.83	2.02	2.37
Benzene, propyl-	0.33	0.31	0.32	0.60
Benzene, 1-ethyl-3-methyl-	2.55	0.73	2.51	3.71
Benzene, 1-ethyl-2-methyl-	-	6.89	-	2.33
o-Cymene	0.18	-	-	-
Benzene, 1,2,3-trimethyl-	-	-	-	-
Benzene, (1-methylethyl)-	-	1.02	-	0.33
Benzene, 1-ethyl-4-methyl-	-	-	-	1.23
Benzene, 4-ethyl-1,2-dimethyl-	-	-	-	0.51
Mesitylene	-	1.22	-	2.29
Indane	0.32	0.65	0.33	0.51
Benzene, 1-methyl-3-(1-methylethyl)-	-	-	0.18	-
Benzene, 1,4-diethyl-	-	0.98	-	0.58
Benzene, 1-methyl-3-propyl-	-	0.93	-	0.75
Benzene, 1-methyl-2-propyl-	1.24	0.72	1.32	0.86
Benzene, 1,2-diethyl-	0.59	1.40	0.63	0.44
Benzene, 2-ethyl-1,4-dimethyl-	-	0.42	0.18	1.71
Benzene, 1-methyl-2-propyl-	-	0.39	-	0.82
Indan, 1-methyl-	0.37	0.31	0.40	0.72
Benzene, 1-ethyl-2,4-dimethyl-	0.32	-	0.16	0.43
1H-Indene, 2,3-dihydro-5-methyl-	-	0.48	-	0.51
Benzene, 1-ethyl-4-(1-methylethyl)-	-	0.85	-	0.33
Benzene, 1-methyl-4-(1-methylpropyl)-	0.54	0.27	0.57	0.59
Benzene, 1-methyl-2-(2-propenyl)-	0.50	-	0.58	1.03
Benzene, pentyl-	0.28	-	0.15	-
Benzene, 1,4-dimethyl-2-(2-methylpropyl)-	0.17	-	0.18	-
Benzene, (1,3-dimethylbutyl)-	0.43	-	0.44	-
1-Methyl-2-n-hexylbenzene	0.33	-	0.36	-
Benzene, 1-ethyl-3-(1-methylethyl)-	-	-	-	0.28
Benzene, 1-ethyl-4-(1-methylethyl)-	-	-	-	0.35
Benzene, 1-methyl-4-butyl	0.70	0.42	0.69	0.67
Naphthalene	1.12	1.05	1.16	3.15
Benzene, 1-methyl-4-(1-methyl-2-propenyl)-	-	0.97	-	0.28
1H-Indene, 2,3-dihydro-1,6-dimethyl-	0.39	0.62	0.43	0.71

Benzene, 1-ethyl-2,4-dimethyl-	-	2.14	-	-
Benzene, 1-ethenyl-3-ethyl-	-	0.30	-	-
Benzene, 1-methyl-4-(1-methylpropyl)-	-	0.75	-	-
Benzene, 1-methyl-2-(2-propenyl)-	-	1.05	-	-
Naphthalene, 1-methyl-	0.82	-	0.88	3.87
Naphthalene, 2-methyl-	0.77	0.34	0.81	1.62
Naphthalene, 2-ethyl-	0.21	2.42	0.23	1.15
Naphthalene, 1,6-dimethyl-	0.25	1.15	0.28	1.71
Benzene, (1-methylheptyl)-	0.30	-	0.32	-
Benzene, (1-methyldecyl)-	1.75	-	0.85	-
Benzene, undecyl-	0.18	-	0.19	-
Benzene, (1,1-dimethylnonyl)-	0.24	-	-	-
2-Ethyl-2,3-dihydro-1H-indene	-	-	-	0.54
Naphthalene, 1,2,3,4-tetrahydro-5,7-dimethyl-	-	-	-	0.27
Naphthalene, 1,2-dimethyl-	-	-	-	1.38
Naphthalene, 2,6-dimethyl-	-	0.80	-	0.72
Naphthalene, 1,3-dimethyl-	-	-	-	0.26
1,4-Dimethylazulene	-	-	-	0.36
Naphthalene, 1-propyl-	-	-	-	0.27
Naphthalene, 2-(1-methylethyl)-	-	0.98	-	0.83
Naphthalene, 2,3,6-trimethyl-	-	-	-	0.44
Naphthalene, 2,3,6-trimethyl-	-	-	-	0.27
Benzene, (1,3-dimethylbutyl)-	-	0.99	-	-
Bicyclo[4.2.1]nona-2,4,7-triene, 7-ethyl-	-	0.46	-	-
Fluorene	0.37	-	0.54	0.53
9H-Fluorene, 9-methyl-	0.34	0.43	0.49	1.26
9H-Fluorene, 2-methyl-	-	-	0.18	0.41
9H-Fluorene, 9,9-dimethyl-	0.17	-	0.19	-
Naphthalene, 1,8-dimethyl-	-	0.37	-	-
Phenanthrene	0.42	-	0.45	0.56
Phenanthrene, 2-methyl-	-	-	-	0.26
<b>Total</b>	<b>19.90</b>	<b>49.17</b>	<b>18.88</b>	<b>63.63</b>

The elemental analysis of the oil products from the cracking reactions were used to plot their van Krevelen diagrams, which is a two-dimensional graph used as a tool to characterise fuels by their elemental ratios. For instance, in this case, the molar ratios of hydrogens to carbons (H/C), and molar ratios of oxygens to carbons (O/C) are often plotted against each other. The H/C shows the degree of saturation, while the O/C shows the concentration of oxygen present. The conversion of the compounds to their corresponding elemental formulas is a prerequisite for estimating these ratios. For comparison, the H/C to O/C ratios of gasoline, kerosene, and diesel have been included in the diagram alongside with those of the products of interest. Figure 7.6 shows an overlap between the reactions at 400°C and 450°C in the absence of a catalyst, with both having relatively higher H/C ratios than the reactions

carried out in the presence of ZSM-5. As shown in Table 7.5, the oils from the catalytic tests were dominated by aromatics, which explains the observations in the H/C ratios. All the oil products had negligible oxygen contents and so, the molar ratios were along the y-axis of the diagram like the other hydrocarbon fuels. Figure 7.6 also shows the extent of deoxygenation achieved from the RSO, the hydrolysed RSO, the decarboxylated oils and the post-cracking oil products.

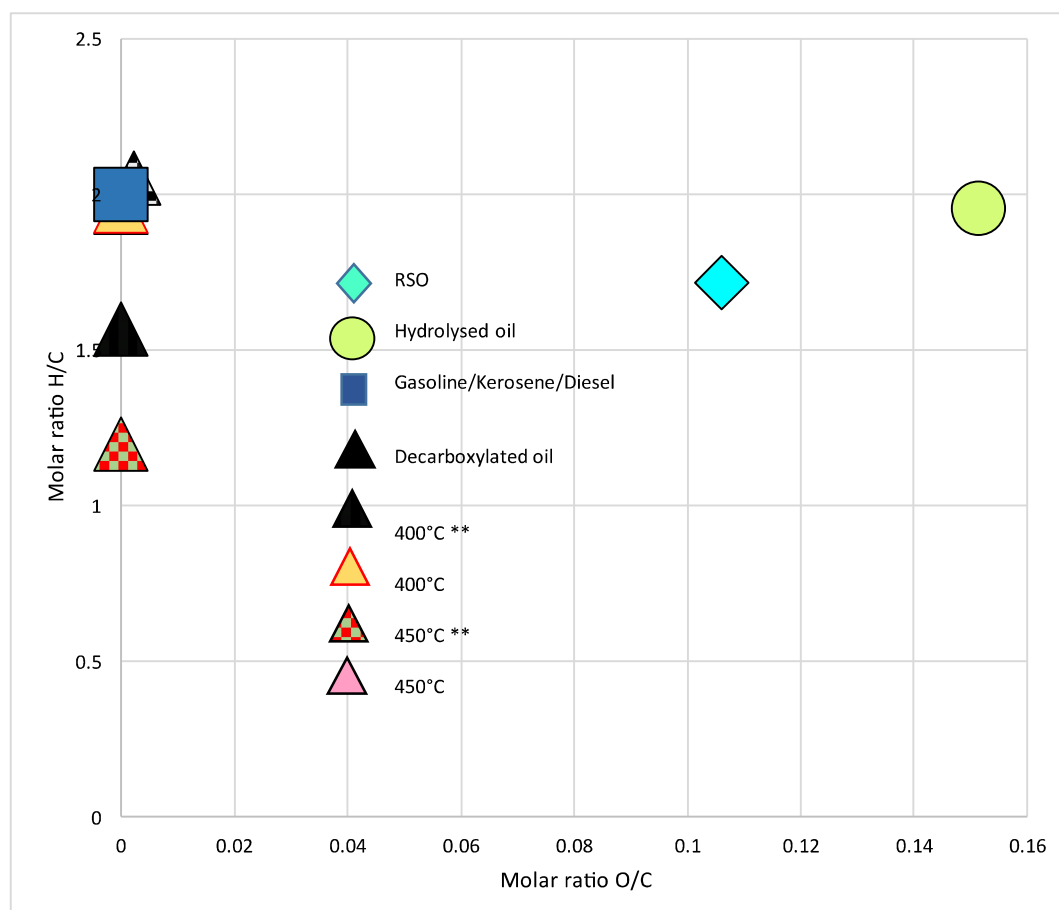


Figure 7.6: Van Krevelen plot of the liquid/wax products from RSO to the post-cracking oil product in comparison with conventional hydrocarbon fuels

To further assess the compatibility of the products obtained with existing engine fuels, Figure 7.7 presents the simulated distillation curves of the product oils obtained from varying reaction temperature with and without ZSM-5 in comparison with gasoline, kerosene, and diesel. The boiling range of the non-catalysed reactions showed a shift to higher boiling points, with 95% of the oils falling higher than gasoline but lower than kerosene. While the profile of the catalysed reactions showed the boiling range distribution was almost 100% below that of gasoline. Both reactions carried out with catalyst also have very comparable profiles to the commercially available gasoline but the catalysed reaction at 400 °C had the most similar profile to gasoline.

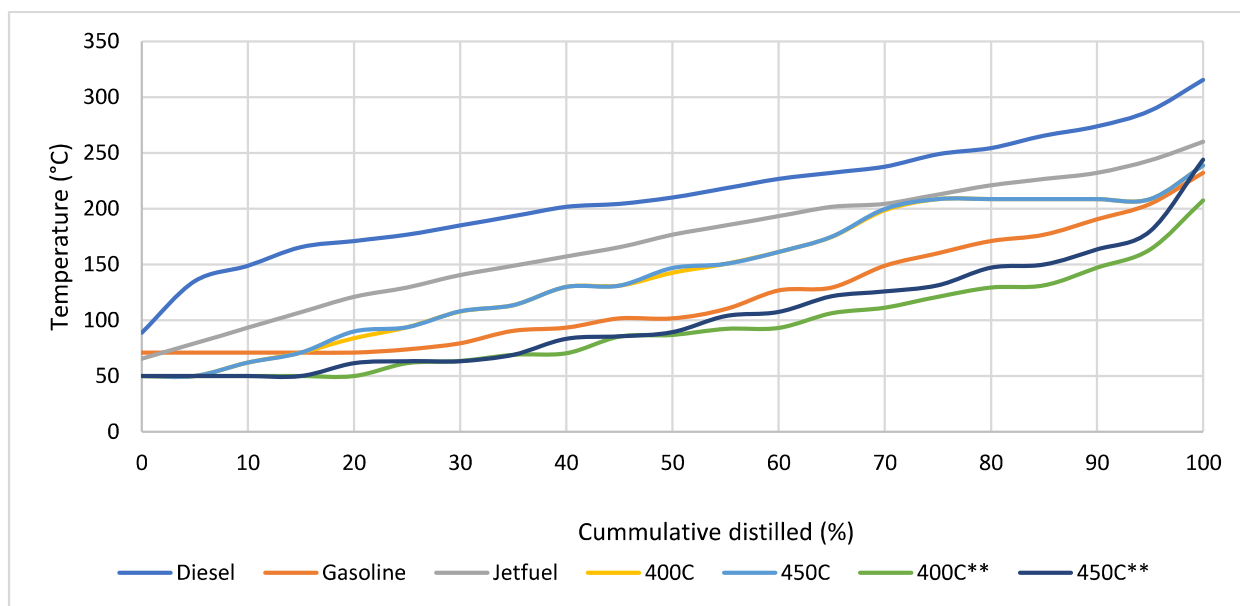


Figure 7.7: Simulated distillation curves from varying reaction temperature (ASTM D2887)

## 7.4 Comparison of different catalyst for cracking of decarboxylated oil

In this section, the results from the catalytic cracking of the decarboxylated oil are reported. The additional catalysts used in this work include zeolite Y, MCM-41, and Ru/Al<sub>2</sub>O<sub>3</sub>. Except the Ru-based catalysts, all the other catalyst are zeolite-based, which are commercially used for catalytic cracking (Xie et al., 2023). Ru-based catalyst have been reported to be efficient in C-C bonds, leading to the formation of simple hydrocarbon gases (mainly methane) (Onwudili and Williams, 2013). However, it has also been reported that such severe cracking reactions occurred with oxides of ruthenium such as RuO<sub>2</sub> and RuO. Hence, in this present work, the Ru-based catalyst was first reduced to the metal under hydrogen gas flow before use, to investigate its activity for mild cracking reactions. All the catalysts were crushed and sieved to >10mm siezes (similar to the ZSM-5) and used for cracking experiments. Based on the composition of aromatic compounds in the oils obtained in Section 7.3 with ZSM-5, the test with these different catalysts were carried out at 400 °C for 1 h under 5 bar N<sub>2</sub> pressure. A temperature of 400 °C was chosen for these tests, to minimise the formation of heavy aromatic hydrocarbons. Some of the properties of these catalysts are shown in Table 7.2. The yields and compositions of the products obtained are discussed in this section in comparison with the ZSM-5 catalyst.



### 7.4.1 Product yields and mass balance in relation of different catalysts

The product distributions and mass balances from the cracking of hydrocarbons with different catalysts are shown in Table 7.6. In comparison with ZSM-5, all the catalyst produced higher oil yields, lower gases and similar or higher solid yields. From Table 7.6, the reactions with the other catalysts gave higher mass balance closures compared to ZSM-5, an indication that the oil products from these catalysts were less volatile and hence little or no mass losses occurred during product recovery and handling.

Table 7.6: Mass balance for reaction products from cracking at 400 °C, 1 h with various catalysts

Catalyst	Solid (wt%)	Oil product (wt%)	Gas phase (wt%)	Balance (wt%)
ZSM-5	1.97	82.55	2.59	87.18
Zeolite Y	1.27	95.20	0.48	96.96
MCM-41	5.10	89.52	0.48	95.16
Ru/Al <sub>2</sub> O <sub>3</sub>	5.68	91.62	0.68	98.03

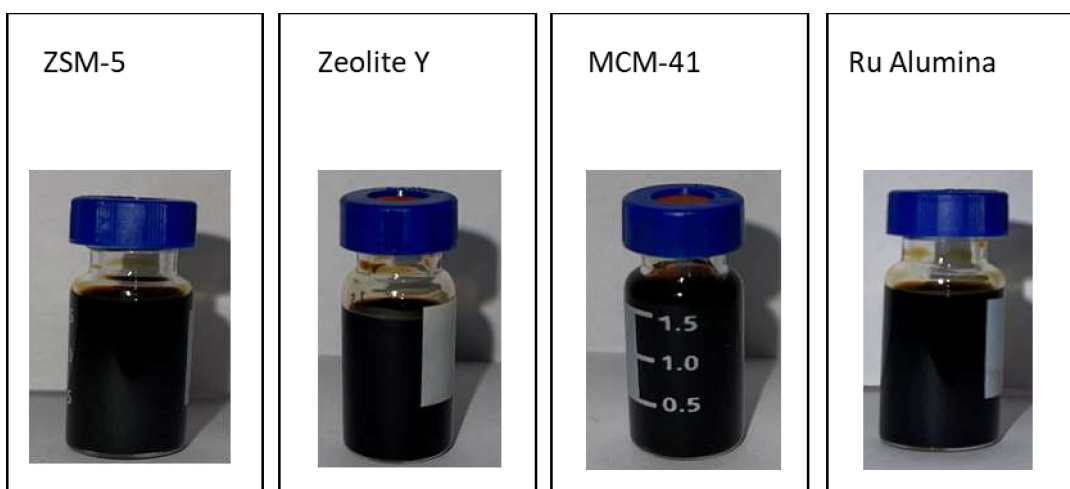


Figure 7.8: Appearance of liquid products obtained with the different cracking catalysts

The reaction with ZSM-5 also produced the most gases, and possibly lower molecular weight compounds, which would be revealed by comparing the GC/MS analysis data of these oils. All the catalysts produced dark easy-flowing oils (Figure 7.8).

### 7.4.2 Gas composition in relation to different catalysts

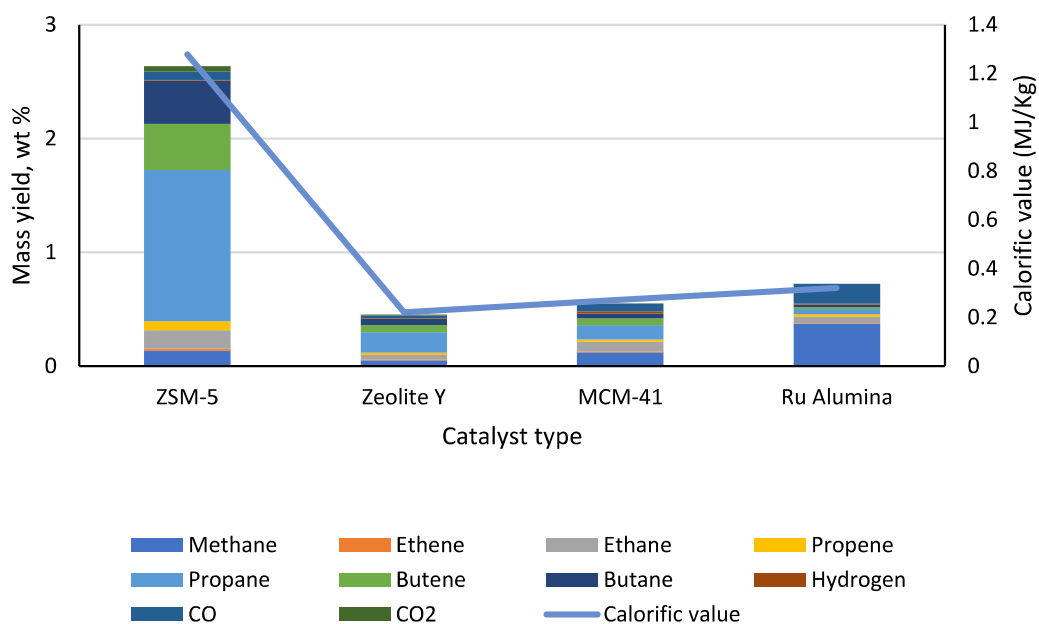


Figure 7.9: Mass yields of gas products obtained from cracking of decarboxylated oil at 400 °C with various catalysts for 1 h

Figure 7.9 shows the composition of gas products obtained from the catalytic cracking experiments using different catalysts. The calorific value of gases obtained ranged from 0.22 MJ/kg to 1.28 MJ/kg. ZSM-5 produce the most gases, which was reflected in it having the highest calorific value of 1.28 MJ/kg. These gases with a high calorific value are preferred for high-value gases. Interestingly, the gas product from ZMS-5 was dominated by propane (1.33 wt%), while the Ru-based catalyst produced the most methane (0.37 wt%). As discussed earlier, ZSM-5 also produce high yields of butane and butene. The selective production of propane during the process of bio-liquids such as pyrolysis oils have been reported during in situ and ex situ upgrading have been variously reported (Kostyniuk et al., 2021; Sankaranarayanan et al., 2018).

### 7.4.3 Characterisation of liquid products obtained from cracking with different catalysts

#### 7.4.3.1 Physico-chemical properties of the liquid products

Table 7.7 shows the elemental composition and calorific content of the product oils. Considering all other factors were kept constant besides the type of catalyst, there were no huge differences in the properties of the oils and based of the similarly fuel-range calorific values, all the oil products have potential to be used as liquid fuels (Staffell, 2011).

Table 7.7: Colour, elemental composition and calorific value obtained from varying catalysts

Catalyst	Main organic product	C (wt %)	H (wt %)	N (wt %)	S (wt %)	O (wt %)	HHV (MJ/kg)
ZSM-5	Dark light oil	88.46	11.54	0.09	nd	nd	46.58
Zeolite Y	Dark light oil	86.16	13.84	0.22	nd	nd	49.12
MCM-41	Dark light oil	87.84	12.16	0.2	nd	nd	47.26
Ru/Al <sub>2</sub> O <sub>3</sub>	Dark light oil	86.18	13.82	0.2	nd	nd	49.1

#### 7.4.3.2 Chemical composition of liquid products obtained with different catalysts

##### 7.4.3.2.1 Composition by compound classes

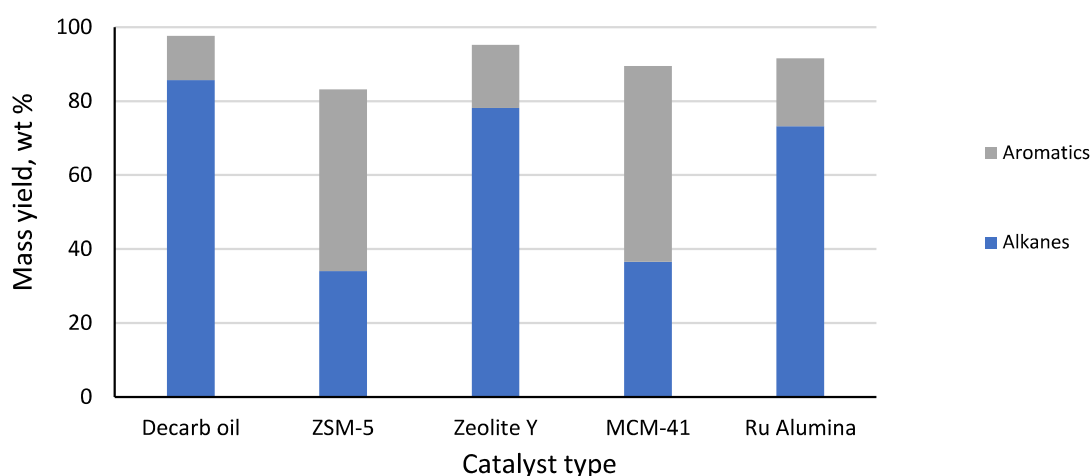


Figure 7.10: Mass yields of compound groups in oil products obtained from the cracking of decarboxylated oil at 400 °C with various catalysts for 1 h

The results in Figure 7.10 show that Zeolite Y and reduced Ru/Al<sub>2</sub>O<sub>3</sub> gave similar and minimal effects on the cracking of hydrocarbons in the decarboxylated oils obtained from hydrolysed RSO. These two catalysts produced nearly similar yields of alkanes and aromatics to the decarboxylated oil feedstock, which suggests minimal catalytic activity. On the other hand, ZSM-5 and MCM-41 showed similar yields with 53% less alkanes, and almost four folds more aromatics when compared to the decarboxylated oil feedstock. This implied ZSM-5 and MCM-41 had stronger selectivities towards aromatics than Zeolite Y and Ru/Al<sub>2</sub>O<sub>3</sub>. This was not unexpected as ZSM-5 and MCM-41 are known to have high acidity due to their low silica/alumina ratio; hence they have been reported to promote aromatisation and coke formation during cracking of alkanes due to having strong binding sites (Jin et al., 2020; Guo et al., 2022). However, MCM-41 produced higher yields of both groups of compounds and overall oil yields than ZSM-5.

#### 7.4.3.2.2 Composition by carbon number

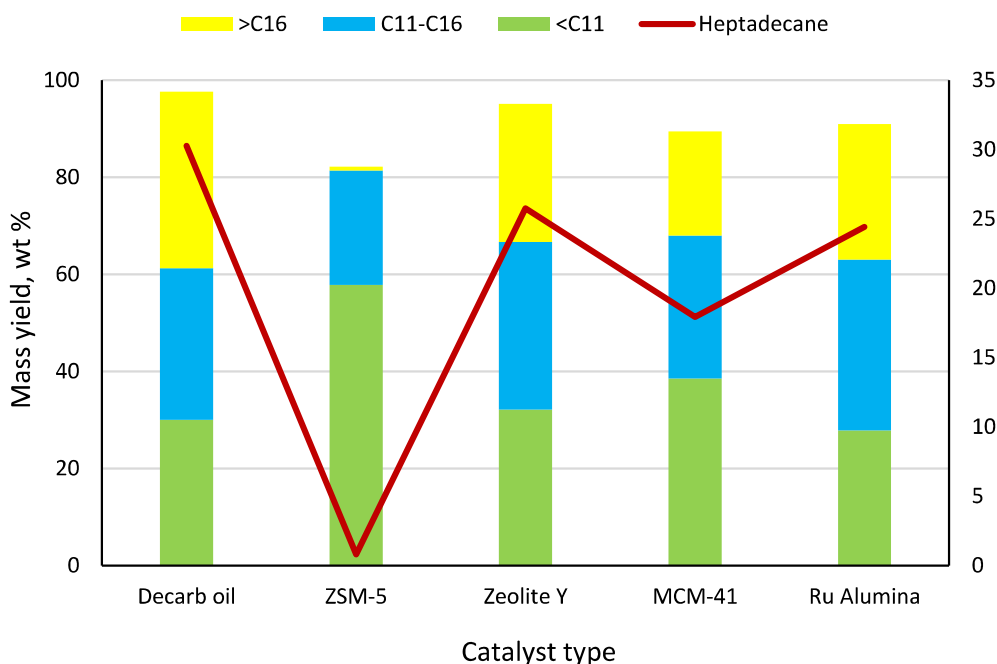


Figure 7.11: Yield wt% of heptadecane and other hydrocarbon products obtained from cracking of hydrocarbons at 400 °C, 1 h with various catalysts

Figure 7.11 shows the distribution of the hydrocarbons in the oils obtained from the different catalysts based on carbon numbers after GC/MS analyses. As discussed in Section 7.4.3.2.1, the use of Zeolite Y and reduced Ru/Al<sub>2</sub>O<sub>3</sub> increased the aromatic contents to around 20% for each catalyst, compared to 12.3% in the decarboxylated oil. The similarity between Zeolite Y and Ru/Al<sub>2</sub>O<sub>3</sub> that was highlighted in Figure 7.10 in terms of the yields of their corresponding aliphatic and aromatic compounds can also be seen in Figure 7.11 as oil from both catalysts gave very similar carbon number profiles. Figure 7.10 shows that both ZSM-5 and MCM-41 produced similar aromatic contents of about 59%, however detailed GC/MS characterisation revealed that the compositions of compounds in the oils differed significantly. From Figure 7.11, ZSM-5 produced the highest yield of <C11 hydrocarbons (57.8 wt%) and retained the least heptadecane (0.82 wt%) compared to other catalysts including MCM-41. Indeed, the MCM-41 still contained 21.5 wt% of >C16 compounds, including nearly 18 wt% of heptadecane. Hence, in terms of fuel range compositions, cracking with ZSM-5 produced hydrocarbons within the gasoline and kerosene range, while the other catalysts gave oil products with gasoline, kerosene and diesel fractions. This implied that the ZSM-5 catalyst had the greatest cracking effect when compared to the other catalysts. Another interesting point to note is that Zeolite Y, MCM-41, and Ru/Al<sub>2</sub>O<sub>3</sub> had similar profiles to the decarboxylated oil in Figure 7.11. However, there was a notable increase in the aromatic content of MCM-41 in Figure 7.10. This suggests that MCM-41 has

a selective potential to produce aromatics as well. Table 7.8 shows the list of compounds identified and quantified from the oils obtained with the different catalysts. Table 7.8 shows the compounds that make up the aliphatic and aromatic groups and is consistent with Figure 7.10. Three of the catalysts, namely ZSM-5, Zeolite Y and MCM-41 produced similar yields of  $C_{11}$  alkanes with yields of 24.76 wt%, 27.24 wt% and 25.42 wt%, respectively, while the Ru-based catalyst produced the lowest yield (18.13 wt%) within this carbon number.

Table 7.8: List of hydrocarbon compounds in the oil products obtained with the different catalysts at 400 °C for 1 h

Alkanes	Yield, wt %			
	ZSM-5	Zeolite Y	MSM-41	Ru/Al <sub>2</sub> O <sub>3</sub>
Hexane, 3-methyl-	0.76	0.33	1.14	-
Heptane	4.19	2.69	2.99	2.07
Heptane, 2-methyl-	0.65	0.45	0.42	-
Heptane, 3-methyl-	0.72	0.37	0.47	-
Heptane, 2,4-dimethyl-	-	-	-	4.22
Octane	6.41	4.82	5.60	-
Nonane	6.50	6.19	7.26	5.82
Nonane, 3-methyl-	0.64	6.36	-	-
Decane	4.89	6.03	7.54	6.02
Undecane	3.32	5.85	0.73	5.76
Dodecane	2.70	-	1.53	5.55
Dodecane, 4-methyl-	-	-	-	0.34
Tridecane	1.29	4.62	0.41	4.53
Tetradecane	0.62	3.97	0.76	3.87
Tetradecane, 2-methyl-	-	-	-	0.42
Pentadecane	0.48	5.75	0.70	5.66
Hexadecane	0.82	1.37	0.44	1.35
Tetradecane, 4-methyl-	-	-	-	0.36
Pentadecane, 2-methyl-	-	-	-	0.94
2,6,10-Trimethyltridecane	-	0.79	0.54	0.65
Undecane, 6-methyl-	-	0.39	-	-
Decane, 2,5-dimethyl-	-	-	1.06	-
Tetradecane, 4-methyl-	-	0.39	0.38	-
Hexadecane, 2-methyl-	-	0.96	0.49	-
Heptadecane, 2-methyl-	-	0.65	1.16	0.65
Heptadecane	-	25.75	0.82	24.43
Octadecane	-	-	0.54	-
Nonadecane	-	0.55	0.37	0.57
<b>Total</b>	<b>33.99</b>	<b>78.21</b>	<b>36.53</b>	<b>73.22</b>

Aromatics	Yield, wt %			
	ZSM-5	Zeolite Y	MCM-41	Ru/Al <sub>2</sub> O <sub>3</sub>
Benzene	1.48	-	-	-

Toluene	4.16	1.23	1.36	0.56
Ethylbenzene	2.63	1.09	1.32	0.71
p-Xylene	4.64	0.96	0.91	0.43
o-Xylene	2.83	1.44	1.79	1.69
Benzene, propyl-	0.31	0.40	0.51	0.31
Benzene, 1-ethyl-3-methyl-	0.73	0.77	1.41	-
Benzene, 1-ethyl-2-methyl-	2.48	0.38	1.60	2.08
Benzene, 1-ethyl-2-methyl-	4.41	1.42	-	-
Benzene, 1,2,3-trimethyl-	-	0.33	0.40	-
Benzene, (1-methylethyl)-	1.02	-	-	-
Benzene, (1,3,3-trimethylnonyl)-	-	-	-	0.56
Mesitylene	1.22	-	-	0.24
Indane	0.65	0.23	0.30	0.23
Benzene, 1,4-diethyl-	0.98	0.25	0.36	-
Benzene, 1,2-diethyl-	1.40	-	-	0.56
Benzene, 1-methyl-3-propyl-	0.93	0.32	0.46	-
p-Mentha-1,5,8-triene		0.54	-	0.43
Benzene, 2-ethyl-1,4-dimethyl-	0.42	0.49	0.65	1.32
Benzene, 1-methyl-2-propyl-	1.11	0.77	0.91	-
Benzene, n-butyl-	-	-	0.71	-
Indan, 1-methyl-	0.31	0.32	0.39	0.39
Benzene, (1,1-dimethylpropyl)-	-	0.23	4.21	-
Benzene, 1-ethyl-2,4-dimethyl-	2.14	-	-	-
Benzene, 1-ethenyl-3-ethyl-	0.30	-	-	-
1-Phenyl-1-butene	-	0.50	0.25	-
Benzene, 1-methyl-4-(1-methylpropyl)-	0.75	0.26	-	0.51
1H-Indene, 2,3-dihydro-5-methyl-	0.62	-	-	-
Benzene, 1-methyl-3-(1-methylethyl)-	-	-	-	0.22
Benzene, pentyl-	-	0.24	0.60	0.25
Benzene, 1-methyl-2-(2-propenyl)-	1.05	-	-	0.50
Benzene, 1-methyl-4-butyl	0.42	0.39	0.26	0.77
Naphthalene	1.05	0.77	0.45	0.79
1H-Indene, 2,3-dihydro-1,6-dimethyl-	1.00	0.26	3.81	0.39
Benzene, (1,3-dimethylbutyl)-	-	0.21	0.31	-
Benzene, 1-methyl-4-(1-methyl-2-propenyl)-	1.44	-	-	-
Naphthalene, 2-methyl-	0.34	1.35	4.03	0.62
Naphthalene, 1-methyl-	-	-	-	0.64
Naphthalene, 2-ethyl-	2.42	0.31	2.62	-
Naphthalene, 1,6-dimethyl-	1.15	0.35	0.37	-
2-Ethyl-2,3-dihydro-1H-indene	-	-	0.45	0.61
Benzene, 1,4-dimethyl-2-(2-methylpropyl)-	-	-	-	0.20
Benzene, (1,3-dimethylbutyl)-	-	-	-	0.54
Bicyclo[4.2.1]nona-2,4,7-triene, 7-ethyl-	0.46	-	-	-
Naphthalene, 1,3-dimethyl-	-	0.35	0.44	-
Naphthalene, 2-(1-methylethyl)-	-	0.18	0.24	-
Benzene, (1-methyldecyl)-	-	0.17	0.27	0.27
Benzene, (1-methyldecyl)-	-	0.28	0.32	0.38

Benzene, (1-methyldecyl)-	-	-	-	-
Benzene, undecyl-	-	0.19	-	0.21
1-Methyl-2-n-hexylbenzene	-	-	-	0.31
Naphthalene, 1,8-dimethyl-	0.37	-	-	0.27
Benzene, (1-methylheptyl)-	-	-	-	0.28
Fluorene	-	-	-	0.26
9H-Fluorene, 9-methyl-	0.43	-	-	0.32
Naphthalene, 2,6-dimethyl-	0.80	-	-	-
Naphthalene, 2-(1-methylethyl)-	0.98	-	-	-
Benzene, 1,4-dimethyl-2-(2-methylpropyl)-	-	-	-	0.27
Phenanthrene	-	-	-	0.27
<b>Total</b>	<b>49.17</b>	<b>17.00</b>	<b>52.99</b>	<b>18.40</b>

Among the four catalysts, ZSM-5 and MCM-41 produced lower yields of C<sub>11</sub>-C<sub>16</sub> alkanes with 9.23 wt% and 6.55 wt%, respectively compared to Zeolite Y (23.13 wt%) and Ru/Al<sub>2</sub>O<sub>3</sub> (29.43 wt%). Table 7.8 also shows that ZSM-5 produced no alkanes with >C<sub>16</sub> carbon numbers, whereas high yields of these compounds were found in the oils obtained from the cracking reactions with Zeolite Y (27.91 wt%) and Ru/Al<sub>2</sub>O<sub>3</sub> (25.65 wt%). In terms of aromatics, majority of these compounds were mostly alkyl benzenes with branch chain lengths from C<sub>7</sub> (toluene) to C<sub>11</sub> (methyldecyl). Detailed analysis showed that ZSM-5 produced nearly three times more <C<sub>11</sub> aromatics with a yield of 33 wt%. This was followed by MCM-41 (13.1 wt%) while both Zeolite Y and Ru/Al<sub>2</sub>O<sub>3</sub> produced around 10 wt% each. Hence, the high total yields of <C<sub>11</sub> compounds (57.8 wt%) obtained from ZSM-5 could explain the poor mass balance closures presented in Table 7.7, confirming the relatively higher volatility of the oil product from this catalyst. In contrast, Ru/Al<sub>2</sub>O<sub>3</sub> (4.17 wt%) produced the lowest yield of heavy aromatic compounds with fused rings (naphthalenes and other PAHs) while the other three catalysts produced about twice more with 8.5 wt% from ZSM-5, 8.95 wt% from Zeolite Y and 8.6 wt% from MCM-41. The presence of these soot-forming aromatics would lead to particulate emissions and also be detrimental to engine performance and efficiency (Tree and Svensson, 2007; Abu-Jrai et al., 2009; Reijnders et al., 2016). Hence, further processing in terms of distillation may be required to obtain lighter fuel fractions from the oils.

The elemental compositions of the oil products obtained from cracking the decarboxylated oil from RSO were further processed to plot the van Krevelen diagram using the H/C and O/C ratios, and compared with those of conventional fuels (gasoline, kerosene, and diesel). With their zero oxygen contents, Figure 7.12 shows all four catalysts produced hydrocarbon oils whose properties were similar to those of the conventional fuels. However, there was an overlap of Zeolite Y and Ru/Al<sub>2</sub>O<sub>3</sub>, which implied remarkably similar H/C ratios of the oil products, which were higher than those obtained from ZSM-5 and MCM-41. The lower H/C

ratios in the oils from ZSM-5 and MCM-41 were due to the high aromatic contents of the oil products obtained from these two catalysts, and therefore the degree of unsaturation as mentioned in Section 7.3.3.2.2. Hence, the data in Figure 7.12 supported the results reported in Figure 7.10, Figure 7.11 and Table 7.8 which show that both catalysts produced the highest amounts of aromatics and highest amount of <C11.

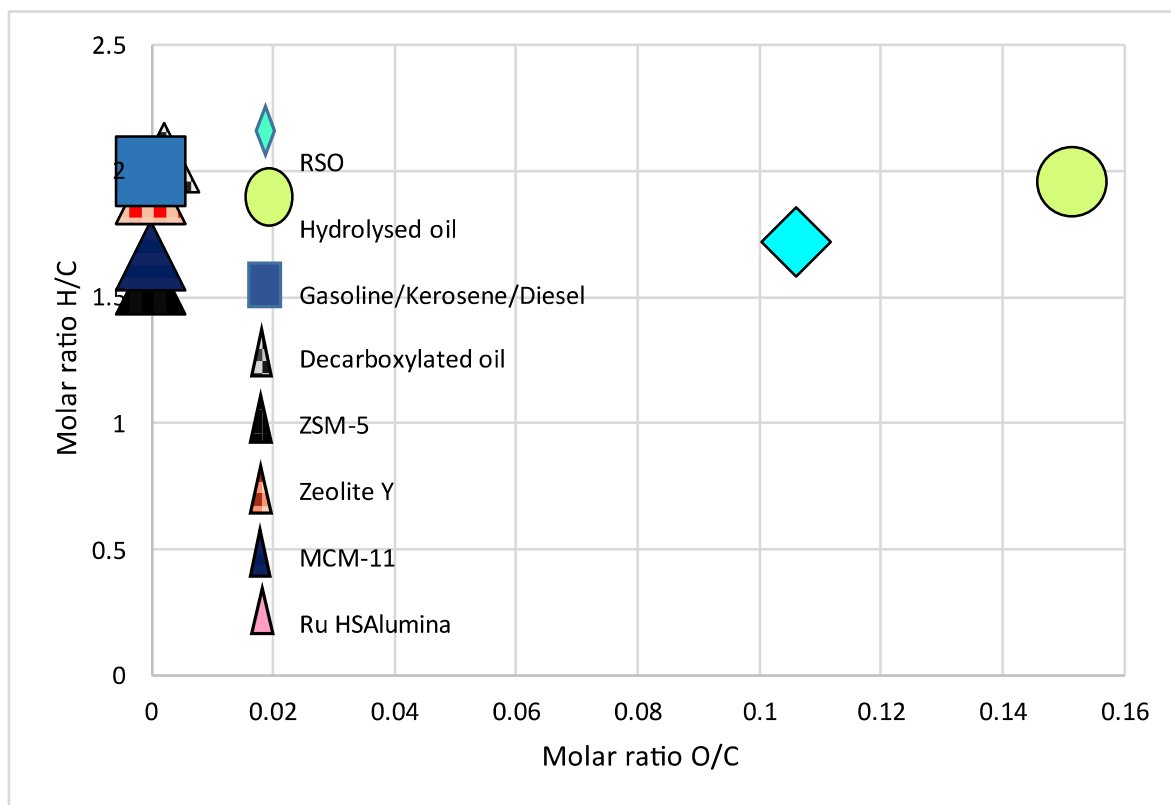


Figure 7.12: Van Krevelen plots of the oil products obtained with different catalysts at 400 °C for 1 h in comparison with conventional fuels



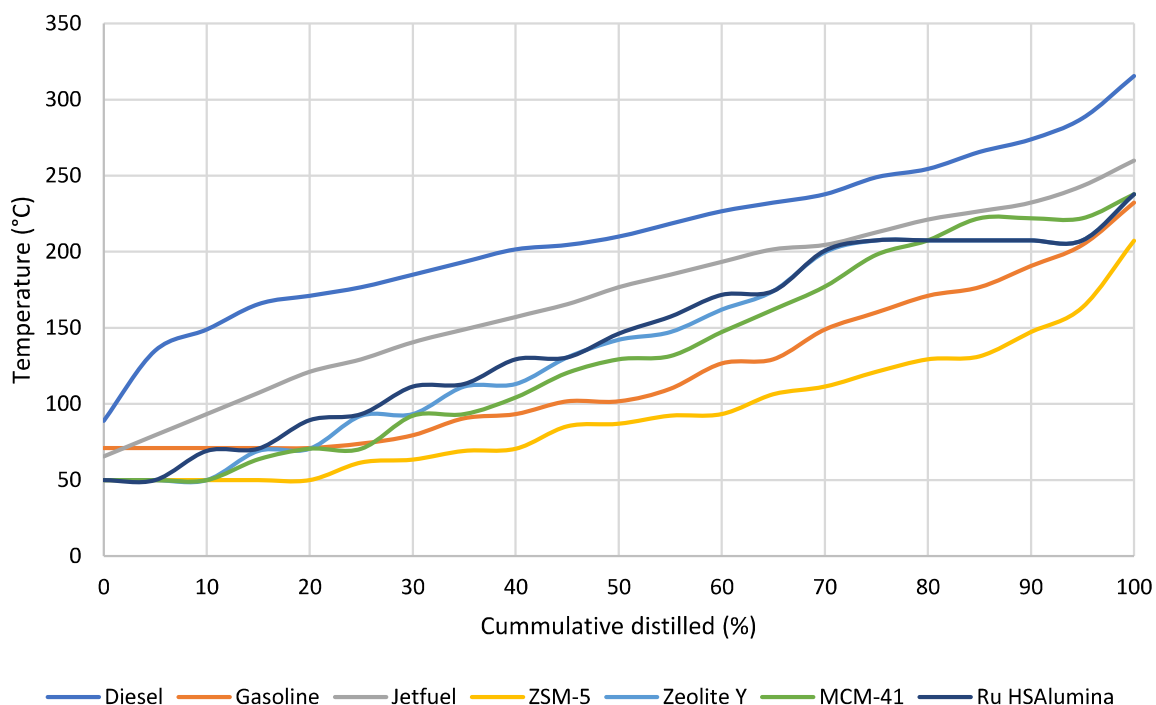


Figure 7.13: Simulated distillation curves for oil products obtained with different catalysts at 400 °C for 1 h

Figure 7.13 shows the boiling range distribution of the oil products obtained from reactions with the various catalysts. The graph shows that the boiling point range of all the oil products were lower than 250°C, with the product obtained using ZSM-5 at an even lower range below 220°C. The oil product from ZSM-5 had a 100% boiling point range fraction below gasoline, while just about 20% of the oils from the three other catalysts were within the gasoline range. Indeed, these three catalysts, Zeolite Y, MCM-41, and Ru/Al<sub>2</sub>O<sub>3</sub> had almost 80% boiling point range fraction below the kerosene fraction. None of the oils overlapped with diesel fuel boiling point range. Hence, all the oils produced with the four different catalysts can potentially be used as gasoline and kerosene fuels, however polishing will be required to remove soot-forming PAHs.

The study investigates the catalytic cracking of hydrocarbons using different catalysts and examines the impact of these catalysts on product yields and characteristics. The results, as presented in Table 7.6, reveal that compared to ZSM-5, Zeolite Y, MCM-41, and Ru/Al<sub>2</sub>O<sub>3</sub> produced higher oil yields, lower gas yields, and similar or higher solid yields. Additionally, mass balance closures were higher with other catalysts, suggesting that the oil products from these catalysts were less volatile, resulting in minimal mass losses during recovery and handling. ZSM-5, in particular, produced more gases, indicating possibly lower molecular weight compounds. Further analysis in Figure 7.8 illustrates that all catalysts yielded dark, easily flowing oils. The gas composition, as depicted in Figure 7.9, shows variations among

the catalysts, with ZSM-5 producing the most gases and having the highest calorific value. Notably, gas product from the reaction with ZSM-5 was dominated by propane, while the Ru-based catalyst produced the most methane.

The physico-chemical properties of the liquid products, detailed in Table 7.7, demonstrate minimal differences among the oils from different catalysts. They all exhibit potential for use as liquid fuels based on similar fuel-range calorific values. Further characterization in Figures 7.10 and 7.11 reveals that ZSM-5 and MCM-41 had stronger selectivities towards aromatics, while Zeolite Y and Ru/Al<sub>2</sub>O<sub>3</sub> showed minimal catalytic activity in this regard. ZSM-5, in particular, exhibited the greatest cracking effect, producing hydrocarbons within the gasoline and kerosene range. Table 7.8 lists hydrocarbon compounds in the oil products, indicating that ZSM-5 and MCM-41 produced lower yields of C11-C16 alkanes compared to Zeolite Y and Ru/Al<sub>2</sub>O<sub>3</sub>. ZSM-5 also produced a higher yield of <C11 aromatics, contributing to poor mass balance closures and indicating higher volatility. The van Krevelen diagram (Figure 7.12) supports these findings, showing similar H/C ratios for Zeolite Y and Ru/Al<sub>2</sub>O<sub>3</sub>, which were higher than those for ZSM-5 and MCM-41 due to the latter's higher aromatic contents.

Finally, simulated distillation curves in Figure 7.13 indicate that all oils can potentially be used as gasoline and kerosene fuels, with ZSM-5 having a lower boiling point range. However, further processing may be required to remove soot-forming PAHs, especially for oils from Zeolite Y, MCM-41, and Ru/Al<sub>2</sub>O<sub>3</sub>.

#### 7.4.3.3 Carbon balance from the cracking of decarboxylated oils with different catalysts

Based on the results obtained from the various analytical techniques, the carbon balance across the various products including the solid residues (spent catalyst and char), the amount of carbon in the used catalysts was done with the CHNS analyser as described in Chapter 3. Table 7.9 shows the carbon balance results from this study. The carbon balances were >90%, showing good closures. Results showed that most of the carbon atoms in the decarboxylated oil feedstock was retained in the target oil product, with more than 86 wt% and correlated with the CHNS result reported earlier in Table 7.7. Interestingly, the Ru/Al<sub>2</sub>O<sub>3</sub> had about 86% carbon content, which agreed with the results in Table 7.7. Although, Zeolite Y produced the lowest char yields among the catalysts, the char contained higher carbon contents than the char from ZSM-5, indicating its potential ease of deactivation by coke formation.

Table 7.9: Distribution of carbon in cracking products

Catalyst	Oil (wt%)	Solid residue (wt. %)	Gas (wt. %)	Total (wt. %)
ZSM-5	85.99	2.38	2.50	90.86

Zeolite Y	89.98	7.75	0.45	98.19
MCM-41	86.16	8.47	0.45	95.07
Ru/Al <sub>2</sub> O <sub>3</sub>	86.86	11.82	0.63	99.30

#### 7.4.3.4 Characterisation of spent catalysts

The spent catalysts were characterised using x-ray diffraction (XRD) after calcination. The procedure for calcination of the spent catalyst has been described in Chapter 3, Section 3.2.2.3. Briefly, the used catalysts were dried in the oven at 110 °C for 2 hours and weighed before calcining at 550 °C for 2 h. The colours of the catalysts before and after each experiment are shown in Figure 7.14. Clearly, all the whitish zeolite-based catalysts turned black due to carbon deposition and mixing with char products. Recalcination was able to mostly restore these zeolites to their original colours.













Catalyst	Fresh	Uncalcined used	Calcined used
ZSM-5			
Zeolite Y			
MCM-41			
Ru Alumina			

Figure 7.14: Appearance of the fresh, used and recalcined catalysts used for the cracking reactions

Figure 7.15 shows the powder XRD patterns of the catalysts used in this present study. The four catalysts had different diffraction patterns. All of the peaks shown in Figure 7.15a that emerged at 23–27° in the XRD patterns of the ZSM-5 sample may be correlated to the usual MFI structural framework (JCPDS-44-0003) (Wang et al., 2022; Anh -Tuyen et al., 2017; Krisnandi et al., 2019). The peaks located at  $2\theta$  10°, 12°, 16°, 19°, 20°, 24°, 27°, 31°, 32°, 33°, and 35° correspond to the Zeolite Y peaks reported by Salahudeen et al. (2015); Rosman et al. (2014), and Eghbali et al. (2016) (Figure 7.15b). The slight decrease in the intensity of the peaks observed in the uncalcined used catalysts may be due to the partial loss of structural cations of the zeolite Y. The diffractograms of ZSM-5 and Zeolite Y had

minimal changes in spite of the change in colour noted in Figure 7.14, meaning their crystalline phases did not change much but the change in surface area in Table 7.10 clearly indicated poisoning by carbon deposition. Figure 7.15c displays the XRD patterns of the MCM-41 catalyst of which are well in accord with those described in the literature (Baskaran et al., 2016) and the broad peaks were observed indicated the highly amorphous nature of the material. The  $\text{Al}_2\text{O}_3$  peaks identified at  $43.1^\circ$ ,  $45.9^\circ$ , and  $67.1^\circ$  in  $\text{Ru}/\text{Al}_2\text{O}_3$ , and MCM-41 correlates with those reported by Suryawanshi et al. (2015) (JCPDS file No. 10-0425). The broad XRD peaks of  $\text{SiO}_2$  were observed in the range  $20\text{--}30^\circ$  in MCM-41 (Pandya et al., 2018). The XRD analysis revealed peaks for  $\text{RuO}_2$  at  $28.5^\circ$ ,  $35^\circ$ , and  $54^\circ$  and for Ru metal at  $38.4^\circ$  (JCPDS Card no. 06-0663) (Chen et al., 2016; Fovanna et al., 2020; Zhang et al., 2017). The absence of the  $\text{RuO}_2$  peak around  $28^\circ$  (Fovanna et al., 2020) in the used catalyst before calcination showed that the catalyst was stable and remained mostly as the metal during the reaction. The intensity of the  $\text{RuO}_2$  peaks indicated the rapid oxidation of the Ru metal during recalcination (Figure 7.15d), meaning that the catalyst would need to be reduced before reuse. Interestingly, no graphitic carbon was observed in any of the used catalysts.

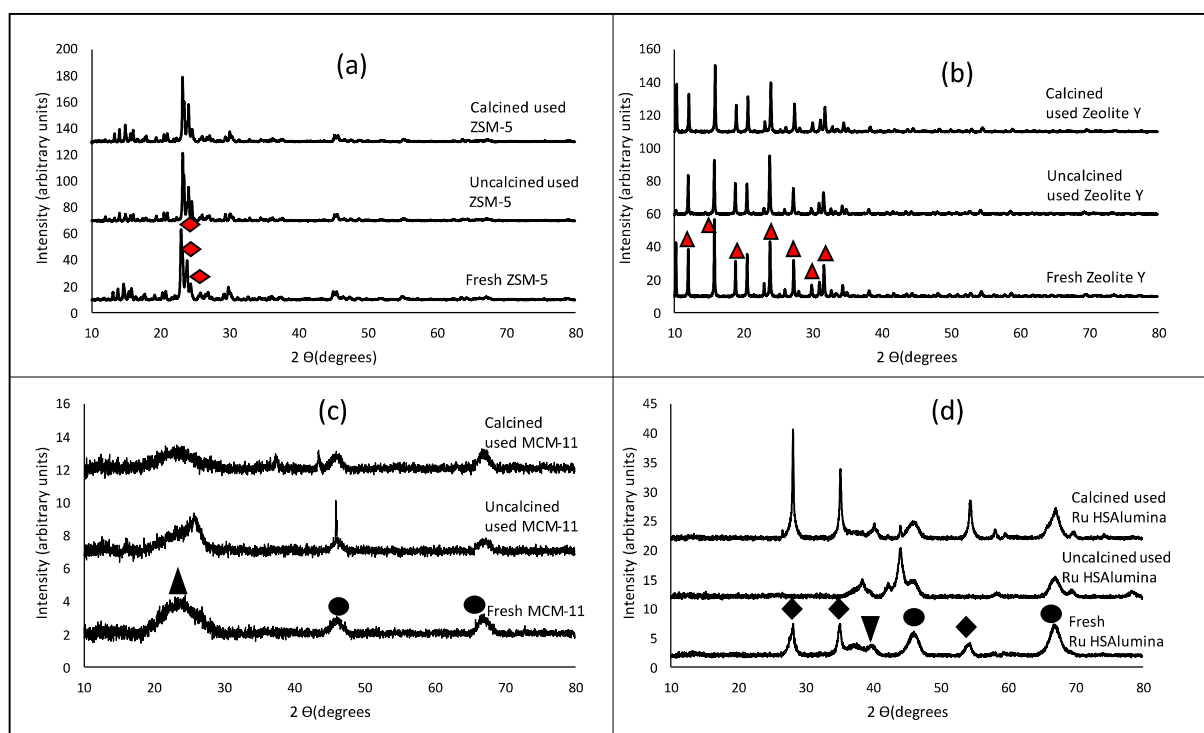


Figure 7.15: XRD patterns of (a) ZSM-5 (b) Zeolite Y (c) MCM-41 (d) Ru HSA alumina (● =  $\text{Al}_2\text{O}_3$ , ▲ =  $\text{SiO}_2$ , ▼ = Ru, ◆ =  $\text{RuO}_2$ , ▲ = Zeolite Y, ◆ = ZSM-5)

Table 7.10 shows the changes in the surface areas, pore volumes and pore diameter of the catalysts used in cracking reactions before and after the recalcination. These properties have been compared with those of the fresh catalyst earlier presented in Table 7.2. The results showed that all the catalyst suffered losses of surface areas after the reactions. However, these properties were somewhat restored after calcination, supporting observations presented in Table 7.8 on the restoration of the colours of the zeolite catalysts.

Table 7.10: Surface areas, pore volumes and pore diameters of used and recalcined catalysts used for the cracking reactions

Catalyst	Surface area (m <sup>2</sup> g <sup>-1</sup> )			Pore volume (cc/g)			Pore diameter (nm)		
	Fresh	Uncalcined used	Calcined used	Fresh	Uncalcined used	Calcined used	Fresh	Uncalcined used	Calcined used
ZSM-5	306.98	31.17	310.85	0.19	0.07	0.26	3.89	3.37	3.85
Zeolite Y	534.91	116.48	452.05	0.19	0.25	0.29	3.83	3.09	3.40
MCM-41	627.26	69.85	520.18	0.24	0.09	0.28	3.43	3.14	3.47
Ru/Al <sub>2</sub> O <sub>3</sub>	154.92	20.12	115.81	0.4	0.14	0.32	8.11	3.37	7.99

\*Surface area and pore volumes obtained from N<sub>2</sub> adsorption porosimetry

## 7.5 Effect of reaction time on the cracking of decarboxylated oil from RSO

So far, using ZSM-5 at a temperature of 400 °C for a reaction time of 1 h appeared to give the best yields of fuel range liquid hydrocarbons from the cracking of decarboxylated oil from RSO. Further optimisation was attempted in this section by varying the reaction time from 0 h to 2 h at the optimal temperature of 400 °C.

### 7.5.1 Product yields and mass balance in relation to reaction time for cracking

Table 7.11 shows there was a decrease in mass balance closures as reaction time increased from 96.77 wt% at 0 h to 82.58 wt% after 2 h of reaction. There was also a decrease in the liquid products while the yields of both gas and solid products increased with increasing reaction time. The decline in the mass balance closures as the time of reaction increased was typically due to the loss of volatiles as previously explained. This correlated with the increase in yields of gas products with time, which also included some unidentified and unquantified gas components observed during gas analysis. The product oils obtained from each reaction time were all dark thin liquids (Figure 7.16).

Table 7.11: Mass balance for reaction products from the cracking of decarboxylated oils at 400 °C with different reaction times

Time (h)	Product			Balance (wt%)
	Solid (wt%)	Oil product (wt%)	Gas product (wt%)	
0	1.10	93.52	1.15	96.77
0.5	1.79	86.51	2.43	90.74
1	1.98	82.55	2.59	87.18
2	2.97	75.67	3.91	82.58

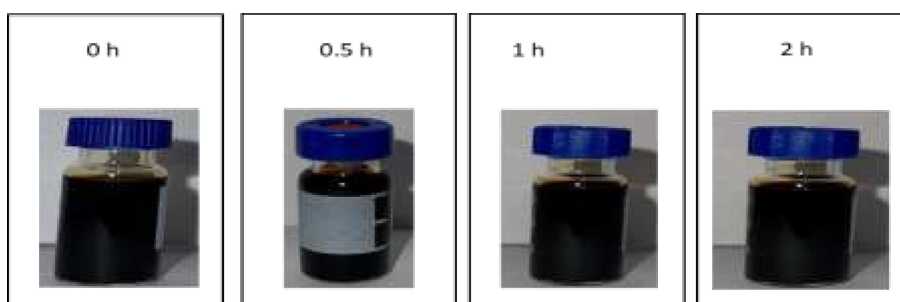


Figure 7.16: Appearance of liquid products obtained from the catalytic cracking of the decarboxylated oils from RSO at different reaction times



### 7.5.2 Gas composition in relation to reaction time

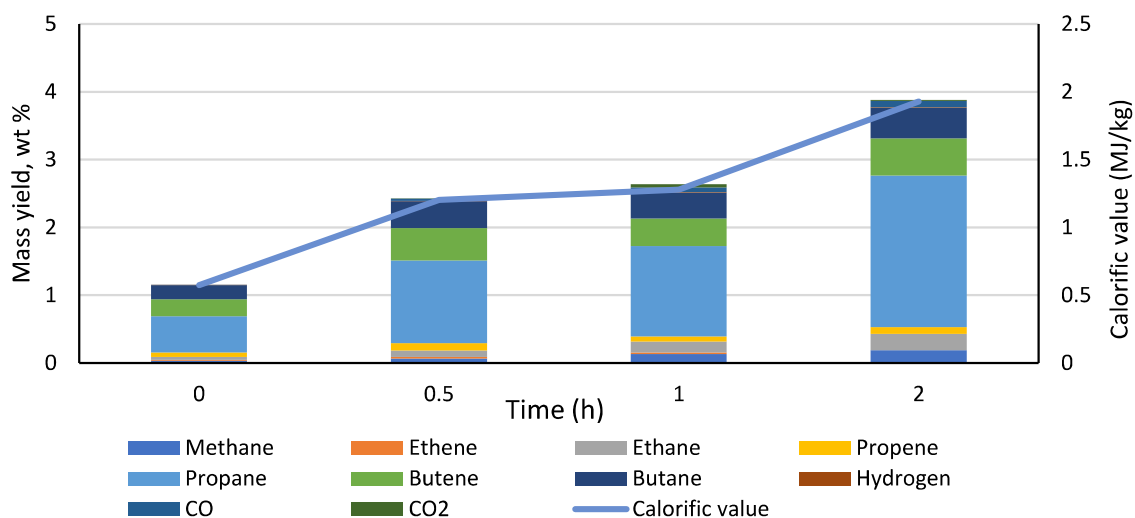


Figure 7.17: Mass yield, wt % of gases obtained from cracking hydrocarbons at 400 °C with different reaction times

Figure 7.17 shows the components in the gas products obtained from the cracking reactions in relation to reaction time. All reactions had similar gaseous compounds profiles in terms of the components present and overall, there was a superior selectivity towards propane across all reactions. While there was a dramatic increase in gas yields between 0 h and 0.5 h, no major differences were observed between the gas yields and compositions from 0.5 h and 1 h. Increasing the reaction time to 2 h again led to a dramatic increase in gas yields and also the proportion of propane in the gas product. Indeed, gas yield increased by 51% when reaction time was increased from 1 h to 2 h, and during this time, propane yield increased by 75.2%. The increased yield of gas components, especially propane, led to increase in the calorific values of the gas products with increasing reaction time, which may be used for process heating.

### 7.5.3 Characterisation of liquid products in relation to reaction time during cracking

#### 7.5.3.1 Physico-chemical properties of the liquid products

Table 7.12 shows the elemental composition and calorific content of the product oils obtained from varying reaction time. There was a reduction in the HHV of the oils as reaction time increased, which could be due to the increase in formation of smaller chain hydrocarbons with less energy density. However, the calorific values ranged from 44.6 MJ/kg to 48.2 MJ/kg and were comparable to those of conventional liquid fuels (Staffell, 2011).



Table 7.12: Colour, elemental composition and calorific value obtained from varying reaction time

Time (h)	Main organic product	C (wt %)	H (wt %)	N (wt %)	S (wt %)	O (wt%)	HHV (MJ/kg)
0	Dark light oil	86.99	13.01	0.27	0	0	48.19
0.5	Dark light oil	88	11.99	0.11	0	0	47.08
1	Dark light oil	88.46	11.54	0.09	0	0	46.58
2	Dark light oil	90.25	9.75	0.14	0	0	44.6

### 7.5.3.2 Chemical composition of oil products in relation to reaction time during cracking

#### 7.5.3.2.1 Composition by compound classes

Figure 7.18 shows the results from the GC/MS analysis of the liquid hydrocarbons from the cracking reactions in relation to reaction time. The figure shows that only alkanes and aromatic compounds were identified and quantified by the GC/MS, and the overall yields were nearly equivalent to the actual yields of liquid products in Table 7.11. The increased severity of the cracking process in terms of reaction time, led to gradual changes in the compositions of the oils. Even at 0 h, there was already a three-fold increase in aromatics compared to the aromatics observed in the decarboxylated oil feedstock. Furthermore, as reaction time increased, a consistent growth in the yield of aromatics could be observed, so that from 0.5 h, there was more aromatics than alkanes in the oil products. In the decarboxylated oil feedstock the mass ratio of aromatics to alkanes was 0.14, at 0 h, this increased to 0.61 and beyond 0.5 h this ratio increased further to 1.18. After 1h and 2h reaction times, the mass ratio of aromatics to alkanes were 1.45 and 5.94, respectively. This meant that increasing reaction time favoured the formation of aromatics .

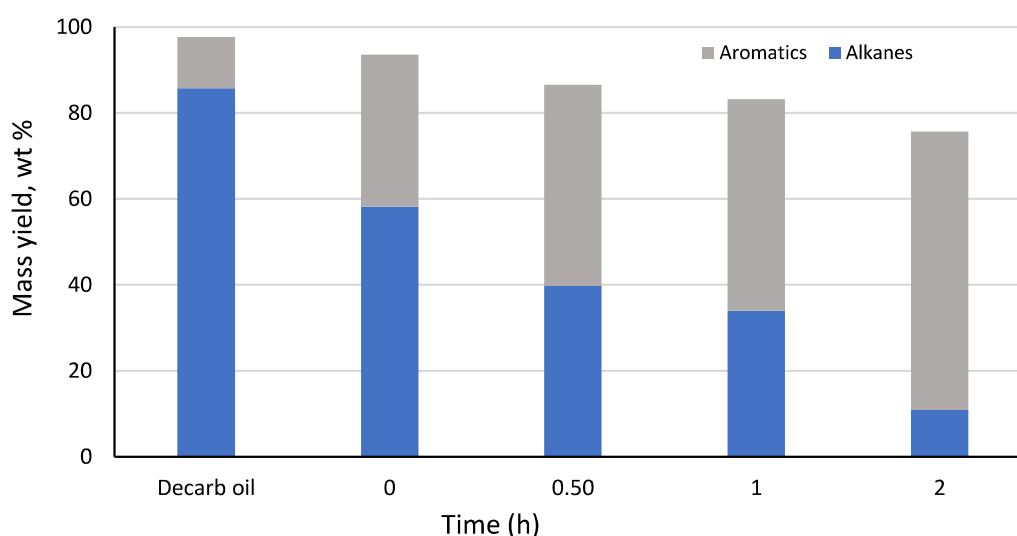


Figure 7.18: Mass yields of groups of hydrocarbon products obtained from cracking of decarboxylated oil at 400 °C in relation to reaction time

### 7.5.3.2.2 Composition of oil products by carbon number

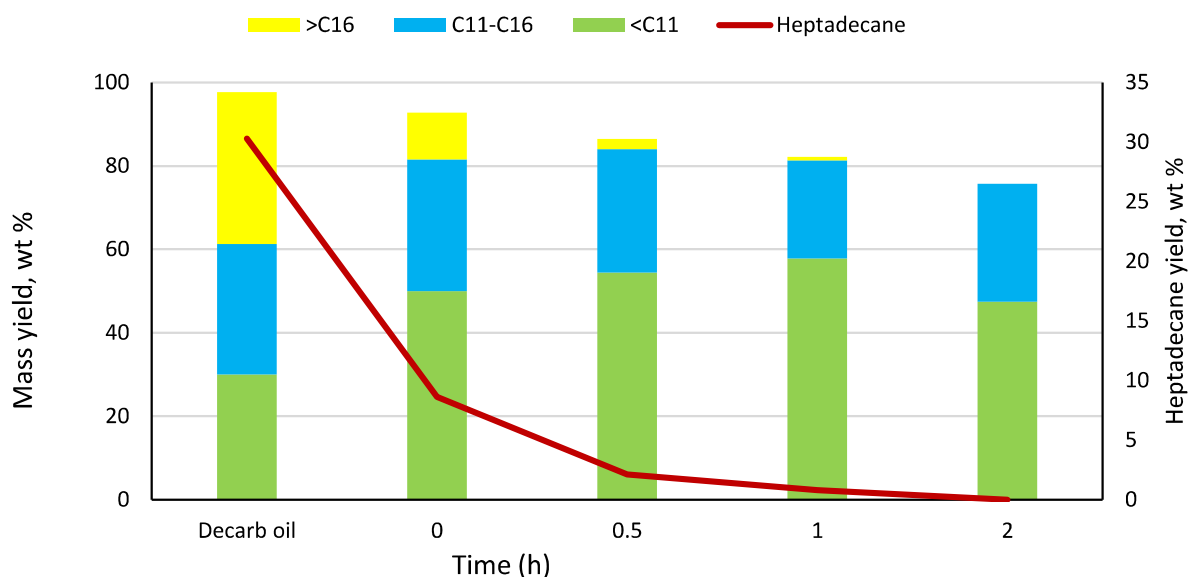


Figure 7.19: Mass yields of heptadecane and other hydrocarbon in the oil products obtained from cracking decarboxylated oil at 400 °C in relation to reaction time

Figure 7.19 shows results from the analysis of the hydrocarbons obtained from the cracking reactions in relation to reaction time. The compounds have been grouped according to their carbon numbers. By 0 h, the <C11 hydrocarbons had increased by 74%, C11-16 by 6%, and the >C16 and heptadecane yields had decreased by 71% compared to the decarboxylated oil feedstock. As time of reaction increased to 2 h, the >C16 and heptadecane yields reached 0 wt%, meaning complete cracking of this major long-chain alkane obtained from the decarboxylation of the predominant C18 fatty acids in RSO. The list of compounds present in the oils obtained from the cracking reactions in relation to reaction time are presented in Table 7.13.

Table 7.13: List of compounds in the oils obtained from the cracking reactions in relation to reaction time

Alkanes	Yield, wt%			
	0 h	0.5 h	1 h	2 h
n-Hexane	1.44	-	-	0.53
Hexane, 2-methyl-	1.47	-	-	2.10
Hexane, 3-methyl-	-	0.61	0.76	0
Heptane	3.99	3.66	4.19	0
Heptane, 2-methyl-	-	0.72	0.65	3.20
Heptane, 3-methyl-	0.8	0.74	0.719	0
Heptane, 2,4-dimethyl-	-	6.38	-	2.69
Octane	6.99	-	6.41	0
Nonane	8.18	7.18	6.5	1.58

Nonane, 3-methyl-	-	-	0.64	-
Decane	7.21	5.87	4.89	-
Undecane	5.87	4.3	3.32	-
Dodecane	5.18	3.51	2.7	-
Tridecane	3.36	1.9	1.29	-
Tetradecane	2.27	1.09	0.62	-
Pentadecane	2.75	1.13	0.48	-
Heptadecane	8.63	2.12	0.81	-
<b>Total</b>	<b>58.13</b>	<b>39.76</b>	<b>33.99</b>	<b>10.92</b>

<b>Aromatics</b>	<b>Yield, wt%</b>			
	<b>0 h</b>	<b>0.5 h</b>	<b>1 h</b>	<b>2 h</b>
Toluene	1.62	3.01	4.16	5.81
Benzene	-	-	1.48	1.28
Ethylbenzene	1.75	2.34	2.63	2.67
p-Xylene	-	3.37	4.64	6.7
o-Xylene	2.69	2.84	2.83	2.44
Benzene, 1,3-dimethyl-	1.87	-	-	-
Benzene, (1-methylethyl)-	-	0.28	-	0.34
Benzene, propyl-	0.63	0.75	0.31	0.65
Benzene, 1-ethyl-3-methyl-	-	1.83	0.73	-
Benzene, 1-ethyl-2-methyl-	5.39	4.7	-	4.75
Mesitylene	-	1.22	1.22	2.35
Benzene, 1,2,3-trimethyl-	0.52	-	-	-
Indane	0.54	0.56	0.65	0.45
Benzene, 1,3-diethyl-	0.979	-	-	-
Benzene, 1,2-diethyl-	0.89	-	-	-
Benzene, (1-methylethyl)-	-	-	1.02	-
Benzene, 1,4-diethyl-	-	0.42	0.98	0.56
o-Cymene	-	-	-	0.77
Benzene, 1,2-diethyl-	-	0.83	1.4	0.46
Benzene, 1-methyl-2-propyl-	1.82	1.66	0.72	0.88
Benzene, 1-methyl-3-propyl-	-	0.51	0.93	0.8
Benzene, (1-methylpropyl)-	-	1.03	-	-
Benzene, 1-ethyl-2,4-dimethyl-	0.37	0.39	-	0.45
Benzene, 2-ethyl-1,4-dimethyl-	-	0.73	0.42	1.81
Benzene, 1-ethenyl-3-ethyl-	-	0.31	-	0.28
Benzene, 1-methyl-2-propyl-	-	-	0.39	0.89
Indan, 1-methyl-	0.84	0.92	0.31	0.75
Benzene, 1-methyl-4-(1-methylpropyl)-	0.93	-	-	-
Benzene, (1,1-dimethylpropyl)-	-	0.28	-	-
Benzene, 1-ethyl-2,4-dimethyl-	-	-	2.14	-
Benzene, 1-ethenyl-3-ethyl-	-	-	0.3	-
Benzene, 1-methyl-2-(2-propenyl)-	0.89	-	-	-
Benzene, 1-methyl-4-butyl	1.07	-	-	-
Benzene, 1-methyl-4-(1-methylpropyl)-	-	1.06	0.75	0.35
1H-Indene, 2,3-dihydro-5-methyl-	1.52	0.4	0.62	0.54
Benzene, 1-methyl-2-(2-propenyl)-	-	1.06	1.05	1.04
7-Methyl-1,2,3,5,8,8a-hexahydronaphthalene	-	0.4	-	-
Benzene, pentamethyl-	-	0.6	-	-

Benzene, 1-methyl-4-butyl	-	1.04	0.42	-
Benzene, 1-ethyl-2,4,5-trimethyl-	-	-	-	0.59
Benzene, 1-methyl-4-(1-methylpropyl)-	-	-	-	0.7
Benzene, (1-methylbutyl)-	-	-	-	0.38
Naphthalene	1.55	1.9	1.05	2.84
Naphthalene, 2-methyl-	2.11	-	0.34	1.55
Naphthalene, 1-methyl-	-	2.93	-	3.97
Naphthalene, 1-ethyl-	0.42	-	-	-
Naphthalene, 2-ethyl-	-	0.67	2.42	1.17
Bicyclo[4.2.1]nona-2,4,7-triene, 7-ethyl-	1.13	-	0.46	-
Benzene, 1-methyl-4-(1-methyl-2-propenyl)-	-	0.27	0.97	-
Benzene, (1,3-dimethylbutyl)-	0.71	0.51	-	-
Benzene, 1,4-dimethyl-2-(2-methylpropyl)-	-	0.3	-	0.24
1H-Indene, 2,3-dihydro-1,6-dimethyl-	-	0.81	0.99	0.77
Naphthalene, 1,2,3,4-tetrahydro-1-methyl-	-	-	-	0.4
2-Ethyl-2,3-dihydro-1H-indene	-	1.14	-	0.55
1-Methyl-2-n-hexylbenzene	0.48	0.31	-	-
Benzene, 1-methyl-4-(1-methyl-2-propenyl)-	-	-	0.48	-
Naphthalene, 1,8-dimethyl-	0.49	0.81	-	-
Naphthalene, 1,6-dimethyl-	-	0.67	1.15	1.9
Naphthalene, 1,2-dimethyl-	-	-	-	1.48
Naphthalene, 2,6-dimethyl-	-	0.32	0.8	0.77
Naphthalene, 1,3-dimethyl-	-	-	-	0.25
Naphthalene, 2,3-dimethyl-	-	-	-	0.38
Naphthalene, 1-propyl-	-	0.38	-	0.25
Naphthalene, 2-(1-methylethyl)-	-	0.29	0.98	1.03
Naphthalene, 1,4,6-trimethyl-	-	-	-	0.36
Naphthalene, 1,4,6-trimethyl-	-	-	-	0.25
Naphthalene, 2-(1-methylethyl)-	-	-	-	0.26
Naphthalene, 2,3,6-trimethyl-	-	-	-	0.29
Naphthalene, 1,6,7-trimethyl-	-	-	-	0.25
Naphthalene, 1,8-dimethyl-	-	-	0.37	-
Spiro[4.4]nona-1,3-diene, 1,2-dimethyl-	-	-	-	0.29
Benzene, (1-methylheptyl)-	0.47	0.29	-	-
Benzene, 1-(2-butenyl)-2,3-dimethyl-	-	-	-	0.31
Naphthalene, 2-methyl-1-propyl-	-	-	-	0.62
Fluorene	-	0.41	-	0.5
9H-Fluorene, 9-methyl-	0.43	0.53	0.43	0.95
9H-Fluorene, 1-methyl-	0.75	-	-	0.35236
Benzene, (1-methyldecyl)-	1.92	0.33	-	-
Benzene, (1,1-dimethylnonyl)-	0.61	-	-	-
Phenanthrene	-	0.35	-	0.45
<b>Total</b>	<b>35.4</b>	<b>46.76</b>	<b>49.17</b>	<b>64.76</b>

The list of compounds mirrored the results presented in Figure 7.18 and 7.19, showing that the oil products obtained from 0.5 h and above were dominated by gasoline and kerosene range compounds. Interestingly, the oil product obtained after 2 h seemed to contain more kerosene range compounds than the oil at 1 h. However, a careful analysis of the data would show that the oil from the longer reaction time contained of significantly higher yields of PAHs (about 21 wt%, compared to 8.65 wt% from the 1 h reaction). The prominent compounds in Table 7.13 show that dimerisation and trimerisation reactions occurred. This would lead to lower thermal efficiency due to poor combustion of fuels and also promote the formation of harmful particulate matter. Therefore, after considering the composition of the oils as well as their yields, the cracking reaction at 1 h was chosen as the optimum condition.

Furthermore, the fuel properties of the oil products obtained in relation to reaction time were assessed using the van Krevelen plot in Figure 7.20. Again, the H/C and O/C ratios of conventional fuels were included for comparison. As no oxygen was present in the oils, their H/C ratios can be found along the y-axis in Figure 7.20. The H/C ratios of the oil products decreased with time due to increased formation of aromatic hydrocarbons.

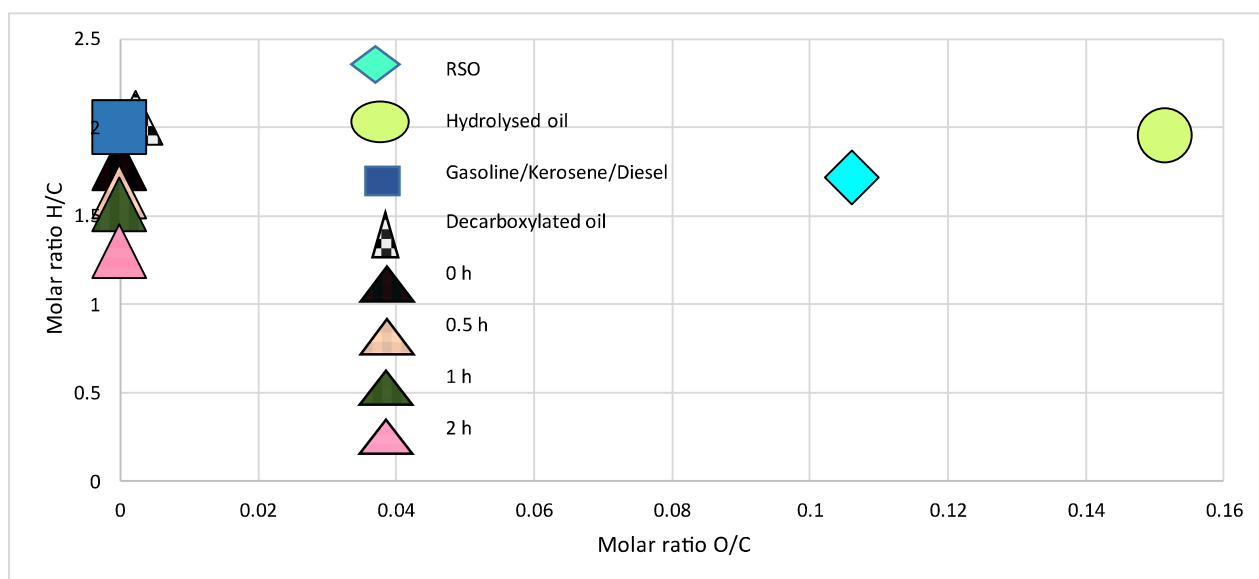


Figure 7.20: Liquid fuels characterisation from varying reaction time by H/C and O/C molar ratios in Van Krevelen diagram

Figure 7.21 shows that all 95% of components in all the oil products obtained in relation to rarefaction time had boiling points below 200 °C, with profiles most similar to gasoline. In general, there was a shift to lower boiling points with the increase in reaction time. These reflect a shift in the molecular weight range as previously highlighted in Figure 7.19. In addition, in these oil products between 75% and 90% of the components could be distilled off

at 150 °C, while for conventional gasoline this number was 70%. Hence, the oils were slightly lighter than gasoline but maybe better blended with other fractions to give better fuel.

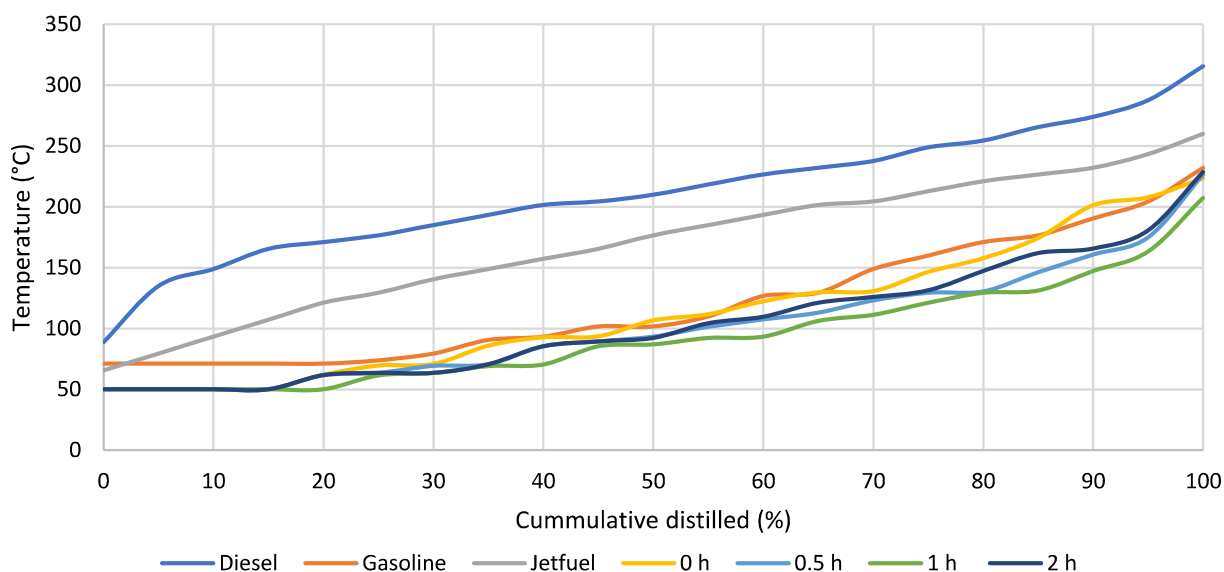


Figure 7.21: Simulated distillation curves from varying reaction time

## 7.6 Simple distillation of oil products from cracking of decarboxylated oil

The decarboxylated oils (clear yellow colour in Chapter 6) turned to darker colours following the cracking reactions as seen from the previous section in this chapter. However, GC/MS results showed the presence of simple aliphatic and aromatic compounds, which are mostly colourless. Therefore, a simple distillation, following the method described in Section 3.2.3.5.6 was carried out on the oil product obtained from the cracking of the decarboxylated oil at 400 °C for 1 h using ZSM-S was used. Figure 7.22 shows photos of the oil products before distillation, the distillate and the bottom products. The distillate was a clear colourless liquid, and subsequently analysed by GC/MS. Figure 7.23a shows the GC/MS chromatogram of the oil product obtained from cracking, while Figure 7.23b shows the chromatogram of the distillate from this oil product. The comparison of both chromatograms showed that they contained similar and almost identical compounds even though there is a shift to lower chain hydrocarbons as presented in Figure 7.24. These compounds are very similar to those present in gasoline (Amaral et al., 2021). Therefore, the conventional fuels could be obtained from this fraction by distillation. This implied the distillation process was successful in separating the important light components of the oil, leaving the heavier fractions, comprising of PAHs in the bottom product. These PAHs and small portions of non-volatile compounds must be responsible for the dark-coloured oils from the cracking reactions. Hence, as

mentioned earlier, a simple distillation process may be used to separate the useful compounds from the soot-forming and highly polluting heavier fractions to obtain higher quality fuels. However, comparing the results of the distillation with the actual yields of lighter compounds indicate that the distillation apparatus used in this work was not very efficient as only 53 wt% of the light compounds could be recovered (U.S. Energy Information Administration, 2012).

---

Pre-distillation sample



---

Distillate



53 wt%

---

Bottom product



47 wt%

---

Figure 7.22: Distribution and appearance of liquid products after distillation

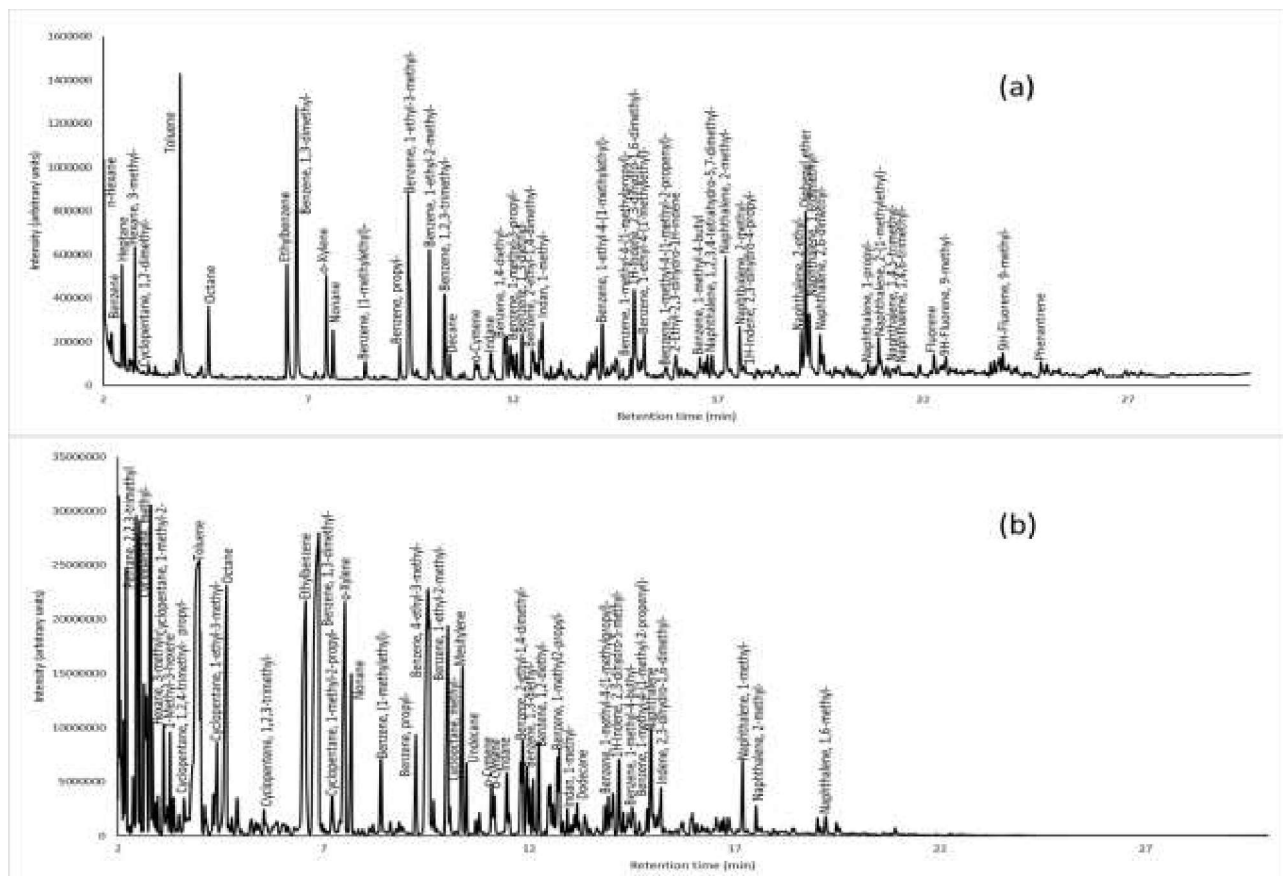


Figure 7.23: (a) GC-MS chromatogram of pre-distilled cracked oil (b) GC-MS chromatogram of distilled cracked oil

Figure 7.23 shows the compiled GC/MS results of the peak area percent of hydrocarbons in the oil product obtained after cracking and the distillate. The figures show the shift of compounds from heavier fractions to lighter chain compounds between the oil obtained directly from cracking and the distillates. The graph in Figure 7.24 has been extracted from the chromatogram in Figure 7.23. Figure 7.24 shows the shift of the C11-16 to <C11 after distillation in terms of peak area %.



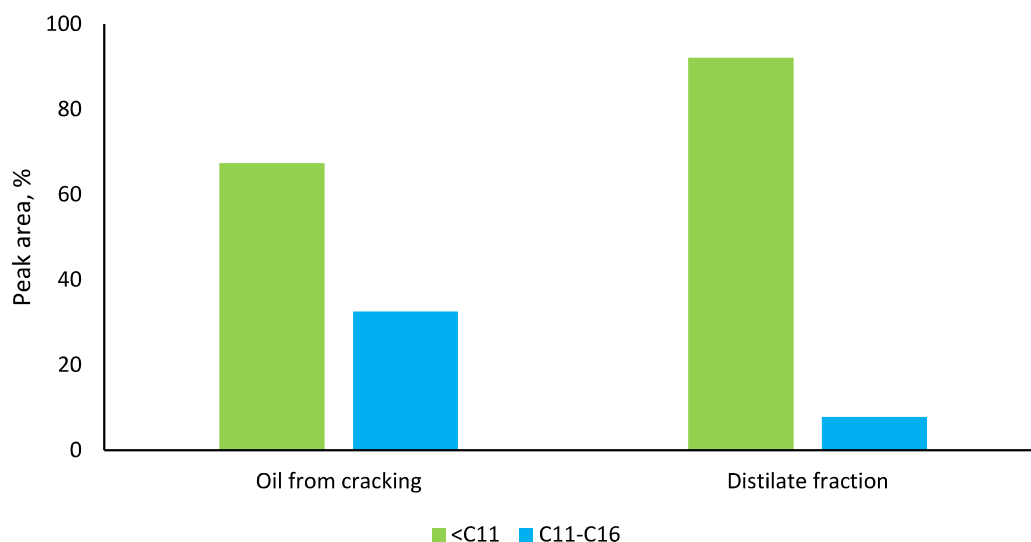


Figure 7.24: Comparison of peak area between cracked and distilled oils

## 7.7 Mechanism for formation of aromatics during cracking

Throughout the different experimental conditions tested, the increase in cracking reaction severity in terms of reaction time and temperature led to an increase in aromatic contents of the oil. While aromatics may not be essentially useful as fuel components, especially the heavier ones, some of them are essential raw materials in the petroleum industry.

Results discussed previously in Section 7.3.3.2.1 showed that reactions without catalysts at 400 °C and 450 °C produced low aromatic yields and minimal profile change from the decarboxylated oil feedstock. However, upon the introduction of ZSM-5, there was a notable increase in the yields of aromatics. In particular, there was an increase in the yields of BTEX compounds. Zhang et al. (2019) and Ono (1992) reported the shape selective potential of ZSM-5 for the production of single ring aromatics such as BTEX from alkanes due to its large pore diameter. The reason being that the surface of ZSM-5 has Lewis acid sites that stimulate hydrogen transfer, and Brønsted acid sites promote the production and transfer of carbon positive ions (Nguyen et al., 2013).

Singh et al. (2019) suggested the conversion of alkanes to aromatics could occur in one of two ways. Either by the aromatisation of the cycloalkenes produced via the Diels-Alder reaction of a substituted alkene and a conjugated diene or oligomerisation of aliphatics followed by cyclisation of resulting oligomers and dehydrogenation reactions of the cyclic intermediates to produce aromatics. Figure 7.25 shows the possible reaction pathway for the catalytic cracking of hydrocarbons to aromatics in this present study. The absence of

cycloalkenes in the results of the cracked oil obtained from the GC/MS suggests that the latter (oligomerisation→cyclisation→dehydrogenation) was the preferred pathway followed (Figure 7.23a). However, unlike the report from Singh et al. (2019) that followed just one path, the chromatogram of the distilled fraction obtained from the oil obtained after cracking did show the presence of alkenes, cycloalkanes and cycloalkenes (Figure 7.23b). This indicated that both routes were possible.

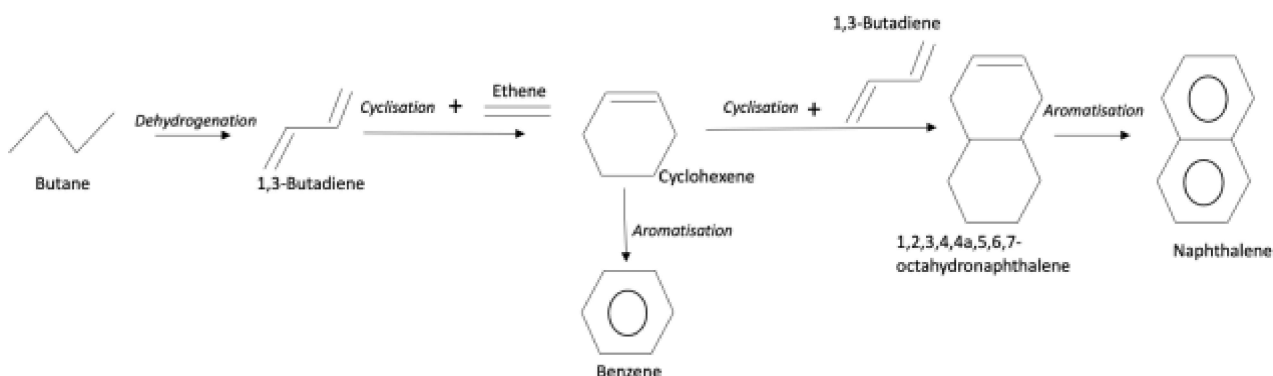


Figure 7.25: Reaction pathways for the catalytic cracking of hydrocarbons (Singh et al., 2021)

## 7.8 Cracking of decarboxylated oils from real-world waste cooking oils (WCOs)

### 7.8.1 Product yields and mass balance

Table 7.14 shows the product yields from the cracking of decarboxylated oils from real-world waste cooking oils, in comparison with similar oils from RSO. Kraiem et al. (2016) performed the non-catalytic cracking of waste frying oils at 500 °C which gave an oil yield of 76%, while Londoño Feria et al. (2021) achieved a liquid product yield of 51.94% by cracking WCOs in the absence of a catalyst at 400 °C. In Table 7.14, higher liquid yields are reported due to the influence of the catalyst, ZSM-5, and all the oil products were dark coloured similar to the one originating from RSO as shown in Figure 7.26.

Table 7.14: Mass balance for reaction products from cracking of decarboxylated oils from RSO and WCOs with ZSM-5 at 400 °C for 1 h

Sample	Product			Balance (wt%)
	Solid (wt%)	Oil product (wt%)	Gas phase (wt%)	
Decarboxylated RSO	1.98	82.55	2.59	87.18
Decarboxylated WCO-A	3.01	78.68	3.20	84.79
Decarboxylated WCO-B	3.91	76.38	2.95	83.23



Figure 7.26: Appearance of liquid products from the cracking of decarboxylated oils with ZSM-5 at 400 °C, for 1 h

### 7.8.2 Gas composition from the cracking of decarboxylated oils from three feedstocks

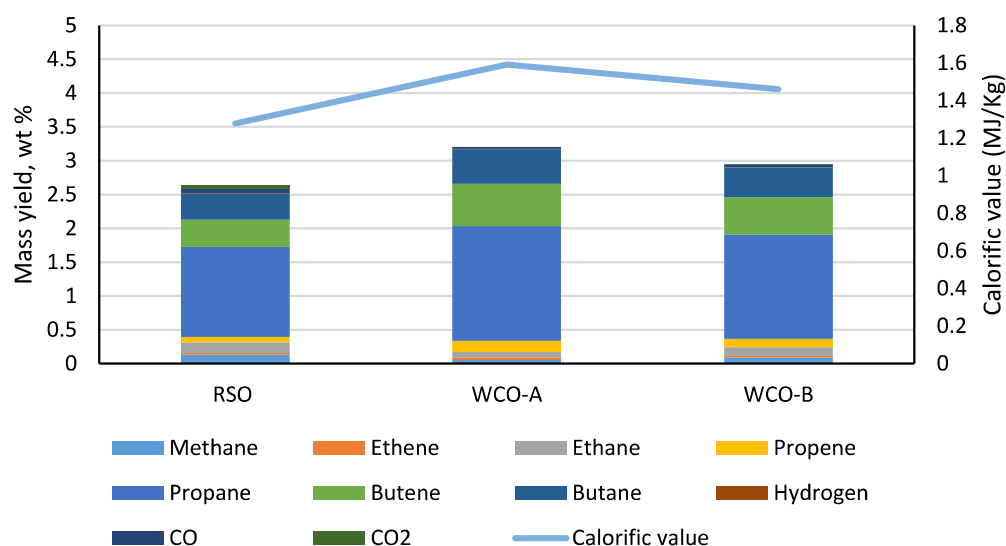


Figure 7.27: Mass yields of gas products obtained from cracking of decarboxylated oils from WCOs at 400 °C for 1 h in comparison with RSO

The gas products obtained from cracking the WCO samples are presented in Figure 7.27. Saturated hydrocarbons were the most dominant group of gases across all three samples. The presence of these alkanes implied that cracking of longer chain hydrocarbons to shorter chain hydrocarbons occurred. The calorific value of the gases obtained from cracking of decarboxylated oils from the WCOs were similar to those obtained from the decarboxylated oil from RSO ranging from 1.28 MJ/kg to 1.59 MJ/kg.

### 7.8.3 Characterisation of liquid products obtained from the cracking of WCOs

#### 7.8.3.1 Physicochemical properties of the liquid products

Table 7.15: Elemental composition and calorific values of the oil products from the cracking of decarboxylated WCOs

Sample	C (wt%)	H (wt%)	N (wt%)	S (wt%)	O (wt%)	HHV (MJ/Kg)
RSO	88.46	11.54	0.19	-	-	46.58
WCO-A	88.96	11.11	0.26	-	-	46.13
WCO-B	89.03	10.96	0.28	-	-	45.93

Table 7.15 presents the elemental composition and calorific content of the WCOs and RSO sample. The decarboxylated oils from the WCOs yielded oils with high calorific values similar to those obtained from RSO. The HHV values of between 46 MJ/kg and 47 MJ/kg fall within the values reported for gasoline, kerosene and diesel (Stafell, 2011) and were clearly higher than those reported by (Li et al., 2021) who carried out direct cracking of biomass. Therefore, all the oils obtained from the cracking process could be used as alternatives to conventional liquid hydrocarbon fuels, after simple further processing such as by distillation. Hence, the same process used for the fresh samples worked exactly the same for the WCOs, showing the robustness of the staged processing of these lipid feedstocks to hydrocarbons. This suggests the product oils can be considered as good fuel substitutes.

#### 7.8.3.2 Chemical composition of liquid products from cracking of decarboxylated WCOs

##### 7.8.3.2.1 Composition by compound classes

Figure 7.28 shows a decrease in the alkane yields, and an increase in the aromatic yields of all three feedstock sources after cracking under the optimum operating conditions of 400 °C for 1 h with ZSM-5. The results have been compared with those from the decarboxylated RSO. Interestingly, the oil products from the cracking of the decarboxylated WCOs contained higher aromatic compounds and even small amounts of alkenes compared to the oil from decarboxylated RSO. The aromatic to alkane mass ratios were respectively 2.5 for decarboxylated from WCO-A and 2.12 for decarboxylated oil from WCO-B, whereas it was 1.45 for decarboxylated oil from RSO. Hence, the slight differences could be attributed to the original lipid feedstocks from which the decarboxylated oils were obtained. Possibly the repeated use of the WCOs led to the formation of hydrocarbons with a higher propensity to form aromatics. Cooking oils have been reported to form hydroxyl groups from oxidation

during cooking, and these can aid dehydration reactions to form alkenes and subsequently aromatics.

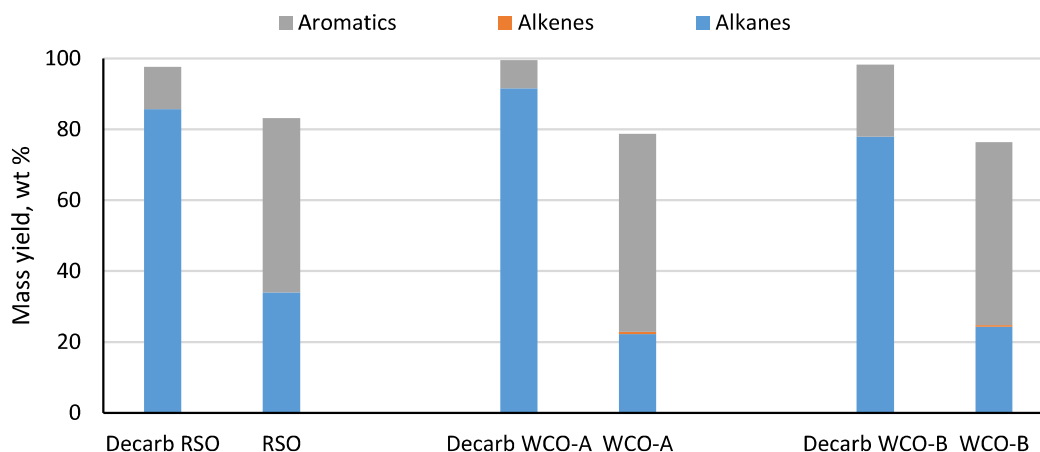


Figure 7.28: Mass yields of groups of hydrocarbons obtained from cracking of decarboxylated WCOs

Figure 7.29 shows the yields of hydrocarbons obtained from the decarboxylated oils from WCOs gave similar profiles as that of decarboxylated RSO. Hence, even the WCOs could still be transformed to high- value hydrocarbons using this three-stage process designed in this study. Giving that the same spectrum of products were obtained from the WCOs and RSO, this implied that the process employed was effective for the conversion of used cooking oils to fuel range hydrocarbons. In comparison with one-pot reactions in literature, this process yielded better quality liquid fuels. For instance, Ge et al. (2022) carried out cracking or conversion of waste cooking oils and obtained a 70 wt% yield of liquid products with CaO/SBA-15 as catalyst.

### 7.8.3.2.2 Composition of oil products by carbon number

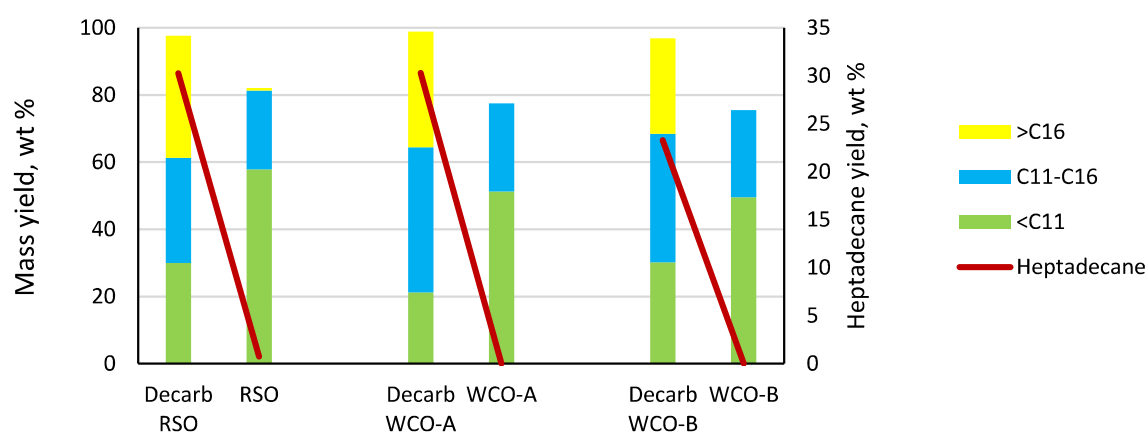


Figure 7.29: Mass yields of hydrocarbon products obtained from cracking WCOs according to carbon number

Further comparison of the oil products obtained from the cracking of the decarboxylated WCOs and RSO oils are provided in the breakdown of compounds in the oils presented in Table 7.16. The presence of branched alkanes and isomers of several aromatic compounds, which are highlighted in the table, shows the occurrence of aromatisation and isomerization reactions. The results in Table 7.16 revealed the main differences and similarities between the oil products from the two sets of feedstocks, the fresh RSO and WCOs. The oil products from decarboxylated RSO contained more <C11 alkanes (28.1 wt%) than the other two, with both WCO-A and WCO-B contained around 20 wt%. All the three oil products from the cracking reactions contained similar yields of <C11 aromatics of around 30 wt%. However, their heavy aromatic contents differed with 8.65 % from RSO-derived oil, compared to 12.7 wt% and 18.32 wt% from oils derived from cracking decarboxylated WCO-A and WCO-B, respectively.

Table 7.16: List of compounds in the oil products obtained from the cracking of decarboxylated WCOs

Alkanes	Yield, wt%		
	RSO	WCO-A	WCO-B
n-Hexane	-	1.56	0.91
Hexane, 3-methyl-	0.76	0.96	0.63
Heptane	4.19	3.26	3.12
Heptane, 2-methyl-	0.65	0.7	0.72
Heptane, 3-methyl-	0.72	0.96	0.64
Heptane, 2,4-dimethyl-	-	-	4.23
Octane	6.41	3.98	-
Nonane	6.5	3.92	4.53
Nonane, 3-methyl-	0.64	-	-

Decane	4.89	2.82	3.61
Undecane	3.32	1.83	2.5
Dodecane	2.70	1.62	2.01
Dodecane, 4-methyl-	-	-	-
Tridecane	1.29	0.64	0.65
Tetradecane	0.62	-	-
Tetradecane, 2-methyl-	-	-	-
Pentadecane	0.48	-	0.54
Heptadecane	0.81	-	-
<b>Total</b>	<b>33.99</b>	<b>22.25</b>	<b>24.09</b>

<b>Alkenes</b>	<b>Yield, wt%</b>		
	<b>RSO</b>	<b>WCO-A</b>	<b>WCO-B</b>
3-Methyl-3-hexene	-	-	0.44
1-Heptene, 5-methyl-	-	0.63	-
<b>Total</b>	<b>-</b>	<b>0.63</b>	<b>0.44</b>

<b>Aromatics</b>	<b>Yield, wt%</b>		
	<b>RSO</b>	<b>WCO-A</b>	<b>WCO-B</b>
Benzene	1.48	-	1.12
Toluene	4.16	3.9	3.68
Ethylbenzene	2.63	2.54	2.38
p-Xylene	4.64	5.46	4.09
o-Xylene	2.83	2.27	2.54
Benzene, propyl-	0.31	0.75	0.7
Benzene, 1-ethyl-3-methyl-	0.73	3.11	2.34
Benzene, 1-ethyl-2-methyl-	6.89	4.45	4.55
Benzene, (1-methylethyl)-	1.02	0.36	0.27
Mesitylene	1.22	-	1.02
Benzene, 4-ethyl-1,2-dimethyl		1.38	-
o-Cymene	-	0.67	-
Indane	0.65	0.58	0.55
Benzene, 1,4-diethyl-	0.98	0.69	0.5
Benzene, 1-methyl-3-propyl-	0.93	0.83	0.61
Benzene, 1-methyl-2-propyl-	0.72	1.15	0.92
Benzene, 1,2-diethyl-	1.4	1.04	1.23
Benzene, 2-ethyl-1,4-dimethyl-	0.42	0.56	1.11
Benzene, 1-methyl-4-propyl-	-	1.7	1.58
Benzene, 1-methyl-2-propyl-	0.39	-	-
Benzene, 1-ethyl-2,4-dimethyl-	-	0.73	0.36
Benzene, 1-ethenyl-3-ethyl-	-	-	0.29
Benzene, 1-ethenyl-4-ethyl-	-	0.37	-
Indan, 1-methyl-	0.31	0.98	0.87
Benzene, 1-methyl-4-(1-methylpropyl)-		0.36	0.28

1H-Indene, 2,3-dihydro-5-methyl-	0.48	0.6	0.46
Benzene, 1-methyl-4-(1-methylpropyl)-	0.27	1.10	1.14
Benzene, 1-methyl-2-(2-propenyl)-	-	1.24	0.95
Benzene, (1-methylbutyl)-	-	0.36	0.67
Benzene, 1-ethyl-4-(1-methylethyl)-	-	0.69	-
Benzene, 1-methyl-4-butyl	0.42	0.89	0.62
Naphthalene	1.05	2.60	2.50
Benzene, 1-methyl-4-(1-methyl-2-propenyl)-	0.97	0.33	0.27
1H-Indene, 2,3-dihydro-1,6-dimethyl-	0.62	1.89	1.21
2-Ethyl-2,3-dihydro-1H-indene		1.37	1.08
Benzene, 1-ethyl-2,4-dimethyl-	2.14	-	-
Benzene, 1-ethenyl-3-ethyl-	0.3	-	-
Benzene, 2-ethyl-1,4-dimethyl-		-	-
Benzene, 1-methyl-4-(1-methylpropyl)-	0.75	-	-
Benzene, 1-methyl-2-(2-propenyl)-	1.05	-	-
Benzene, 1,4-dimethyl-2-(2-methylpropyl)-	-	0.29	-
Naphthalene, 1-methyl-	-	2.52	3.41
Naphthalene, 2-methyl-	0.34	1.16	1.63
Naphthalene, 2-ethyl-	2.42	0.78	1.19
1-Methyl-2-n-hexylbenzene	-	-	0.2
Naphthalene, 1-propyl-	-	0.45	0.4
Naphthalene, 1,6-dimethyl-	1.15	1.11	1.4
Benzene, (1,3-dimethylbutyl)-	-	-	0.39
Naphthalene, 1,2,3,4-tetrahydro-5,7-dimethyl-	-	0.34	0.26
Naphthalene, 1,8-dimethyl-	0.37	0.8	1.25
Naphthalene, 2,6-dimethyl-	0.8	0.41	0.64
Naphthalene, 1,3-dimethyl-	-	-	0.22
Benzene, (1-methylheptyl)-	-	-	0.2
Benzene, (1-methyldecyl)-	-	0.36	-
Naphthalene, 2-(1-methylethyl)-	0.98	0.61	1.02
Fluorene	-	0.48	0.56
Naphthalene, 1,4,6-trimethyl-	-	-	0.26
Benzene, (1,3-dimethylbutyl)-	0.99	0.46	-
Bicyclo[4.2.1]nona-2,4,7-triene, 7-ethyl-	0.46	-	-
9H-Fluorene, 9-methyl-	0.43	0.64	1.12
Anthracene, 9,10-dihydro-2-methyl-	-	-	0.24
Phenanthrene	-	-	0.67
Phenanthrene, 2-methyl-	-	-	0.76
<b>Total</b>	<b>48.56</b>	<b>55.35</b>	<b>55.71</b>

The van Krevelen plots of the oil products from the cracking reactions with ZSM-5 at 400 °C for 1 h are shown Figure 7.30, which also include data for gasoline, kerosene and diesel fuels. The oils obtained from the three original feedstocks overlap on the y-axis of the plot and all had slightly lower H/C ratios than these conventional fuels due to their high aromatic contents.



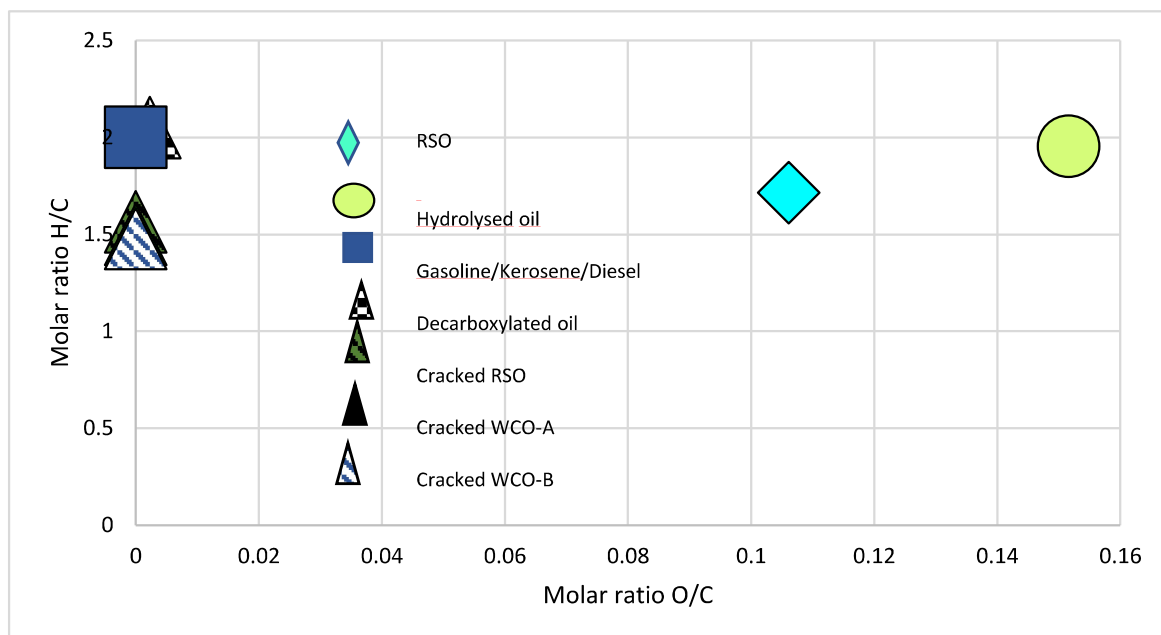
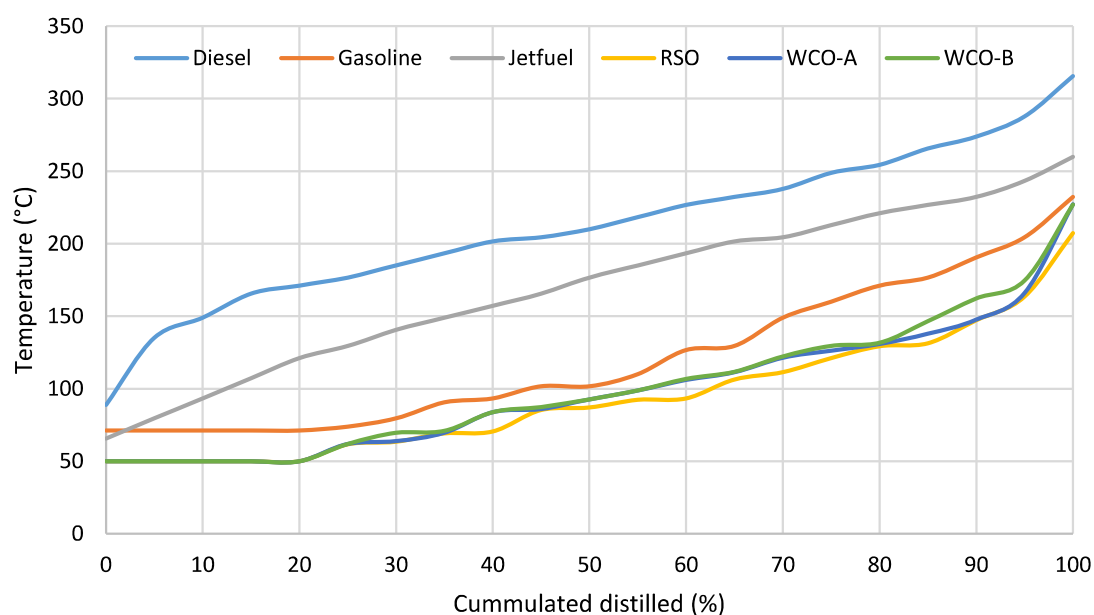


Figure 7.30: Van Krevelen plots of the oil products from cracking of decarboxylated WCOs in comparison with conventional fuels

Figure 7.31 compares the simulated distillation curves of the product oils obtained from the various feedstock sources with gasoline, kerosene, and diesel in order to assess their compatibility with conventional engine fuels. The boiling range distribution was 100% lower than those of all three standard fuels, according to the profile of the different oil products. The production of the gasoline fraction with a high percentage of aromatics is favoured by oils and fats with a relatively high yields of <C11 hydrocarbons (Araújo et al., 2017).



## 7.9 Improving yield of single ring aromatic compounds

Experiments were carried out at longer residence times up to 12 h to explore the possibility of producing oil with a lighter colour comparable to existing fuels. As expected, the mass balance closures presented in Table 7.17 shows a decrease with increase in time due to increased formation and loss of volatile compounds. There was negligible increase in char product after 6 h. However, there was an 85% increase in gas when reaction time increased from 1 h to 6 h but this slowed from 6 h to 12 with an increase was only about 11%. Figure 7.32 shows that the product oil did get slightly lighter after 6 h but after 12 h the oil became darker and more viscous. This could be due to a number of factors including polymerisation and oligomerisation, resulting in the occurrence of random reactions rather than selective reactions as the catalyst deactivated. Table 7.17 also shows the density of the oil increased at 12 h. This is possibly due to the formation of more 2 ring aromatic compounds, which are denser than single ring aromatic compounds. For example, naphthalene has a density of 1140 kg/m<sup>3</sup> and benzene has density of 876 kg/m<sup>3</sup>.

Table 7.17: Product distribution, mass balances and densities of oil product from the extended reaction times at 400 °C, 1 h with various catalysts

Time (h)	Product			Balance (wt%)	Density of oil (kg/m <sup>3</sup> )
	Solid (wt%)	Oil product (wt%)	Gas phase (wt%)		
1	1.99	82.55	1.99	87.18	916
6	4.30	66.73	3.70	74.75	914
12	4.00	63.40	4.10	71.53	947

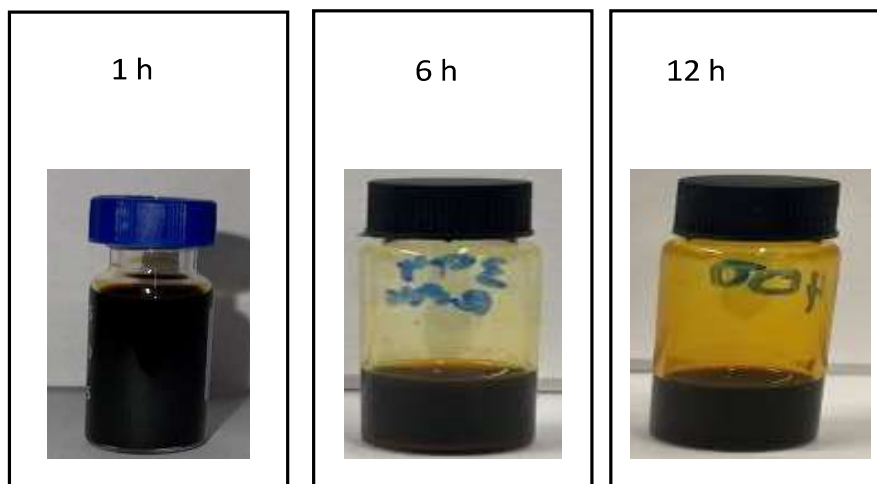


Figure 7.32: Appearance of liquid products from the cracking of decarboxylated oils with ZSM-5 at 400 °C, for longer reaction times

### 7.9.1 Chemical composition of oil products from cracking at extended residence times

The yields of the compounds identified from the oil obtained after cracking reactions for extended reaction times of up to 12 h have been compiled in Table 7.18. There was an 83.38% decrease in the alkanes identified at 1 h when reaction time increased to 6 h, and at 12 h there were no aliphatic compounds identified. Hence, there was an increase in the aromatic yield by 25.82 wt% at 6 h and 30.58 wt% at 12 h compared to yields at 1 h reaction time. This suggested that the increased reaction severity in terms of time promoted aromatisation reactions (Zhang et al., 2023). While the extended reaction time increased the yield of useful BTEX compounds, the yields of PAHs more than double between 6 h and 12 h reaction times. However, the middle aromatics comprising alkyl benzenes with longer chains of up to ten carbon atoms, completely disappeared and instead dialkylbenzenes and trialkylbenzenes became the dominant middle aromatics. Although, the BTEX compounds could be separated by simple distillation, there would be little justification for using extended reaction times for cracking the decarboxylated oil from lipids giving that significant yields of non-useful higher aromatics were also formed.

Table 7.18: List of compounds in the oil products obtained from cracking decarboxylated RSO for extended reaction times

Alkanes	Yield, wt %		
	1 h	6 h	12 h
Hexane, 3-methyl-	0.76	0.49	-
Heptane	4.19	1.12	-

Heptane, 2-methyl-	0.65	-	-
Heptane, 3-methyl-	0.72	-	-
Heptane, 2,4-dimethyl-	-	-	-
Octane	6.41	1.50	-
Nonane	6.5	1.28	-
Nonane, 3-methyl-	0.64	-	-
Decane	4.89	0.77	-
Undecane	3.32	0.48	-
Dodecane	2.7	-	-
Dodecane, 4-methyl-	-	-	-
Tridecane	1.29	-	-
Tetradecane	0.62	-	-
Tetradecane, 2-methyl-	-	-	-
Pentadecane	0.48	-	-
Hexadecane	-	-	-
Pentadecane, 7-methyl-	-	-	-
Pentadecane, 4-methyl-	-	-	-
Heptadecane	0.81	-	-
Heptadecane, 3-methyl-	-	-	-
Octadecane	-	-	-
Nonadecane	-	-	-
<b>Total</b>	<b>33.99</b>	<b>5.65</b>	<b>0</b>

<b>Aromatics</b>	<b>Yield, wt %</b>		
	<b>1 h</b>	<b>6 h</b>	<b>12 h</b>
<b>BTX compounds</b>			
Benzene	1.48	1.63	1.10
Toluene	4.16	6.79	7.21
Xylene	7.47	8.44	11.36
<b>Total</b>	<b>13.11</b>	<b>16.86</b>	<b>19.68</b>

<b>Other single ring compounds</b>	<b>1 h</b>	<b>6 h</b>	<b>12 h</b>
Ethylbenzene	2.63	2.47	2.36
Benzene, 1,3-dimethyl-	-	2.67	-
Benzene, propyl-	0.31	0.52	0.51
Benzene, (1-methylethyl)-	1.02	0.30	0.36
Benzene, 1-ethyl-3-methyl-	0.73	3.63	3.91
Benzene, 1-ethyl-2-methyl-	6.89	1.47	1.01
Benzene, 1-ethyl-4-methyl-	-	-	1.47
Mesitylene	1.22	3.70	3.14
o-Cymene	-	-	0.75
Indane	0.65	0.37	0.37
Benzene, 1,2,4-trimethyl-	-	0.51	-
Benzene, 1-ethyl-2-methyl-	-	1.96	-
Benzene, 1,4-diethyl-	0.98	0.51	0.46

Benzene, 1-methyl-2-propyl-	1.11	2.10	1.80
Benzene, 1-methyl-3-propyl-	0.93	-	-
Benzene, 1,2-diethyl-	1.4	0.35	0.31
Benzene, 2-ethyl-1,4-dimethyl-	0.42	1.03	1.25
Benzene, 1-ethyl-2,4-dimethyl-	-	0.39	0.39
Benzene, 1-ethenyl-3-ethyl-	-	0.25	0.20
Benzene, 1-ethyl-3,5-dimethyl-	-	0.77	0.41
Benzene, 1-ethyl-2,4-dimethyl-	2.14	-	-
Indan, 1-methyl-	0.31	0.71	0.63
1H-Indene, 2,3-dihydro-5-methyl-	0.48	0.48	0.53
Benzene, 1-ethyl-4-(1-methylethyl)-	0.85	-	0.29
Benzene, 1-methyl-4-(1-methylpropyl)-	0.27	-	-
Benzene, 1,3-diethyl-5-methyl-	-	0.30	-
Benzene, (1,1-dimethylpropyl)-	-	0.49	0.41
Benzene, (1,2-dimethylpropyl)-	-	0.30	-
Benzene, 1-ethyl-2,4,5-trimethyl-	-	0.77	-
Benzene, 1-methyl-2-(2-propenyl)-	1.05	0.87	0.98
Benzene, 1-ethenyl-3-ethyl-	0.3	-	-
Benzenepropanal, .beta.-methyl-	-	-	0.22
Benzene, 1-methyl-4-(1-methyl-2-propenyl)-	0.97	0.25	0.22
Benzene, 1-methyl-4-butyl	0.42	-	-
Benzene, 1,4-diethyl-2-methyl-	-	-	0.27
1H-Indene, 2,3-dihydro-4,7-dimethyl-	0.62	0.28	0.26
1H-Indene, 2,3-dihydro-1,6-dimethyl-	-	0.72	1.01
2-Ethyl-2,3-dihydro-1H-indene	-	-	0.61
Benzene, 1,2,4-triethyl-	-	-	0.33
Benzene, 1-methyl-4-(1-methylpropyl)-	0.75	-	-
2-Ethyl-2,3-dihydro-1H-indene	-	0.49	-
Benzene, (1,3-dimethylbutyl)-	0.99	0.26	-
1H-Indene, 2,3-dihydro-4-propyl-	-	-	0.25
Bicyclo[4.2.1]nona-2,4,7-triene, 7-ethyl-	0.46	-	-
<b>Total</b>	<b>27.9</b>	<b>28.92</b>	<b>24.73</b>

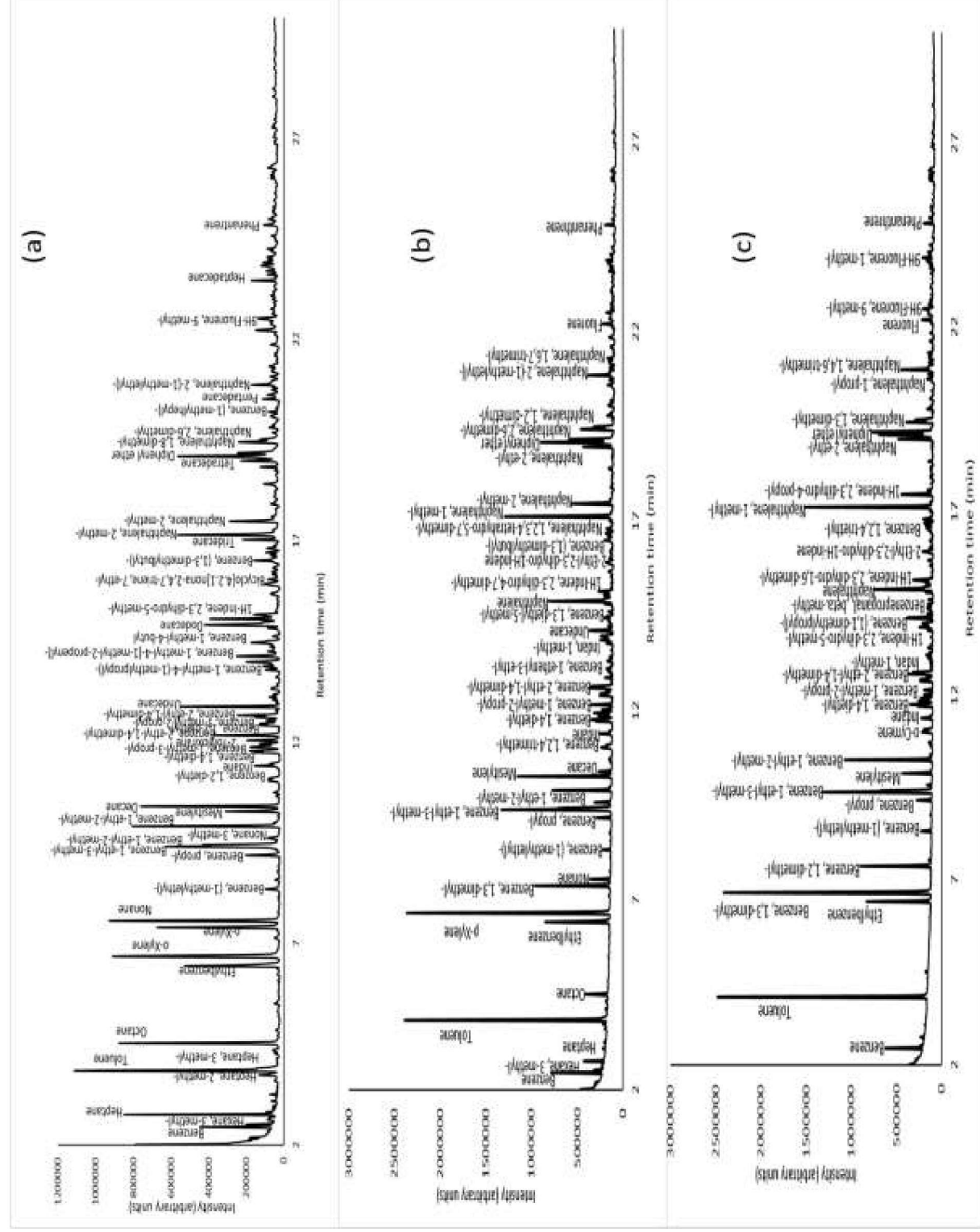
<b>Naphthalenes and alkyl naphthalenes</b>	<b>1 h</b>	<b>6 h</b>	<b>12 h</b>
Naphthalene	1.05	2.71	2.75
Naphthalene, 1,2,3,4-tetrahydro-	-	-	0.49
Naphthalene, 1,2,3,4-tetrahydro-5,7-dimethyl-	-	0.27	0.41
Naphthalene, 1-methyl-	-	5.21	5.80
Naphthalene, 2-methyl-	0.34	-	-
Naphthalene, 2-ethyl-	2.42	1.01	1.17
Naphthalene, 2,6-dimethyl-	-	2.65	2.67
Naphthalene, 1,2-dimethyl-	-	1.29	1.10
Naphthalene, 1,6-dimethyl-	1.15	-	-
Naphthalene, 2,6-dimethyl-	0.8	-	0.72
Naphthalene, 1,3-dimethyl-	-	-	0.21

Naphthalene, 2-(1-methylethyl)-	0.98	0.82	0.37
Naphthalene, 1,4,6-trimethyl-	-	0.25	0.27
Naphthalene, 1-propyl-	-	-	0.20
Naphthalene, 2-(1-methylethyl)-	-	-	1.12
Naphthalene, 1,6,7-trimethyl-	-	0.37	-
Naphthalene, 1,8-dimethyl-	0.37	-	-
<b>Total</b>	<b>7.12</b>	<b>14.59</b>	<b>17.28</b>

<b>Fluorene +</b>	<b>1 h</b>	<b>6 h</b>	<b>12 h</b>
Fluorene	-	0.39	0.38
9H-Fluorene, 1-methyl-	-	-	0.34
9H-Fluorene, 9-methyl-	0.43	-	0.61
Phenanthrene	-	0.33	0.38
<b>Total</b>	<b>0.43</b>	<b>0.73</b>	<b>1.72</b>

Figure 7.33 shows the GC/MS chromatograms for the oil products obtained from the cracking of decarboxylated RSO at 1 h, 6 h, and 12 h reaction times. The conversion of all aliphatics to aromatics when reaction time increased from 6 h to 12 h actually favoured the production of PAHs, which may explain the increased viscosity and density as well as the darker colour of the final oil product. The minimal change in the oil yield reported in Table 7.17 in comparison with Table 7.18 implies that increasing reaction time from 6 to 12 h there was negligible impact on the yield of the product oil, instead there was greater effect on the chemical compositions.



Parameter	Dependent variables tested	Independent variables	Summary of main findings
Temperature	400 °C (no catalyst) 450 °C (no catalyst) 400 °C (with ZSM-5) 450 °C (with ZSM-5)	Feed: 10 g oil Reaction time: 1 h Catalyst: 1 g	<p>The investigation into hydrocarbon cracking, focusing on the impact of temperature and the ZSM-5 catalyst, revealed notable outcomes. The presence of ZSM-5 led to lower mass balance closures, emphasising its influence on product distribution. Temperature increase and catalyst utilisation resulted in augmented gas and solid products at the expense of oil yields (Table 7.3). Gas composition was notably affected by ZSM-5, particularly in the production of C<sub>3</sub> – C<sub>4</sub> hydrocarbons, highlighting the catalyst's superior impact over temperature (Fig 7.3). Physico-chemical analysis of liquid products indicated a decrease in calorific values with the catalyst (Table 7.4), aligning with the generation of lighter compounds (Fig 7.4). A comparison of non-catalytic and catalytic tests at 400 °C indicated a notable increase in aromatic content with the presence of ZSM-5, making aromatic hydrocarbons the dominant compounds. At 450 °C, ZSM-5 induced a more dramatic rise in aromatic yields (Fig 7.4). Figure 7.5 further illustrates the yields of heptadecane and various hydrocarbons in oil products, revealing a substantial decrease in heptadecane and diesel range compounds with ZSM-5 at 400 °C. Simulated distillation curves suggested that the catalysed reaction at 400 °C exhibited a profile closely resembling gasoline, indicating potential compatibility with conventional engine fuels (Fig 7.7). Overall, the study demonstrated the pivotal role of ZSM-5 in influencing the composition and characteristics of cracked hydrocarbons, presenting promising prospects for generating high-quality liquid fuels.</p>
Catalyst type	ZSM-5 Zeolite Y	Feed: 10 g oil Temperature: 450	<p>In this section, the results of catalytic cracking of decarboxylated oil are presented using different catalysts. In comparison with ZSM-5, all other catalysts produced higher oil yields, lower gases, and similar or higher solid yields. Zeolite Y, MCM-41, and Ru/Al<sub>2</sub>O<sub>3</sub> showed higher mass balance closures</p>



	MCM-41 Ru/Al <sub>2</sub> O <sub>3</sub>	<p>°C Reaction time: 1 h Catalyst: 1 g</p>	<p>indicating less volatility in the oil products (Table 7.6). The gas composition varied among catalysts, with ZSM-5 producing the most gases, dominated by propane (Fig 7.9). Chemical composition analysis revealed that ZSM-5 and MCM-41 had stronger selectivity towards aromatics than Zeolite Y and Ru/Al<sub>2</sub>O<sub>3</sub> (Fig 7.10). ZSM-5 showed the greatest cracking effect, producing hydrocarbons within the gasoline and kerosene range (Fig 7.11). Van Krevelen plot (Fig 7.12) and simulated distillation curve (Fig 7.13) further supported the potential of the oil products for use as gasoline and kerosene fuels, though further processing may be needed to remove soot-forming PAHs.</p>
Time (h)  0, 0.5, 1, 2		<p>Feed: 10 g oil Temperature: 400 °C Catalyst: 1 g ZSM-5</p>	<p>These experiments focused on the impact of varying reaction times (0-2 h). It was observed as reaction time increased, there was a decline in mass balance closures, with a decrease in liquid products and increase in gas and solid products (Table 7.11). Gas analysis revealed a notable selectivity towards propane, with increased yields and calorific values with increased reaction severity (Fig 7.17). GC/MS analysis showed a shift towards aromatics in the liquid products, with a consistent growth in aromatic yield as reaction time increased (Fig 7.18). The liquid fuels were characterised using van Krevelen diagrams, indicating a decrease in H/C ratios with time (Fig 7.20). Simulated distillation curves showed a shift towards lower boiling points with increasing reaction time, suggesting the potential for better blending with other fractions to enhance fuel properties (Fig 7.21). This study selected the 1 h reaction time as the optimum condition, considering both composition and yield, despite longer reaction times resulting in higher yields of kerosene-range compounds, which could adversely affect combustion efficiency and promote harmful particulate matter formation.</p>
Lipid feedstock		<p>Feed: 10 g oil Reaction time: 1 h</p>	<p>Following the compilation of the results obtained from each parametric study, these optimum conditions were tested with the WCOs. The product yields distribution from the cracking of decarboxylated oils</p>

	<p>Temperature: 400 °C</p> <p>Catalyst: 1 g ZSM-5</p>	<p>derived from WCOs in comparison with RSO were quite similar (Table 7.14) . The use of ZSM-5 catalyst at 400 °C increased liquid yields, and all products exhibited dark coloration similar to RSO-derived oil (Fig 7.26). Figure 7.27 displays gas yields from WCO cracking, dominated by saturated hydrocarbons, suggesting the transformation of longer chains into shorter ones, with their gas calorific values closely matching those from RSO. The cracking process effectively converted WCOs into fuel-range hydrocarbons, as shown in Figures 7.28 and 7.29. Alkane yields decreased, while aromatics increased compared to RSO, possibly due to WCOs' original composition. Table 7.16 details the composition of cracked WCOs and RSO oils, indicating similarities in the spectrum of hydrocarbons. Van Krevelen plots (Figure 7.30) show slightly lower H/C ratios for the product oils than conventional fuels, owing to their high aromatic content. Simulated distillation curves (Figure 7.31) reveal compatibility with conventional engine fuels, emphasising the potential of cracked WCOs as alternatives to conventional hydrocarbon fuels.</p>
--	---	--

Table 7.19: Summary table showing compiled results of cracking experiments

To conclude, in order to increase the yields of aromatics in the oil product, experiments were carried out varying time, temperature, catalyst type, and catalyst loading (Table 7.19). Similarly, to Chapters 5 and 6, analysis of the oil products was done with CHNS and GC/MS, and analysis tools such as Van Krevelen and simulated distillation being employed. Even though increasing the severity of the reactions in terms of time and temperature favoured aromatics formation, the optimum reaction conditions were 400 °C for 1 h with 1 g ZMS-5. This increased the aromatic content of the oil by almost seven folds. Tests were also carried out at longer reaction times, and this favoured the formation of PAHs. However, these conventional fuels, gasoline and kerosene, are dominated by monocyclic aromatics rather than PAHs, which makes the extended reaction times less attractive to this research project.

## 7.10References

- Abu-Jrai, A., Rodríguez-Fernández, J., Tsolakis, A., Megaritis, A., Theinnoi, K., Cracknell, R. F., and Clark, R. H. (2009). Performance, combustion and emissions of a diesel engine operated with reformed EGR. Comparison of diesel and GTL fuelling. *Fuel*, 88(6), 1031–1041. <https://doi.org/10.1016/j.fuel.2008.12.001>.
- Amaral, L. V., Santos, N. D. S. A., Roso, V. R., Sebastião, R. d. C. d. O., and Pujatti, F. J. P. (2021). Effects of gasoline composition on engine performance, exhaust gases and operational costs. *Renewable and Sustainable Energy Reviews*, 135, 110196. <https://doi.org/10.1016/j.rser.2020.110196>.
- 10.1016/j.renene.2016.09.058.
- Anh Tuyen, L., Quang Hung, N., Chi Cuong, L., Duy Khiem, D., Trong Phuc, P., Ly Nguyen, L., Ngoc Hue, N. T., Thi Hue, P., & Van Phuc, D. (2017). Simultaneous existence of defects and mesopores in nanosized ZSM-5 zeolite studied by positron annihilation and X-ray diffraction spectroscopies. *Journal of Applied Physics*, 121(8), 084303. <https://doi.org/10.1063/1.4977013>.
- Baskaran, T., Joshi, A., Kamalakar, G., and Sakthivel, A. (2016). A solvent free method for preparation of  $\beta$ -amino alcohols by ring opening of epoxides with amines using MCM-22 as a catalyst. *Applied Catalysis A: General*, 524, 50–55. <https://doi.org/10.1016/j.apcata.2016.05.029>.
- Buzetzkı, E., Sidorová, K., Cvengrošová, Z., Kaszonyi, A., and Cvengroš, J. (2011). The influence of zeolite catalysts on the products of rapeseed oil cracking. *Fuel Processing Technology*, 92(8), 1623–1631. <https://doi.org/10.1016/j.fuproc.2011.04.009>.
- de Jong, E. and Gosselink, R.J.A. (2014) 'Lignocellulose-based chemical products', *Bioenergy Research: Advances and Applications*, pp. 277–313. doi:10.1016/b978-0-444-59561-4.00017-6.
- Eghbali, P., Şahin, E. and Masteri-Farahani, M. (2016) 'Immobilization of a molybdenum-glycine Schiff base complex within the nanocages of zeolite Y with flexible ligand method', *Journal of Porous Materials*, 24(1), pp. 39–44. doi:10.1007/s10934-016-0234-8.
- Fovanna, T., Campisi, S., Villa, A., Kambolis, A., Peng, G., Rentsch, D., Kröcher, O., Nachttegaal, M., and Ferri, D. (2020). Ruthenium on phosphorous-modified alumina as an effective and stable catalyst for catalytic transfer hydrogenation of furfural. *RSC Advances*, 10(19), 11507–11516. <https://doi.org/10.1039/d0ra00415d>.
- Fuels - higher and lower calorific values Engineering ToolBox. Available at: [https://www.engineeringtoolbox.com/fuels-higher-calorific-values-d\\_169.html](https://www.engineeringtoolbox.com/fuels-higher-calorific-values-d_169.html).

- Ge, S., Ganesan, R., Sekar, M., Xia, C., Shanmugam, S., Alsehli, M., and Brindhadevi, K. (2022). Blending and emission characteristics of biogasoline produced using CaO/SBA-15 catalyst by cracking used cooking oil. *Fuel*, 307, 121861. <https://doi.org/10.1016/j.fuel.2021.121861>.
- Guo, T., Ma, X., Li, Z., Zheng, L., Fan, Q., Ding, X., Hu, S., and Fu, P. (2022). Enhancing high selectivity production of light aromatics from in-situ catalytic upgrading of cellulose pyrolysis vapors by regulating hierarchical core-shell ZSM-5@MCM-41. *Journal of Analytical and Applied Pyrolysis*, 105774. <https://doi.org/10.1016/j.jaap.2022.105774>.
- Hagmann, C. and Richards, P.L. (1995) 'Specific heat of stainless steel', *Cryogenics*, 35(5), p. 345. doi:10.1016/0011-2275(95)95355-i.
- Hasan, A. O., Al-Rawashdeh, H., Abu-jrai, A., Gomaa, M. R., and Jamil, F. (2022). Impact of variable compression ratios on engine performance and unregulated HC emitted from a research single cylinder engine fueled with commercial gasoline. *International Journal of Hydrogen Energy*. <https://doi.org/10.1016/j.ijhydene.2022.09.025>.
- Isa, K. M., Snape, C. E., Uguna, C., Meredith, W., and Deng, H. (2016). Pyrolysis oil upgrading in high conversions using sub- and supercritical water above 400 °C. *Journal of Analytical and Applied Pyrolysis*, 119, 180–188. <https://doi.org/10.1016/j.jaap.2016.03.004>.
- Jin, F., Yan, Y. and Wu, G. (2020) 'Ethylene oligomerization over H- and ni-form aluminosilicate composite with ZSM-5 and MCM-41 structure: Effect of acidity strength, nickel site and porosity', *Catalysis Today*, 355, pp. 148–161. doi:10.1016/j.cattod.2019.06.050.
- Kostyniuk, A., Bajec, D. and Likozar, B. (2021) 'Catalytic hydrogenation, hydrocracking and isomerization reactions of biomass tar model compound mixture over ni-modified zeolite catalysts in packed bed reactor', *Renewable Energy*, 167, pp. 409–424. doi:10.1016/j.renene.2020.11.098.
- Kraiem, T., Hassen, A. B., Belayouni, H., and Jeguirim, M. (2016). Production and characterization of bio-oil from the pyrolysis of waste frying oil. *Environmental Science and Pollution Research*, 24(11), 9951–9961. <https://doi.org/10.1007/s11356-016-7704-z>.
- Krisyuningsih Krisnandi, Y., Nurani, D., Reza, M., Samodro, B., Suwardiyanto, Susianto, N., Putrananda, A., Saragi, I., Umar, A., Choi, S., Howe, R. (2019) "Partial oxidation of methane to methanol on cobalt oxide-modified hierarchical ZSM-5," *Biogas - Recent Advances and Integrated Approaches* [Preprint]. Available at: <https://doi.org/10.5772/intechopen.86133>.

- Li, P., Shi, X., Wang, X., Song, J., Fang, S., Bai, J., Zhang, G., Chang, C., and Pang, S. (2021). Bio-oil from biomass fast pyrolysis: Yields, related properties and energy consumption analysis of the pyrolysis system. *Journal of Cleaner Production*, 328, 129613. <https://doi.org/10.1016/j.jclepro.2021.129613>.
- Londoño Fera, J.M., Nausa Galeano, G.A. and Malagón-Romero, D.H. (2021) 'Production of Bio-oil from waste cooking oil by pyrolysis', *Chemical Engineering and Technology*, 44(12), pp. 2341–2346. doi:10.1002/ceat.202100018.
- Maher, K.D. and Bressler, D.C. (2007) 'Pyrolysis of triglyceride materials for the production of renewable fuels and chemicals', *Bioresource Technology*, 98(12), pp. 2351–2368. doi:10.1016/j.biortech.2006.10.025.
- NIST Office of Data and Informatics (no date) *Nitrogen*. Available at: <https://webbook.nist.gov/cgi/cbook.cgi?ID=C7727379&Type=JANAFG&Plot=on#JANAFG> (Accessed: 30 October 2023).
- Nguyen, T. S., Zabeti, M., Lefferts, L., Brem, G., and Seshan, K. (2013). Catalytic upgrading of biomass pyrolysis vapours using faujasite zeolite catalysts. *Biomass and Bioenergy*, 48, 100–110. <https://doi.org/10.1016/j.biombioe.2012.10.024>.
- Ono, Y. (1992) 'Transformation of lower alkanes into aromatic hydrocarbons over ZSM-5 Zeolites', *Catalysis Reviews*, 34(3), pp. 179–226. doi:10.1080/01614949208020306.
- Onwudili, J.A. and Williams, P.T. (2013) 'Hydrogen and methane selectivity during alkaline supercritical water gasification of biomass with ruthenium-alumina catalyst', *Applied Catalysis B: Environmental*, 132–133, pp. 70–79. doi:10.1016/j.apcatb.2012.11.033.
- Pan, H., Zhou, X., Xie, S., Du, Z., Li, G., Zhang, C., Luo, Y., and Zhang, X. (2022). Selective production of monocyclic aromatic hydrocarbon from agricultural waste wheat straw for aviation fuel using Ni/ZSM-5 catalyst. *Biomass and Bioenergy*, 165, 106592. <https://doi.org/10.1016/j.biombioe.2022.106592>.
- Pandya, R., Mane, R. and Rode, C.V. (2018) "Cascade dehydrative amination of glycerol to oxazoline," *Catalysis Science and Technology*, 8(11), pp. 2954–2965. Available at: <https://doi.org/10.1039/c8cy00185e>.
- Qian, M., Zhao, Y., Huo, E., Wang, C., Zhang, X., Lin, X., Wang, L., Kong, X., Ruan, R., and Lei, H. (2022). Improving catalytic production of aromatic hydrocarbons with a mesoporous ZSM-5 modified with nanocellulose as a green template. *Journal of Analytical and Applied Pyrolysis*, 166, 105624. <https://doi.org/10.1016/j.jaap.2022.105624>.

Rahimi, N. and Karimzadeh, R. (2011) 'Catalytic cracking of hydrocarbons over modified ZSM-5 zeolites to produce light olefins: A Review', *Applied Catalysis A: General*, 398(1–2), pp. 1–17. doi:10.1016/j.apcata.2011.03.009.

Reijnders, J., Boot, M. and de Goey, P. (2016) 'Impact of aromaticity and cetane number on the soot-nox trade-off in conventional and low temperature combustion', *Fuel*, 186, pp. 24–34. doi:10.1016/j.fuel.2016.08.009.

Rosman, N., Harun, Z., & Jamalludin, M. R. (2014). The Characteristic of Synthesized Zeolite Rice Husk Particles via Different Routes. *Jurnal Teknologi*, 69(9).  
<https://doi.org/10.11113/jt.v69.3410>.

Salahudeen, N., Ahmed, A. S., Al-Muhtaseb, A. H., Jibril, B. Y., Al-Hajri, R., Waziri, S. M., Dauda, M., & Al-Sabahi, J. (2015). Microwave-Assisted Adsorptive Desulfurization of Model Diesel Fuel Using Synthesized Microporous Rare Earth Metal-Doped Zeolite Y. *The Journal of Engineering Research [TJER]*, 12(1), 44.  
<https://doi.org/10.24200/tjer.vol12iss1pp44-52>.

Sankaranarayanan, T. M., Kreider, M., Berenguer, A., Gutiérrez-Rubio, S., Moreno, I., Pizarro, P., Coronado, J. M., and Serrano, D. P. (2018). Cross-reactivity of guaiacol and propionic acid blends during hydrodeoxygenation over Ni-supported catalysts. *Fuel*, 214, 187–195. <https://doi.org/10.1016/j.fuel.2017.10.059>.

Santos, J.C. *et al.* (2005) 'Comparative study of specific heat capacities of some vegetable oils obtained by DSC and microwave oven', *Journal of Thermal Analysis and Calorimetry*, 79(2), pp. 283–287. doi:10.1007/s10973-005-0050-x.

Singh, O., Sharma, T., Ghosh, I., Dasgupta, D., Vempatapu, B. P., Hazra, S., Kustov, A. L., Sarkar, B., and Ghosh, D. (2019). Converting Lignocellulosic Pentosan-Derived Yeast Single Cell Oil into Aromatics: Biomass to Bio-BTX. *ACS Sustainable Chemistry and Engineering*, 7(15), 13437–13445. <https://doi.org/10.1021/acssuschemeng.9b02851>.

Singh, O., Agrawal, A., Dhiman, N., Vempatapu, B. P., Chiang, K., Tripathi, S., and Sarkar, B. (2021). Production of renewable aromatics from jatropha oil over multifunctional ZnCo/ZSM-5 catalysts. *Renewable Energy*, 179, 2124–2135.  
<https://doi.org/10.1016/j.renene.2021.08.011>.

Staffell, I. (2011) The Energy and Fuel Data Sheet. Available at: [https://www.claverton-energy.com/wordpress/wp-content/uploads/2012/08/the\\_energy\\_and\\_fuel\\_data\\_sheet1.pdf](https://www.claverton-energy.com/wordpress/wp-content/uploads/2012/08/the_energy_and_fuel_data_sheet1.pdf) (Accessed: January 2023).

Stauffer, E., Dolan, J.A. and Newman, R. (2008) 'Chemistry and physics of fire and liquid fuels', *Fire Debris Analysis*, pp. 85–129. doi:10.1016/b978-012663971-1.50008-7.

Suryawanshi, Y. R., Chakraborty, M., Jauhari, S., Mukhopadhyay, S., Shenoy, K. T., and Sen, D. (2015). Selective hydrogenation of Dibenzo-18-crown-6 ether over highly active monodisperse Ru/ $\gamma$ -Al<sub>2</sub>O<sub>3</sub> nanocatalyst. *Bulletin of Chemical Reaction Engineering and Catalysis*, 10(1). <https://doi.org/10.9767/bcrec.10.1.7141.23-29>.

Tree, D.R. and Svensson, K.I. (2007) 'Soot processes in compression ignition engines', *Progress in Energy and Combustion Science*, 33(3), pp. 272–309.  
doi:10.1016/j.pecs.2006.03.002.

U.S. Energy Information Administration, E. (2012) Crude oil distillation and the definition of refinery capacity, Homepage - U.S. Energy Information Administration (EIA). Available at: <https://www.eia.gov/todayinenergy/detail.php?id=6970> (Accessed: 21 March 2023).

Wang, P., Xiao, X., Pan, Y., Zhao, Z., Jiang, G., Zhang, Z., Meng, F., Li, Y., Fan, X., Kong, L., and Xie, Z. (2022). Facile Synthesis of Nanosheet-Stacked Hierarchical ZSM-5 Zeolite for Efficient Catalytic Cracking of n-Octane to Produce Light Olefins. *Catalysts*, 12(3), 351. <https://doi.org/10.3390/catal12030351>.

Xie, Y., Zhang, Y., He, L., Jia, C. Q., Yao, Q., Sun, M., and Ma, X. (2023). Anti-deactivation of zeolite catalysts for residue fluid catalytic cracking. *Applied Catalysis A: General*, 119159. <https://doi.org/10.1016/j.apcata.2023.119159>.

Yuan, H., Li, C., Shan, R., Zhang, J., and Chen, Y. (2023). Aromatics production from catalytic pyrolysis of waste cassava residue using La and P modified ZSM-5: Experimental and kinetic study. *Industrial Crops and Products*, 198, 116753. <https://doi.org/10.1016/j.indcrop.2023.116753>.

Zhang, C., Kwak, G., Park, H.-G., Jun, K.-W., Lee, Y.-J., Kang, S. C., and Kim, S. (2019). Light hydrocarbons to BTEX aromatics over hierarchical HZSM-5: Effects of alkali treatment on catalytic performance. *Microporous and Mesoporous Materials*, 276, 292–301. <https://doi.org/10.1016/j.micromeso.2018.10.005>.

Zhang, J., Ma, M., Chen, Z., Zhang, X., Yang, H., Wang, X., Feng, H., Yu, J., and Gao, S. (2023). Production of monocyclic aromatics and light olefins through ex-situ catalytic pyrolysis of low-density polyethylene over Ga/P/ZSM-5 catalyst. *Journal of the Energy Institute*, 101235. <https://doi.org/10.1016/j.joei.2023.101235>.



## 8 Conclusion and future work

The goal of this research project was to create a unique, three-stage process for converting triglycerides into high yields of liquid hydrocarbon fuels, which may then be used to produce a significant amount of aviation fuel without the need for hydrogen. This technique will involve cracking reactions, decarboxylation, and hydrothermal hydrolysis. The significant hydrogen gas consumption required to deoxygenate the available biomass-derived feedstocks for conversion is one of the main obstacles to the production of biojet fuels. The objective is to discover a different, hydrogen-free process that can generate large amounts of liquid hydrocarbons. This approach is expected to lower the cost of converting biomass-derived feedstocks into alternative sustainable hydrocarbon fuels, which may be used to produce SAF. The technical advancement of the processing route will be the main emphasis of this endeavour. In order to commence tests, an in-depth literature review was carried out in Chapter 2 on the development of biojet fuels from biomass-based feedstocks. This highlighted the five SAF technologies and their relative properties that are currently ASTM approved. This showed that there is still a substantial difference, especially between the fuels obtained through these ASTM approved technologies, and the commercially available, fossil-derived jet fuel (Jet-A). In addition to this, a review was also carried out the research that has been done on conversion of biomass-derived feedstocks to jet fuel range hydrocarbons. This review included the various feedstock sources, reaction conditions, as well the yields obtained.

The methodology in Chapter 3 was designed to cover the conversion of both fresh and used for cooking vegetable oils. The process included hydrolysis to convert the vegetable oil to fatty acids, decarboxylation to convert the fatty acids into hydrocarbons by removing oxygen in the form of carbondioxide, and cracking to hydrocarbons in the gasoline and jet fuel range, with more focus on alkanes and aromatics. Various analytical methods were employed such as titration, TGA, XRD, porosimetry, CHNS, GC/MS, and GC/FID. The findings of the tests carried out in each chapter have been summarised in the following sections.

### 8.1 Conclusion to results chapters

In chapter 4, various characterisation methods including TGA, acid-base titration and GC/MS were employed to analyse the three samples and their main hydrolysis products in this work. In particular, the use of TGA for characterisation has been successful in showing the three stages of degradation or volatilisation of the liquid samples. These were categorised as Stage I (glycerol-rich), Stage II (free fatty acid-rich) and Stage III (lipids-rich). The TGA

thermograms showed that Stage III components had the highest proportions in the feedstocks. In contrast, GC/MS was only capable of analysing FAMES after a simple but incomplete esterification process, while acid-base titration gave the yields of free fatty acids in the feedstocks.

Hydrolysis of the three samples were achieved under subcritical water (hydrothermal) conditions under 1 h reaction time in a stirred batch reactor, after optimisation using rapeseed. In the absence of any external catalyst, hydrothermal hydrolysis was found to be highly effective in producing fatty acids from lipids. The optimum set of conditions for hydrolysis was found to be a temperature of 300 °C, sample - water mass ratio of 1:2 and reaction time of 1 h to give quantitative yields of fatty acids. The set of optimised conditions was used to prepare fatty acids for the decarboxylation stage, which is the next stage in the process to produce hydrocarbons from lipid feedstocks.

In chapter 5, the decarboxylation of the hydrolysis products (mainly fatty acids) obtained from the optimum hydrolysis conditions was attempted in this chapter. Clearly, the parametric studies showed that temperature, reaction time and the use of catalysts could have a profound effect on the extent of decarboxylation. Initial results showed that increased in temperature led to increased deoxygenation, but this was not very selective towards decarboxylation as many different gases were formed indicating evidence of random C-C bond breaking and product formation. The use of commercial Pt/C catalyst confirmed literature reports of its efficiency in decarboxylation of fatty acids. Beyond this, the present work has shown that the catalysts can be effective in the controlled cracking of long chain hydrocarbons to produce significant yields of gasoline, jet fuel and diesel range liquid products. The physico-chemical properties of the liquid product were like those of common fuels from the parametric studies but on the liquid products from Pt/C and at higher reaction severities (400 °C and reaction times > 1 h) could produce clear liquid products that looked and smelt like hydrocarbon fuels. The chosen reaction conditions in this work seemed to minimise both char and gas formation and favoured the production of liquid hydrocarbon fuels. The optimum set of conditions for the decarboxylation of the RSO-derived fatty acids to produce a liquid product dominated by alkanes was: 10 g of hydrolysed product, 2 g of catalyst, 400 °C, and 2 h reaction time. While complete decarboxylation was achieved and high yields of hydrocarbons (mostly alkanes) obtained, the resulting liquid product still contained significantly fewer aromatic compounds compared to standard Jet-A fuel. Therefore, further attempts would be made in subsequent chapters in this work to address this deficiency.

In chapter 6, several experiments have been carried out in attempts to produce gasoline and jet fuel range liquid hydrocarbons through simultaneous catalytic decarboxylation and cracking of hydrolysed vegetable oils using Pt-based catalyst. Reactions were carried out with RSO at 420 °C and 450 °C for 1 h in the presence of 5 wt% Pt/C. Near complete decarboxylation was achieved at 450 °C, yielding an oil with 2.34 wt% acid content compared with the no-catalysed reaction, which gave acid yield of nearly 23%. Other Pt-based catalysts (Pt/MgSilicate and Pt/Al<sub>2</sub>O<sub>3</sub>) on supports that could be much easily regenerated were compared with Pt/C under the same reaction conditions, but they achieved lower results in terms of decarboxylation, even though Pt/Al<sub>2</sub>O<sub>3</sub> produced an oil with high gasoline range compounds. Furthermore, the influence of reaction time was investigated at 450 °C from 0 h – 2 h with the Pt/C catalyst and although, the reaction at 2 h produced more gasoline and jet fuel hydrocarbons, the yields of essential aromatics reduced. Hence the use of 2 h rather than 1 h was not found to be justifiable. Hydrolysis products from real-world waste cooking oils were also subjected to the same reactions as the hydrolysed RSO and the oil products were in many ways similar to those of the fresh vegetable oils, confirming that WCOs could be used in this process without problems. The reusability test of the 5 wt% Pt/C catalyst over three cycles showed rapid deactivation occurred, which could be attributed to the increased formation of char, which made the catalyst surface inaccessible. Giving that Pt/C catalysts are not easily regenerated by calcination or carbon-burn-off, the use of supports that could easily be regenerated would be an important consideration for future work.

In chapter 7, the production of aromatics through catalytic cracking of feedstock produced in Chapter 6 by decarboxylation and cracking of hydrolysed RSO at 450 °C for 1 h with Pt/C. The oil products were analysed using GC/MS. The parametric studies were carried out varying temperature, time, catalyst type, and catalyst loading, and these all had considerable impacts on the production of aromatics. The results showed that increasing reaction severity in terms of time and temperature favoured the production of aromatics. Tests were carried out at longer reaction times, up to 12 h, and these showed substantial increase in the yield of BTX compounds. However, the high energy cost does not compensate these outputs. Additionally, zeolites are commonly used in literature for cracking in the petroleum industry, and the findings support this as ZSM-5 had the highest selectivity towards aromatics. Analysis tools such as the Van Krevelen, and simulated distillation were explored to assess the oxygen to carbon ratios, and boiling points of the product oils respectively. The simple distillation was carried out to extract clear oil that looks more like commercial fuels. Even though this separation was successful, finding operating conditions, and distillation systems that could obtain higher than the 53% yield obtained from this work should be considered as future work.

Hydrolysis	88.60%	88.60%	88.60%
	↓	↓	↓
Decarboxylation with Pt/C @ 400 °C	71.98%	-	-
	↓	↓	↓
Decarboxylation and cracking with Pt/C @ 450 °C	-	70.98%	70.98%
	↓	↓	↓
Cracking, aromatisation with ZSM-5 @ 400 °C	-	-	83.16%
	63.77%	62.88%	52.30%

Figure 8.1: Overall yields of liquid hydrocarbons from the 3-stage conversion of rapeseed oil

Figure 8.1 shows the overall yields of final fuel range products from the three-stage conversion of rapeseed oil. The results showed that the final liquid products (after cracking) gave a total liquid hydrocarbon yield of around 50 wt.%. This present work has produced better results than those reported in recent literature using direct cracking of lipids with ZSM-5. For instance, Zhao et al., (2015) reported a maximum yield of 30.1 wt.% hydrocarbons from the direct cracking of non-edible sunflower oil with ZMS-5 at a temperature 550 °C. This three-stage process produced 'neat' hydrocarbons with non-detectable oxygen content, compared to the work of Zhao et al. (2015) who reported up to 7% oxygen content in the upgraded oil product.

In addition to this, the design of this reaction process provides accommodation for robust processes. For instance, jet fuel contains 47% alkanes and 18% aromatics (Edwards, 2002). While gasoline contains 44.7% alkanes and 43.8% aromatics (Botero et al., 2016). Therefore, based on the compositions of the oils from decarboxylation in Chapter 6 (60.82% alkanes and 8.5% aromatics), and from the cracking stage in Chapter 7 (33.99% alkanes and 49.17%), both fractions can be blended. In other words, 61% of the decarboxylated oil with 26% of the cracked oil can produce a blend with the potential to substitute jet fuel, and 47% of the oil decarboxylated oil with 47% of the cracked oil can provide the required quantities of alkanes and aromatics in gasoline.

## 8.2 Overall recommendation and future work

The aqueous phase that was the by-product of the hydrolysis of vegetable oil contains some glycerol. This research project found the glycerol fraction recovered to be about 10 wt.% of the feedstock, vegetable oil, which did not seem like much when feedstock mass per batch was 10 g. However, at a scaled-up level, “10%” could represent a significantly higher mass. Therefore, further work could be done on recovering the glycerol and exploring economically useful applications. Currently, significant amount of research is ongoing to find uses for the glycerol glut arising from biodiesel production. The aqueous glycerol fraction from this hydrolysis step may find similar uses. Main uses of glycerol include production of acrolein (a versatile chemical for several application from military to plastics), monoglycerides, polyglycerol, polyols, polyurethanes, solketal, lactic acid, and bio-oil. It can also be used in the production of hydrogen through aqueous phase reforming (APR) and hydrothermal gasification.

Even though this research project has only explored just WCOs from a pub and cafeteria, other sustainable second-generation lipids including non-edible oils, oil-rich effluents from oilseed processing, animal fats, industrial wastes and by-products, lipid derived algae, could be explored and tested. These are all made up of triglycerides and so could serve as non-food sources of hydrocarbons using the methods investigated in this thesis. Using these feedstocks could also expand the available bio-derived hydrocarbons to make significant impact on the displacement of fossil hydrocarbons to achieve Net Zero.

In this present work all experiments were carried out in batch reactors, which are not essentially favoured for large-scale production. Instead, continuous processes are more industrially relevant due to the advantages such as simpler scaling up, reduced space requirements, reduced waste generation from process, and increase of both process and energy efficiency, which would deliver products at reduced costs. However, these need to be investigated as some of the steps researched in this work (e.g., the hydrolysis product was obtained as a semi-solid, which may be challenging for continuous isolation via known industrial-scale separation technologies) may not be easily amenable to continuous operations. Therefore, a combination of batch and continuous operations may be more appropriate i.e., by accommodating cooling, separation and reheating steps for the hydrolysis product steps before the next stages.

It was observed that the distillation process for the products of catalytic cracking was inefficient due to the design of the apparatus used. For instance, clear liquids could be seen condensing and returning to the holding flask, which could have been part of the distillate. Hence, more appropriate distillation apparatus would be recommended for more efficient

separation of the useful fuel fractions from the dissolved carbon to improve the purity of the fuels.

Further investigations could be conducted with different catalysts because Pt/C is expensive and not easily regenerable. Therefore, the use of cheaper catalysts could reduce the overall cost of the process as well as make recycling easier. Other cheaper catalysts based on Ni, Co and Nb have been reported in literature but with serious deactivation challenges. More research could be carried out to improve the stability of these catalysts to ensure low product costs.

Finally, considering the excellent results obtained in this work, in terms of overall conversion and yields of liquid hydrocarbons (including significant biojet yield), it would be important to assess the economic viability and environmental sustainability of this three-stage process. This can be used to compare it with other lipid-to-hydrocarbons processing routes reported in literature. A study of the possible adverse impact on production, from sourcing the feedstock to the conversion, the energy and materials balances, logistics and GHG emissions (including carbon accounting) should be considered in a life cycle assessment (LCA). In addition, modelling of the three-stage process in continuous flow can be conducted and used for technoeconomic assessment to understand the economic performance of the process.

### 8.3 References

- Botero, M.L., Mosbach, S. and Kraft, M. (2016) 'Sooting tendency and particle size distributions of n-heptane/toluene mixtures burned in a wick-fed diffusion flame', *Fuel*, 169, pp. 111–119. doi:10.1016/j.fuel.2015.12.014.
- Edwards, T. (2002) "'kerosene" fuels for aerospace propulsion - composition and properties', 38th AIAA/ASME/SAE/ASEE Joint Propulsion Conference and amp; Exhibit [Preprint]. doi:10.2514/6.2002-3874.
- Zhao, X., Wei, L., Cheng, S., Huang, Y., Yu, Y. and Julson, J. (2015). Catalytic cracking of camelina oil for hydrocarbon biofuel over ZSM-5-Zn catalyst. *Fuel Proc. Technol.*, 139, 117-126.